Dynamic Resource Allocation in Wireless Fading Channels with Delay Requirements

A DISSERTATION
SUBMITTED TO THE FACULTY OF THE GRADUATE SCHOOL
OF THE UNIVERSITY OF MINNESOTA
BY

Juyul Lee

IN PARTIAL FULFILLMENT OF THE REQUIREMENTS
FOR THE DEGREE OF
DOCTOR OF PHILOSOPHY

Professor Nihar Jindal, Adviser

January, 2010

Acknowledgements

I would like to thank a number of people for their contribution to my PhD study. First of all, I express my sincerest gratitude to Professor Nihar Jindal for his guidance and continual support. His advice, supervisions and encouragement have made any success in this undertaking possible. The time, effort and discipline he graciously provided me on many engineering issues enabled me to improved the ability to approach their solutions in a consistent and efficient manner.

I acknowledge the efforts of Professor Georgios B. Giannakis, Professor Zhi-Quan (Tom) Luo and Professor William L. Cooper as my committee members. Their many useful suggestions, along with their classes, have been invaluable in my work.

I want to thank my laboratory companions, including Niranjay Ravindran, Peng Wu, Mariam Kaynia, Joseph Blomer, John Marcos, Amogh Rajanna, Omar Mehanna and Balasubramanian Gopalakrishnan, for their many kindnesses and helpful discussions that contributed to a pleasant and productive working atmosphere. I also thank my department friends, including Stephen Wu, Pepe Barbe, Yao Huang, Hao Zhu, Shahrokh Faramand and Mercedeh Khajavikhan, for encouraging me to press on in my researches during my PhD study. The unselfish help of my Korean friends including Seung-jun Kim, Sangmin Kim, Woojoon Lee, Hyoungsuk Yoo, Daesun Oh and Taehyoun Oh, can not be passed over.

In publishing this dissertation, including journal and conference publications, Niranjay Ravindran, Joseph Blomer, Michael Sheehan and Steve Carnes are also acknowledged for their assistance in honing my English writing and speaking.

Above all, my deepest thanks go to my parents for their continuous support, understanding and encouragement. Without their patience and forbearance, the preparation of this dissertation would have been impossible.

Abstract

In this dissertation we investigate resource allocation in fading channels with delay constraints. We first consider scheduling communication resources over time-varying channels when constrained by a hard deadline requirement. The basic problem setting is given as follows: a packet of B bits must be transmitted by a hard deadline of T time slots over a time-varying channel. The transmitter/scheduler must determine how many bits to transmit, or equivalently how much energy to transmit with, during each time slot based on the current channel quality and the number of unserved bits, with the objective of minimizing expected total energy. Our focus is on the interplay between opportunism (adapting to the fading behavior) and the delay requirements. Under the Shannon energy cost function, the optimal solution can only be numerically determined in general, and thus we develop simple and near-optimal policies, which are shown to be asymptotically optimal. Then, we consider monomial cost, under which we can obtain the optimal policy in closed form. We attempt to extend the result to the case for multi-user scheduling and scheduling with outage. In these resource allocation problems, our interests are in formulating an analytical solution. Additionally, we consider parallel/MIMO channel scheduling and wideband scheduling with a hard deadline constraint. As an alternative view of delay requirements, we consider the fairness of each user's traffic. In this regard, we investigate the symmetric capacity of MIMO broadcast channels along with high SNR analysis of MIMO broadcast channels.

Contents

List of Tables

List of Figures

Chapter 1

Introduction

Due to the enormous popularity and endless demand for mobile applications during the last two decades, wireless technologies have been of great interest and have evolved tremendously. In the mid 1990s, 2G (Second Generation) mobile services were a big success with simple voice and short message services (SMS), thanks to the advances in integrated circuit (IC) technologies. Likewise, Wi-Fi (Wireless Fidelity) became widespread all over the world for computer networks in fixed wireless environments. While creating huge consumer industries, these two technologies have continued to evolve to 3G (Third Generation) and 4G (Fourth Generation) technologies such as WCDMA (Wideband Code Division Multiple Access), CDMA2000 (Code Division Multiple Access 2000), LTE (Long Term Evolution), and WiMAX (Worldwide Interoperability for Microwave Access).

From the system engineering perspective, for the development of wireless technologies, an important issue is the short-term performance associated with delay requirements. For example, a VoIP (Voice over Internet Protocol) packet should have less than 150 msec one-way delay for "acceptable communication" [ITU03]. Audio and video streaming services are other examples of delay-constrained data traffic. Without taking such delay limits into account, communication resource allocation can end up being inefficient. Notice that radio transmission technologies designed for best average performance are not necessarily adequate for delay-constrained setups and large amounts of resources may be consumed or transmission tasks may fail to meet the delay requirements. With all these concerns, this dissertation deals with efficient resource allocations for wireless communications when a delay requirement is imposed. As communication devices get lighter and smaller to meet the high demand for portability, efficient power resource allocation

is of great importance for longer battery life. Let us start with a motivating example in the next section.

1.1 A Motivating Example

In this section, we consider an example of hard deadline scheduling. We suppose that we have a VoIP packet of 200 bits that has a hard deadline of 50 msec and a channel coherence time of 25 msec. In other words, the packet of 200 bits is required to be transmitted within two time slots. We want to design a discrete-time bit allocation policy that minimizes total transmit energy.

At the first time slot, the transmitter should determine how many of the 200 bits to transmit given the knowledge of the channel state of the first slot, but without the knowledge of the channel state for the second slot. Notice that the remaining bits, that is the bits that are not transmitted in the first slot, must be transmitted in the second slot. When the channel quality is good, it is desirable to transmit more than 100 bits. When the quality is poor, it is desirable to transmit fewer than 100 bits. Since the transmitter does not know the channel realization for the future (second) slot, leaving many bits to the future slot is potentially risky. Again, the question is how many of the 200 bits should be sent at the first time slot if only the current (first slot) channel state is available.

We now point out several challenging issues from the example. All the discussions focus on bit allocation in the first time slot, because the bit allocation in the second slot is trivial, i.e., all the unserved bits are to be served at the second slot.

First, this allocation problem has a hard deadline constraint. That is, the transmitter knows that the next time slot is the deadline and is aware that all the deferred bits are to be transmitted at the second slot, i.e., no outage is allowed. Thus, the bit allocation should be conservative rather than aggressive in that the bit allocation process is affected by the deadline constraint, although it is dependent on the current channel quality as well. As a result, there is a tension between serving bits when the channel is good and leaving too many bits to the second slot. If we consider an extension of the allocation example to three slots, the bit allocation at the first time slot is expected to be less conservative (or more aggressive) than that of the two slot case. In general, the allocation process is expected to be more dependent on the current channel quality and less dependent on the deadline as the deadline is far away. At the limit, i.e., no hard deadline, the bit allocation is then expected to be purely channel-dependent.

Second, the unpredictability of the variation of the wireless channel with respect to time makes *causal* knowledge of the channel state a fundamental property: the future channel cannot be known at the present. That is, the number of bits to transmit should be determined without the knowledge of the channel state of the second slot. Let us consider the following two cases that are different from our example. The first case is that the transmitter does not know both channel states. Then, transmitting 100 bits equally for each slot would be desirable. The second case is that the transmitter knows both channel states. Then, the bit allocation can be determined by solving a convex optimization and the solution (which will later be shown to be "waterfilling") allocates more bits for a better channel. When we go back to our example, however, only the channel state information of the first slot is available because of causality. With only the current channel information, we need to determine how good or poor the current channel condition is, in order to determine the bit allocation at the present time. To judge the quality of the channel state at present, we should find a measure of the goodness/badness of the channel state. One can propose a comparison with the average value of the random channel states. However, the optimality of choosing the average value is not clear. Another question is whether the criterion of the goodness/badness of the channel state is constant with respect to time or is a function of the number of the slots to the deadline.

Above all, the objective of the bit allocation process is the minimization of the expected energy expenditure of transmitting 200 bits over two time slots. To calculate the energy expenditure, we need a relationship between the number of transmit bits and the incurred energy. In this dissertation, we deals with two function types: the Shannon function and monomial functions. The Shannon function is the inverse of the channel capacity of the additive white Gaussian noise channel, which will be discussed in the next section. Among the policies that satisfy the hard deadline constraint and require only causal channel information, we should adopt the policy that minimizes the expected energy. This will guarantee the short-term performance of delay-constrained traffic.

Although the example is very simple, it has introduced many interesting issues. In this dissertation, we will develop algorithms for resource allocation for such delay constrained traffic.

Notice that the example can be formulated as a dynamic program, and moreover, any extension to an arbitrary deadline constraint can also be formulated as a dynamic program. Dynamic programming is, in general, a sequence of problems, each of which determines parts of the entire variables [Bel03, Ber05]. Dynamic programming is applicable to many areas such as

stock markets in economics and inventory control in industrial engineering. Our example here can be understood as a finite-horizon dynamic program. In many cases, dynamic programs can only be solved numerically. However, we will focus on the system engineering intuition and the manner in which parameters such as the deadline length, causal channel state information, and energy-bit functions affect the optimal resource allocation policy, rather than numerical computations of the dynamic program.

1.2 Wireless Background

In this dissertation, we study dynamic resource allocation over *wireless* fading channels. To provide an understanding of wireless basics, this section briefly introduces background materials based on standard wireless communication textbooks such as [Gol05, TV05].

One of the most challenging issues in wireless communications is the time-varying nature of the wireless channel. Figure 1.1 illustrates a typical example of wireless communication between an access point (or base station) and multiple user terminals. If the position of mobile terminals or the surrounding environment is varying in time, such as due to moving vehicles, the wireless channels between the access point and the user terminals change with respect to time. This time-varying behavior of wireless channels induces changes in scattering, reflections, multi-path, etc. Thus, the overall propagation model is varying in time and the phenomenon is referred to as *fading*. Although there are many issues and concerns related to fading, we will adopt a very simple fading model and discuss resource allocation over this model in this section.

1.2.1 Fading Channels and Resource Allocation

Our discussion begins with channel capacity, which plays an important role in the equivalence between the incurred energy and the number of transmit bits. Then we will discuss resource allocation for fading channels.

Channel capacity is a fundamental measure in a communication link that represents the maximum achievable communication rate [Sha48]. For the additive white Gaussian noise channel depicted in Fig. 1.2, the capacity C is [CT91]

$$C = \log(1+gP) \quad [\text{nats/sec/Hz}], \tag{1.1}$$

where g denotes a constant channel gain (a non-negative quantity, usually measured in power

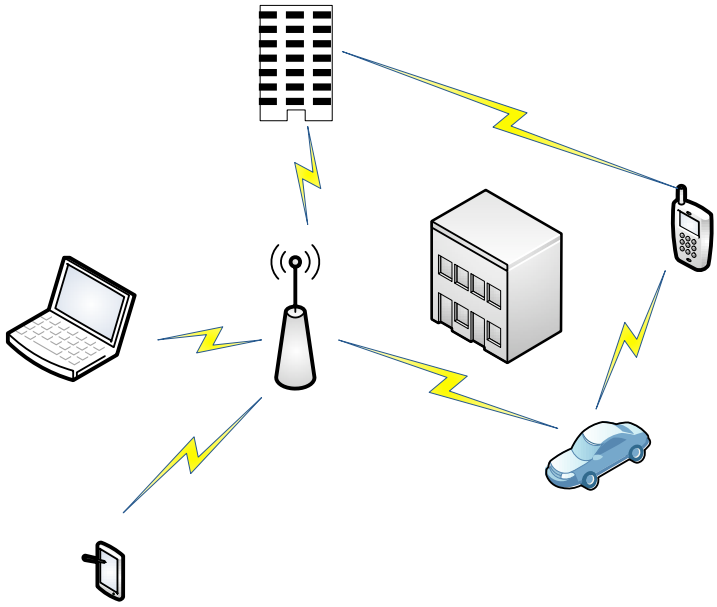

Figure 1.1: Typical wireless communication environment

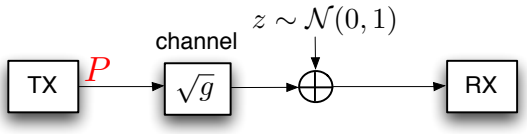

Figure 1.2: Additive white Gaussian noise channel

units), assuming that the additive noise z (in Fig. 1.2) is a Gaussian random variable with zero mean and unit variance and transmit power P. The relation (1.1) shows the equivalence between power P and rate C for a fixed channel state g. That is, the maximum achievable rate C is an increasing function of the transmission power P for a given channel state g. By the monotonicity of the logarithm, we can also find the inverse relation which determines the minimum required power to transmit at a rate of C is:

$$P = \frac{e^C - 1}{g}. \tag{1.2}$$

When the channel fades due to the time-varying nature of the wireless environment, the channel gain state g is random and thus the capacity C is also random. To characterize the capacity of wireless fading channels, many notions of capacity has been proposed: ergodic capacity, outage capacity, and zero-outage (delay-limited) capacity. The ergodic capacity, for

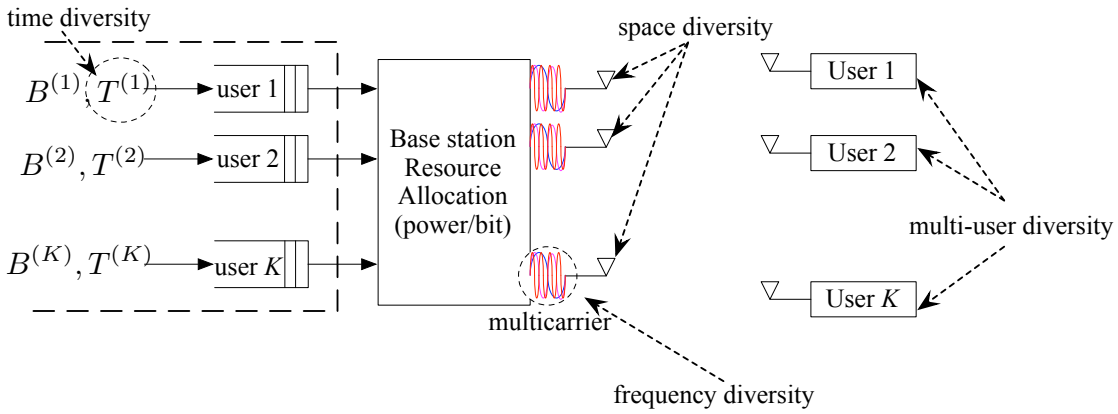

Figure 1.3: The downlink resource allocation problem in various diversity environment

example, denotes the maximum achievable rate averaged over all fading states and is given by

$$C^{\text{erg}} = \mathbb{E}\left[\log(1+gP)\right], \tag{1.3}$$

where the expectation is taken over the fading distribution of g. Thus, this ergodic capacity is useful when the channel fade state changes fast enough such that all the possible realizations occur during the averaging interval. When fading is slow, however, this notion is not suitable to characterize the fading channel. Outage capacity or zero-outage capacity is more appropriate for slow fading cases (see [Gol05, TV05] for detail).

When a communication link is in "deep fade", i.e., the channel gain g in Fig. 1.2 is very small, the capacity gets smaller and the reliability is reduced. To improve reliability, diversity combining is a useful technique, which uses the fact that it is less likely for two independent paths to be in deep fade simultaneously. Diversity can be implemented in various domains such as time, frequency, and space as illustrated in Fig. 1.3. Transmitting over multiple time slots provides time diversity when each slot experiences fading independent from the other slots. Similarly, multiple carrier subchannels provide frequency diversity and multiple antennas provide space diversity. In a multiple access or broadcast scenario, each wireless link to the user provides multiuser diversity [VTL02].

Since diversity is furnished by independent fading paths, it can be modeled with a set of parallel channels as illustrated in Fig. 1.4. When the transmitter has a power constraint P, it

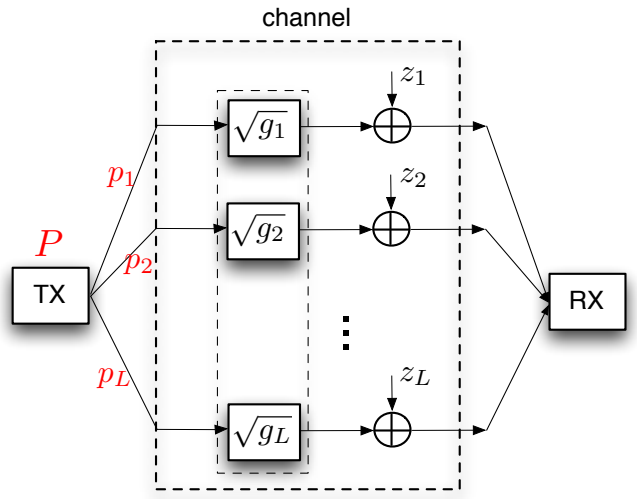

Figure 1.4: Parallel channels

can distribute the power to the parallel channel components of the set in any manner so that the sum power is no greater than P. Depending on the way of distributing the power, the achievable rate varies considerably. Therefore, power allocation is a very important issue for improving the utilization of communication resources.

Let us consider a set of parallel channels that consists of L parallel components with $g_1, g_2, \cdots, g_L$ path gains and zero-mean unit variance additive white Gaussian noise as depicted in Fig. 1.4. First, we consider the case when the transmitter has perfect knowledge of the channel state information of the parallel channels. For this case, the transmitter can adapt the power allocation according to the channel states of the paths, and thus the capacity is given by the following optimization:

$$\begin{aligned} C^{\text{parallel, perfect CSI}} = \max_{p_1, p_2, \cdots, p_L} \quad & \sum_{l=1}^{L} \log\left(1 + g_l p_l\right), \\ \text{subject to} \quad & \sum_{l=1}^{L} p_l \leq P, \\ & p_l \geq 0, \quad \forall l, \end{aligned} \tag{1.4}$$

where p_l denotes the power allocation to the l-th path. By the Lagrangian method [BV04], the

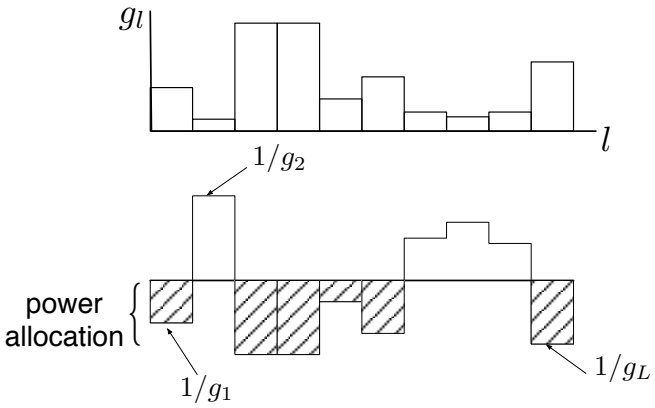

Figure 1.5: Waterfilling when CSI is available

solution to the optimization in (1.4) is given by

$$\frac{p_l}{P} = \begin{cases} \frac{1}{g_{\text{th}}} - \frac{1}{g_l}, & g_l \geq g_{\text{th}}, \\ 0, & g_l < g_{\text{th}}, \end{cases} \tag{1.5}$$

where g_{th} is determined to satisfy

$$\sum_{l=1}^{L} p_l = P. \tag{1.6}$$

Figure 1.5 illustrates both the channel gain states and the optimal power allocation according to (1.5), in which the amount of power allocated for each path component is depicted as the difference between a threshold level and the noise gain of the path component (i.e., the inverse of the channel gain). By analogy, this solution is referred to as *waterfilling* and the threshold is called *water-level* [CT91, Gol05]. Comparing the two plots in Fig. 1.5, we can observe that more power is allocated for the path component that has a stronger channel gain. This leads to the concept of *opportunistic* communication: transmitting with more power (and rate) where the channel quality is good and less power (and rate) where the channel is in a poor state.

When the transmitter does not have knowledge of the channel states of the parallel channels, it allocates the same amount of power uniformly to all the paths. Thus, the channel capacity is given by

$$C^{\text{parallel, no CSI}} = \sum_{l=1}^{L} \mathbb{E}\left[\log\left(1 + \frac{P}{L} g_l\right)\right] = L\,\mathbb{E}\left[\log\left(1 + \frac{P}{L} g\right)\right], \tag{1.7}$$

assuming that $g_1, \cdots, g_L$ are identically distributed.

Depending on the information available to the transmitter, we have seen two power allocation schemes. When the transmitter has perfect knowledge of the channel state information, it performs waterfilling. When the transmitter has no knowledge, it performs uniform power allocation. Instead of maximizing the achievable rate with a power constraint, we can alternatively consider minimizing power with a rate constraint, which is practically useful in battery-powered mobile applications for a fixed service rate. Because these two problems are the dual of one another (in the sense of convex optimization [BV04]), the opportunistic behavior of optimal resource allocation is expected here as well. Connected to the example of Section 1.1, it is interesting to know what the resource allocation should be if the transmitter knows one state of the channel but does not know the other state. To capture this, we consider resource allocation problems in time-domain, especially with a finite horizon. Inherently, the transmitter can only know past channel states and (at best) current channel states, but does not know future channel states due to causality. This discussion is followed in the next subsection.

1.2.2 Resource Allocation over Time-Domain

In this dissertation, we use a block fading model that assumes that the channel state is constant for a certain block period (during the coherence time interval) and changes independently to a new value for the next block period, and thus the channel state is modeled by a random sequence $g_t, t = 1, 2, \cdots$, where t denotes a slotted time index. If we consider a resource allocation problem over a certain interval T, then the communication link with the channel states $g_1, g_2, \cdots, g_T$ form a set of parallel channels as illustrated in Fig. 1.4 by replacing the channel index l with t and the total number of parallel channels L with T.

In time-domain resource allocation, as pointed out in the example of Section 1.1, the transmitter knows, at best, the current channel state but cannot know the future channel states because of causality. Let us consider an example of sequential power allocation problem as illustrated in Fig. 1.6. As in Fig. 1.6a, the transmitter knows the channel state of the first slot but does not know the other states. Thus, the transmitter should determine the amount of power to allocate only with the current channel state information. Similarly, in the second time slot (Fig. 1.6b) the power allocation should be determined only with the channel states of the first and second slots without the rest of the channel states. The process can continue as in Fig. 1.6c and Fig. 1.6d, and so forth.

To perform opportunistic resource allocation, it is essential to determine whether a channel is

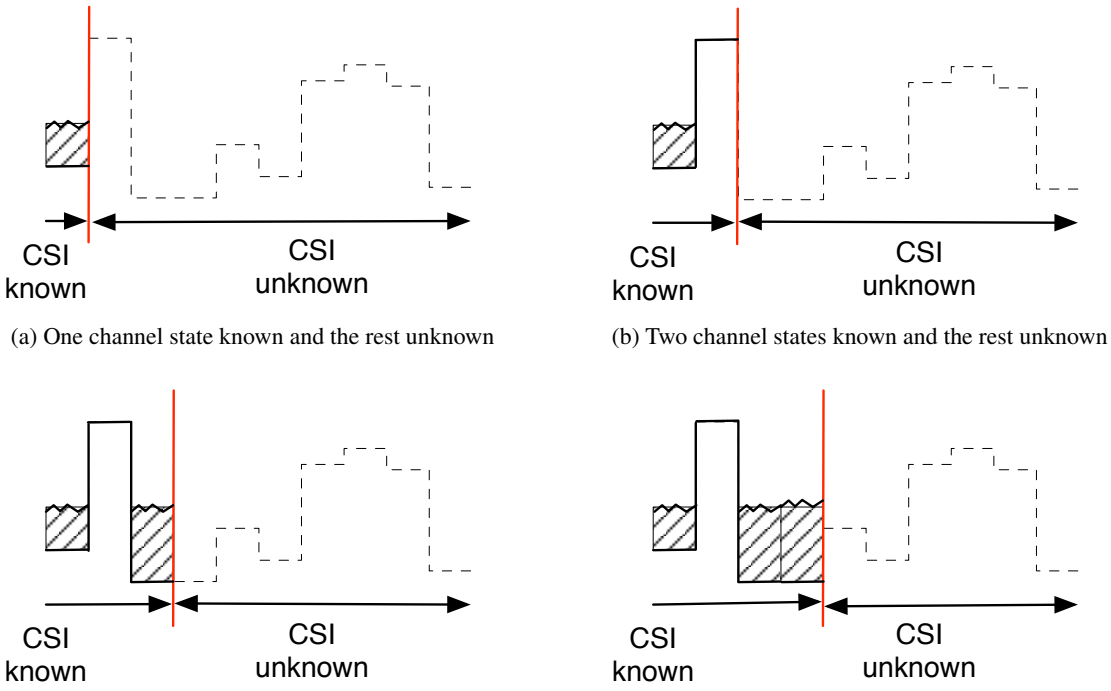

(a) One channel state known and the rest unknown

(b) Two channel states known and the rest unknown

(c) Three channel states known and the rest unknown

(d) Four channel states known and the rest unknown

Figure 1.6: Progressive waterfilling when only parts of CSI are known

good or bad, and to what extent. The critical parameter for this issue is the water-level, which can be determined by (1.5) and (1.6) for the parallel channel setup in Fig. 1.4, and requires complete knowledge of the channel states beforehand. The question is how we should approach this if the transmitter only knows some of the states. When there are infinite channel components, we can determine the water-level based entirely on the fading distribution. The problem of interest is then how to determine the water-level if the transmitter knows only some of the states when the total number of channel components is finite.

If the transmitter had perfect knowledge of the channel states, it could determine the water-level and perform waterfilling like (1.5) and (1.6) as illustrated in Fig. 1.5. If the transmitter had no knowledge of the channel states, it should perform uniform allocation. Thus, the scheduling problem with this kind of partial knowledge lies in between the two strategies when the water-level can not be determined by (1.5) and (1.6).

Finite-horizon time resource allocation problems have been studied in the context of delay

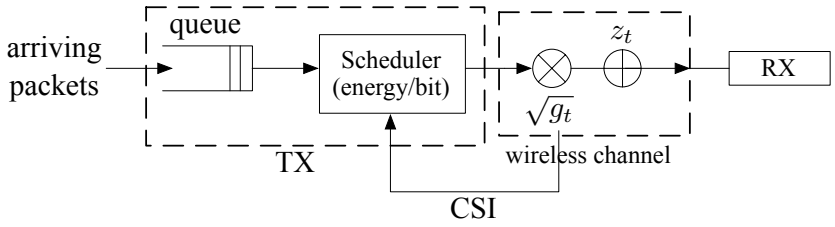

Figure 1.7: Delay-constrained packet scheduling model

constrained scheduling. Purely opportunistic communication is optimal from the perspective of long-term average rate, but not necessarily appropriate for delay-constrained traffic which requires guaranteed short-term performance. To account for a short-term performance, we may consider the delay-limited capacity (a.k.a. zero outage capacity) that represents the maximum achievable constant rate for all fading states [HT98, Gol05]. This notion, however, applies to the cases with only one time slot in the scheduling problem. Thus, another notion to account for a finite-time horizon with more than one time slot is required. In this regard, we focus on the interplay between fading, finite-horizon, and causal channel information in the dissertation.

In addition to power allocation, the issue of bandwidth allocation is also relevant to recent OFDM systems such as WiMAX [Nua07] and LTE [HT07]. Additionally, we can consider other types of cost functions instead of the Shannon function as in (1.1) such as monomial functions, which may be obtained from experimental data.

1.3 Prior Work

Delay constrained scheduling in wireless communication systems has been actively studied in various network settings under different arriving traffic models and delay constraints. As illustrated in Fig. 1.7 for a single-user scheduling, delay-constrained data packets are arriving at the queue of transmitter and then are to be scheduled over the wireless fading channel to the receiver.

An example of the arrivals at the queue is illustrated in Fig. 1.8, in which data packets arrive randomly in time each with different packet sizes (depicted in the height of the bar) and with different delay requirements (indicated by the scheduling period). Then the scheduler arranges the transmission of the data packet to meet the delay requirements with the objective of

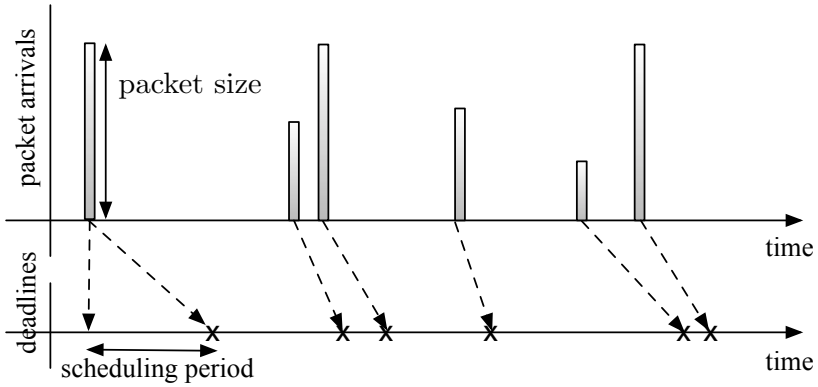

Figure 1.8: Randomly arriving traffic

minimizing the transmission power. Depending on the wireless channel fading states, the power required to transmit a fixed number of bits varies as in (1.2). Therefore, the scheduler should be designed to take care of the two random sources of packet arrivals and channel fading, in order to fulfill minimizing the transmission power while satisfying the delay requirements. This problem is generally complicated and the relevant work will be discussed in Section 1.3.1.

Another traffic model is illustrated in Fig. 1.9, in which data packets arrive regularly, i.e., the packet arrival is periodic and each packet has the same size and the same delay requirement. Since there is no randomness in packet arrivals, wireless fading is the only random source. In this sense, the regular traffic model is simpler than the randomly arriving traffic model, but the optimal scheduling for the regular traffic is also complicated to design and is important for audio/video streaming applications. The relevant work will be introduced in Section 1.3.2.

Instead of categorizing in terms of the type of packet arrivals, prior work can be grouped depending on its delay constraint, i.e., average versus hard delay constraint, where the latter has a strict deadline constraint while the former is constrained on the average. Typically, regularly arriving traffic such as streaming services have stringent deadlines so it is usually constrained with hard deadlines. For randomly arriving traffic, scheduling with hard deadline constrains is more complicated than that with average delay constraints. The scheduling problem in this dissertation deals mainly with a regularly arriving traffic with a hard deadline constraint.

Moreover, a scheduler can also be classified either as offline or online depending on the availability of future channel states. If a scheduler can operate without future channel information, it is an online scheduler. From the literature in higher layer scheduling, it is observed that many

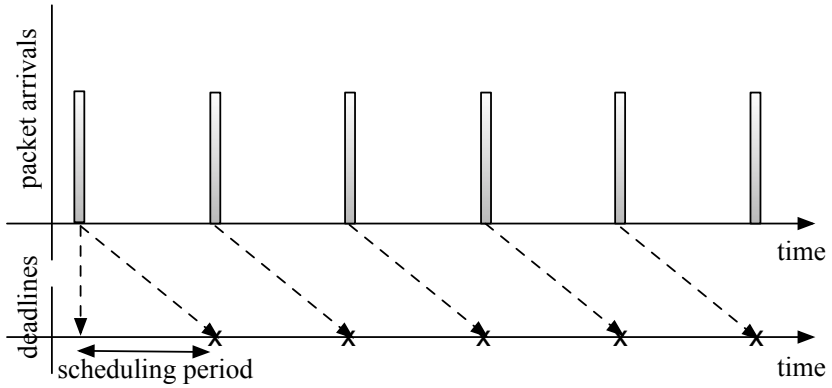

Figure 1.9: Regularly arriving traffic

online scheduling algorithms have been developed from heuristic variations of optimal offline algorithms. Notice that our problem corresponds to an online scheduling. To emphasize our treatment of physical-layer issues, however, we use the terms *causal* and *non-causal* rather than online and offline to indicate whether a scheduler has knowledge of future channel states.

Many other issues can be considered such as the number of users, outage, types of cost/utility, and so on. Although our research focus is narrow in delay constrained scheduling, we will go over some of the highlights of a general delay constrained scheduling problem for wireless fading channels by categorizing into the arrival types.

1.3.1 Random Packet Arrivals

When packets arrive randomly at the queue of the physical layer transmitter, a scheduling policy should be designed in accordance with the queue dynamics as well as the channel fading state. A general objective is the minimization of the average transmit power/energy while satisfying the delay requirement or vice versa. Notice that the average transmit power has a tradeoff relationship with the delay requirements. For example, if a data packet has an imminent deadline, the scheduler has no time to wait for a better channel condition so that it needs to transmit the packet even at a poor channel state, and thus the average transmit power increases. If a data packet has a long deadline or is insensitive to short-term performance, the scheduler can wait until the channel condition is sufficiently good such that transmit power can be saved. In this regard, more transmit power is consumed with short deadlines.

According to the survey in [UBG04], the joint queue/fading scheduling problem dates back

to 1999 when Collins and Cruz considered minimizing average transmission power under an average delay constraint and a peak power constraint for the two-state Gilbert-Elliott channel model ("good" and "bad" states) [CC99], which results in a linear cost function. By formulating a dynamic programming (DP), they proposed a policy of when to transmit depending on backlog size and channel state. Rajan, Sabharwal, and Aazhang considered a similar setup by allowing arbitrary channel states [RSA04]. Instead of being limited to a linear cost function, they adopted the Shannon cost function, i.e., the power and rate are related by (1.1). Berry and Gallager investigated the tradeoff between power and delay by formulating a multiobjective optimization problem that is a weighted sum of average power and average delay [Ber00, BG02]. By varying the weight, they obtained the optimal average power curve with respect to average delay and found properties of the curve.

Prabhakar, Uysal-Biyikoglu, and El Gamal studied a minimum energy transmission scheduler by adjusting packet transmission time [PUBG01, UBPG02]. They devised a so-called "lazy" scheduling policy that adapts transmission times according to backlog but did not incorporate wireless fading. Uysal-Biyikoglu and El Gamal considered scheduling by jointly adapting backlog and fading channel conditions for minimizing transmission energy [UBG04]. From the formulation of a non-causal setting, they developed an iterative algorithm called "FlowRight" for the optimal non-causal scheduling and then proposed a heuristic causal algorithm that performs "look-ahead waterfilling". Chen, Mitra, and Neely extended the FlowRight algorithm for individual deadline constraints [CNM07a, CNM07b].

1.3.2 Regular Data Traffic

Compared to the random arrival traffic, scheduling of regular traffic, as depicted in Fig. 1.9, has been less extensively studied. Typically, this type of traffic comes with a stringent or a hard delay deadline requirement. Satisfying the hard deadline is crucial for continuing streaming applications. Since there is no need to take care of the random behavior of the queue dynamics in this traffic model, the scheduler is to be developed concerning with the number of unserved bits and the fading states over the scheduling period constrained by a hard deadline.

Negi and Cioffi considered the maximization of the expected number of transmitted bits in a finite number of slots subject to a finite energy constraint, which is the dual problem of the one considered here [NC02]. They provided iterative algorithms in dynamic programming and suggested asymptotic policies for high and low SNR: equal-power scheduling that allocates the

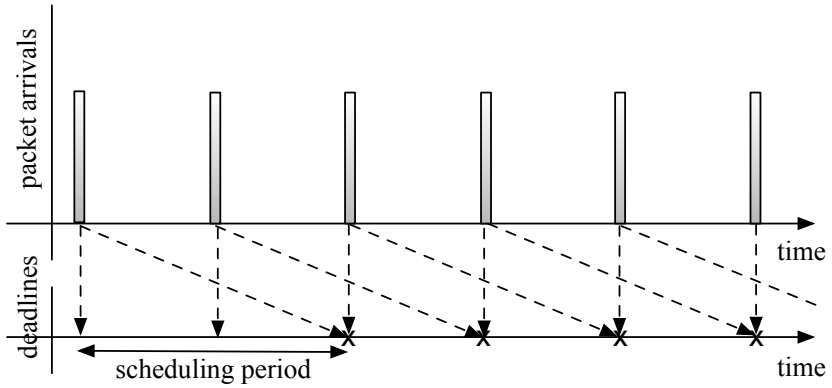

Figure 1.10: Regularly arriving traffic with underflow constraints

same amount of power at each slot for high SNR while a one-shot threshold policy for low SNR. Their work was extended to multiple-access channels in [CTV04].

Fu, Modiano, and Tsitsiklis considered a scheduling problem of a single packet transmission over a block fading channel, subject to a hard deadline, and formulated it as a finite-horizon DP [FMT06]. For general cost functions, this DP can only be solved numerically, but in [FMT06] a closed-form description of the optimal policy is derived for the special case where the cost function is linear and the channel state is restricted to be an integer multiple of some constant. A linear cost function is also considered in [SL08] and [SL] under strict underflow constraints. In their formulation, an overlapping deadline constraint, as illustrated in Fig. 1.10, is imposed in order to guarantee a continuous playback of a streaming service with a underflow constraint.

Zafer and Modiano extended the work of [FMT06] to a setting where the channel evolves according to a continuous Markov process, and they derived the optimal scheduler for the case where the cost function is given by the AWGN capacity formula under particular assumptions on the channel model (channels with *drift*) [ZM07].

1.4 Overview of Contributions

This dissertation focuses on the regular data traffic with a hard delay constraint setting where each packet must be transmitted within a certain time duration without an outage. Based on relatively simple model, we derive closed-form solutions and provide an interpretation of the interplay between fading, hard deadlines, and causal information of the channel states. This

setup reasonably models delay-constrained applications such as VoIP and streaming services, where packets arrive regularly and each must be received within a short delay window.

In general, a hard deadline delay constraint problem of regular traffic can be formulated as follows. If we let $C(b;g)$ be the cost to transmit b bits under channel quality g, the objective of scheduling is to minimize the expected sum of costs, i.e.,

$$\begin{aligned} \text{minimize} \quad & \mathbb{E}_{g_1,\cdots,g_T}\left[\sum_{t=1}^{T} C(b_t;g_t)\right], \\ \text{subject to} \quad & \sum_{t=1}^{T} b_t = B, \\ & b_t \geq 0, \quad \forall t. \end{aligned} \tag{1.8}$$

where T is the hard deadline constraint, B is the total size of packet, and b_t is the number of scheduled bits at time slot t.

Depending on the available information on the channel states at each instance of transmission, various problems can be imposed. One can assume that all the channel states are available at the beginning of scheduling, or the channel states are not available. Considering that resource allocation occurs across time slots, it is more reasonable to assume that the channel states are provided in a causal manner, i.e., the scheduler has knowledge of the past and the current channel, but not of the future channel. Another aspect is channel correlation across time slots. In this dissertation, however, we explore the simpler case where the channel states are i.i.d. (independently and identically distributed) across time slots and are known causally. This is a simple setting, but solving the scheduling problem (1.8) under this setting is non-trivial. In addition, this simple setting suggests how the scheduler should balance the desire to be opportunistic, i.e., wait to serve many of the bits when the channel is in a good state, with the hard deadline.

The choice of the cost function may vary depending on the operating environment. For example, if we operate a scheduler at AWGN capacity and want to minimize the total transmit power, the exponential function in (1.2) is a proper choice, while we can obtain a cost function from a predefined form (e.g., monomial functions) by curve-fitting. According to [UBPG02], the cost function C should be non-negative, increasing, and strictly convex, e.g., exponential functions and monomial functions. The choice of the cost function also affects the availability of the closed-form solution.

This dissertation mainly deals with the cost associated with the AWGN channel capacity:

$$b = W\log(1+gE), \tag{1.9}$$

where b is transmittable with given energy E and given bandwidth W under channel state g.

In Chapter 2, we consider an energy-efficient scheduling problem where the cost function is given by the energy incurred to transmit b bits under channel state g:

$$C(b;g)(=E) = \frac{e^b-1}{g}. \tag{1.10}$$

From this setup, we develop low-complexity scheduling policies for delay-constrained causal scheduling, and prove the optimality in different asymptotic regimes. The scheduling policy in this setup is a set of bit allocation at each time instant $b_1, b_2, \cdots, b_T$, where each b_t is a function of the number of unserved bits β_t at the beginning of time slot t (t is in descending order and thus represents the number of remaining slots) and the current channel state g_t. Because of the causality and the i.i.d. block fading assumption, the future channel states are not available and the past channel states are not relevant, respectively. In particular, we show that:

- When the total number of bits B is large, the optimal scheduling policy is a linear combination of a delay-associated term and an opportunistic-term.

$$b_t = \underbrace{\frac{1}{t}\beta_t}_{\text{delay associated}} + \underbrace{\frac{t-1}{t}\log\left(\frac{g_t}{\eta_t}\right)}_{\text{opportunistic}}, \tag{1.11}$$

  where b_t is the number of bits to serve (from the unserved bits β_t) at time slot t and η_t denotes a channel threshold determined by the channel statistics and the particular policy. If the current channel quality is equal to the threshold level, then a fraction $\frac{1}{t}$ of the remaining bits are transmitted. If the channel quality is better/worse than the threshold, then additional/fewer bits are transmitted. The scheduler acts very opportunistically when the deadline is far away (t large) but less so as the deadline approaches.

- When the number of bits B is small, a one-shot threshold policy where all B bits are transmitted in the first slot in which the channel quality is above a specified threshold is optimal.

- When the number of bits B and the time horizon T are both large, a waterfilling-like policy is optimal.

In Chapter 3, we consider extensions of the energy-efficient scheduling in Chapter 2, such as incorporation of outage and scheduling for multi-user systems. Additionally, we deal with an efficient bandwidth scheduling problem in which the transmission energy is fixed (without loss of generality, $E = 1$), and thus the cost is given by

$$C(b;g)(=W) = \frac{b}{\log(1+g)}. \tag{1.12}$$

This will be useful in channel allocation for OFDM environments. Without a peak bandwidth constraint, a one-shot policy is optimal since the problem is a linear program. When there is a peak bandwidth constraint for each slot, the problem becomes identical to the setting in [FMT06]. This setting is more relevant to frequency-flat fading environment where the channel gain state with respect to frequency is constant. As an alternative, we also consider scheduling for parallel/MIMO channels for minimizing the total transmission energy.

In Chapter 4, we investigate the scheduling problem with monomial cost functions rather than the Shannon function:

$$C(b;g) = a\frac{b^n}{g}, \tag{1.13}$$

where a is a constant and n is a monomial order. We obtain the optimal scheduler in closed form. The optimal scheduler determines the ratio of the number of bits (b_t) to be allocated in the current slot t (t denotes the number of remaining slots to the deadline) to the deferred bits ($\beta_t - b_t$) such that

$$b_t : (\beta_t - b_t) = (g_t)^{\frac{1}{n-1}} : \eta_{n,t}, \tag{1.14}$$

where $\eta_{n,t}$ denotes a statistical quantity determined by the channel distribution and the number of remaining slots t. From the properties of $\eta_{n,t}$, we can observe that the scheduler behaves very opportunistically when the deadline is far away (t large) but less so as the deadline approaches, since $\eta_{n,t}$ is an increasing function of t.

In Chapter 5, we slightly change the focus to resource allocation for multi-user broadcast channels. First, we compare the achievable throughput with the optimal strategy to that achievable with linear precoding. One of the interesting results is that the weighted sum rate is maximized at asymptotically high SNR by allocating power directly proportional to user weights. This result appears to generalize the well-known property that equal power allocation asymptotically maximizes sum rate in a number of different single-user and multi-user settings. In a multi-user setting, fairness can be an alternative view of delay requirements. Thus, secondly, we study the

symmetric capacity of MIMO broadcast channels, which is the maximum achievable symmetric rate of all the users.

In Chapter 6, we conclude the dissertation and discuss directions for future research.

Chapter 2

Delay Constrained Scheduling for the Shannon Cost Function

In this chapter we consider the problem of transmitting a packet of B bits over T time slots, where the channel fades independently from slot to slot and the transmitter has perfect *causal* channel information (i.e., knowledge of the current channel, but not of the future channel). During each slot, the transmitter (or scheduler hereafter) determines how many bits to transmit based on the current channel quality and the number of bits yet to be served. The scheduler must balance the desire to be opportunistic, i.e., wait to serve many of the bits when the channel is in a good state, with the hard deadline. We investigate the setting where there is a single packet to be transmitted (i.e., no other packets are scheduled during the T slot delay horizon), the packet must be transmitted by the deadline, and transmission occurs at capacity of the underlying Gaussian noise channel where the relation between the required energy E to transmit b bits are governed by the Shannon function:

$$b = \log(1 + gE), \tag{2.1}$$

where g denotes a channel state. In this framework our objective is to design a scheduling policy that minimize the expected energy consumed.

This setup reasonably models delay-constrained applications such as VoIP, where packets arrive regularly and each must be received within a short delay window. In such a setting perhaps the most important design objective is to minimize the resources (in our case, energy) needed to meet the delay requirements. In the cellular uplink, for example, an energy-minimizing policy

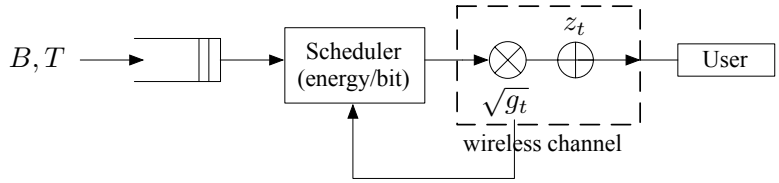

Figure 2.1: Single-user delay constrained scheduling

would extend the battery life of mobile terminals. Some of the work in this chapter is published in [LJ08, LJ09a, LJ09b, LJ09d].

2.1 Problem Formulation

We consider a single-user delay constrained scheduling problem as illustrated in Fig. 2.1: a packet of B bits[1] must be transmitted within T time slots through a fading channel, in which T is referred to as the *delay-limit* or *deadline*. We assume no other packet is scheduled during the T time slots, and that the packet must be transmitted by the deadline (i.e., no outage is allowed). Although these two assumptions may not be entirely realistic, even for relatively deterministic traffic (e.g., in VoIP, the next packet generally arrives before the deadline of the previous has expired; furthermore, a small percentage of packets are allowed to miss their deadlines), these assumptions allow for a relatively tractable problem and allow us to focus on the central issue of meeting deadlines based upon causal channel information. The purpose of the scheduler is to determine the energy, or equivalently the number of bits, to be served during each time slot such that the expected energy is minimized and the bits are served by the deadline T.

The discrete-time slots are indexed by t in descending order, i.e., $t = T$ is the initial slot, $t = T-1$ is the 2nd slot, ..., and $t = 1$ is the final slot before the deadline; in doing so, t represents the number of remaining slots. The channel state (at slot t), in power units, is denoted by g_t. We assume that the channel states $\{g_t\}_{t=1}^{T}$ are independently and identically distributed (i.i.d.) and the probability density function (PDF) and the cumulative distribution function (CDF) are denoted by f and F, respectively.[2] The scheduler is assumed to have only *causal* knowledge

[1] We operate in "nats" instead of "bits" since we adopt log-base e expression in the capacity formula to avoid constant factors in the analysis. We use "bits" and "bit allocation" as generic terms.

[2] The fading distribution must have a non-zero delay-limited capacity, i.e., $\mathbb{E}[1/g] < \infty$, for this problem to be feasible.

of channel states (i.e., at time t, $g_T, g_{T-1} \cdots, g_t$ are known but $g_{t-1}, \cdots, g_1$ are unknown). In this context, we refer to this type of scheduler as a *causal scheduler*.

Assuming unit variance Gaussian additive noise and transmission at capacity, the number of transmitted bits, denoted as b_t, if E_t energy is used is given as in (2.1). By solving for E_t we arrive at a formula for the energy cost in terms of the channel state g_t, and the number of bits[3] served b_t:

$$E_t(b_t, g_t) = \frac{e^{b_t} - 1}{g_t}. \tag{2.2}$$

The queue state is denoted by β_t, which is the number of unserved bits at the beginning of slot t. Then, β_t can be calculated recursively as $\beta_t = \beta_{t+1} - b_{t+1}$. Given this setup, a scheduler is a sequence of functions $\{b_t\}_{t=1}^T$ that maps from the current queue and the current channel state[4] to the bit allocation: $\{b_T(\beta_T, g_T), b_{T-1}(\beta_{T-1}, g_{T-1}), \cdots, b_1(\beta_1, g_1)\}$, and each $b_t : \mathbb{R}_+ \times \mathbb{R}_{++} \to [0, \beta_t]$. As for terminology, the entire set $\{b_T(\cdot,\cdot), b_{T-1}(\cdot,\cdot), \cdots, b_1(\cdot,\cdot)\}$ is referred to as a *policy* or a *scheduler*, and each element of it is referred to as a *policy function* or a *scheduling function*. Notice that the definition of b_t for given t remains the same irrespective of T.

2.2 Optimal Scheduler

The optimal energy-efficient scheduler is the set of scheduling functions $\{b_t^{\text{opt}}(\cdot,\cdot)\}_{t=1}^T$ that minimizes the total expected energy cost (summed over the T slots): i.e.,

$$\min_{b_T, \cdots, b_1} \mathbb{E}\left[\sum_{t=1}^{T} E_t(b_t, g_t)\right] \tag{2.3}$$

subject to $\sum_{t=1}^T b_t = B$ and $b_t \geq 0$ for all t.

The optimization in (2.3) can be formulated sequentially (via dynamic programming) with the remaining bits β_t as a state variable that summarizes the bit allocation up until the previous

[3] An implicit assumption is that each slot spans n channel symbols, for n reasonably large, and that powerful coding allows for transmission of nb_t bits in the t-th slot. Thus, the quantity b_t should be thought of as the number of bits transmitted per channel symbol during the t-th scheduling slot; it therefore need not be restricted to integer values.

[4] Because the channel states are assumed to be i.i.d., it is sufficient to make scheduling decisions based only on the current channel (while ignoring past channels). If channels are correlated across time slots, then the past and present channel should be used to compute the conditional distributed of future channel states and all expected future energy costs should be computed with respect to these conditional distributions.

Table 2.1: Definitions of variables

Variable	Description
T	hard delay deadline; time horizon span
B	total number of bits to transmit within T slots
t	discrete-time index in descending order; $t = T$ (initial), $t = T-1, \cdots, t = 1$ (final)
g_t	channel state at time slot t (measured in power unit)
g	generic channel state assuming $\{g_t\}$ are iid
z_t	additive white Gaussian noise with zero-mean and unit variance
f	probability density function of g
F	cumulative distribution function of g
b_t	number of bits to transmit at time slot t
β_t	unserved bits at the beginning of scheduling at time slot t
E_t	incurred energy at time slot t
J_t	sum of total energy expenditure up to time slot t, i.e., $J_t = \sum_{s=1}^{t} E_t$
$\mathbb{R}_+$	set of non-negative real numbers
$\mathbb{R}_{++}$	set of positive real numbers

time step.

$$b_t^{\text{opt}}(\beta_t, g_t) = \begin{cases} \arg\min\limits_{0 \le b_t \le \beta_t} \left\{ E_t(b_t, g_t) + \mathbb{E}\left[\sum\limits_{s=1}^{t-1} E_s(b_s, g_s) \middle| b_t \right] \right\}, & t = T, \ldots, 2, \\ \beta_1, & t = 1. \end{cases} \tag{2.4}$$

This is the standard backward iteration: we first determine the optimal action at $t = 1$, then find the optimal policy at $t = 2$ by taking into account the optimal policy to be used at $t = 1$, and so forth. Since g_t is known but future channel states $g_{t-1}, \ldots, g_1$ are unknown, the quantity E_t is not random but the future energy costs $E_{t-1}, \ldots, E_1$ are random. Note also that the optimization (2.4) should be performed for all possible values of β_t and g_t. In other words, deriving the optimal scheduling function b_t^{opt} is equivalent to finding the optimal decision rule for all possible pairs (β_t, g_t).

Notice that (2.4) can be equivalently formulated as a finite-horizon dynamic program (DP):

$$J_t^{\text{opt}}(\beta_t, g_t) = \begin{cases} \min\limits_{0 \le b_t \le \beta_t} \left(\frac{e^{b_t} - 1}{g_t} + \bar{J}_{t-1}^{\text{opt}}(\beta_t - b_t) \right), & t \ge 2 \\ \frac{e^{\beta_1} - 1}{g_1}, & t = 1, \end{cases} \tag{2.5}$$

where

$$\bar{J}_{t-1}^{\text{opt}}(\beta) = \mathbb{E}_g[J_{t-1}^{\text{opt}}(\beta, g)] \tag{2.6}$$

is the cost-to-go function, i.e., the expected cost to serve β bits in $t-1$ slots if the optimal policy is used.

Unfortunately, an analytic expression is obtained only when $T = 2$ (besides the $T = 1$ trivial case). For $T > 2$, we discuss the difficulty in obtaining an analytic expression. When the scheduler has non-causal knowledge of the future channel states, however, deriving an optimal scheduler is possible; the optimal non-causal scheduler provides useful intuition and is derived in Section 2.7.1. In the present section, however, we assume causal channel state information at the scheduler.

2.2.1 Optimal Scheduler for $T = 1$

The scheduler is required to transmit all B bits regardless of the channel state g_1, due to the hard delay constraint. Thus, the energy cost is given by

$$E_1(B, g_1) = \frac{e^B - 1}{g_1} \tag{2.7}$$

or all g_1, and the expected cost to serve B bits is

$$\bar{J}_1^{\text{opt}}(B) = \mathbb{E}_{g_1}\left[E_1(B,g_1)\right] = \mathbb{E}\left[\frac{1}{g}\right](e^B - 1), \tag{2.8}$$

where the general definition of $\bar{J}_1^{\text{opt}}$ is in (2.6).

2.2.2 Optimal Scheduler for $T = 2$

In the final time slot ($t = 1$), the scheduling function b_1 is identical with the $T = 1$ scheduler since we denote t in descending order. Thus, the expected cost to serve β_1 bis is given by

$$\bar{J}_1^{\text{opt}}(\beta_1) = \mathbb{E}\left[\frac{1}{g}\right](e^{\beta_1} - 1). \tag{2.9}$$

At $t = 2$, g_2 is known but g_1 is unknown. The scheduler needs to determine b_2, based on g_2 and B, while balancing the current energy cost (of serving b_2 bits in the current slot) and the *expected* future cost (of deferring $B - b_2$ bits to the last slot). Thus, from (2.5) the optimum scheduler is the solution to the following minimization:

$$\begin{aligned} b_2^{\text{opt}}(B,g_2) &= \arg\min_{0\le b_2\le B}\left(\underbrace{\frac{e^{b_2}-1}{g_2}}_{\text{current energy cost}} + \underbrace{\bar{J}_1^{\text{opt}}(B-b_2)}_{\text{expected future cost}}\right) \\ &= \arg\min_{0\le b_2\le B}\left(\frac{1}{g_2}\left(e^{b_2}-1\right) + \mathbb{E}\left[\frac{1}{g_1}\right]\left(e^{B-b_2}-1\right)\right). \end{aligned} \tag{2.10}$$

The objective function in (2.10) is convex, and therefore the minimizer is found by setting the derivative to zero while taking into account the constraints on b_2. Some simple manipulation yields the following:

$$b_2^{\text{opt}}(B,g_2) = \left\langle \frac{1}{2}B + \frac{1}{2}\log\left(g_2\nu_1\right)\right\rangle_0^B, \tag{2.11}$$

where $\langle\cdot\rangle_0^B$ denotes truncation below 0 and above B, and $\nu_1 \triangleq \mathbb{E}[1/g]$ is a constant that depends only on the distribution of the channel state g (see Section 2.7.2 for the definition of constants ν_m for $m = 1,2,\ldots$). Note that this policy[5] depends only on the number of unserved bits and the current channel state.

[5] This policy is only meaningful when ν_1 is finite; this rules out Rayleigh fading, in which case g is exponentially distributed and thus $\mathbb{E}[1/g]$ is not finite.

Notice that the optimal scheduling function (2.11) has two additive terms: (a) $\frac{1}{2}B$ corresponds to an equal distribution to time slots $t=1$ and $t=2$, and (b) $\frac{1}{2}\log(g_2\nu_1)$ associated with a measure of the channel quality at $t=2$. That is, if the channel quality g_2 is bigger than the threshold $1/\nu_1$, then more than $\frac{1}{2}B$ bits are allocated; if g_t is smaller than the threshold then fewer bits are allocated and more bits are deferred to the final slot.

2.2.3 Optimal Scheduler for $T > 2$

The DP in (2.5) is a one-dimensional convex optimization (pp. 87-88 in [BV04]) over b_t and the optimal solution satisfies (2.12)

$$b_t^{\text{opt}}(\beta_t, g_t) = \begin{cases} 0, & g_t \le \frac{1}{(\bar{J}_{t-1}^{\text{opt}})'(\beta_t)}, \\ \arg_b \left\{ \frac{e^b}{g_t} = (\bar{J}_{t-1}^{\text{opt}})'(\beta_t - b) \right\}, & \frac{1}{(\bar{J}_{t-1}^{\text{opt}})'(\beta_t)} < g_t < \frac{e^{\beta_t}}{(\bar{J}_{t-1}^{\text{opt}})'(0)}, \\ \beta_t, & g_t \ge \frac{e^{\beta_t}}{(\bar{J}_{t-1}^{\text{opt}})'(0)}, \end{cases} \tag{2.12}$$

where $\arg_b\{\cdot\}$ represents the solution[6] of the argument equation. The differentiability of $\bar{J}_{t-1}^{\text{opt}}$ can be verified by the properties of convexity and infimal convolution (pp. 254-255 in [Roc70]).

When $t=2$, the cost-to-go function $\bar{J}_1^{\text{opt}}(\beta_1) = (e^{\beta_1}-1)\nu_1$ (as well as its derivative) takes on a very simple form and thus (2.12) can be solved in closed form as in (2.11). However, the same is not true for $t>2$. Because the optimal policy for $t=2$ is known, the cost-go-to $\bar{J}_2^{\text{opt}}(\beta_2)$ can be written in closed form. The derivative $(\bar{J}_2^{\text{opt}})'(\beta_2)$ can also be written in closed form but cannot be analytically inverted; thus, the optimal policy for $t=3$ can only be written in the form of (2.12) with the second condition given by the following fixed point equation:

$$\frac{e^{b_3}}{g_3} = e^{\beta_3 - b_3} \int_0^{\frac{e^{-(\beta_3-b_3)}}{\nu_1}} \nu_1 dF(x) + e^{\frac{\beta_3-b_3}{2}} \nu_1^{\frac{1}{2}} \int_{\frac{e^{-(\beta_3-b_3)}}{\nu_1}}^{\frac{e^{\beta_3-b_3}}{\nu_1}} \left(\frac{1}{x}\right)^{\frac{1}{2}} dF(x) + e^{\beta_3-b_3} \int_{\frac{e^{\beta_3-b_3}}{\nu_1}}^{\infty} \frac{1}{x} dF(x), \tag{2.13}$$

where F is the cumulative distribution function of the channel state g. As a result, no analytical characterization of $\bar{J}_3^{\text{opt}}(\beta_3)$ is possible, and thus neither $b_t^{\text{opt}}(\cdot,\cdot)$ nor $\bar{J}_t^{\text{opt}}(\beta_t)$ can be found in closed form for $t \ge 4$.

Alternately, we can numerically find the optimal scheduler by the discretization method [Ber75]. However, large complexity and memory is required for sufficiently fine discretization.

[6] Because of the convexity, the solution exists uniquely if it exists.

More importantly, this numerical method gives little insight on how the delay constraint and channel state affect the scheduling function.

Although we are not able to obtain an analytical description of the optimal scheduler when $T > 2$, we examine the behavior from (2.12) in each of the three operating regions as follows. On the one hand, we consider the case when g_t is fixed and β_t is increasing from 0. Depending on the given fixed value of g_t as opposed to $\frac{1}{(\bar{J}_{t-1}^{\text{opt}})'(0)}$, the optimum is determined at either the boundary case, i.e., $b_t^{\text{opt}} = 0$ or $b_t^{\text{opt}} = \beta_t$ when β_t is near 0, which is non-decreasing in β_t. As β_t increases, $\frac{1}{(\bar{J}_{t-1}^{\text{opt}})'(\beta_t)}$ gets smaller and $\frac{e^{\beta_t}}{(\bar{J}_{t-1}^{\text{opt}})'(0)}$ gets larger and thus $g_t \in \left(\frac{1}{(\bar{J}_{t-1}^{\text{opt}})'(\beta_t)}, \frac{e^{\beta_t}}{(\bar{J}_{t-1}^{\text{opt}})'(0)} \right)$, in which b_t^{opt} is determined to satisfy $\frac{e^{b_t^{\text{opt}}}}{g_t} = (\bar{J}_{t-1}^{\text{opt}})'(\beta_t - b_t^{\text{opt}})$. Because of the monotonicity of the exponential function and $(\bar{J}_{t-1}^{\text{opt}})'$, b_t^{opt} is also non-decreasing in β_t. On the other hand, we consider the case when β_t is fixed and g_t is increasing. When g_t is smaller than $\frac{1}{(\bar{J}_{t-1}^{\text{opt}})'(\beta_t)}$, then it starts with $b_t^{\text{opt}} = 0$, which is constant and thus non-decreasing. As g_t gets bigger than $\frac{1}{(\bar{J}_{t-1}^{\text{opt}})'(\beta_t)}$, b_t^{opt} is determined to satisfy $\frac{e^{b_t^{\text{opt}}}}{g_t} = (\bar{J}_{t-1}^{\text{opt}})'(\beta_t - b_t^{\text{opt}})$. By the same token as the previous case, b_t^{opt} is non-decreasing in β_t because of the monotonicity of the exponential function and $(\bar{J}_{t-1}^{\text{opt}})'$. As g_t is bigger than $\frac{e^{\beta_t}}{(\bar{J}_{t-1}^{\text{opt}})'(0)}$, $b_t^{\text{opt}} = \beta_t$ and thus constant in g_t. More precise arguments are given in the following.

Proposition 2.1. *The optimal policy function $b_t^{opt}(\beta_t, g_t)$ has the following monotonicity properties:*

(a) For any fixed value $g_t(>0)$, b_t^{opt} and $(\beta_t - b_t^{opt})$ are non-decreasing in β_t. Furthermore, there exists $\mathfrak{B}_0$ such that b_t^{opt} and $(\beta_t - b_t^{opt})$ are strictly increasing in β_t for all $\beta_t > \mathfrak{B}_0$.

(b) For any fixed value $\beta_t(>0)$, b_t^{opt} is non-decreasing in g_t.

Proof. See Section 2.7.3. □

Intuitively, monotonicity in the queue β_t and the channel state g_t is expected because more bits should be served when there remain more unserved bits or when the channel is strong.

2.3 Suboptimal Schedulers

Because the optimal scheduler cannot be written in closed form, it is of interest to develop suboptimal schedulers. Before introducing suboptimal schedulers, we briefly mention the

baseline strategy of equal-bit scheduling. The first scheduler is based on the intuition from the optimal $T = 2$ policy, and the second is found by solving a relaxed version of the optimization. The one-shot threshold scheduler is derived by forming an optimal stopping problem, i.e., determine causally to transmit the entire packet at one time slot. Finally, the delay-constrained ergodic scheduler is developed by modifying the ergodic waterfilling algorithm to meet the hard deadline constraint.

2.3.1 Equal-Bit Scheduler

First off, we consider one of the simplest causal schedulers: equal-bit scheduler. This policy allocates B/T bits in each time slot, regardless of channel conditions, i.e.,

$$b_t^{\mathrm{eq}}(\beta, g_t) = \frac{B}{T} = \frac{1}{t}\beta_t. \tag{2.14}$$

The corresponding expected energy is given by

$$\bar{J}_t^{\mathrm{eq}}(\beta) = t(e^{\frac{\beta}{t}} - 1)\,\mathbb{E}\left[\frac{1}{g}\right] = t(e^{\frac{\beta}{t}} - 1)\nu_1. \tag{2.15}$$

This channel-blind strategy will serve as a baseline for comparison with channel-aware policies.

2.3.2 Expectation Substitution Scheduler

If we compare the optimal causal scheduler for $T = 2$ (Section 2.2.2) to the optimal non-causal scheduler (see Section 2.7.1), we can immediately notice that the optimal scheduler determines b_2^{opt} by inverse-waterfilling over channels g_2 and $1/\nu_1$, whereas the non-causal scheduler inverse waterfills over g_2 and the actual value of g_1[7] . This is because of the particularly simple form of the expected future cost. Although the expected future cost does not take on such a simple form for $T > 2$, we can get a suboptimal scheduler by simply applying this inverse-waterfilling at every time slot t. This is a technique of certainty equivalence control that substitutes uncertain state information with nominal values [BST74, Ber05]. In other words, at time step t, perform inverse-waterfilling over the following t channels:

$$g_t, \underbrace{\frac{1}{\nu_1}, \ldots, \frac{1}{\nu_1}}_{t-1}$$

[7] When both g_2 and g_1 are known at $t = 2$, the optimal non-causal scheduling policy is given by $b_2^{\mathrm{IWF}}(B, g_2) = \left\langle \frac{1}{2}B + \frac{1}{2}\log\left(\frac{g_2}{g_1}\right)\right\rangle_0^B$ from (2.65), in which "IWF" stands for *inverse waterfilling* (see Section 2.7.1 for detail).

to determine how many of the unserved β_t bits to serve now. We refer to this bit allocation policy as *expectation substitution policy* and denote it as $b_t^{\text{expectation}}$. Since $t-1$ of the t channels are equal, the inverse-waterfilling operation is very simple and the policy is given by

$$b_t^{\text{expectation}}(\beta_t, g_t) = \left\langle \frac{1}{t}\beta_t + \frac{t-1}{t}\log\left(\frac{g_t}{\eta_t^{\text{expectation}}}\right)\right\rangle_0^{\beta_t}, \tag{2.16}$$

where $\eta_t^{\text{expectation}} = 1/\nu_1$ serves as the channel threshold. Notice that this threshold value depends only on the channel statistics and is constant with respect to t.

When the deadline is far away (large t), the first term in (2.16) is negligible and the bit allocation is almost completely dependent on the instantaneous channel quality. As the deadline approaches (t decreases toward 1), the weight of the channel-dependent second term decreases and the weight of the delay-associated first term increases.

2.3.3 Boundary-Relaxed Scheduler

The inability to find a general analytic solution to the original optimization (2.5) is due to complications caused by the constraint $0 \le b_t \le \beta_t$ (for each t) in the dynamic optimization. However, if we relax this constraint, i.e., allow $b_t < 0$ and $b_t > \beta_t$ while maintaining the constraint $\sum_{t=1}^{T} b_t = B$, we can derive a policy in closed form.

We define the cost-to-go function for the relaxed problem as $\bar{U}_t(\beta_t)$. As we show below, the cost-to-go can be written in closed form for general t:

$$\bar{U}_t(\beta_t) = te^{\frac{\beta_t}{t}}\,\mathbb{G}(\nu_t, \nu_{t-1}, \ldots, \nu_1) - t\nu_1 \tag{2.17}$$

where $\nu_1, \nu_2, \cdots$ are the fractional moments defined in Section 2.7.2 and $\mathbb{G}$ denotes the geometric mean operator (i.e., $\mathbb{G}(x_1, \cdots, x_n) = (\prod_{k=1}^{n} x_k)^{1/n}$).

When $t = 1$, (2.17) holds trivially. If we assume (2.17) holds for $t-1$, then the relaxed optimization for the next time step is given by

$$U_t(\beta_t, g_t) = \min_{b_t}\left(\frac{e^{b_t}-1}{g_t} + \bar{U}_{t-1}(\beta_t - b_t)\right) \tag{2.18}$$

and the solution (i.e., the optimum for the relaxed problem) is found by setting the derivative of the objective to zero due to the simple form of the cost-to-go function $\bar{U}_{t-1}$:

$$b_t = \frac{1}{t}\beta_t + \frac{t-1}{t}\log\left(g_t\,\mathbb{G}(\nu_{t-1}, \ldots, \nu_1)\right). \tag{2.19}$$

By plugging in the optimum value of b_t in (2.19) into (2.18) and taking expectation with respect to g_t, we reach (2.17). This completes the proof that the expression in (2.17) is the cost-to-go function for the relaxed problem.

To obtain a policy for the actual unrelaxed problem, we simply truncate the policy function in (2.19) at 0 and β_t, to obtain what we refer to as the *boundary-relaxed scheduler*:

$$b_t^{\text{relax}} = \left\langle \frac{1}{t}\beta_t + \frac{t-1}{t}\log\left(\frac{g_t}{\eta_t^{\text{relax}}}\right)\right\rangle_0^{\beta_t}, \tag{2.20}$$

where

$$\eta_t^{\text{relax}} = \frac{1}{\mathbb{G}\left(\nu_{t-1}, \nu_{t-2}, \cdots, \nu_1\right)}. \tag{2.21}$$

Note that these thresholds depend only on the statistics, and not the realizations. Note also that this policy is optimal for $t = 2$, i.e., $b_2^{\text{relax}} = b_2^{\text{opt}}$ for all β_2 and g_2 since $(\bar{U}_1)' = (\bar{J}_1^{\text{opt}})'$.

This same scheduling policy can be reached using the high-SNR approximation $\log(1+x) \approx \log(x)$. More specifically, if the energy-bit relationship in (2.2) is approximated by:

$$E_t(b_t, g_t) = \frac{e^{b_t} - 1}{g_t} \approx \frac{e^{b_t}}{g_t}. \tag{2.22}$$

and the optimal policy is found with the same relaxation as above, the policy in (2.19) is also reached.

From (2.16) and (2.20), we can see that the expectation substitution scheduler and the boundary-relaxed scheduler have a very similar form with the only difference term being the threshold η_t. Based on the policy formulations, we investigate the common and differing characteristics of the two suboptimal schedulers.

The two schedulers can be cast into a single framework:

$$b_t(\beta_t, g_t) = \left\langle \frac{1}{t}\beta_t + \frac{t-1}{t}\log\left(\frac{g_t}{\eta_t}\right)\right\rangle_0^{\beta_t}, \tag{2.23}$$

where η_t is the channel threshold, as determined by the individual algorithms. This simple allocation strategy reveals how the delay constraint affects the scheduling algorithms: at time step t serve a fraction $1/t$ of the remaining bits plus/minus a quantity that depends on the strength of the current channel compared to a channel threshold. If the current channel is good (i.e., g_t is bigger than the threshold η_t), additional bits are served (up to β_t), while fewer bits are served when the current channel is poorer than the threshold. Furthermore, note that when t is large (i.e., far from the deadline), the first term β_t/t is very small and the number of bits served is

almost completely determined by the current channel conditions. This agrees with intuition that we should make aggressive, almost completely channel dependent (and deadline independent) decisions when the deadline is far away, while we should make more conservative (more deadline dependent, less channel dependent) decisions near the deadline (small t).

Using $\log_2 10 \approx 3$ we can rewrite the policy in dB units as:

$$b_t(\beta_t, g_t) \approx \left\langle \frac{1}{t}\beta_t + \left(\frac{t-1}{t}\right)\left(\frac{g_t^{\mathrm{dB}} - \eta_t^{\mathrm{dB}}}{3}\right)\right\rangle_0^{\beta_t}. \tag{2.24}$$

For large t, approximately one bit[8] is allocated for every 3 dB by which the channel exceeds the threshold.

The difference between the two policies is in the threshold values, which are illustrated in Fig. 2.2 for a particular channel distribution. The expectation substitution scheduler has a constant threshold $\eta_t^{\text{expectation}} = 1/\nu_1$ for all t, whereas the boundary-relaxed scheduler has a threshold that increases with t (by Proposition 2.8 in Section 2.7.2). It is intuitive to use a larger threshold when the deadline is far away (large t), as the scheduler can be more selective because many different channels remain to be seen before the deadline is reached.

By using a constant threshold, the expectation substitution scheduler is not selective enough and transmits too many bits when the deadline is far away. To see this, consider the average number of bits transmitted in slot t (ignoring truncation):

$$\begin{aligned} \mathbb{E}_{g_t}[b_t(\beta_t, g_t)] &= \mathbb{E}_{g_t}\left[\frac{1}{t}\beta_t + \frac{t-1}{t}\log\left(\frac{g_t}{\eta_t}\right)\right] \\ &= \frac{1}{t}\beta_t + \frac{t-1}{t}\,\mathbb{E}\left[\log\left(\frac{g_t}{\eta_t}\right)\right]. \end{aligned} \tag{2.25}$$

Because $\eta_t^{\text{expectation}} = 1/\nu_1$,

$$\begin{aligned} \mathbb{E}\left[\log\left(\frac{g_t}{\eta_t^{\text{expectation}}}\right)\right] &= \mathbb{E}[\log g] + \log \nu_1 \\ &= -\,\mathbb{E}\left[\log\left(\frac{1}{g}\right)\right] + \log \nu_1 \\ &\overset{(a)}{=} -\log \nu_\infty + \log \nu_1 \\ &\overset{(b)}{>} 0 \end{aligned} \tag{2.26}$$

[8] The "bit" in this case represents the real bit not nat.

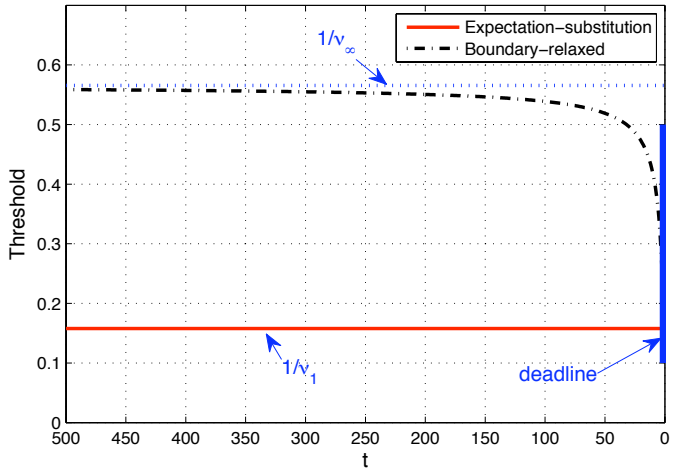

Figure 2.2: Thresholds $\eta_t^{\text{expectation}}$ for the expectation substitution scheduler and η_t^{relax} for the boundary-relaxed scheduler when the distribution of the channel state is the truncated exponential with $\gamma_0 = 0.001$

where both (a) and (b) follow from Proposition 2.8a in Section 2.7.2. Thus, the expectation substitution scheduler transmits more than $\frac{B}{T}$ bits on average when scheduling begins, which is in some sense overly aggressive. On the other hand, the quantity $\mathbb{E}_{g_t}\left[\log\left(g_t/\eta_t^{\text{relax}}\right)\right]$ decreases as t increases and the limit is given by (see Proposition 2.8b in Section 2.7.2)

$$\lim_{t\to\infty} \mathbb{E}_{g_t}\left[\log\left(\frac{g_t}{\eta_t^{\text{relax}}}\right)\right] = 0. \tag{2.27}$$

This implies that the boundary-relaxed scheduler allocates B/T bits on the average when the deadline is far away and thus, unlike the expectation substitution scheduler, is not overly aggressive. Numerical results given later support the fact that the boundary-relaxed scheduler generally performs better than the expectation substitution scheduler.

If the expectation substitution, the boundary-relaxed, and the equal-bit schedulers are compared to the optimal non-causal policy (inverse waterfilling), one can see that each of the algorithms mimics inverse waterfilling using either the current channel or channel statistics for the future channels, as summarized in Table 2.2.

If we investigate the behavior of the boundary-relaxed scheduler for the overall T slots when B is large, it is clear that the average rate of the bounary-relaxed scheduler is less than

Table 2.2: Waterfilling interpretation

	At each t, perform IWF over the following
Equal-bit scheduler	$g_t, \underbrace{g_t, g_t, \cdots, g_t}_{t-1}$
Expectation substitution scheduler	$g_t, \underbrace{\frac{1}{\nu_1}, \frac{1}{\nu_1}, \cdots, \frac{1}{\nu_1}}_{t-1}$
Boundary-relaxed scheduler	$g_t, \frac{1}{\nu_{t-1}}, \frac{1}{\nu_{t-2}}, \cdots, \frac{1}{\nu_1}$
Non-causal IWF	$g_t, g_{t-1}, g_{t-2}, \cdots, g_1$

(or may possibly be equal to) the delay-limited (zero-outage) capacity [Gol05] under a same power constraint. Due to the nature of the problem that the rate is fixed B/T, we compare the power consumption. Specifically, we examine the maximum achievable rate (ergodic capacity) with the power that is used for the boundary-relaxed scheduler. From (2.17), the average power consumption of the boundary-relaxed scheduler for the rate B/T is roughly (which will be shown later) $\mathbb{E}[J_T]/T = 2^{\frac{B}{T}} \left[\mathbb{G}(\nu_T, \cdots, \nu_1) - e^{-\frac{B}{T}} \nu_1 \right]$. Thus, the maximum achievable rate is given by

$$\mathbb{E}\left[\log\left(1 + \frac{\mathbb{E}[J_T]}{T} g \right) \right] = \mathbb{E}\left[\log\left(e^{\frac{B}{T}} \mathbb{G}(\nu_T, \cdots, \nu_1) g \right) + \delta \right] = \frac{B}{T} + \delta',$$

for some $\delta, \delta' > 0$. This implies that the average rate achieved by the boundary-relaxed scheduler is strictly less than the ergodic capacity; i.e., there exists strict difference of the energy consumption between the boundary-relaxed scheduler and the water-filling that achieves the ergodic capacity. This gap corresponds to the loss due to the causal knowledge of the channel gain information as opposed to the non-causal knowledge.

Behavioral Difference with Ergodic Watefilling

We have analyzed the performance of the delay-constrained scheduler over the whole scheduling horizon, which is specified the delay deadline T. From the analysis, we have observed that the optimal scheduler behaves more opportunistic in the initial time steps, which are when t is large. It is interesting to investigate the behavior of the very beginning step as compared to the average ergodic scheduler, i.e., the pure waterfilling algorithm.

Since the boundary-relaxed scheduler performs close to the optimal when the packet size B is large, we consider the very beginning of the optimal scheduler with the boundary-relaxed

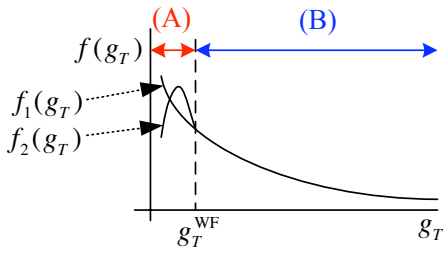

Figure 2.3: Waterfilling algorithms for the fading distributions with the two pdfs f_1 and f_2 are identical but they are different in the boundary-relaxed scheduler

scheduler which form is given by

$$\lim_{T\to\infty} E_T^{\mathrm{relax}} = \begin{cases} e^{\frac{B}{T}}\nu_\infty - \frac{1}{g_T}, & g_T \geq \frac{1}{\nu_\infty}e^{-\frac{B}{T}}, \\ 0, & g_T < \frac{1}{\nu_\infty}e^{-\frac{B}{T}}, \end{cases} \tag{2.28}$$

assuming that $\frac{B}{T} > \bar{b}$ for sufficiently large $\bar{b}$ (see Section 2.7.13 for derivation). If we compare this with (4.12) in [Gol05] that is given by

$$\frac{E_T^{\mathrm{WF}}}{E^{\mathrm{ref}}} = \begin{cases} \frac{1}{g_{\mathrm{th}}^{\mathrm{WF}}} - \frac{1}{g_T}, & g_T \geq g_{\mathrm{th}}^{\mathrm{WF}}, \\ 0, & g_T < g_{\mathrm{th}}^{\mathrm{WF}}, \end{cases} \tag{2.29}$$

where E^{ref} denotes the total energy level and $g_{\mathrm{th}}^{\mathrm{WF}}$ is determined to satisfy:

$$\int_{g_T^{\mathrm{WF}}}^{\infty} \left(\frac{1}{g_{\mathrm{th}}^{\mathrm{WF}}} - \frac{1}{g_T} \right) f(g_T) dg_T = 1. \tag{2.30}$$

As can be seen, the only difference is the threshold values, i.e., $\frac{1}{\nu_\infty}e^{-\frac{B}{T}}$ versus $g_{\mathrm{th}}^{\mathrm{WF}}$. The former depends on ν_∞ and thus is affected by the *entire support* of PDF of g_T. On the contrary, the quantity $g_{\mathrm{th}}^{\mathrm{WF}}$ is affected by the support of PDF such that $g_T > g_T^{\mathrm{WF}}$. Figure 2.3 illustrates this effect with two PDF functions. If we separate the support of PDF by g_T^{WF} and refer to the two regions as (A) and (B) as shown in the figure. The two PDFs f_1 and f_2 are identical in region (B) but different in region (A). The quantity $g_{\mathrm{th}}^{\mathrm{WF}}$ is the same when the PDF of g_T is both f_1 and f_2. But this is not the case for $\frac{1}{\nu_\infty}e^{-\frac{B}{T}}$. When the region (A) gets smaller, the boundary-relaxed scheduler perform closer to waterfilling. We can conclude that the behavioral difference between the boundary-relaxed scheduler (emulating the optimal scheduler for large B) and the waterfilling is affected by the fading distribution.

2.3.4 One-Shot Threshold Scheduler

In some settings it may be undesirable to split the packet across multiple time slots, e.g., because there is a large overhead associated with each slot used for transmission. In this scenario we may wish to find only one time slot among the T slots for the transmission of B bits; i.e., the action b_t can be either 0 or B.

We consider a policy by modifying the boundary constraint into a stronger constraint $b_t \in \{0, \beta_t\}$ (equivalently, $b_t \in \{0, B\}$), i.e., in each slot either the entire packet is transmitted or nothing is transmitted. Then, the dynamic program in this setting can be written as

$$J_t^{\text{one}}(\beta_t, g_t) = \begin{cases} \min\limits_{b_t \in \{0,\beta_t\}} \left(\frac{e^{b_t}-1}{g_t} + \bar{J}_{t-1}^{\text{one}}(\beta_t - b_t) \right), & t \geq 2, \\ \frac{e^{\beta_1}-1}{g_1}, & t = 1, \end{cases} \tag{2.31}$$

where $\bar{J}_t^{\text{one}}(\beta) = \mathbb{E}_g[J_t^{\text{one}}(\beta, g)]$. Equivalently, we can express the above DP as an optimal stopping problem [Ber05] (this can be shown inductively with $\beta_T = B$):

$$J_t^{\text{one}}(B, g_t) = \begin{cases} \min\left\{ \frac{e^{B}-1}{g_t},\ \bar{J}_{t-1}^{\text{one}}(B) \right\}, & t \geq 2, \\ \frac{e^{B}-1}{g_1}, & t = 1. \end{cases} \tag{2.32}$$

The optimal solution to the stopping problem is a *sequential* threshold policy [Ber05]:

$$b_t = \begin{cases} B, & \text{first } t \text{ such that } g_t > 1/\omega_t, \\ 0, & \text{otherwise}, \end{cases} \tag{2.33}$$

where $1/\omega_t$ is the channel threshold in slot t, and is recursively computed as (see Section 2.7.4 for derivation):

$$\omega_t = \begin{cases} \mathbb{E}\left[\min\left(\frac{1}{g}, \omega_{t-1} \right) \right], & t = T, \cdots, 3, \\ \mathbb{E}\left[\frac{1}{g} \right], & t = 2, \\ \infty, & t = 1. \end{cases} \tag{2.34}$$

Notice that the thresholds depend only on the channel statistics and are independent of B, and that the thresholds decrease as the deadline approaches (i.e., as t decreases), which is because the expected cost-to-go increases as t decreases.

Figure 2.4 illustrates the thresholds for the truncated exponential g with $\gamma_0 = 0.001$ and the chi-squared g with 4 degrees of freedom. Figure 2.5 illustrates the energy usage (normalized by

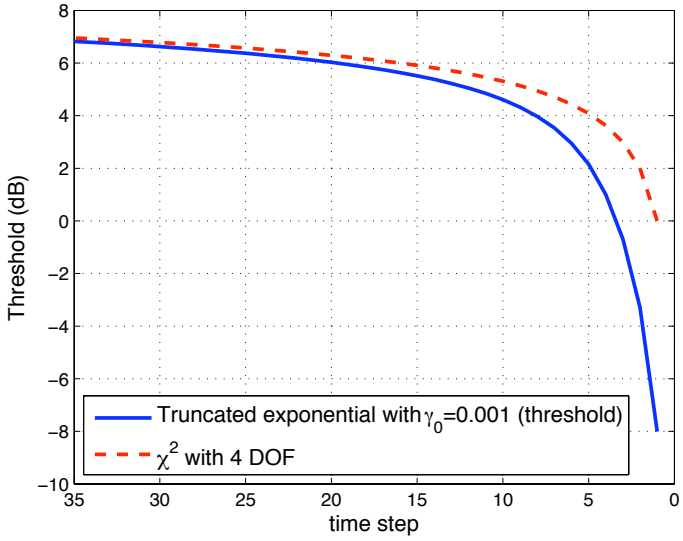

Figure 2.4: Thresholds for the one-shot threshold scheduler

T) of the optimal one-shot allocation policy and the multiple slot policies. The $B/T = 0.1$ and $B/T = 1$ curves illustrate performance for relatively small and large values of B, respectively. When B is small, the energy of the one-shot allocation is nearly the same as the optimal policy that allows for multiple slots to be used. However, this one-shot allocation is not appropriate when B is relatively large because the required energy of the one-shot policy grows exponentially with B.

2.3.5 Delay-Constrained Ergodic Scheduler

The previous suboptimal policies are developed to solve the DP, formulated in (2.5), by simplifying the cost-to-go function. Unlike these previous policies, we now consider a policy by modifying the ergodic scheduling policy to meet the hard deadline constraint. The ergodic policy is the optimal solution to a problem of minimizing the average energy to transmit a certain *average* number of bits (i.e., no hard deadline constraint). If we denote this average rate constraint as $\bar{b}$, the ergodic scheduling policy function $b(g)$, which does not depend on t and determines how many bits to transmit based only upon the channel state g, is determined by

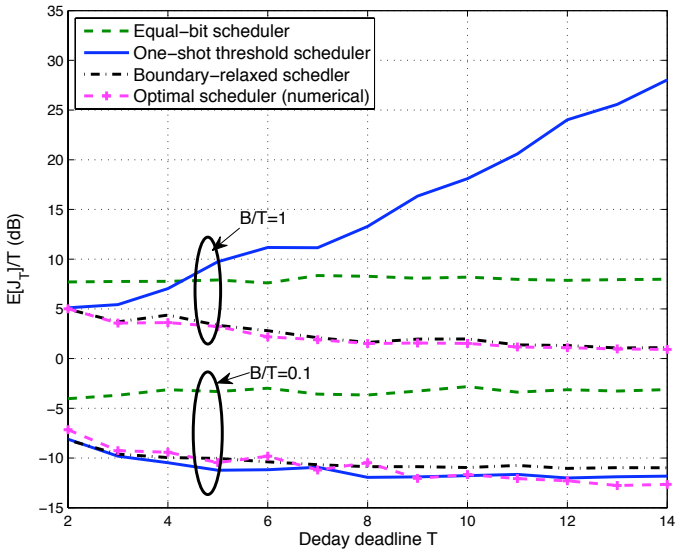

Figure 2.5: Performance of the optimal one-shot allocation compared with multi-slot allocation algorithms

solving:

$$\begin{aligned} \bar{E}^{\text{erg}}(\bar{b}) = \quad & \min_{b(g)} \quad \mathbb{E}_g\left[\frac{e^{b(g)}-1}{g}\right], \\ & \text{subject to} \quad \mathbb{E}_g[b(g)] \geq \bar{b}, \\ & \qquad\qquad b(g) \geq 0. \end{aligned} \tag{2.35}$$

This optimization is readily solvable by standard waterfilling [Gol05] and the solution is given by

$$b^{\text{erg}}(\bar{b},g) \;=\; \left\langle \log\left(\frac{g}{\eta^{\text{erg}}}\right)\right\rangle_0^{\infty} \;=\; \begin{cases} \log\left(\frac{g}{\eta^{\text{erg}}}\right), & g \geq \eta^{\text{erg}}, \\ 0, & \text{else}, \end{cases} \tag{2.36}$$

where η^{erg} serves as a channel threshold and is the solution to:

$$\mathbb{E}[b^{\text{erg}}(\bar{b},g)] = \bar{b}. \tag{2.37}$$

When the time-horizon T is large, we intuitively expect the ergodic policy to perform well in the delay-limited setting considered here. In order to meet the deadline constraint, we utilize the

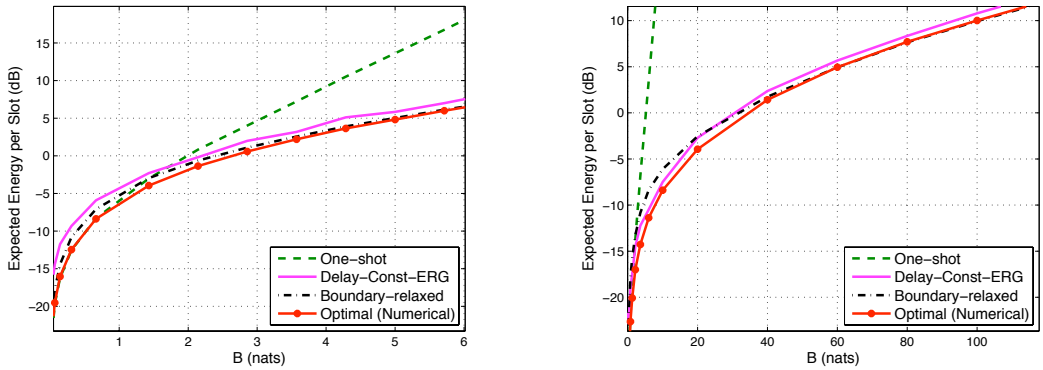

(a) $T = 5$ (b) $T = 50$

Figure 2.6: Per slot energy cost for $T = 5$ and $T = 50$

ergodic policy, with $\bar{b} = \frac{B}{T} + \delta$ for some $\delta > 0$,[9] at each time step with the exception that all remaining unserved bits are transmitted in the final step:

$$b_t^{\text{constrained-erg}}\left(\frac{B}{T}, g_t; \delta\right) = \begin{cases} b^{\text{erg}}\left(\frac{B}{T} + \delta, g_t\right), & t = T, T-1, \cdots, 2, \\ \beta_1, & t = 1, \end{cases} \tag{2.38}$$

which is referred to as the *delay-constrained ergodic scheduler*. The value of δ can be numerically obtained to minimize the energy cost.

2.3.6 Numerical Results: Policy Comparison

In order to compare the different asymptotically optimal policies, we compare their respective energy costs for different time-horizons (T). Since the analytical expression for the optimal policy is not available for $T > 2$, we solve the dynamic programming (2.5) numerically by the discretization method [Ber75]. In Fig. 2.6 the per-slot energy consumption of the suboptimal schedulers is plotted for $T = 5$ and $T = 50$ assuming that the fading $\{g_t\}_{t=1}^{T}$ are i.i.d. truncated exponential with a support of $[0.001, 10^6]$, i.e.,

$$f(g) = \begin{cases} ce^{-(g-0.001)}, & \text{if } 0.001 \le g \le 10^6, \\ 0, & \text{otherwise}, \end{cases} \tag{2.39}$$

[9] This policy is motivated by Theorem 3 of [CTV04], where a modified version of the ergodic rate-maximizing policy is shown to maximize the expected transmitted rate over a finite time-horizon when the transmitter is subject to a finite energy constraint (which is the dual of the problem considered here).

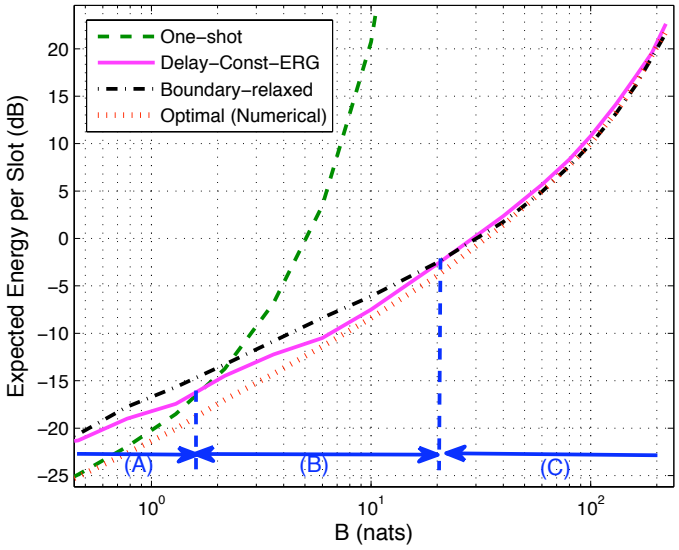

Figure 2.7: Average energy cost per slot for $T = 50$ when g is a truncated exponential variable with support $[0.001, 10^6]$

where c is a normalization factor. As can be seen, the one-shot scheduler is near-optimal only when B is small. The other schedulers performs close to the optimal through all ranges of B. When $T = 5$, as in Fig. 2.6a, the delay-constrained ergodic scheduler performs worse than the boundary-relaxed for all B. This is because $T = 5$ is too small for the delay-constrained ergodic scheduler to perform like the optimal. When $T = 50$, as in Fig. 2.6b, there exists a range of B such that the delay-constrained ergodic scheduler outperforms the boundary-relaxed scheduler. This phenomenon can be clearly illustrated in Fig. 2.7, where the number of bits are given in logarithmic scale. As can be seen in Fig. 2.7, the one-shot scheduler performs best for small B (region A) and the boundary-relaxed scheduler outperforms when B is very large (region C). In the middle range (region B), the delay-constrained ergodic scheduler performs better than the other two.

2.4 Asymptotic Optimality

Motivated by the numerical results in the previous section, we investigate the asymptotic optimality of the suboptimal schedulers. The optimality can be analyzed in two ways: optimality in

policy and optimality in the associated energy cost. Both forms of optimality are shown for the boundary-relaxed scheduler and the one-shot scheduler, whereas energy optimality is shown for the delay-constrained ergodic scheduler.

2.4.1 Large B and Finite T: Asymptotic Optimality of Boundary-Relaxed Scheduler

We first prove that the boundary-relaxed scheduler converges to the optimal policy when T is fixed and the number of bits B is taken to infinity. When B is large, we intuitively expect that the optimal policy will allocate strictly positive bits to all T time slots with high probability due to the nature of the Shannon energy-bit function. Thus, we expect the boundary-relaxed scheduler to coincide with the optimal policy when the number of bits to serve is large. The following theorem makes this relationship precise:

Theorem 2.2. *Let the PDF f of g_t be continuous on $[g_{\min}, g_{\max}]$ with Support$(f) = [g_{\min}, g_{\max}]$, where $g_{\min} > 0$ and $g_{\max} < \infty$. For every time step t, the boundary-relaxed policy function in* (2.20) *converges to the optimal scheduling policy function uniformly on $[g_{\min}, g_{\max}]$ as the number of unserved bits β goes to infinity: for every given $\varepsilon > 0$, there exists $\mathfrak{B}_0$ such that*

$$\left| b_t^{relax}(\beta, g_t) - b_t^{opt}(\beta, g_t) \right| < \varepsilon, \quad \forall g_t \in [g_{\min}, g_{\max}]. \tag{2.40}$$

for $\beta > \mathfrak{B}_0$.

Proof. See Section 2.7.5. □

Figure 2.8a illustrates the behaviors of $b_3^{\text{relax}}(\beta, g_3)$ and $b_3^{\text{opt}}(\beta, g_3)$ vs. g_3 for different values of β and Fig. 2.8b illustrates the behaviors in terms of β for different values of g_3, when g is a truncated exponential variable with a support of $[0.001, 10^6]$[10] . When $g_3 = 0.5$, for instance, it can be seen that the difference between b_3^{relax} and b_3^{opt} gets smaller as β increases in both Fig. 2.8a and Fig. 2.8b. Notice also that the value of β making the difference between b_3^{relax} and b_3^{opt} small varies with the value of g_3. As can be seen in Fig. 2.8b, larger β is required for larger g_3. Additionally, we can observe from Fig. 2.8b that the slope of the plots is 1 in small β and the slope changes to $\frac{1}{3}$ for some larger β depending on the value of g_3, which is due to the policy function in (2.20).

[10] The density of the usual truncated exponential distribution has only a lower limit, i.e., $f(g) = e^{-(g-\gamma_0)}$ for $g \geq \gamma_0$ and 0 for elsewhere. However, the truncated exponential variable in this subsection has both a lower and a upper limits. See (2.39) for the pdf.

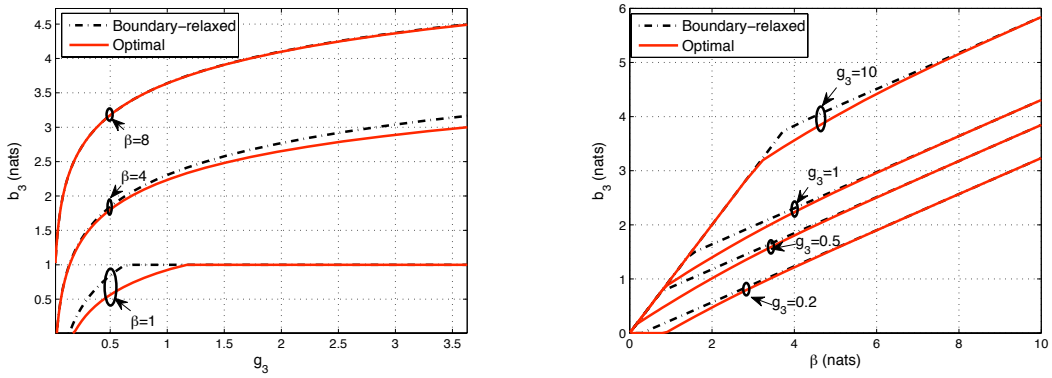

(a) $b_3^{\text{relax}}(\beta, g_3)$ and $b_3^{\text{opt}}(\beta, g_3)$ with respect to g_3

(b) $b_3^{\text{relax}}(\beta, g_3)$ and $b_3^{\text{opt}}(\beta, g_3)$ with respect to β

Figure 2.8: The behavior of b_3^{relax} and b_3^{opt} when $\{g_t\}$ are truncated exponential variables with support $[0.001, 10^6]$

We now compare the incurred energy costs of the two polices. We first define the incurred energy with the boundary-relaxed scheduler as:

$$J_t^{\text{relax}}(\beta_t, g_t) = \begin{cases} \frac{e^{b_t^{\text{relax}}}-1}{g_t} + \bar{J}_{t-1}^{\text{relax}}(\beta_t - b_t^{\text{relax}}), & t = T, T-1, \cdots, 2, \\ \frac{e^{\beta_1}-1}{g_1}, & t = 1, \end{cases} \tag{2.41}$$

where $\bar{J}_{t-1}^{\text{relax}}(\beta) = \mathbb{E}_g[J_{t-1}^{\text{relax}}(\beta, g)]$. Notice that (2.41) is not an optimization but is instead a calculation based upon the definition of b_t^{relax} in (2.20). Also notice that $\bar{J}_t^{\text{relax}}$ denotes the cost for the actual un-relaxed problem (the energy cost with a policy satisfying $0 \leq b_t \leq \beta_t$ for all t), while the function $\bar{U}_t$ defined in Section 2.3.3 denotes the cost for the relaxed problem (the energy cost with a policy that may not satisfy $0 \leq b_t \leq \beta_t$).

Theorem 2.3. *Let the PDF f of g_t be continuous on $[g_{\min}, g_{\max}]$ with Support$(f) = [g_{\min}, g_{\max}]$, where $g_{\min} > 0$ and $g_{\max} < \infty$. For any number of time slots T, the energy cost of the boundary-relaxed scheduler converges to the optimal energy cost as the number of bits B goes to infinity:*

$$\lim_{B\to\infty} \left[\bar{J}_T^{relax}(B) - \bar{J}_T^{opt}(B)\right] = 0. \tag{2.42}$$

Proof. See Section 2.7.6. □

While proving Theorem 2.3, we obtain the asymptotic relations between the actual cost of the boundary-relaxed scheduler, the cost of the relaxed version, and the cost of the optimal

one, i.e., $\lim_{B\to\infty}\left[\bar{J}_T^{\text{relax}}(B)-\bar{U}_T(B)\right]=0$ and $\lim_{B\to\infty}\left[\bar{U}_T(B)-\bar{J}_T^{\text{opt}}(B)\right]=0$. Since we have a closed-form expression of $\bar{U}_T(B)$ shown in (2.17), these relations help us understand the behavior of the optimal cost for large B, which will be discussed in Section 2.5.1.

Although the analytic form of the optimal scheduler is not available, the above two theorems tell us that the boundary-relaxed scheduler, which has a very simple form that can be easily implemented, is asymptotically optimal when the number of bits to transmit (B) is sufficiently large. Furthermore, the scheduling function (2.20) provides intuition on the interplay between the channel quality and the deadline. When the deadline is far away (large t), the bit allocation is almost completely determined by the channel quality; on the other hand, as the deadline approaches (small t), the policy becomes less opportunistic.

2.4.2 Small B and Finite T: Asymptotic Optimality of One-Shot Scheduler

We now show that the one-shot scheduling policy is asymptotically optimal when T is fixed and B is taken to zero. We first show convergence in terms of the policy function, and then in terms of the energy cost.

Theorem 2.4. *For arbitrary time step t, the one-shot policy function in* (2.33) *converges to the optimal scheduling policy function as the number of unserved bits β tends to zero, i.e., the optimal policy becomes a threshold policy and the threshold coincides with the threshold of the one-shot policy:*

$$\lim_{\beta\to 0}\sup\{g: b_t^{opt}(\beta,g)=0\}=\lim_{\beta\to 0}\inf\{g: b_t^{opt}(\beta,g)=\beta\}=\frac{1}{\omega_t}, \tag{2.43}$$

where $1/\omega_t$ is the threshold of the one-shot policy as in (2.33) *and* (2.34)*.*

Proof. See Section 2.7.7. □

Furthermore, we claim that the costs of the two policies also converge to one another. Since the average costs for the two policies converge to zero as $B\to 0$, cost convergence is investigated by studying the ratio, rather than the absolute difference, between the two costs:

Theorem 2.5. *For arbitrary delay deadline T, the energy cost of the one-shot scheduler converges to the optimal energy cost as the number of bits B goes to zero:*

$$\lim_{B\to 0}\frac{\bar{J}_T^{one}(B)}{\bar{J}_T^{opt}(B)}=1. \tag{2.44}$$

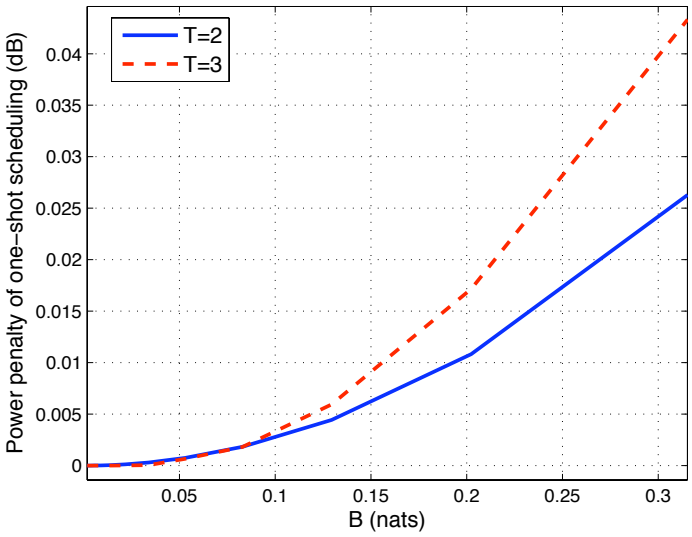

Figure 2.9: Additional power cost of one-shot scheduling relative to optimal scheduling as a function of B, when g is a truncated exponential variable with support $[0.001, 10^6]$

Proof. See Section 2.7.8. □

In Fig. 2.9 the additional power cost of one-shot scheduling relative to optimal scheduling (i.e., $10\log_{10}\frac{\bar{J}_T^{\text{one}}(B)}{\bar{J}_T^{\text{opt}}(B)}$) is plotted versus the number of bits B for $T=2$ and $T=3$ when g is a truncated exponential variable with a support of $[0.001, 10^6]$. As can be seen, the ratio converges to 1 (0 dB) as B converges to 0.

The optimality of one-shot scheduling can also be seen by upper and lower bounding the energy-bit function by linear functions. Using $x \le e^x - 1 \le xe^B$ for $0 \le x \le B$, we have:

$$\frac{b_t}{g_t} \le E_t(b_t, g_t) \le \frac{b_t e^B}{g_t}. \tag{2.45}$$

If we solve the DP using either of these bounds on the energy-bit function, the optimization in (2.5) becomes a linear program and thus a one-shot policy is optimal because a constrained linear program has a solution at a boundary of the constraint. Furthermore, the one-shot policy based on the upper and lower bounds converge to the one-shot policy described in Section 2.3.4 as $B \to 0$ because the bounds themselves converge.

2.4.3 Large T: Asymptotic Optimality of Causal Delay-Constrained Ergodic Scheduler

When B and T are simultaneously taken to infinity at a particular ratio (i.e., $B,T \to \infty$ with $B = \bar{b}T$ for some constant $\bar{b} > 0$), we can show the energy-cost optimality of the ergodic policy in Section 2.3.5. Unlike the above two cases, a weaker convergence is analyzed for the delay-constrained ergodic scheduler in terms of the average per-slot energy cost. That is, instead of analyzing the absolute difference of the total energy costs, the converge is analyzed for the average energy per slot.

The average energy cost of the delay-constrained ergodic scheduler is given by

$$\bar{J}_T^{\text{constrained-erg}}(\bar{b}T;\delta) = \mathbb{E}\left[\sum_{t=1}^{T} \frac{e^{b_t^{\text{constrained-erg}}} - 1}{g_t}\right] = \mathbb{E}\left[\sum_{t=2}^{T} \frac{e^{b_t^{\text{erg}}(\bar{b}+\delta,g_t)} - 1}{g_t}\right] + \mathbb{E}\left[\frac{e^{\beta_1} - 1}{g_1}\right], \tag{2.46}$$

where β_1 denotes the remaining bits at the final slot and the value of δ is chosen such that

$$\bar{J}_T^{\text{constrained-erg}}(\bar{b}T) = \inf_{\delta>0} \bar{J}_T^{\text{constrained-erg}}(\bar{b}T;\delta). \tag{2.47}$$

Theorem 2.6. *For any given average rate $\bar{b}(>0)$, the per-slot energy cost of the delay-constrained ergodic policy converges to the optimal ergodic energy cost as T tends to infinity:*

$$\lim_{T\to\infty} \frac{1}{T} \bar{J}_T^{\textit{constrained-erg}}(\bar{b}T) = \lim_{T\to\infty} \frac{1}{T} \bar{J}_T^{opt}(\bar{b}T) = \bar{E}^{erg}(\bar{b}). \tag{2.48}$$

Proof. See Section 2.7.9. □

The effect of the hard-deadline becomes inconsequential for large T because the channel realizations over the deadline horizon closely match the fading distribution. As a result, the delay-constrained ergodic scheduler performs similar to the ergodic scheduler when T is large. Moreover, the delay-constrained ergodic scheduler becomes causal optimal since any causal policy cannot be better than the ergodic policy.

2.5 Scheduling Gain

We have shown that the boundary-relaxed and the one-shot schedulers are asymptotically optimal as $B \to \infty$ and $B \to 0$, respectively. Another interesting issue is quantifying the advantage these

schedulers provide compared to a non-opportunistic equal-bit scheduler in Section 2.3.1 that simply transmits B/T bits during each time slot.

Recall that the expected energy cost of the equal-bit scheduler is given by

$$\bar{J}_T^{\text{equal}}(B) = \mathbb{E}\left[\sum_{t=1}^{T} \frac{e^{\frac{B}{T}} - 1}{g_t}\right] = T\left(e^{\frac{B}{T}}\nu_1 - \nu_1\right), \tag{2.49}$$

since the equal-bit scheduler chooses $b_t = B/T$ for all t. Notice that the equal-bit scheduler achieves the delay-limited capacity [CTB99, HT98] (i.e., zero-outage capacity) with rate B/T.

We define the scheduling gain as the ratio between the expected energy expenditures:

$$\Delta_T^{\text{opt}}(B) \triangleq \frac{\bar{J}_T^{\text{equal}}(B)}{\bar{J}_T^{\text{opt}}(B)} \tag{2.50}$$

and quantify its behavior in the following theorem:

Theorem 2.7. *For any T, the scheduling gain $\Delta_T^{\text{opt}}(B)$ is monotonically decreasing with respect to B. Furthermore, the limiting scheduling gains are given by:*

$$\lim_{B\to 0} \Delta_T^{\text{opt}}(B) = \lim_{B\to 0} \frac{\bar{J}_T^{\text{equal}}(B)}{\bar{J}_T^{\text{one}}(B)} = \frac{\nu_1}{\omega_{T+1}}, \tag{2.51}$$

and if the PDF of the fading distribution is compactly supported and continuous,

$$\lim_{B\to\infty} \Delta_T^{\text{opt}}(B) = \lim_{B\to\infty} \frac{\bar{J}_T^{\text{equal}}(B)}{\bar{J}_T^{\text{relax}}(B)} = \frac{\nu_1}{\mathbb{G}(\nu_T, \cdots, \nu_1)}. \tag{2.52}$$

Proof. See Section 2.7.10. □

Since the boundary-relaxed scheduler is optimal as $B \to \infty$, the scheduling gain of the optimal scheduler and that of the boundary-relaxed scheduler are the same as $B \to \infty$; the same is true for the optimal and the one-shot scheduler as $B \to 0$. The plot of scheduling gain vs. B in Fig. 2.10 agrees with the results of Theorem 2.7. Intuitively, scheduling delivers a larger power gain for small B because in such scenarios one can be very opportunistic and transmit the entire packet once a sufficiently good channel state is realized. For larger B, however, it is inefficient to transmit the entire packet in a single slot (because energy increases exponentially with the number of bits) and thus transmissions must be spread across many slots (in fact, all slots are used as $B \to \infty$), which reduces the channel quality during those transmissions and thus reduces the benefit of scheduling.

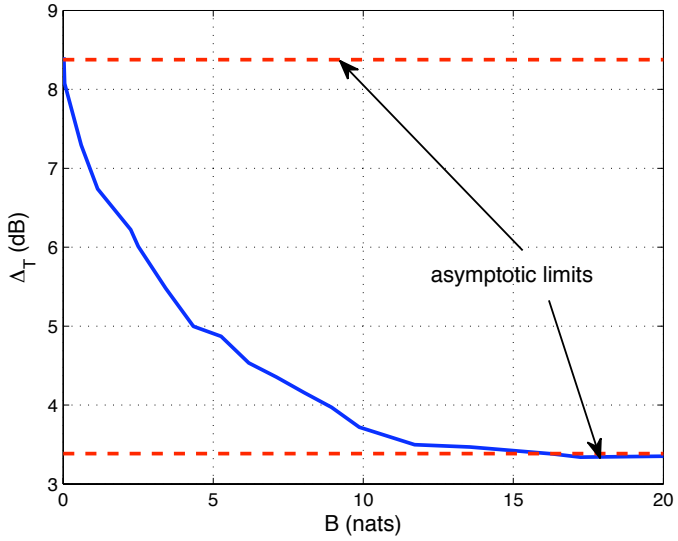

Figure 2.10: Scheduling gain Δ_5 when g is a truncated exponential variable with support $[0.001, 10^6]$

In Table 2.3 the limited scheduling gains are showed for various fading distributions. As intuitively expected, the scheduling gain is larger for more severe fading distributions and for larger time horizons T. From the fact that both $\mathbb{G}(\nu_T, \cdots, \nu_1)$ and ω_{T+1} decrease as T increases as in Proposition 2.8, the asymptotic scheduling gains in (2.51) and (2.52) increase with T.

2.5.1 Large B Behavior (High SNR)

When B is large relative to T, it is useful to interpret the scheduling gain in terms of the well-known affine approximation to high-SNR (P) capacity [SV01] :

$$C(P) = \mathcal{S}_\infty(\log P - \mathcal{L}_\infty) + o(1), \tag{2.53}$$

where $\mathcal{S}_\infty$ denotes the slope representing the multiplexing gain and $\mathcal{L}_\infty$ denotes the constant term representing the power/rate offset (see Section 5.2 also). We define the average SNR on a per-slot basis, i.e., $P = \bar{J}_T/T$. Similarly, the average rate is defined as $R_T = B/T$, which represents the average spectral efficiency per slot. Then, we investigate R_T in terms of P and T:

$$R_T(P) = \mathcal{S}_\infty(\log P - \mathcal{L}_{\infty,T}) + o(1). \tag{2.54}$$

Table 2.3: Scheduling gain examples for several fading distributions

distribution of channel state g	$T=5$		$T=10$		$T=50$	
	$\lim_{B\to\infty}\Delta_5^{\text{opt}}$	$\lim_{B\to 0}\Delta_5^{\text{opt}}$	$\lim_{B\to\infty}\Delta_{10}^{\text{opt}}$	$\lim_{B\to 0}\Delta_{10}^{\text{opt}}$	$\lim_{B\to\infty}\Delta_{50}^{\text{opt}}$	$\lim_{B\to 0}\Delta_{50}^{\text{opt}}$
trunc. exp. with $[0.1, 10^6]$	0.97 dB	4.42 dB	1.26 dB	5.98 dB	1.63 dB	8.59 dB
trunc. exp. with $[0.01, 10^6]$	2.19 dB	6.72 dB	2.80 dB	8.63 dB	3.52 dB	11.51 dB
trunc. exp. with $[0.001, 10^6]$	3.38 dB	8.38 dB	4.22 dB	10.44 dB	5.17 dB	13.40 dB

With algebraic calculations, we can obtain $\mathcal{S}_\infty$ and $\mathcal{L}_{\infty,T}$ for the equal-bit policy, the optimal scheduler (which is equal to the boundary-relaxed scheduler in this regime[11]), as well as the ergodic capacity (see Section 2.7.11 for derivation). The three policies have the same multiplexing gain (degrees of freedom) per slot ($\mathcal{S}_\infty = 1$), but the offsets $\mathcal{L}_{\infty,T}$ are different:

$$\mathcal{L}_{\infty,T}^{\text{equal}} = \log \nu_1, \tag{2.55}$$

$$\mathcal{L}_{\infty,T}^{\text{opt}} = \log \mathbb{G}\left(\nu_T, \nu_{T-1}, \cdots, \nu_1\right), \tag{2.56}$$

$$\mathcal{L}_{\infty,T}^{\text{erg}} = \log \nu_\infty. \tag{2.57}$$

The offset of the equal-bit scheduler is independent of T since it does not take advantage of time diversity. On the other hand, the offset of the boundary-relaxed scheduler decreases with T since $\mathbb{G}\left(\nu_T, \nu_{T-1}, \cdots, \nu_1\right)$ decreases by Proposition 2.8. Moreover, the offset of the boundary-relaxed scheduler converges to that of the ergodic capacity because $\mathbb{G}\left(\nu_T, \nu_{T-1}, \cdots, \nu_1\right) \to \nu_\infty$ as $T \to \infty$ by Proposition 2.8. Figure 2.11 illustrates the offsets $\mathcal{L}_{\infty,T}$ for several fading distributions. As can be seen, $\mathcal{L}_{\infty,T}^{\text{opt}}$ for all the fading distributions decreases from $\mathcal{L}_{\infty,T}^{\text{equal}}$ as T increases and converges to $\mathcal{L}_{\infty,T}^{\text{erg}}$. We can also see that the offsets $\mathcal{L}_{\infty,T}$ have larger values for more severe fading distributions.

Figure 2.12 illustrates the behavior of the spectral efficiency versus SNR. The dashed lines are obtained from the affine approximations in (2.54) while the solid lines are obtained numerically by running the optimal scheduling policy. As can be seen, the affine approximations are very accurate when SNR is 20dB or higher. Furthermore, as T increases the spectral efficiency increases from the delay-limited capacity (achieved with the $T = 1$ optimal scheduling or the equal-bit scheduling) to the ergodic capacity (achieved with the $T = \infty$ optimal scheduling).

[11] We obtain this result in the process of proving Theorem 2.3, and thus we limit the fading distribution as conditioned in Theorem 2.3, i.e., the PDF f is compactly supported and is continuous on the support.

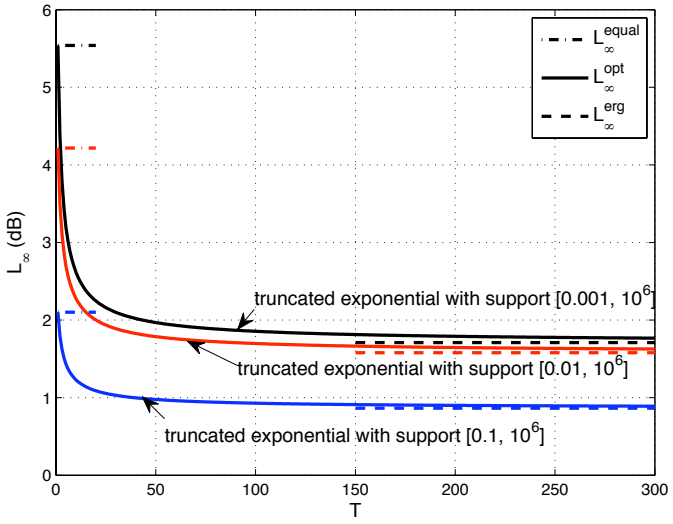

Figure 2.11: $\mathcal{L}_{\infty,T}$ for several fading distributions

It is interesting to note that for the dual problem of rate maximization over a finite time horizon when subject to a per-realization energy constraint (i.e., for every realization of channel gains $g_T, \cdots, g_1$ the amount of energy used by the scheduling policy cannot exceed some constraint E considered in [NC02] and [CTV04], at high SNR the optimal policy converges to uniform power allocation (independent of channel state) and there is no advantage to using an intelligent scheduling policy. This is to be contrasted with the setting considered here, where there is a non-vanishing benefit to using the optimal scheduler even at high SNR (i.e., large B).

2.5.2 Small B Behavior (Low SNR)

In this regime, we characterize the linear approximation to the spectral efficiency versus $\frac{E_b}{N_0}$ curve based on the wideband analysis in [Ver02]. The linear approximation consists of a constant term $\left(\frac{E_b}{N_0}\right)_{\min}$ and a slope $\mathcal{S}_0$ that represent the minimum energy per bit for reliable communication and the growth of spectral efficiency with respect to $\frac{E_b}{N_0}$. To be clear, we adopt the notion of E_b as the required energy per slot to transmit one bit per slot instead of the required energy to transmit

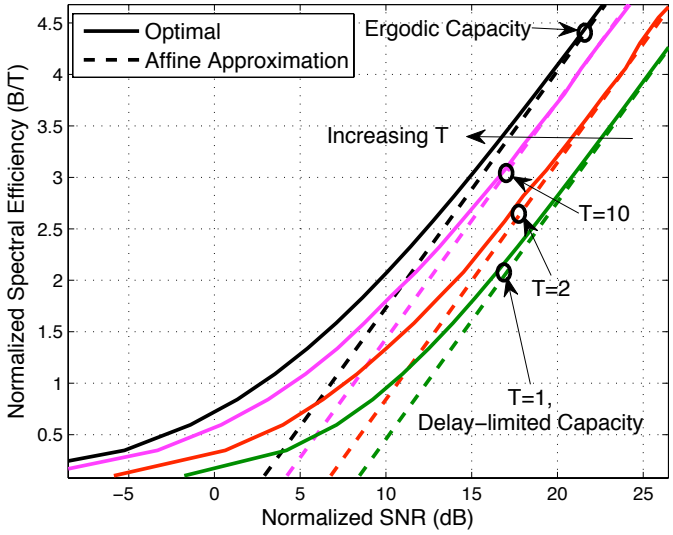

Figure 2.12: High SNR behavior when g is a truncated exponential variable with support $[0.001, 10^6]$

one bit throughout the entire T slots:

$$R_T\left(\frac{E_b}{N_0}\right) \approx \mathcal{S}_{0,T}\left(\frac{\frac{E_b}{N_0}\Big|_{\text{dB}} - \left(\frac{E_b}{N_0}\right)_{\min,T}\Big|_{\text{dB}}}{3\text{ dB}}\right). \tag{2.58}$$

These parameters $\mathcal{S}_{0,T}$ and $\left(\frac{E_b}{N_0}\right)_{\min,T}$ can be obtained for the equal-bit scheduler and the one-shot scheduler, which is optimal for $B \to 0$, (see Section 2.7.12 for derivations):

$$\mathcal{S}_{0,T}^{\text{eq}} = 2, \tag{2.59}$$

$$\mathcal{S}_{0,T}^{\text{one}} = \frac{2}{T}, \tag{2.60}$$

$$\left(\frac{E_b}{N_0}\right)_{\min,T}^{\text{eq}} = (\log 2)\nu_1, \tag{2.61}$$

$$\left(\frac{E_b}{N_0}\right)_{\min,T}^{\text{one}} = (\log 2)\,\mathbb{E}\left[\min\left(\frac{1}{g_T}, \mathbb{E}\left[\min\left(\frac{1}{g_{T-1}}, \cdots \mathbb{E}\left[\min\left(\frac{1}{g_2}, \mathbb{E}\left[\frac{1}{g_1}\right]\right)\right]\right)\right]\right)\right] \tag{2.62}$$

and both $\mathcal{S}_{0,T}^{\text{erg}}$ and $\left(\frac{E_b}{N_0}\right)_{\min,T}^{\text{erg}}$ are zero for ergodic capacity.

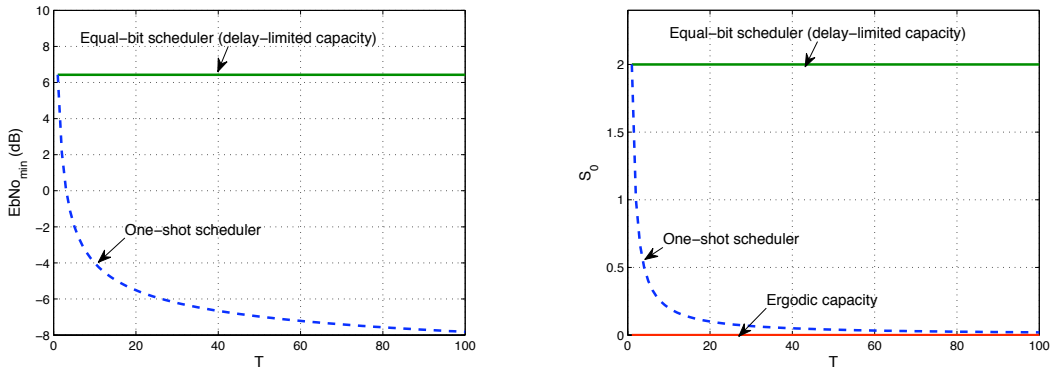

(a) $\left(\frac{E_b}{N_0}\right)_{\min,T}$ versus T (b) $\mathcal{S}_{0,T}$ versus T

Figure 2.13: Low SNR behavior when g is a truncated exponential variable with support $[0.001, 10^6]$

Figure 2.13 illustrates the behavior of $\left(\frac{E_b}{N_0}\right)_{\min,T}$ and $\mathcal{S}_{0,T}$ with respect to T. As can be seen, both $\left(\frac{E_b}{N_0}\right)_{\min,T}$ and $\mathcal{S}_{0,T}$ decrease from the delay-limited values to the ergodic capacity values as $T \to \infty$ due to the available time diversity.

2.6 Summary

In this chapter we considered the problem of bit/energy allocation for transmission of a finite number of bits over a finite delay horizon, assuming perfect instantaneous channel state information is available to the transmitter and that the energy and rate are related by the Shannon-type (exponential) function. We derived the optimal scheduling policy when the deadline spans two time slots, and derived suboptimal policies for general deadlines. The proposed schedulers have a simple and intuitive form that gives insight into the optimal balance between channel-awareness (i.e., opportunism) and deadline-awareness in a delay-limited setting.

Moreover, we have shown the asymptotic optimality of three different scheduling policies for delay-constrained transmission over a fading channel. When only a small number of bits need to be served, a one-shot threshold policy is optimal: once a sufficiently good channel state is experienced, the entire packet is transmitted. On the other hand, when the number of bits is large, the number of transmitted bits at each time step should be a weighted sum of the unserved

bits and a channel state-related term, where the weight is inversely proportional to the time to deadline. Furthermore, a modification of the ergodic waterfilling policy is shown to be optimal when the number of bits and the time horizon are both large.

2.7 Supplementary Materials and Proofs

2.7.1 Non-Causal Scheduling

If the channel states are known non-causally, i.e., $g_T, \ldots, g_1$ are known at $t = T$, the optimal scheduling/allocation is determined by waterfilling because each time slot serves as a parallel channel. While conventional waterfilling maximizes rate subject to a power constraint, this is the dual of minimizing power/energy subject to a rate/bit constraint and is referred to as *inverse-waterfilling* (IWF):

$$J_T^{\mathrm{IWF}}(B, \{g_t\}_{t=1}^T) = \min_{b_T, \cdots, b_1} \sum_{t=1}^{T} \frac{e^{b_t} - 1}{g_t}, \tag{2.63}$$

subject to $\sum_{t=1}^{T} b_t = B$ and $b_t \geq 0$. This is a convex optimization problem and can be easily solved using the standard Lagrangian method:

$$b_t^{\mathrm{IWF}} = \left\langle \log\left(\frac{g_t}{g_{\mathrm{th}}}\right) \right\rangle_0^{\infty}, \tag{2.64}$$

where g_{th} is the solution to $\sum_{i=1}^{T} \left\langle \log\left(\frac{g_i}{g_{\mathrm{th}}}\right) \right\rangle_0^{\infty} = B$. A time slot t is called *utilized* if a positive bit is scheduled at t, i.e., $b_t > 0$ or equivalently $g_t > g_{\mathrm{th}}$. With algebraic manipulations, we can express this IWF policy in (2.64) sequentially like other causal scheduling policies as

$$b_t^{\mathrm{IWF}}(\beta_t, g_t) = \frac{1}{t'}\beta_t + \frac{t'-1}{t'} \log\left(\frac{g_t}{\eta_t^{\mathrm{IWF}}}\right), \qquad \text{if } g_t > g_{\mathrm{th}}, \tag{2.65}$$

otherwise $b_t^{\mathrm{IWF}}(\beta_t, g_t) = 0$, where $t' = \sum_{i=1}^{t} 1_{\{g_i \geq g_{\mathrm{th}}\}}$ and $\eta_t^{\mathrm{IWF}} = \left(\prod_{i=1}^{t-1} g_i^{1_{\{g_i > g_{\mathrm{th}}\}}}\right)^{1/(t'-1)}$. Notice that $g_{t-1}, \cdots, g_1$ are relatively future quantities at slot t.

Like causal scheduling, the bit allocation process is described in two stages: first the remaining bits are divided equally amongst the utilized slots and then bits are added/subtracted depending on the channel state.

2.7.2 Channel Characterization by Fractional Moments

We characterize the statistics of the channel states by using the fractional moments of the inverse of the channel states g. We define the following quantity for $m = 1, 2, \ldots$,

$$\nu_m = \left(\mathbb{E}\left[\left(\frac{1}{g} \right)^{\frac{1}{m}} \right] \right)^m . \tag{2.66}$$

Then, the properties of these quantities are summarized as follows:

Proposition 2.8. *The channel statistics defined according to* (2.66) *for a non-degenerate*[12] *positive random variable have the following properties:*

(a) the sequence $\{\nu_m\}$ *is strictly decreasing and the limit exists:*

$$\nu_\infty \left(= \lim_{m\to\infty} \nu_m \right) = e^{\mathbb{E}[\log(1/g)]}. \tag{2.67}$$

(b) the sequence $\{(\nu_m \nu_{m-1} \cdots \nu_1)^{1/m}\}$ *is also strictly decreasing and its limit is also* ν_∞.

Proof. (a) First, we show the sequence $\{\nu_m\}$ is monotonically decreasing. Let $Y = 1/g$ and $f_Y(y)$ be the pdf of Y. By the Hölder's inequality [Rud87],

$$\begin{aligned}
\mathbb{E}\left[Y^{\frac{1}{m+1}} \right] &= \int_0^\infty y^{\frac{1}{m+1}} f_Y(y) dy \\
&= \int_0^\infty \left(y^{\frac{1}{m}} f_Y(y) \right)^{\frac{m}{m+1}} \left(f_Y(y) \right)^{\frac{1}{m+1}} dy \\
&< \left(\int_0^\infty y^{\frac{1}{m}} f_Y(y) dy \right)^{\frac{m}{m+1}} \left(\int_0^\infty f_Y(y) dy \right)^{\frac{1}{m+1}} \\
&= \left(\mathbb{E}[Y^{\frac{1}{m}}] \right)^{\frac{m}{m+1}} .
\end{aligned}$$

The strict inequality is due to the fact that Y is not a point-mass density. Raising both sides to the power $(m+1)$ gives $\nu_{m+1} < \nu_m$.

Second, we show convergence of the sequence. Let $\phi_m(y) = y^{\frac{1}{m}}$ for $y > 0$ and $\psi(y) = 1 + y$ for $y > 0$. Then, it is clear that $\lim_{m\to\infty} \phi_m(y) = 1$ for all $y > 0$, and $0 < \phi_m(y) \le \psi(y)$ for all $y > 0$. Additionally, $\int_0^\infty \psi(y) f_Y(y) dy < \infty$. By the dominated convergence theorem [Rud87], we have

$$\begin{aligned}
\lim_{m\to\infty} \mathbb{E}[Y^{\frac{1}{m}}] &= \lim_{m\to\infty} \int_0^\infty \phi_m(y) f_Y(y) dy \\
&= \int_0^\infty 1 \cdot f_Y(y) dy = 1.
\end{aligned}$$

[12] *This eliminates a delta-type density (point-mass) function.*

Let x be a positive real number. By the continuity of the logarithmic function, we have $\lim_{x\to 0} \ln \mathbb{E}[Y^x] = 0$. By L'Hospital rule,

$$\lim_{x\to 0} \frac{\ln \mathbb{E}[Y^x]}{x} = \lim_{x\to 0} \frac{\mathbb{E}[Y^x \ln Y]}{\mathbb{E}[Y^x]} = \mathbb{E}[\ln Y]$$

since $\lim_{x\to 0} \mathbb{E}[Y^x] = 1$ and $\lim_{x\to 0} \mathbb{E}[Y^x \ln Y] = \mathbb{E}[\ln Y]$ (due to the dominated convergence theorem). By the continuity of the exponential function, $\lim_{x\to 0} e^{\frac{1}{x}\ln \mathbb{E}[Y^x]} = e^{\mathbb{E}[\ln Y]}$. Since the above limit exists and x is in the superset of integers, we have the result.

(b) The monotonicity of the sequence $\{(\nu_m \nu_{m-1} \cdots \nu_1)^{1/m}\}$ follows immediately from the monotonicity of the sequence $\{\nu_m\}$ and its positivity.
By the property of the exponential function, we have $(\nu_m \nu_{m-1} \cdots \nu_1)^{\frac{1}{m}} = e^{\frac{1}{m}\ln(\nu_m \nu_{m-1} \cdots \nu_1)} = e^{\frac{1}{m}\sum_{n=1}^{m} \ln \nu_n}$. Since $\lim_{m\to\infty} \nu_m = \nu_\infty$ and log is continuous, $\lim_{m\to\infty} \ln \nu_m = \ln \nu_\infty$. By Cesáro mean, $\lim_{m\to\infty} \frac{1}{m}\sum_{n=1}^{m} \ln \nu_n = \ln \nu_\infty$. From the continuity of the exponential function, we have the result.

□

Notice that ν_1 and ν_∞ represent the arithmetic mean and the geometric mean of random variable $1/g$, respectively. All other values in the sequence $\{\nu_m\}$ lie between these two means.

2.7.3 Proof of Proposition 2.1

(a) (i) We show the monotonicity of b_t^{opt} in β_t. When $g_t \le \frac{1}{(\bar{J}_{t-1}^{\mathrm{opt}})'(\beta_t)}$, $b_t^{\mathrm{opt}} = 0$ and thus is non-decreasing in β_t. When $\frac{1}{(\bar{J}_{t-1}^{\mathrm{opt}})'(\beta_t)} < g_t < \frac{e^{\beta_t}}{(\bar{J}_{t-1}^{\mathrm{opt}})'(0)}$, we suppose that b_t^{opt} decreases in β_t. Then, $(\beta_t - b_t^{\mathrm{opt}})$ increases and $(\bar{J}_{t-1}^{\mathrm{opt}})'(\beta_t - b_t^{\mathrm{opt}})$ increases. As a result, b_t^{opt} increases but this leads a contradiction. Thus, b_t^{opt} is non-decreasing in β_t when $\frac{1}{(\bar{J}_{t-1}^{\mathrm{opt}})'(\beta_t)} < g_t < \frac{e^{\beta_t}}{(\bar{J}_{t-1}^{\mathrm{opt}})'(0)}$. When $g_t \ge \frac{e^{\beta_t}}{(\bar{J}_{t-1}^{\mathrm{opt}})'(0)}$, $b_t^{\mathrm{opt}} = \beta_t$ and thus is non-decreasing in β_t.

(ii) We show the strict monotonicity of b_t^{opt} for large β_t. To do this, we first show the unboundedness of $(\bar{J}_{t-1}^{\mathrm{opt}})'$. Suppose not, i.e., there exists $M(<\infty)$ such that $(\bar{J}_{t-1}^{\mathrm{opt}})'(\beta) \le M$ for all $\beta(\ge 0)$. By integrating both sides, we have $\bar{J}_{t-1}^{\mathrm{opt}}(\beta) \le M\beta$ for all $\beta(\ge 0)$. Note also that $\bar{J}_{t-1}^{\mathrm{opt}}(\beta) \ge \mathbb{E}\left[\frac{e^{\beta/t}-1}{\max(g_{t-1},\cdots,g_1)}\right]$ for all $\beta(\ge 0)$ by (2.5). Consequently, we have $\mathbb{E}\left[\frac{e^{\beta/t}-1}{\max(g_{t-1},\cdots,g_1)}\right] \le M\beta$ for all $\beta(\ge 0)$, which leads a contradiction. Therefore, $(\bar{J}_{t-1}^{\mathrm{opt}})'$ is unbounded.

Since $(\bar{J}_{t-1}^{\mathrm{opt}})'$ is unbounded and monotonically increasing, for any given g_t there exists $\mathfrak{B}_0$ such that $\frac{1}{(\bar{J}_{t-1}^{\mathrm{opt}})'(\beta_t)} < g_t < \frac{e^{\beta_t}}{(\bar{J}_{t-1}^{\mathrm{opt}})'(0)}$ for all $\beta_t > \mathfrak{B}_0$. In this region of g_t, we showed that b_t^{opt} is non-decreasing in β_t by (i). Suppose b_t^{opt} maintains a constant value as β_t increases in this region of g_t. Then, $(\beta_t - b_t^{\mathrm{opt}})$ increases and $(\bar{J}_{t-1}^{\mathrm{opt}})'(\beta_t - b_t^{\mathrm{opt}})$ increases. As a result, b_t^{opt} increases but this leads a contradiction, too. Therefore, b_t^{opt} increases strictly in β_t if $\beta_t > \mathfrak{B}_0$.

(iii) Finally, we show the monotonicity of $(\beta_t - b_t^{\mathrm{opt}})$ in β_t. Since b_t^{opt} is non-decreasing in β_t, $\frac{e^{b_t^{\mathrm{opt}}}}{g_t}$ is non-decreasing. Since $(\bar{J}_{t-1}^{\mathrm{opt}})'(\cdot)$ is an increasing function, $(\beta_t - b_t^{\mathrm{opt}})$ must be non-decreasing in β_t. If $\beta_t > \mathfrak{B}_0$, then b_t^{opt} is strictly increasing by (ii) and thus $(\beta_t - b_t^{\mathrm{opt}})$ is strictly increasing by the same argument.

(b) If $g_t \leq \frac{1}{(\bar{J}_{t-1}^{\mathrm{opt}})'(\beta_t)}$ and $g_t \geq \frac{e^{\beta_t}}{(\bar{J}_{t-1}^{\mathrm{opt}})'(0)}$, b_t^{opt} is constant as g_t increases, and thus is non-decreasing with respect to g_t. When $\frac{1}{(\bar{J}_{t-1}^{\mathrm{opt}})'(\beta_t)} < g_t < \frac{e^{\beta_t}}{(\bar{J}_{t-1}^{\mathrm{opt}})'(0)}$,

$$b_t^{\mathrm{opt}} = \log g_t + \log\left[(\bar{J}_{t-1}^{\mathrm{opt}})'(\beta_t - b_t^{\mathrm{opt}})\right]. \tag{2.68}$$

If we suppose that b_t^{opt} decreases strictly as g_t increases, $(\beta_t - b_t^{\mathrm{opt}})$ will increase and thus $(\bar{J}_{t-1}^{\mathrm{opt}})'(\beta_t - b_t^{\mathrm{opt}})$ will also increase. This leads a contradiction because the left hand side of (2.68) decreases strictly while the right hand side increases. Therefore, b_t^{opt} is non-decreasing in g_t.

2.7.4 Derivation of (2.34)

From (2.32) the threshold ω_t is related to the expected cost-to-go by $\omega_t = \frac{1}{e^B-1}\mathbb{E}[J_{t-1}(B,g)]$. The one-step cost-to-go is $\mathbb{E}[J_1(B,g)] = (e^B-1)\,\mathbb{E}\left[\frac{1}{g}\right]$ and therefore $\omega_2 = \mathbb{E}\left[\frac{1}{g}\right]$. For $t > 2$, we expand the cost-to-go in terms of ω_{t-1} to give:

$$\begin{aligned}\omega_t &= \frac{1}{e^B-1}\mathbb{E}[J_{t-1}(B,g)] \\ &= \frac{1}{e^B-1}\left(\mathbb{E}\left[\frac{e^B-1}{g_{t-1}}\middle|\frac{1}{g_{t-1}} < \omega_{t-1}\right]\Pr\left\{\frac{1}{g_{t-1}} < \omega_{t-1}\right\} + \right. \\ &\qquad\qquad \left. \mathbb{E}\left[\mathbb{E}[J_{t-2}(B,g)]\middle|\frac{1}{g_{t-1}} < \omega_{t-1}\right]\Pr\left\{\frac{1}{g_{t-1}} \geq \omega_{t-1}\right\}\right)\end{aligned} \tag{2.69}$$

By substituting $\mathbb{E}[J_{t-2}(B,g)] = (e^B-1)\omega_{t-1}$, we have the result.

2.7.5 Proof of Theorem 2.2

We show the result by induction, i.e., we show that if the scheduling functions converge at time step $t-1$, then the functions also converge at time step t. The base cases occur at $t=1$ and $t=2$: by construction, $b_2^{\text{relax}}(\beta,g_2) = b_2^{\text{opt}}(\beta,g_2)$ for every (β,g_2), and $b_1^{\text{relax}}(\beta,g_1) = b_1^{\text{opt}}(\beta,g_1)$ for every (β,g_1).

In order to show policy convergence, it is useful to write b_t^{relax} as:

$$b_t^{\text{relax}}(\beta_t,g_t) = \begin{cases} 0, & g_t \le \frac{1}{(\bar{U}_{t-1})'(\beta_t)}, \\ \arg_b \left\{ \frac{e^b}{g_t} = (\bar{U}_{t-1})'(\beta_t - b) \right\}, & \frac{1}{(\bar{U}_{t-1})'(\beta_t)} < g_t < \frac{e^{\beta_t}}{(\bar{U}_{t-1})'(0)}, \\ \beta_t, & g_t \ge \frac{e^{\beta_t}}{(\bar{U}_{t-1})'(0)}, \end{cases} \tag{2.70}$$

which is identical to the expression for b_t^{opt} in (2.12) except replacing $(\bar{J}_{t-1}^{\text{opt}})'$ with $(\bar{U}_{t-1})'$. Since $\bar{J}_{t-1}^{\text{opt}}$ and $\bar{U}_{t-1}$ are convex, $(\bar{J}_{t-1}^{\text{opt}})'$ and $(\bar{U}_{t-1})'$ are increasing and moreover unbounded (shown in Section 2.7.3 (a)(ii)). Since $g_{\min} > 0$ and $g_{\max} < \infty$ where $g_{\min}$ and $g_{\max}$ are the lower and the upper bounds of the support of the PDF f (Support$(f) = [g_{\min}, g_{\max}]$), there exists $\mathfrak{B}_0$ such that if $\beta > \mathfrak{B}_0$ then

$$g_{\min} > \max\left(\frac{1}{(\bar{U}_{t-1})'(\beta)}, \frac{1}{(\bar{J}_{t-1}^{\text{opt}})'(\beta)} \right) \tag{2.71}$$

$$g_{\max} < \min\left(\frac{e^{\beta}}{(\bar{U}_{t-1})'(0)}, \frac{e^{\beta}}{(\bar{J}_{t-1}^{\text{opt}})'(0)} \right). \tag{2.72}$$

Henceforth, we only consider $\beta > \mathfrak{B}_0$, and thus, no truncation occurs in both policy functions, i.e., b_t^{relax} and b_t^{opt} are determined by

$$\frac{e^{b_t^{\text{relax}}}}{g_t} = \phi(\beta - b_t^{\text{relax}}), \tag{2.73}$$

$$\frac{e^{b_t^{\text{opt}}}}{g_t} = \psi(\beta - b_t^{\text{opt}}), \tag{2.74}$$

for $\beta > \mathfrak{B}_0$, where $\phi(\beta) = (\bar{U}_{t-1})'(\beta)$ and $\psi(\beta) = (\bar{J}_{t-1}^{\text{opt}})'(\beta)$.

Let $\varepsilon > 0$ be given. By Lemma 2.9 (stated later in Section 2.7.5), there exists $\mathfrak{B}_1 (\ge \mathfrak{B}_0)$ such that if $\xi > \mathfrak{B}_1$, then

$$|\phi(\xi) - \psi(\xi)| < \varepsilon. \tag{2.75}$$

Since $\beta - b_t^{\text{opt}}$ and b_t^{opt} are strictly increasing in β (when β is sufficiently large) by Proposition 2.1 and $\beta - b_t^{\text{opt}} (= \psi^{-1}(e^{b_t^{\text{opt}}}/g_t))$ is unbounded due to the unboundedness and the monotonicity of ψ, there exists $\mathfrak{B}_2$ such that $\beta > \mathfrak{B}_2$ implies

$$\beta - b_t^{\text{opt}}(\beta, g_t) > \mathfrak{B}_1, \qquad \forall g_t \in [g_{\min}, g_{\max}]. \tag{2.76}$$

Therefore, if $\beta > \mathfrak{B}_2$,

$$\left|\phi(\beta - b_t^{\text{opt}}(\beta, g_t)) - \psi(\beta - b_t^{\text{opt}}(\beta, g_t))\right| < \varepsilon, \quad \forall g_t \in [g_{\min}, g_{\max}]. \tag{2.77}$$

If $b_t^{\text{opt}} \leq b_t^{\text{relax}}$,

$$\phi(\beta - b_t^{\text{relax}}) \leq \phi(\beta - b_t^{\text{opt}}) < \psi(\beta - b_t^{\text{opt}}) + \varepsilon, \tag{2.78}$$

where the last inequality follows from (2.77). Additionally, we have

$$\phi(\beta - b_t^{\text{relax}}) = \frac{e^{b_t^{\text{relax}}}}{g_t} \geq \frac{e^{b_t^{\text{opt}}}}{g_t} = \psi(\beta - b_t^{\text{opt}}). \tag{2.79}$$

Combining (2.78) and (2.79), we have $\phi(\beta - b_t^{\text{relax}}) - \psi(\beta - b_t^{\text{opt}}) < \varepsilon$. By the same argument for $b_t^{\text{opt}} > b_t^{\text{relax}}$, we have $\psi(\beta - b_t^{\text{opt}}) - \phi(\beta - b_t^{\text{relax}}) < \varepsilon$. Thus, we obtain

$$\left|\phi(\beta - b_t^{\text{relax}}(\beta, g_t)) - \psi(\beta - b_t^{\text{opt}}(\beta, g_t))\right| < \varepsilon, \qquad \forall g_t \in [g_{\min}, g_{\max}]. \tag{2.80}$$

By (2.73), (2.74), and the continuity, $b_t^{\text{relax}}(\cdot, g_t) \to b_t^{\text{opt}}(\cdot, g_t)$ uniformly on $[g_{\min}, g_{\max}]$ is obtained. □

Lemma 2.9. *If $b_{t-1}^{relax}(\cdot, g_{t-1}) \to b_{t-1}^{opt}(\cdot, g_{t-1})$ uniformly on $[g_{\min}, g_{\max}]$, then*

$$\lim_{\beta \to \infty} \left[(\bar{U}_{t-1})'(\beta) - (\bar{J}_{t-1}^{opt})'(\beta)\right] = 0. \tag{2.81}$$

Proof. From (2.5) and (2.12), we write the expected cost-to-go as:

$$\begin{aligned} \bar{J}_{t-1}^{\text{opt}}(\beta) = \int_0^{\frac{1}{(\bar{J}_{t-2}^{\text{opt}})'(\beta)}} \bar{J}_{t-2}^{\text{opt}}(\beta) dF(x) + \int_{\frac{e^\beta}{(\bar{J}_{t-2}^{\text{opt}})'(0)}}^{\infty} \frac{e^\beta - 1}{x} dF(x) \\ + \int_{\frac{1}{(\bar{J}_{t-2}^{\text{opt}})'(\beta)}}^{\frac{e^\beta}{(\bar{J}_{t-2}^{\text{opt}})'(0)}} \left[\frac{e^{b_{t-1}^{\text{opt}}} - 1}{x} + \bar{J}_{t-2}^{\text{opt}}(\beta - b_{t-1}^{\text{opt}})\right] dF(x), \end{aligned} \tag{2.82}$$

where b_{t-1}^{opt} is a function of β (and x). By differentiating $\bar{J}_{t-1}^{\text{opt}}$ using integral calculus[13] , the derivative (with respect to β) of $\bar{J}_{t-1}^{\text{opt}}$ is:

$$(\bar{J}_{t-1}^{\text{opt}})'(\beta) = \int_0^{\frac{1}{(\bar{J}_{t-2}^{\text{opt}})'(\beta)}} (\bar{J}_{t-2}^{\text{opt}})'(\beta) f(x)dx + e^{\beta} \int_{\frac{e^{\beta}}{(\bar{J}_{t-2}^{\text{opt}})'(0)}}^{\infty} \frac{1}{x} f(x)dx + \int_{\frac{1}{(\bar{J}_{t-2}^{\text{opt}})'(\beta)}}^{\frac{e^{\beta}}{(\bar{J}_{t-2}^{\text{opt}})'(0)}} \frac{d}{d\beta} \left[\frac{e^{b_{t-1}^{\text{opt}}} - 1}{x} + \bar{J}_{t-2}^{\text{opt}}(\beta - b_{t-1}^{\text{opt}}) \right] dF(x) \quad (2.83)$$

Since $(\bar{J}_{t-2}^{\text{opt}})'$ is unbounded increasing and $\text{Support}(f) = [g_{\min}, g_{\max}]$, $\frac{1}{(\bar{J}_{t-2}^{\text{opt}})'(\beta)} < g_{\min}$ and $\frac{e^{\beta}}{(\bar{J}_{t-2}^{\text{opt}})'(0)} > g_{\max}$ for sufficiently large β, and thus

$$\lim_{\beta \to \infty} \int_0^{\frac{1}{(\bar{J}_{t-2}^{\text{opt}})'(\beta)}} (\bar{J}_{t-2}^{\text{opt}})'(\beta) f(x)dx = 0, \quad (2.84)$$

$$\lim_{\beta \to \infty} e^{\beta} \int_{\frac{e^{\beta}}{(\bar{J}_{t-2}^{\text{opt}})'(0)}}^{\infty} \frac{1}{x} f(x)dx = 0. \quad (2.85)$$

Since $\frac{e^{b_{t-1}^{\text{opt}}}}{x} = (\bar{J}_{t-2}^{\text{opt}})'(\beta - b_{t-1}^{\text{opt}})$ for $x \in \left(\frac{1}{(\bar{J}_{t-2}^{\text{opt}})'(\beta)}, \frac{e^{\beta}}{(\bar{J}_{t-2}^{\text{opt}})'(0)} \right)$ by (2.12),

$$\frac{d}{d\beta} \left[\frac{e^{b_{t-1}^{\text{opt}}} - 1}{x} + \bar{J}_{t-2}^{\text{opt}}(\beta - b_{t-1}^{\text{opt}}) \right] = \frac{e^{b_{t-1}^{\text{opt}}}}{x}. \quad (2.86)$$

As a result, the derivative of the expected cost-to-go can be stated simply in the limit of large β:

$$\lim_{\beta \to \infty} (\bar{J}_{t-1}^{\text{opt}})'(\beta) = \lim_{\beta \to \infty} \int_{\frac{1}{(\bar{J}_{t-2}^{\text{opt}})'(\beta)}}^{\frac{e^{\beta}}{(\bar{J}_{t-2}^{\text{opt}})'(0)}} \frac{e^{b_{t-1}^{\text{opt}}(\beta,x)}}{x} dF(x). \quad (2.87)$$

From (2.17), we have

$$\begin{aligned} \lim_{\beta \to \infty} \left[(\bar{U}_{t-1})'(\beta) - (\bar{J}_{t-1}^{\text{opt}})'(\beta) \right] &= \lim_{\beta \to \infty} \left[e^{\frac{\beta}{t-1}} \, \mathbb{G}_{\mathbb{T}}(\nu_{t-1}, \cdots, \nu_1) - \int_{\frac{1}{(\bar{J}_{t-2}^{\text{opt}})'(\beta)}}^{\frac{e^{\beta}}{(\bar{J}_{t-2}^{\text{opt}})'(0)}} \frac{e^{b_{t-1}^{\text{opt}}}}{x} dF(x) \right] \\ &= \lim_{\beta \to \infty} \left[e^{\frac{\beta}{t-1}} \, \mathbb{G}_{\mathbb{T}}(\nu_{t-1}, \cdots, \nu_1) - \int_{\frac{1}{(\bar{J}_{t-2}^{\text{opt}})'(\beta)}}^{\frac{e^{\beta}}{(\bar{J}_{t-2}^{\text{opt}})'(0)}} \frac{e^{b_{t-1}^{\text{relax}}}}{x} dF(x) + \int_{\frac{1}{(\bar{J}_{t-2}^{\text{opt}})'(\beta)}}^{\frac{e^{\beta}}{(\bar{J}_{t-2}^{\text{opt}})'(0)}} \frac{e^{b_{t-1}^{\text{relax}}} - e^{b_{t-1}^{\text{opt}}}}{x} dF(x) \right]. \end{aligned} \quad (2.88)$$

[13] $H'(x) = h(x, \varphi(x))\varphi'(x) + \int_a^{\varphi(x)} \frac{\partial h}{\partial x}(x,y)dy$ for $H(x) = \int_a^{\varphi(x)} h(x,y)dy$

Since $\text{Support}(f) = [g_{\min}, g_{\max}] \subset \left[\frac{1}{(\bar{J}_{t-2}^{\text{opt}})'(\beta)}, \frac{e^{\beta}}{(\bar{J}_{t-2}^{\text{opt}})'(0)}\right]$ (for large β) and the induction hypothesis that $b_{t-1}^{\text{relax}}(\beta,x)$ converges to $b_{t-1}^{\text{opt}}(\beta,x)$ uniformly on $x \in [g_{\min}, g_{\max}]$,

$$\lim_{\beta\to\infty} \int_{\frac{1}{(\bar{J}_{t-2}^{\text{opt}})'(\beta)}}^{\frac{e^{\beta}}{(\bar{J}_{t-2}^{\text{opt}})'(0)}} \frac{e^{b_{t-1}^{\text{relax}}} - e^{b_{t-1}^{\text{opt}}}}{x} f(x)dx = \lim_{\beta\to\infty} \int_{g_{\min}}^{g_{\max}} \frac{e^{b_{t-1}^{\text{relax}}} - e^{b_{t-1}^{\text{opt}}}}{x} f(x)dx = 0, \tag{2.89}$$

and thus

$$\lim_{\beta\to\infty} \left[(\bar{U}_{t-1})'(\beta) - (\bar{J}_{t-1}^{\text{opt}})'(\beta)\right] = \lim_{\beta\to\infty} \left[e^{\frac{\beta}{t-1}}\, \mathbb{G}(\nu_{t-1}, \cdots, \nu_1) - \int_{\frac{1}{(\bar{J}_{t-2}^{\text{opt}})'(\beta)}}^{\frac{e^{\beta}}{(\bar{J}_{t-2}^{\text{opt}})'(0)}} \frac{e^{b_{t-1}^{\text{relax}}}}{x} dF(x) \right]. \tag{2.90}$$

By substituting (2.20) into b_{t-1}^{relax} and re-writing $\mathbb{G}(\nu_{t-1}, \cdots, \nu_1)$ as

$$\mathbb{G}(\nu_{t-1}, \cdots, \nu_1) = (\mathbb{G}(\nu_{t-2}, \cdots, \nu_1))^{\frac{t-2}{t-1}} \int \left(\frac{1}{x}\right)^{\frac{1}{t-1}} dF(x), \tag{2.91}$$

we have $\lim_{\beta\to\infty} \left[(\bar{U}_{t-1})'(\beta) - (\bar{J}_{t-1}^{\text{opt}})'(\beta)\right] = 0$. □

2.7.6 Proof of Theorem 2.3

We will prove this by showing that $\lim_{B\to\infty} \left[\bar{J}_T^{\text{relax}}(B) - \bar{U}_T(B)\right] = 0$ and $\lim_{B\to\infty} \left[\bar{U}_T(B) - \bar{J}_T^{\text{opt}}(B)\right] = 0$.

(i) First, we show $\lim\limits_{B\to\infty} \left[\bar{J}_T^{\text{relax}}(B) - \bar{U}_T(B)\right] = 0$ by induction. Notice that $J_t^{\text{relax}}(\beta,g) \geq U_t(\beta,g)$ for all values of β and g by the constructions (2.18) and (2.41), and thus, $\left|J_t^{\text{relax}}(\beta,g) - U_t(\beta,g)\right| = J_t^{\text{relax}}(\beta,g) - U_t(\beta,g)$ and $\left|\bar{J}_t^{\text{relax}}(\beta) - \bar{U}_t(\beta)\right| = \bar{J}_t^{\text{relax}}(\beta) - \bar{U}_t(\beta)$. By (2.17) and (2.41), $\bar{J}_1^{\text{relax}} \equiv \bar{U}_1$. Let $\varepsilon(>0)$ be given. As an induction hypothesis, we assume that

$$\lim_{B\to\infty} \left[\bar{J}_{T-1}^{\text{relax}}(B) - \bar{U}_{T-1}(B)\right] = 0, \tag{2.92}$$

i.e., there exists $\mathfrak{B}_0$ such that if $B > \mathfrak{B}_0$ then $\bar{J}_{T-1}^{\text{relax}}(B) - \bar{U}_{T-1}(B) < \varepsilon$.

To differentiate b_t^{relax} and the solution to (2.18), we let $b_t^{\text{untruncated}}$ be the solution to (2.18), and thus the relation of the two is $b_t^{\text{relax}}(\beta_t, g_t) = \left\langle b_t^{\text{untruncated}}(\beta_t, g_t)\right\rangle_0^{\beta_t}$, where $b_t^{\text{untruncated}}(\beta_t, g_t) = \frac{1}{t}\beta_t + \frac{t-1}{t}\log\left(\frac{g_t}{\eta_t^{\text{relax}}}\right)$ by (2.19).

Notice that

$$\begin{aligned}
\bar{J}_T^{\text{relax}}(B) - \bar{U}_T(B) &= \mathbb{E}\left[J_T^{\text{relax}}(B,g_T) - U_T(B,g_T)\right] \\
&= \mathbb{E}\left[J_T^{\text{relax}}(B,g_T) - U_T(B,g_T)\middle| \frac{1}{(\bar{U}_{T-1})'(B)} < g_T < \frac{e^B}{(\bar{U}_{T-1})'(0)}\right] \Pr\left\{\frac{1}{(\bar{U}_{T-1})'(B)} < g_T < \frac{e^B}{(\bar{U}_{T-1})'(0)}\right\} \\
&+ \mathbb{E}\left[J_T^{\text{relax}}(B,g_T) - U_T(B,g_T)\middle| g_T \le \frac{1}{(\bar{U}_{T-1})'(B)}\right] \Pr\left\{g_T \le \frac{1}{(\bar{U}_{T-1})'(B)}\right\} \\
&+ \mathbb{E}\left[J_T^{\text{relax}}(B,g_T) - U_T(B,g_T)\middle| g_T \ge \frac{e^B}{(\bar{U}_{T-1})'(0)}\right] \Pr\left\{g_T \ge \frac{e^B}{(\bar{U}_{T-1})'(0)}\right\}
\end{aligned} \tag{2.93}$$

When $\frac{1}{(\bar{U}_{T-1})'(B)} < g_T < \frac{e^B}{(\bar{U}_{T-1})'(0)}$, $b_T^{\text{relax}}(B,g_T) = b_T^{\text{untruncated}}(B,g_T)$ by (2.70), i.e., no boundary cases occur,

$$J_T^{\text{relax}}(B,g_T) - U_T(B,g_T) = \bar{J}_{T-1}^{\text{relax}}(B - b_T^{\text{relax}}) - \bar{U}_{T-1}(B - b_T^{\text{relax}}), \tag{2.94}$$

where $b_T^{\text{relax}} = \frac{1}{T}B + \frac{T-1}{T}\log g_T\, \mathbb{G}(\nu_{T-1},\cdots,\nu_1)$ by (2.20) for $g_T \in \left(\frac{1}{(\bar{U}_{T-1})'(B)}, \frac{e^B}{(\bar{U}_{T-1})'(0)}\right)$. Thus,

$$B - b_T^{\text{relax}} = \frac{T-1}{T}B - \frac{T-1}{T}\log g_T\, \mathbb{G}(\nu_{T-1},\cdots,\nu_1), \tag{2.95}$$

which is strictly increasing in B and unbounded. Therefore, there exists $\mathfrak{B}_1$ such that $B > \mathfrak{B}_1$ implies $B - b_T^{\text{relax}} > \mathfrak{B}_0$ uniformly for all $g_T \in [g_{\min}, g_{\max}]$. Thus, $\bar{J}_{T-1}^{\text{relax}}(B - b_T^{\text{relax}}) - \bar{U}_{T-1}(B - b_T^{\text{relax}}) < \varepsilon$ for $B > \mathfrak{B}_1$ uniformly for all $g_T \in [g_{\min}, g_{\max}]$ by (2.92) and consequently,

$$\begin{aligned}
&\lim_{B\to\infty} \mathbb{E}\left[J_T^{\text{relax}}(B,g_T) - U_T(B,g_T)\middle| \frac{1}{(\bar{U}_{T-1})'(B)} < g_T < \frac{e^B}{(\bar{U}_{T-1})'(0)}\right] \Pr\left\{\frac{1}{(\bar{U}_{T-1})'(B)} < g_T < \frac{e^B}{(\bar{U}_{T-1})'(0)}\right\} \\
&\qquad = \lim_{B\to\infty} \int_{\frac{1}{(\bar{U}_{T-1})'(B)}}^{\frac{e^B}{(\bar{U}_{T-1})'(0)}} \left[J_T^{\text{relax}}(B,x) - U_T(B,x)\right] f(x)dx \\
&\qquad = \lim_{B\to\infty} \int_{g_{\min}}^{g_{\max}} \left[J_T^{\text{relax}}(B,x) - U_T(B,x)\right] f(x)dx \\
&\qquad = \lim_{B\to\infty} \int_{g_{\min}}^{g_{\max}} \left[\bar{J}_{T-1}^{\text{relax}}(B - b_T^{\text{relax}}) - \bar{U}_{T-1}(B - b_T^{\text{relax}})\right] f(x)dx = 0
\end{aligned} \tag{2.96}$$

For sufficiently large B, $\frac{1}{(\bar{U}_{T-1})'(B)} < g_{\min}$ since $(\bar{U}_{T-1})'(B) = e^{B/T}\,\mathbb{G}(\nu_{T-1},\cdots,\nu_1)$ and $\frac{e^B}{(\bar{U}_{T-1})'(0)} > g_{\max}$, and thus

$$\Pr\left\{g_T \le \frac{1}{(\bar{U}_{T-1})'(B)}\right\} = \Pr\left\{g_T \ge \frac{e^B}{(\bar{U}_{T-1})'(0)}\right\} = 0. \tag{2.97}$$

Consequently, the induction follows.

(ii) Second we show $\lim_{B\to\infty}\left[\bar{U}_T(B)-\bar{J}_T^{\rm opt}(B)\right]=0$ by induction again.

At $t=1$, all the bits are to be served and thus:

$$\bar{J}_1^{\rm opt}(\beta)=\mathbb{E}\left[\frac{e^\beta-1}{g}\right]=e^\beta\nu_1-\nu_1=\bar{U}_1(\beta),\qquad\forall\beta(\geq 0),\tag{2.98}$$

where ν_1 is defined in (2.66). As an induction hypothesis, we assume that

$$\lim_{\beta\to\infty}\left[\bar{U}_{t-1}(\beta)-\bar{J}_{t-1}^{\rm opt}(\beta)\right]=0.\tag{2.99}$$

From (2.5) and (2.12), we write the expected cost-to-go as:

$$\begin{aligned}\bar{J}_t^{\rm opt}(\beta)=&\int_0^{\frac{1}{(\bar{J}_{t-1}^{\rm opt})'(\beta)}}\bar{J}_{t-1}^{\rm opt}(\beta)f(x)dx+\int_{\frac{e^\beta}{(\bar{J}_{t-1}^{\rm opt})'(0)}}^{\infty}\frac{e^\beta-1}{x}f(x)dx\\&+\int_{\frac{1}{(\bar{J}_{t-1}^{\rm opt})'(\beta)}}^{\frac{e^\beta}{(\bar{J}_{t-1}^{\rm opt})'(0)}}\left[\frac{e^{b_t^{\rm opt}}-1}{x}+\bar{J}_{t-1}^{\rm opt}(\beta-b_t^{\rm opt})\right]dF(x),\end{aligned}\tag{2.100}$$

where $b_t^{\rm opt}$ is a function of β (and x). Since $(\bar{J}_{t-1}^{\rm opt})'$ is unbounded increasing and Support$(f)=[g_{\min},g_{\max}]$, $\frac{1}{(\bar{J}_{t-1}^{\rm opt})'(\beta)}<g_{\min}$ and $\frac{e^\beta}{(\bar{J}_{t-1}^{\rm opt})'(0)}>g_{\max}$ for sufficiently large β as did in Lemma 2.9, and thus

$$\lim_{\beta\to\infty}\int_0^{\frac{1}{(\bar{J}_{t-1}^{\rm opt})'(\beta)}}\bar{J}_{t-1}^{\rm opt}(\beta)f(x)dx=0\tag{2.101}$$

$$\lim_{\beta\to\infty}\int_{\frac{e^\beta}{(\bar{J}_{t-1}^{\rm opt})'(0)}}^{\infty}\frac{e^\beta-1}{x}f(x)dx=0.\tag{2.102}$$

From Theorem 2.2 and the induction hypothesis (2.99),

$$\lim_{\beta\to\infty}\left[b_t^{\rm relax}(\beta,g)-b_t^{\rm opt}(\beta,g)\right]=0\quad\text{uniformly }\forall g\in[g_{\min},g_{\max}],\tag{2.103}$$

$$\lim_{\beta\to\infty}\left[\bar{U}_{t-1}(\beta-b_t^{\rm relax}(\beta,g))-\bar{J}_{t-1}^{\rm opt}(\beta-b_t^{\rm opt}(\beta,g))\right]=0\quad\text{uniformly }\forall g\in[g_{\min},g_{\max}],\tag{2.104}$$

and thus,

$$\lim_{\beta\to\infty}\bar{J}_t^{\rm opt}(\beta)=\lim_{\beta\to\infty}\int_{\frac{1}{(\bar{J}_{t-1}^{\rm opt})'(\beta)}}^{\frac{e^\beta}{(\bar{J}_{t-1}^{\rm opt})'(0)}}\left[\frac{e^{b_t^{\rm relax}}-1}{x}+\bar{U}_{t-1}(\beta-b_t^{\rm relax})\right]dF(x)\tag{2.105}$$

Therefore,

$$\begin{aligned}
&\lim_{\beta\to\infty}[\bar{U}_t(\beta)-\bar{J}_t^{\mathrm{opt}}(\beta)]\\
&=\lim_{\beta\to\infty}\left[te^{\frac{\beta}{t}}\,\mathbb{G}(\nu_t,\nu_{t-1},\cdots,\nu_1)-t\nu_1-\int_{\frac{1}{(\bar{J}_{t-1}^{\mathrm{opt}})'(\beta)}}^{\frac{e^\beta}{(\bar{J}_{t-1}^{\mathrm{opt}})'(0)}}\left[\frac{e^{b_t^{\mathrm{relax}}}-1}{x}+\bar{U}_{t-1}(\beta-b_t^{\mathrm{relax}})\right]dF(x)\right]\\
&=\lim_{\beta\to\infty}\left[te^{\frac{\beta}{t}}\,\mathbb{G}(\nu_t,\nu_{t-1},\cdots,\nu_1)-\int_{\frac{1}{(\bar{J}_{t-1}^{\mathrm{opt}})'(\beta)}}^{\frac{e^\beta}{(\bar{J}_{t-1}^{\mathrm{opt}})'(0)}}\left[\frac{e^{b_t^{\mathrm{relax}}}-1}{x}+(t-1)e^{\frac{\beta-b_t^{\mathrm{relax}}}{t-1}}\,\mathbb{G}(\nu_{t-1},\cdots,\nu_1)\right]dF(x)\right]
\end{aligned}\tag{2.106}$$

By substituting (2.20) into b_t^{relax}, we have $\lim_{\beta\to\infty}[\bar{U}_t(\beta)-\bar{J}_t^{\mathrm{opt}}(\beta)]=0$ as desired. Thus, the induction holds.

By (i) and (ii), we obtain the result as desired.

2.7.7 Proof of Theorem 2.4

First, we show that the optimal scheduler becomes a threshold policy as $\beta\to 0$. As in (2.12), the optimal policy is determined differently by the range of g_t: $g_t\le 1/(\bar{J}_{t-1}^{\mathrm{opt}})'(\beta)$, $1/(\bar{J}_{t-1}^{\mathrm{opt}})'(\beta)<g_t<e^\beta/(\bar{J}_{t-1}^{\mathrm{opt}})'(0)$, or $g_t\ge e^\beta/(\bar{J}_{t-1}^{\mathrm{opt}})'(0)$. Since $\lim_{\beta\to0}e^\beta=1$ and $\lim_{\beta\to0}(\bar{J}_{t-1}^{\mathrm{opt}})'(\beta)=(\bar{J}_{t-1}^{\mathrm{opt}})'(0)$,

$$\lim_{\beta\to0}\left[\frac{e^\beta}{(\bar{J}_{t-1}^{\mathrm{opt}})'(0)}-\frac{1}{(\bar{J}_{t-1}^{\mathrm{opt}})'(\beta)}\right]=0,\tag{2.107}$$

which implies that the case of $1/(\bar{J}_{t-1}^{\mathrm{opt}})'(\beta)<g_t<e^\beta/(\bar{J}_{t-1}^{\mathrm{opt}})'(0)$ occurs with vanishing probability as $\beta\to0$. Thus, the optimal policy is a threshold policy , i.e.,

$$b_t^{\mathrm{opt}}(\beta,g_t)=\begin{cases}\beta, & g_t>\frac{1}{(\bar{J}_{t-1}^{\mathrm{opt}})'(0)},\\ 0, & g_t\le\frac{1}{(\bar{J}_{t-1}^{\mathrm{opt}})'(0)}\end{cases}\tag{2.108}$$

as $\beta\to0$. This implies that

$$\lim_{\beta\to0}\sup\{g:b_t^{\mathrm{opt}}(\beta,g)=0\}=\lim_{\beta\to0}\inf\{g:b_t^{\mathrm{opt}}(\beta,g)=\beta\}=\frac{1}{(\bar{J}_{t-1}^{\mathrm{opt}})'(0)}.\tag{2.109}$$

Second, we show that the thresholds are identical, i.e., $\lim_{\beta\to0}(\bar{J}_{t-1}^{\mathrm{opt}})'(\beta)=\omega_t$ for every t, where ω_t is defined in (2.34). When $t=2$, this holds by construction. As an induction hypothesis,

we suppose that $\lim_{\beta\to 0}(\bar{J}_{t-2}^{\text{opt}})'(\beta) = (\bar{J}_{t-2}^{\text{opt}})'(0) = \omega_{t-1}$. By (2.83) and (2.86),

$$\begin{aligned}
\lim_{\beta\to 0}(\bar{J}_{t-1}^{\text{opt}})'(\beta) &= \lim_{\beta\to 0}\left[\int_0^{\frac{1}{(\bar{J}_{t-2}^{\text{opt}})'(\beta)}}(\bar{J}_{t-2}^{\text{opt}})'(\beta)dF(x) + e^{\beta}\int_{\frac{e^{\beta}}{(\bar{J}_{t-2}^{\text{opt}})'(0)}}^{\infty}\frac{1}{x}dF(x) + \int_{\frac{1}{(\bar{J}_{t-2}^{\text{opt}})'(\beta)}}^{\frac{e^{\beta}}{(\bar{J}_{t-2}^{\text{opt}})'(0)}}\frac{e^{b_{t-1}^{\text{opt}}}}{x}dF(x)\right] \\
&= (\bar{J}_{t-2}^{\text{opt}})'(0)\int_0^{\frac{1}{(\bar{J}_{t-2}^{\text{opt}})'(0)}}dF(x) + \int_{\frac{1}{(\bar{J}_{t-2}^{\text{opt}})'(0)}}^{\infty}\frac{1}{x}dF(x) \\
&= (\bar{J}_{t-2}^{\text{opt}})'(0)\Pr\left\{g_t \le \frac{1}{(\bar{J}_{t-2}^{\text{opt}})'(0)}\right\} + \mathbb{E}\left[\frac{1}{g_t}\middle| g_t > \frac{1}{(\bar{J}_{t-2}^{\text{opt}})'(0)}\right]\Pr\left\{g_t > \frac{1}{(\bar{J}_{t-2}^{\text{opt}})'(0)}\right\} \\
&= \omega_t
\end{aligned} \tag{2.110}$$

where the last equality follows from (2.34) by substituting ω_{t-1} into $(\bar{J}_{t-2}^{\text{opt}})'(0)$ from the induction hypothesis. Thus, the induction holds.

2.7.8 Proof of Theorem 2.5

Since $\bar{J}_1^{\text{one}}(B) = (e^B-1)\,\mathbb{E}\left[\frac{1}{g}\right]$, $(\bar{J}_1^{\text{one}})'(0) = \mathbb{E}\left[\frac{1}{g}\right] = \omega_2$ by (2.34). If we suppose that $\lim_{B\to 0}(\bar{J}_{t-2}^{\text{one}})'(B) = (\bar{J}_{t-2}^{\text{one}})'(0) = \omega_{t-1}$, then from (2.32)

$$\bar{J}_{t-1}^{\text{one}}(B) = \int_0^{\frac{1}{\omega_{t-1}}}\bar{J}_{t-2}^{\text{one}}(B)dF(x) + \int_{\frac{1}{\omega_{t-1}}}^{\infty}\frac{e^B-1}{x}dF(x) \tag{2.111}$$

$$(\bar{J}_{t-1}^{\text{one}})'(B) = \int_0^{\frac{1}{\omega_{t-1}}}(\bar{J}_{t-2}^{\text{one}})'(B)dF(x) + \int_{\frac{1}{\omega_{t-1}}}^{\infty}\frac{e^B}{x}dF(x). \tag{2.112}$$

Thus,

$$\begin{aligned}
\lim_{B\to 0}(\bar{J}_{t-1}^{\text{one}})'(B) &= (\bar{J}_{t-2}^{\text{one}})'(0)\int_0^{\frac{1}{\omega_{t-1}}}dF(x) + \int_{\frac{1}{\omega_{t-1}}}^{\infty}\frac{1}{x}dF(x) \\
&= \omega_{t-1}\Pr\left\{\frac{1}{g} \ge \omega_{t-1}\right\} + \mathbb{E}\left[\frac{1}{g}\middle|\frac{1}{g} \ge \omega_{t-1}\right]\Pr\left\{\frac{1}{g} \ge \omega_{t-1}\right\} = \omega_t.
\end{aligned} \tag{2.113}$$

By induction, $\lim_{B\to 0}(\bar{J}_T^{\text{one}})'(B) = \omega_{T+1}$. In the proof of Theorem 2.4, we have shown that $\lim_{B\to 0}(\bar{J}_T^{\text{opt}})'(B) = \omega_{T+1}$ also. Since $\lim_{B\to 0}\bar{J}_T^{\text{one}}(B) = \lim_{B\to 0}\bar{J}_T^{\text{opt}}(B) = 0$, by L'Hopital's rule, we have

$$\lim_{B\to 0}\frac{\bar{J}_T^{\text{one}}(B)}{\bar{J}_T^{\text{opt}}(B)} = \lim_{B\to 0}\frac{(\bar{J}_T^{\text{one}})'(B)}{(\bar{J}_T^{\text{opt}})'(B)} = 1. \tag{2.114}$$

2.7.9 Proof of Theorem 2.6

By definition,

$$\bar{E}^{\text{erg}}(\bar{b}) \le \frac{1}{T}\bar{J}_T^{\text{opt}}(\bar{b}T) \le \frac{1}{T}\bar{J}_T^{\text{constrained-erg}}(\bar{b}T). \tag{2.115}$$

Let $\varepsilon > 0$ be given. Since $\bar{E}^{\text{erg}}(\bar{b})$ is an increasing continuous function of $\bar{b}$, there exists $\delta > 0$ such that

$$\bar{E}^{\text{erg}}(\bar{b}) + \varepsilon = \bar{E}^{\text{erg}}(\bar{b}+\delta). \tag{2.116}$$

We use this δ for $b_t^{\text{erg-delta}}$. Then, by (2.46) and (2.47),

$$\begin{aligned}\frac{1}{T}\bar{J}_T^{\text{constrained-erg}}(\bar{b}T) &\le \frac{1}{T}\mathbb{E}\left[\sum_{t=2}^{T}\frac{e^{b_t^{\text{erg}}(\bar{b}+\delta,g_t)}-1}{g_t} + \frac{e^{\beta_1}-1}{g_1}\right] \\ &= \frac{T-1}{T}\mathbb{E}\left[\frac{1}{T-1}\sum_{t=2}^{T}\frac{e^{b_t^{\text{erg}}(\bar{b}+\delta,g_t)}-1}{g_t}\right] + \frac{1}{T}\mathbb{E}_{g_1}\left[\mathbb{E}_{\beta_1}\left[\frac{e^{\beta_1}-1}{g_1}\right]\right]\end{aligned} \tag{2.117}$$

Notice that $\left\{\frac{e^{b_t^{\text{erg}}(\bar{b}+\delta,g_t)}-1}{g_t}\right\}_{t=2}^{T}$ are i.i.d. and thus,

$$\mathbb{E}\left[\frac{1}{T-1}\sum_{t=2}^{T}\frac{e^{b_t^{\text{erg}}(\bar{b}+\delta,g_t)}-1}{g_t}\right] = \mathbb{E}\left[\frac{e^{b_t^{\text{erg}}(\bar{b}+\delta,g_t)}-1}{g_t}\right] = \bar{E}^{\text{erg}}(\bar{b}+\delta). \tag{2.118}$$

Since $\{b_t^{\text{erg}}\}_{t=2}^{T}$ are i.i.d., $\frac{1}{T-1}\sum_{t=2}^{T} b_t^{\text{erg}} \to \mathbb{E}[b_t^{\text{erg}}] = \bar{b}+\delta$ almost surely (a.s.) as $T \to \infty$ by the law of large number, and thus, the remaining bits at the final slot is given by

$$\bar{b}T - \sum_{t=2}^{T} b_t^{\text{erg}} = (T-1)\left(\frac{T}{T-1}\bar{b} - \frac{1}{T-1}\sum_{t=2}^{T} b_t^{\text{erg}}\right) \le \bar{b}+\delta \quad \text{a.s.} \tag{2.119}$$

That is, $e^{\beta_1} \le e^{\bar{b}+\delta}$ a.s. and therefore $\mathbb{E}\left[e^{\beta_1}\right] \le e^{\bar{b}+\delta}$.

$$\mathbb{E}_{g_1}\left[\mathbb{E}_{\beta_1}\left[\frac{e^{\beta_1}-1}{g_1}\right]\right] \le \mathbb{E}_{g_1}\left[\frac{e^{\bar{b}+\delta}-1}{g_1}\right] = \min_{b=\bar{b}+\delta}\ \mathbb{E}_{g_1}\left[\frac{e^{b}-1}{g_1}\right] \le \min_{\mathbb{E}[b]=\bar{b}+\delta}\ \mathbb{E}\left[\frac{e^{b}-1}{g_1}\right] = \bar{E}^{\text{erg}}(\bar{b}+\delta) \tag{2.120}$$

Thus,

$$\lim_{T\to\infty}\frac{1}{T}J_T^{\text{constrained-erg}}(\bar{b}T) \le \lim_{T\to\infty}\left[\frac{T-1}{T}\bar{E}^{\text{erg}}(\bar{b}+\delta) + \frac{1}{T}\bar{E}^{\text{erg}}(\bar{b}+\delta)\right] = \bar{E}^{\text{erg}}(\bar{b}+\delta). \tag{2.121}$$

Therefore,

$$\bar{E}^{\text{erg}}(\bar{b}) \le \lim_{T\to\infty}\frac{1}{T}\bar{J}_T^{\text{constrained-erg}}(\bar{b}T) \le \bar{E}^{\text{erg}}(\bar{b}) + \varepsilon. \tag{2.122}$$

Since ε is arbitrary, we have the result.

2.7.10 Proof of Theorem 2.7

First, we show the monotonicity of $\Delta_T^{\rm opt}(B)$. Since

$$\frac{d}{dB}\Delta_T^{\rm opt}(B) = \frac{(\bar{J}_T^{\rm eq})'(B)\bar{J}_T^{\rm opt}(B) - \bar{J}_T^{\rm eq}(B)(\bar{J}_T^{\rm opt})'(B)}{\left(\bar{J}_T^{\rm opt}(B)\right)^2}, \tag{2.123}$$

we will investigate the quantity $(\bar{J}_T^{\rm eq})'(B)\bar{J}_T^{\rm opt}(B) - \bar{J}_T^{\rm eq}(B)(\bar{J}_T^{\rm opt})'(B)$.

From (2.5), (2.12), and (2.49), we have

$$\begin{aligned}
\bar{J}_T^{\rm opt}(B) &= \int_0^{\frac{1}{(\bar{J}_{T-1}^{\rm opt})'(B)}} \bar{J}_{T-1}^{\rm opt}(B)dF(x) + \int_{\frac{1}{(\bar{J}_{T-1}^{\rm opt})'(B)}}^{\frac{e^B}{(\bar{J}_{T-1}^{\rm opt})'(0)}} \left[\frac{e^{b_T^{\rm opt}}-1}{x} + \bar{J}_{T-1}^{\rm opt}(B-b_T^{\rm opt})\right] dF(x) \\
&\quad + \int_{\frac{e^B}{(\bar{J}_{T-1}^{\rm opt})'(0)}}^{\infty} \frac{e^B-1}{x} dF(x) \qquad (2.124) \\
(\bar{J}_T^{\rm opt})'(B) &= \int_0^{\frac{1}{(\bar{J}_{T-1}^{\rm opt})'(B)}} (\bar{J}_{T-1}^{\rm opt})'(B)dF(x) + \int_{\frac{1}{(\bar{J}_{T-1}^{\rm opt})'(B)}}^{\frac{e^B}{(\bar{J}_{T-1}^{\rm opt})'(0)}} \frac{d}{dB}\left[\frac{e^{b_T^{\rm opt}}-1}{x} + \bar{J}_{T-1}^{\rm opt}(B-b_T^{\rm opt})\right] dF(x) \\
&\quad + \int_{\frac{e^B}{(\bar{J}_{T-1}^{\rm opt})'(0)}}^{\infty} \frac{e^B}{x} dF(x) \qquad (2.125) \\
\bar{J}_T^{\rm eq}(B) &= T(e^{\frac{B}{T}}-1)\nu_1 \qquad (2.126) \\
(\bar{J}_T^{\rm eq})'(B) &= e^{\frac{B}{T}}\nu_1 \qquad (2.127)
\end{aligned}$$

When $T=2$,

$$\begin{aligned}
(\bar{J}_2^{\rm eq})'(B)\bar{J}_2^{\rm opt}(B) - \bar{J}_2^{\rm eq}(B)(\bar{J}_2^{\rm opt})'(B) &= \int_0^{\frac{e^{-B}}{\nu_1}} e^{\frac{B}{2}}\nu_1^2(-1)(e^{\frac{B}{2}}-1)^2 f(x)dx \\
&\quad + \int_{\frac{e^{-B}}{\nu_1}}^{\frac{e^B}{\nu_1}} e^{\frac{B}{2}}\nu_1(-1)\left[\left(\frac{1}{x}\right)^{\frac{1}{2}} - \left(\frac{1}{\nu_1}\right)^{\frac{1}{2}}\right]^2 f(x)dx \\
&\quad + \int_{\frac{e^B}{\nu_1}}^{\infty} \frac{e^{\frac{B}{2}}\nu_1}{x}(-1)(e^{\frac{B}{2}}-1)^2 f(x)dx \\
&\le 0.
\end{aligned} \tag{2.128}$$

That is, $\frac{d\Delta_2^{\rm opt}(B)}{dB} \le 0$.

We now suppose that $\frac{d\Delta_{T-1}^{\rm opt}(B)}{dB} \le 0$ and examine $\frac{d\Delta_T^{\rm opt}(B)}{dB}$. That is, we assume that

$$(\bar{J}_{T-1}^{\rm eq})'(B)\bar{J}_{T-1}^{\rm opt}(B) - \bar{J}_{T-1}^{\rm eq}(B)(\bar{J}_{T-1}^{\rm opt})'(B) \le 0, \tag{2.129}$$

where the left hand side is the numerator of $\frac{d\Delta_{T-1}^{\mathrm{opt}}(B)}{dB}$ from (2.123). The numerator of $\frac{d\Delta_{T}^{\mathrm{opt}}(B)}{dB}$ is given by

$$
\begin{aligned}
&(\bar{J}_T^{\mathrm{eq}})'(B)\bar{J}_T^{\mathrm{opt}}(B) - \bar{J}_T^{\mathrm{eq}}(B)(\bar{J}_T^{\mathrm{opt}})'(B) \\
&\qquad = \int_0^{\frac{1}{(\bar{J}_{T-1}^{\mathrm{opt}})'(B)}} \nu_1 \left[e^{\frac{B}{T}} \bar{J}_{T-1}^{\mathrm{opt}}(B) - T(e^{\frac{B}{T}}-1)(\bar{J}_{T-1}^{\mathrm{opt}})'(B) \right] f(x)dx \\
&\qquad + \int_{\frac{e^B}{(\bar{J}_{T-1}^{\mathrm{opt}})'(0)}}^{\infty} \nu_1 \left[e^{\frac{B}{T}} \frac{e^B-1}{x} - T(e^{\frac{B}{T}}-1)\frac{e^B}{x} \right] f(x)dx \\
&\qquad + \int_{\frac{1}{(\bar{J}_{T-1}^{\mathrm{opt}})'(B)}}^{\frac{e^B}{(\bar{J}_{T-1}^{\mathrm{opt}})'(0)}} \nu_1 \left[e^{\frac{B}{T}} \left(\frac{e^{b_T^{\mathrm{opt}}}-1}{x} + \bar{J}_{T-1}^{\mathrm{opt}}(B-b_{T-1}^{\mathrm{opt}}) \right) - T(e^{\frac{B}{T}}-1)\frac{d}{dB}\left(\frac{e^{b_T^{\mathrm{opt}}}-1}{x} + \bar{J}_{T-1}^{\mathrm{opt}}(B-b_{T-1}^{\mathrm{opt}}) \right) \right] f(x)dx
\end{aligned}
\tag{2.130}
$$

From the integrand of the first integral in (2.130),

$$
\begin{aligned}
e^{\frac{B}{T}} \bar{J}_{T-1}^{\mathrm{opt}}(B) - T(e^{\frac{B}{T}}-1)(\bar{J}_{T-1}^{\mathrm{opt}})'(B) = e^{-\frac{B}{T(T-1)}} &\left[e^{\frac{B}{T-1}} \bar{J}_{T-1}^{\mathrm{opt}}(B) - (T-1)(e^{\frac{B}{T-1}}-1)(\bar{J}_{T-1}^{\mathrm{opt}})'(B) \right] \\
&+ \left[T - e^{\frac{B}{T}} - (T-1)e^{-\frac{B}{T(T-1)}} \right] (\bar{J}_{T-1}^{\mathrm{opt}})'(B)
\end{aligned}
\tag{2.131}
$$

From (2.126), (2.127), and the hypothesis (2.129), we have

$$
e^{\frac{B}{T-1}} \bar{J}_{T-1}^{\mathrm{opt}}(B) - (T-1)(e^{\frac{B}{T-1}}-1)(\bar{J}_{T-1}^{\mathrm{opt}})'(B) \le 0. \tag{2.132}
$$

We define a concave function ϕ such that

$$
\phi(z) = T - z^{T-1} - (T-1)z^{-1}, \qquad z > 0. \tag{2.133}
$$

Since the concavity and $\phi'(z) = 0$ yield that ϕ attains its maximum at $z = 1$ and $\phi(1) = 0$, $\phi(z) \le 0$ for all $z > 0$. Since $\phi(e^{\frac{B}{T(T-1)}}) = T - e^{\frac{B}{T}} - (T-1)e^{-\frac{B}{T(T-1)}}$,

$$
T - e^{\frac{B}{T}} - (T-1)e^{-\frac{B}{T(T-1)}} \le 0. \tag{2.134}
$$

From (2.132) and (2.134) along with the fact that $\bar{J}_{T-1}^{\mathrm{opt}}$ is convex, (2.131) becomes

$$
e^{\frac{B}{T}} \bar{J}_{T-1}^{\mathrm{opt}}(B) - T(e^{\frac{B}{T}}-1)(\bar{J}_{T-1}^{\mathrm{opt}})'(B) \le 0. \tag{2.135}
$$

Likewise, from the integrand of the second integral in (2.130), we want to show that

$$
e^{\frac{B}{T}}(e^B - 1) - T(e^{\frac{B}{T}}-1)e^B \le 0, \tag{2.136}
$$

which is equivalent to show $e^B - 1 - T(1 - e^{-\frac{B}{T}})e^B \le 0$. If we define a concave function $\psi(z) = -(T-1)z^T + Tz^{T-1} - 1$ for $z > 0$, $\psi(e^{\frac{B}{T}}) = e^B - 1 - T(1 - e^{-\frac{B}{T}})e^B$. As we did before, we can show that $\psi(z) \le 0$, and thus (2.136) holds.

From the integrand of the third integral in (2.130), we want to show that

$$e^{\frac{B}{T}}\left(e^{b_T^{\mathrm{opt}}}-1\right)-T\left(e^{\frac{B}{T}}-1\right)e^{b_T^{\mathrm{opt}}}\leq 0, \tag{2.137}$$

$$e^{\frac{B}{T}}\bar{J}_{T-1}^{\mathrm{opt}}(B-b_{T-1}^{\mathrm{opt}})-T\left(e^{\frac{B}{T}}-1\right)\frac{d}{dB}\bar{J}_{T-1}^{\mathrm{opt}}(B-b_{T-1}^{\mathrm{opt}})\leq 0. \tag{2.138}$$

To prove (2.137), we can write

$$\begin{aligned}&e^{\frac{B}{T}}\left(e^{b_T^{\mathrm{opt}}}-1\right)-T\left(e^{\frac{B}{T}}-1\right)e^{b_T^{\mathrm{opt}}}=\\&\qquad e^{\frac{B-b_T^{\mathrm{opt}}}{T}}\left[e^{\frac{b_T^{\mathrm{opt}}}{T}}\left(e^{b_T^{\mathrm{opt}}}-1\right)-T\left(e^{\frac{b_T^{\mathrm{opt}}}{T}}-1\right)e^{b_T^{\mathrm{opt}}}\right]-e^{\frac{B-b_T^{\mathrm{opt}}}{T}}Te^{b_T^{\mathrm{opt}}}\left(1-e^{-\frac{B-b_T^{\mathrm{opt}}}{T}}\right)\end{aligned} \tag{2.139}$$

Notice that (2.136) holds for every $B\geq 0$ and thus

$$e^{\frac{b_T^{\mathrm{opt}}}{T}}(e^{b_T^{\mathrm{opt}}}-1)-T(e^{\frac{b_T^{\mathrm{opt}}}{T}}-1)e^{b_T^{\mathrm{opt}}}\leq 0. \tag{2.140}$$

Therefore, (2.137) holds. By the similar argument, (2.138) holds, too. Thus, the third integral in (2.130) is no greater than 0. Consequently, we obtain

$$(\bar{J}_T^{\mathrm{eq}})'(B)\bar{J}_T^{\mathrm{opt}}(B)-\bar{J}_T^{\mathrm{eq}}(B)(\bar{J}_T^{\mathrm{opt}})'(B)\leq 0. \tag{2.141}$$

This shows that the monotonicity of $\Delta_T^{\mathrm{opt}}(B)$ inductively.

Second, the limits are calculated with $\bar{J}_T^{\mathrm{relax}}(B)$ and $\bar{J}_T^{\mathrm{one}}(B)$ since $\bar{J}_T^{\mathrm{opt}}(B)$ converges to the former for large B and to the latter for small B by Theorem 2.3 and Theorem 2.5, respectively.

2.7.11 Derivation of High SNR Affine Approximation Parameters

From (2.49), the spectral efficiency of the equal-bit scheduler can be found by

$$P=(e^{R_T^{\mathrm{eq}}}-1)\nu_1 \quad \text{or} \quad R_T^{\mathrm{eq}}(P)=\log\left(1+\frac{P}{\nu_1}\right). \tag{2.142}$$

Thus, at high SNR

$$R_T^{\mathrm{eq}}(P)=\log P-\log\nu_1+o(1). \tag{2.143}$$

Similarly, from (2.17) and Theorem 2.3, the spectral efficiency of the optimal scheduler at high SNR is given by

$$R_T^{\mathrm{opt}}(P)=\log P-\log\mathbb{G}(\nu_T,\cdots,\nu_1)+o(1). \tag{2.144}$$

At high SNR, the ergodic capacity can be approximately given by the uniform power control:

$$\begin{aligned} R^{\mathrm{erg}}(P) &\approx \mathbb{E}\left[\log(1+gP)\right] \\ &\approx \log P + \mathbb{E}\left[\log g\right] \\ &= \log P - \log e^{\mathbb{E}\left[\log\left(\frac{1}{g}\right)\right]} \\ &= \log P - \log \nu_\infty, \end{aligned} \tag{2.145}$$

where the last equality follows from

$$e^{\mathbb{E}\left[\log\left(\frac{1}{g}\right)\right]} = \lim_{x\to 0} e^{\frac{1}{x}\log \mathbb{E}\left[\left(\frac{1}{g}\right)^x\right]} = \lim_{m\to\infty}\left(\mathbb{E}\left[\left(\frac{1}{g}\right)^{\frac{1}{m}}\right]\right)^m = \nu_\infty. \tag{2.146}$$

2.7.12 Derivation of Low SNR Affine Approximation Parameters

From (2.142),

$$\dot{R}^{\mathrm{eq}}(P) = \frac{1/\nu_1}{1+\frac{P}{\nu_1}}. \tag{2.147}$$

By [Ver02],

$$\left(\frac{E_b}{N_0}\right)^{\mathrm{eq}}_{\min} = \frac{\log 2}{\dot{R}^{\mathrm{eq}}(0)} = (\log 2)\nu_1. \tag{2.148}$$

Then second order analysis is given by

$$\ddot{R}^{\mathrm{eq}}(P) = \frac{-(1/\nu_1)^2}{\left(1+\frac{P}{\nu_1}\right)^2} \tag{2.149}$$

Therefore, by [Ver02],

$$\mathcal{S}_0^{\mathrm{eq}} = -2\frac{\left(\dot{R}^{\mathrm{eq}}(0)\right)^2}{\ddot{R}^{\mathrm{eq}}(0)} = 2. \tag{2.150}$$

By Theorem 2.5, the average total energy cost of the optimal scheduler at low SNR is given by

$$\bar{J}_T^{\mathrm{opt}} = (e^B-1)\,\mathbb{E}\left[\min\left(\frac{1}{g_T},\mathbb{E}\left[\min\left(\frac{1}{g_{T-1}},\cdots\mathbb{E}\left[\min\left(\frac{1}{g_2},\mathbb{E}\left[\frac{1}{g_1}\right]\right)\right]\right)\right]\right)\right]. \tag{2.151}$$

With the per slot basis notations,

$$TP = (e^{TR^{\mathrm{opt}}}-1)\,\mathbb{E}\left[\min\left(\frac{1}{g_T},\mathbb{E}\left[\min\left(\frac{1}{g_{T-1}},\cdots\mathbb{E}\left[\min\left(\frac{1}{g_2},\mathbb{E}\left[\frac{1}{g_1}\right]\right)\right]\right)\right]\right)\right] \tag{2.152}$$

and thus,

$$R^{\mathrm{opt}}(P) = \frac{1}{T}\log\left(1+\frac{TP}{\mathbb{E}\left[\min\left(\frac{1}{g_T},\mathbb{E}\left[\min\left(\frac{1}{g_{T-1}},\cdots\mathbb{E}\left[\min\left(\frac{1}{g_2},\mathbb{E}\left[\frac{1}{g_1}\right]\right)\right]\right)\right]\right)\right]}\right). \tag{2.153}$$

Therefore, we have

$$\dot{R}^{\mathrm{opt}}(P) = \frac{\frac{1}{\mathbb{E}\left[\min\left(\frac{1}{g_T},\mathbb{E}\left[\min\left(\frac{1}{g_{T-1}},\cdots\mathbb{E}\left[\min\left(\frac{1}{g_2},\mathbb{E}\left[\frac{1}{g_1}\right]\right)\right]\right)\right]\right)}}{1+\frac{TP}{\mathbb{E}\left[\min\left(\frac{1}{g_T},\mathbb{E}\left[\min\left(\frac{1}{g_{T-1}},\cdots\mathbb{E}\left[\min\left(\frac{1}{g_2},\mathbb{E}\left[\frac{1}{g_1}\right]\right)\right]\right)\right]\right)}} \tag{2.154}$$

$$\ddot{R}^{\mathrm{opt}}(P) = \frac{\frac{T}{\left(\mathbb{E}\left[\min\left(\frac{1}{g_T},\mathbb{E}\left[\min\left(\frac{1}{g_{T-1}},\cdots\mathbb{E}\left[\min\left(\frac{1}{g_2},\mathbb{E}\left[\frac{1}{g_1}\right]\right)\right]\right)\right]\right)\right)^2}}{\left(1+\frac{TP}{\mathbb{E}\left[\min\left(\frac{1}{g_T},\mathbb{E}\left[\min\left(\frac{1}{g_{T-1}},\cdots\mathbb{E}\left[\min\left(\frac{1}{g_2},\mathbb{E}\left[\frac{1}{g_1}\right]\right)\right]\right)\right]\right)}\right)^2}. \tag{2.155}$$

Thus,

$$\left(\frac{E_b}{N_0}\right)^{\mathrm{one}}_{\min} = \frac{\log 2}{\dot{R}(0)} = (\log 2)\,\mathbb{E}\left[\min\left(\frac{1}{g_T},\mathbb{E}\left[\min\left(\frac{1}{g_{T-1}},\cdots\mathbb{E}\left[\min\left(\frac{1}{g_2},\mathbb{E}\left[\frac{1}{g_1}\right]\right)\right]\right)\right]\right)\right] \tag{2.156}$$

$$\mathcal{S}_0^{\mathrm{one}} = -2\frac{\left(\dot{R}^{\mathrm{one}}(0)\right)^2}{\ddot{R}^{\mathrm{one}}(0)} = \frac{2}{T}. \tag{2.157}$$

See [Ver02] for $\left(\frac{E_b}{N_0}\right)_{\min}$ and $\mathcal{S}_0$ of the ergodic capacity.

2.7.13 Derivation of (2.28)

Since $\lim_{T\to\infty} b_T^{\mathrm{relax}} = \left\langle \frac{1}{T}B + \frac{T-1}{T}\log(g_T\nu_\infty)\right\rangle_0^B$,

$$\begin{aligned} E_T^{\mathrm{relax}} &= \frac{e^{b_T^{\mathrm{relax}}}-1}{g_T} \\ &= \begin{cases} 0, & g_T < \frac{1}{\nu_\infty}e^{-\frac{B}{T-1}}, \\ \frac{e^{\frac{B}{T}}\nu_\infty^{\frac{T-1}{T}}}{(g_T)^{\frac{1}{T}}} - \frac{1}{g_T}, & \frac{1}{\nu_\infty}e^{-\frac{B}{T-1}} \le g_T \le \frac{1}{\nu_\infty}e^{B}, \\ \frac{e^B-1}{g_T}, & g_T > \frac{1}{\nu_\infty}e^{B}. \end{cases} \end{aligned}$$

As $T\to\infty$ while fixing $\frac{B}{T}$, then $B\to\infty$,

$$\lim_{T\to\infty} E_T^{\mathrm{relax}} = \begin{cases} 0, & g_T < \frac{1}{\nu_\infty}e^{-\frac{B}{T}}, \\ e^{\frac{B}{T}}\nu_\infty - \frac{1}{g_T}, & g_T \ge \frac{1}{\nu_\infty}e^{-\frac{B}{T}}. \end{cases}$$

Chapter 3

Extensions to Delay Constrained Scheduling for the Shannon Cost Function

In the previous chapter, we considered a simple hard-deadline scheduling problem of transmitting B bits within T time slots under a causal CSI assumption. Although the problem setup is simple, it is sufficiently rich to reveal the interplay between opportunistic communication and delay-limited communication. In this chapter, we extend the hard-deadline scheduling problem to more general settings and investigate the balance between opportunistic behavior and delay-limited behavior. First, we address the issue of outage. When fading is severe, allowing outage is more desirable from an overall system perspective (in the sense of energy utilization), rather than satisfying a strict deadline constraint at all times. Second, we consider a multi-user scheduling problem in a broadcast setup. In the previous chapter, we developed policies assuming schedulers can transmit at the rate of channel capacity for a single-user channel. In a multiple user setting, a natural extension is to operate on the boundary of capacity region, which is generally complicated. We will rather focus on a two-user broadcast model and discuss difficulties in this setting. Third, we consider scheduling problems for parallel/MIMO channels. Similar to the single channel scheduling problem in the previous chapter, we obtain asymptotic policies for parallel/MIMO channel scheduling. All of these scheduling policies are developed to minimize the energy expenditure. As an alternative, we consider a scheduling problem to minimize the

total bandwidth usage, which is simply formulated by changing the cost function.

3.1 Scheduling with an Outage Penalty

In the previous chapter, we have considered a scheduler that always meets a hard deadline. However, this constraint may be unrealistic in many practical environments because too much power may be required to fulfill the hard deadline constraint when fading is severe. Before reaching the final time slot, the scheduler can defer transmitting to future slots. At the final slot, however, the scheduler must finish transmitting all the unserved bits under whatever channel state is given. To avoid huge power consumption at the final slot, we can consider a scheme where the scheduler is allowed outage at the final time slot. That is, if the energy cost at the final time slot exceeds a given level M, the scheduler will give up transmitting the remaining packet and declare outage. We will refer to this as an *M-outage scheduler*, while we refer to the schedulers in the previous chapter as *non-outage schedulers*.

This M-outage scheduler can be formulated into a DP:

$$J_t^{\text{out}}(\beta_t, g_t) = \begin{cases} \min\limits_{0\le b_t\le \beta_t} \left\{ \frac{e^{b_t}-1}{g_t} + \bar{J}_{t-1}^{\text{out}}(\beta_t - b_t) \right\}, & t = T, \cdots, 2 \\ \min\left\{ \frac{e^{\beta_1}-1}{g_1},\, M \right\}, & t = 1, \end{cases} \tag{3.1}$$

where β_t denotes the remaining bits at time slot t and $\bar{J}_{t-1}^{\text{out}}(\beta) = \mathbb{E}[J_{t-1}^{\text{out}}(\beta, g_{t-1})]$ denotes the cost-to-go.

Since we denote the time index t in descending order, the scheduling functions at t for any T have the same form, e.g., $b_1(\beta_1, g_1)$ for $T = 1$ is identical to $b_1(\beta_1, g_1)$ for $T = 2$. For this reason, we will derive scheduling policies as functions of t and β_t without being concerned with T.

3.1.1 Optimal Scheduling Function at $t = 1$

Since we allow outage, the optimal solution at the final step is no longer "$b_1 = \beta_1$" but is given by

$$b_1^{\text{out}}(\beta_1, g_1) = \begin{cases} 0, & \text{if } g_1 < \frac{e^{\beta_1}-1}{M}, \\ \beta_1, & \text{if } g_1 \ge \frac{e^{\beta_1}-1}{M}. \end{cases} \tag{3.2}$$

That is, when the channel state g_1 is less than a threshold $(e^{\beta_1} - 1)/M$, the transmission is given up and outage is declared. On the other hand, when the channel state is greater than or equal to

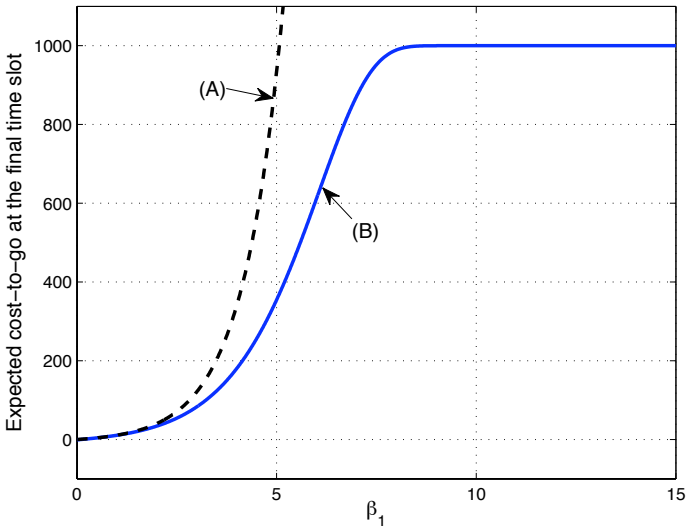

Figure 3.1: The curve (A) illustrates $\bar{J}_1^{\text{non-out}}(\beta_1)$ and the curve (B) illustrates $\bar{J}_1^{\text{out}}(\beta_1)$ for a truncated exponential variable with threshold 0.001 and $M = 1000$

the threshold, all the unserved bits β_1 are transmitted. The resulting expected cost-to-go function is given by

$$\bar{J}_1^{\text{out}}(\beta_1) = \mathbb{E}[J_1^{\text{out}}(\beta_1, g_1)] = \int_0^{\frac{e^{\beta_1}-1}{M}} M dF(x) + \int_{\frac{e^{\beta_1}-1}{M}}^{\infty} \frac{e^{\beta_1}-1}{x} dF(x), \tag{3.3}$$

where F is the cdf of the fading distribution g. Figure 3.1 illustrates the expected cost-to-go function $\bar{J}_1^{\text{out}}$ compared with the non-outage cost-to-go function

$$\bar{J}_1^{\text{non-out}}(\beta_1) = (e^{\beta_1}-1)\,\mathbb{E}\left[\frac{1}{g}\right] = \int_0^{\infty} \frac{e^{\beta_1}-1}{x} dF(x), \tag{3.4}$$

which was derived in (2.8). Notice that $\bar{J}_1^{\text{out}}$ is not convex but quasiconvex because it is nondecreasing, which can be also verified by the first-order conditions[1] [BV04].

When there is no penalty term like (2.5), the expected cost at the last slot $\bar{J}_1^{\text{non-out}}$ is an exponentially increasing function as in (3.4), and thus unbounded. When there is a penalty term like (3.1), however, the expected cost $\bar{J}_1^{\text{out}}$ is monotonically increasing but bounded by M, and

[1] Let $\phi : \mathbb{R}^n \to \mathbb{R}$ be differentiable. The function ϕ is quasiconvex if and only if $\text{Dom}(f)$ is convex and $\phi(y) \leq \phi(x)$ implies $\nabla\phi(x)^T(y-x) \leq 0$, for all $x, y \in \text{Dom}(f)$.

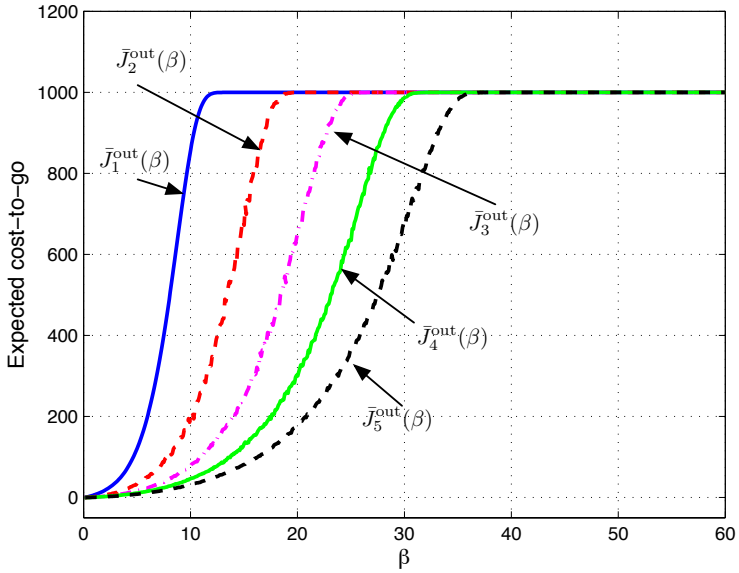

Figure 3.2: Expected cost-to-go function when the fading is i.i.d. truncated exponential with threshold 0.001 and the outage penalty is $M = 1000$

thus,

$$\lim_{\beta_1 \to \infty} \bar{J}_1^{\text{out}}(\beta_1) = M. \tag{3.5}$$

Furthermore, we can observe that

$$\bar{J}_t^{\text{out}}(\beta_t) \leq M, \tag{3.6}$$

for all β_t and t by induction. Figure 3.2 illustrates the expected cost-to-go curves $\bar{J}_t^{\text{out}}$ by numerically evaluating (3.1) for the truncated exponential variable with threshold 0.001 and the outage penalty $M = 1000$. If we let $E_t(b_t, g_t)$ be the energy cost to transmit b_t bits under channel state g_t at slot t, i.e., $E_t(b_t, g_t) = (e^{b_t} - 1)/g_t$, then

$$E_t(b_t, g_t) \leq M \qquad \forall b_t \geq 0, \ \forall g_t \geq 0, \ \forall t \geq 1. \tag{3.7}$$

This implies that the scheduling problem has a peak energy constraint at all time slots.

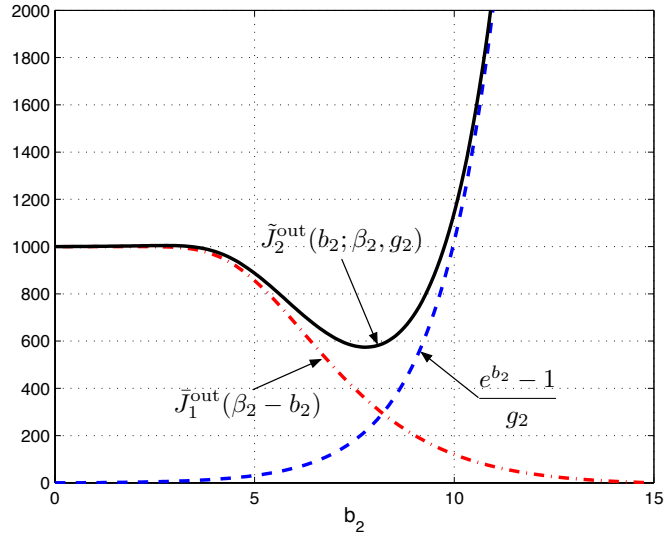

Figure 3.3: Illustration of $\tilde{J}_2^{\text{out}}$ when $\beta_2 = 15$, $M = 1000$, $g_2 = 1$, and g_1 is a truncated exponential variable with threshold 0.001

3.1.2 Optimal Scheduling Function at $t = 2$

Since we adopt the descending time index, the scheduling function in the final time slot ($t = 1$) is identical to the $T = 1$ scheduler. At $t = 2$, the M-outage scheduling problem is given by:

$$J_2^{\text{out}}(\beta_2, g_2) = \min_{0 \le b_2 \le \beta_2} \left\{ \frac{e^{b_2} - 1}{g_2} + \bar{J}_1^{\text{out}}(\beta_2 - b_2) \right\} \tag{3.8}$$

where $\bar{J}_1^{\text{out}}$ is defined in (3.3), which is quasiconvex. This optimization is neither convex nor quasiconvex. If we let $\tilde{J}_2^{\text{out}}$ be the objective function in the optimization (3.8), i.e.,

$$\begin{aligned} \tilde{J}_2^{\text{out}}(b_2;\beta_2,g_2) &= \frac{e^{b_2}-1}{g_2} + \bar{J}_1^{\text{out}}(\beta_2 - b_2) \\ &= \frac{e^{b_2}-1}{g_2} + \int_0^{\frac{e^{\beta_2-b_2}-1}{M}} M dF(x) + \int_{\frac{e^{\beta_2-b_2}-1}{M}}^{\infty} \frac{e^{\beta_2-b_2}-1}{x} dF(x), \end{aligned} \tag{3.9}$$

the optimal solution is determined by minimizing $\tilde{J}_2^{\text{out}}$, whose shape is illustrated in Fig. 3.3 for some parameters. Notice that $\tilde{J}_2^{\text{out}}$ is not necessarily quasiconvex with respect to b_2 for every given β_2, g_2, and M. Figure 3.4 shows an example of $\tilde{J}_2^{\text{out}}$ such that the level sets are not convex for all levels, and therefore $\tilde{J}_2^{\text{out}}$ is not quasiconvex.

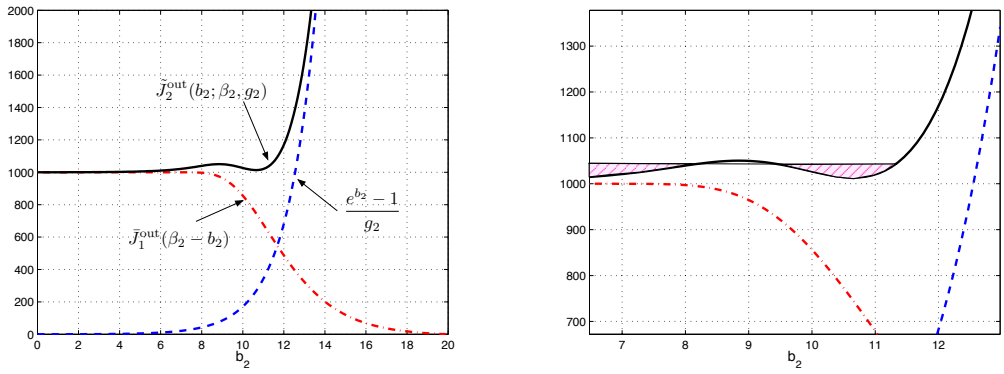

(a) Overall (b) Zoom

Figure 3.4: Non-quasiconvexity of $\tilde{J}_2^{\text{out}}$ when $\beta_2 = 20$, $M = 1000$, $g_2 = 6$, and g_1 is a truncated exponential variable with threshold 0.001

Since the optimization in (3.8) is not convex (nor quasiconvex), systematic approaches such as the KKT conditions (sequence of convex feasibility problems for quasiconvex cases) cannot be applied. Instead, numerical methods are possible approaches. However, our concern is more on the effects of scheduling parameters on the scheduling function, not the approach to the solution. With this concern, we will focus on the optimal solution itself, instead of how to find the solution.

If we assume that the distribution F is continuous (i.e., the channel fading g is a continuous random variable), $\tilde{J}_2^{\text{out}}$ is continuous and differentiable in b_2, and therefore the optimal solution to (3.8) lies either at the boundary points (0 or β_2) or at the stationary points of the objective. In this case, the optimization in (3.8) can be solved by evaluating all possible candidate points, i.e., the boundary points (0 or β_2) and the stationary points of the objective function.

Stationary Points

Since the boundary points are known by default, we focus on the stationary points and their relation to the optimal solution. We first look at the stationary point for the non-outage problem and then compare with the stationary points for the M-outage problem.

For the non-outage scheduling problem at $t = 2$, the optimal bit allocation is determined by

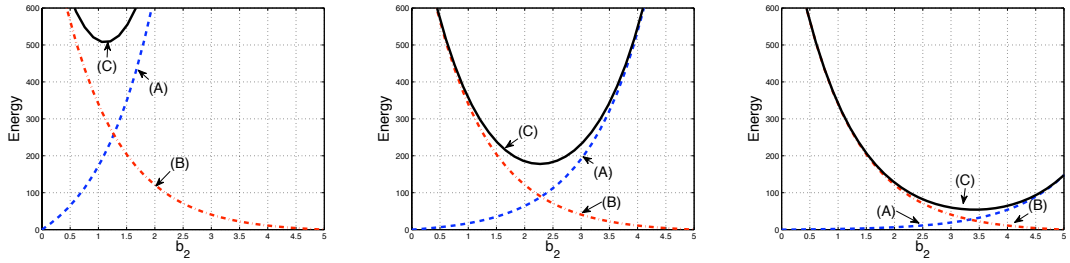

(a) When $g_2 = 0.01$ (b) When $g_2 = 0.1$ (c) When $g_2 = 1$

Figure 3.5: The curves (A) illustrate $E_2^{\text{non-out}}(b_2, g_2)$, the curves (B) illustrate $\bar{J}_1^{\text{non-out}}(\beta_2 - b_2)$, and the curves (C) illustrate $\tilde{J}_2^{\text{non-out}}(b_2; \beta_2, g_2)$ for $g_2 = 0.01, 0.1, 1$ and g_1 is a truncated exponential variable with threshold 0.001

solving (2.10). For the sake of convenience, we re-write the equation as

$$J_2^{\text{non-out}}(\beta_2, g_2) = \min_{0 \le b_2 \le \beta_2} \left[\overbrace{\underbrace{\frac{e^{b_2} - 1}{g_2}}_{E_2^{\text{non-out}}} + \underbrace{(e^{\beta_2 - b_2} - 1)\,\mathbb{E}\left[\frac{1}{g_1}\right]}_{\bar{J}_2^{\text{non-out}}}}^{\tilde{J}_2^{\text{non-out}}} \right], \tag{3.10}$$

where $E_2^{\text{non-out}}$, $\bar{J}_1^{\text{non-out}}$, and $\tilde{J}_2^{\text{non-out}}$ are defined accordingly, similar to the M-outage problem. These $E_2^{\text{non-out}}$, $\bar{J}_1^{\text{non-out}}$, and $\tilde{J}_2^{\text{non-out}}$ are illustrated as functions of b_2 in Fig. 3.5 for several parameters. Notice that $\tilde{J}_2^{\text{non-out}}$ is convex and it has a unique, if any, stationary point such that $(\tilde{J}_2^{\text{non-out}})'(b_2) = 0$, i.e.,

$$b_2^{\text{non-out, stationary}} = \frac{1}{2}\beta_2 + \frac{1}{2}\log\left(g_2\,\mathbb{E}\left[\frac{1}{g_1}\right]\right). \tag{3.11}$$

In Chapter 2, we have studied that the optimal b_2 for the non-outage problem is determined by (2.11). This can be understood in terms of the stationary point in (3.11). If the stationary point is in $[0, \beta_2]$, the stationary point is optimal. If not, either boundary point (0 or β_2) close to the stationary point is the optimal, which is obtained by the truncation operation.

For the M-outage problem, the stationary points can be obtained by differentiating $\tilde{J}_2^{\text{out}}$ in (3.9) with respect to b_2 and setting it to zero, i.e.,

$$b_2^{\text{stationary}} = \frac{1}{2}\beta_2 + \frac{1}{2}\log\left(g_2 \int_{\frac{e^{\beta_2 - b_2^{\text{stationary}}} - 1}{M}}^{\infty} \frac{1}{x} dF(x)\right). \tag{3.12}$$

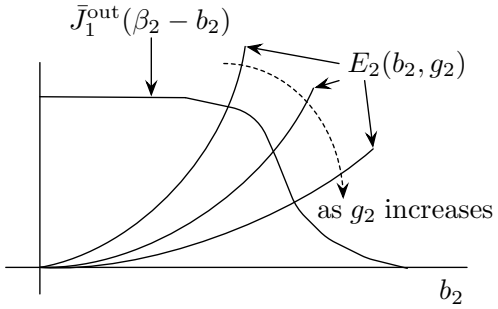

Figure 3.6: Illustration of E_2 and $\bar{J}_1^{\text{out}}$ for $\tilde{J}_2^{\text{out}}$ as varying g_2 when β_2 is fixed

Notice that the formula in (3.12) is very similar to (3.11) except for one term in the argument of the logarithmic function. As a sanity check, we can see that the two different terms coincide when $M \to \infty$. As we have an argument of the balance between opportunistic communication and delay-limited communication for the non-outage problem in Chapter 2, we can have the same interpretation for the M-outage problem from the stationary point formula in (3.12) when the optimal occurs at a stationary point.

Behavior of the Optimal Scheduler at $t = 2$

Because of non-convexity of the expected future cost function, non-smooth allocation may occur. The cost function of the optimal $t = 2$ M-outage scheduler in (3.8) consists of two parts: $E_2(b_2, g_2)$ and $\bar{J}_1^{\text{out}}(\beta_2 - b_2)$ that denote the energy costs at $t = 2$ and $t = 1$, respectively. If the pdf of the channel state $f(x)$ vanishes as x increases, $\bar{J}_1^{\text{out}}(\beta_2 - b_2)$ has a flat region as illustrated in Fig. 3.3 and is no longer convex. Because of this flat region, non-smooth allocation behavior associated with the boundary cases ($b_2^{\text{out}} = 0$ or $b_2^{\text{out}} = \beta_2$) occurs depending on β_2 and g_2. We will investigate the allocation behavior as g_2 increases while fixing β_2 and vice versa.

When β_2 is fixed large enough for $\bar{J}_1^{\text{out}}(\beta_2 - b_2)$ to have a flat region, the optimal bit allocation b_2^{out} increases discontinuously as g_2 increases. To see this, let us examine the total cost function that consists of two costs as illustrated in Fig. 3.6. When g_2 is small, the two curves $E_2(b, g_2)$ and $\bar{J}_1^{\text{out}}(\beta_2 - b_2)$ meet in the region where $\bar{J}_1^{\text{out}}(\beta_2 - b_2)$ is flat such that the sum $\tilde{J}_2^{\text{out}}(b)$ is increasing. Thus, $b_2 = 0$ is optimal. As g_2 increases, the two curves $\bar{J}_1^{\text{out}}(\beta_2 - b_2)$ and $E_2(b, g_2)$ in Fig. 3.6 meet at a non-flat region such that the minimal sum occurs no longer at $b_2 = 0$. The value of g_2 such that the sum of $\bar{J}_1^{\text{out}}(\beta_2 - b_2)$ and $E_2(b, g_2)$ is smaller that the cost of the flat region

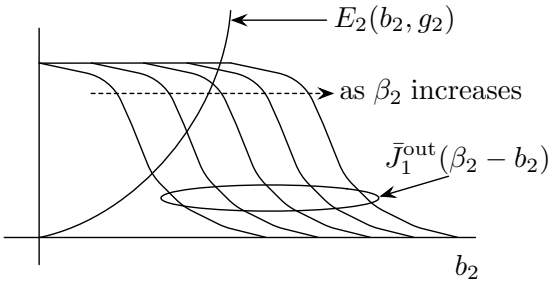

Figure 3.7: Illustration of E_2 and $\bar{J}_1^{\text{out}}$ for $\tilde{J}_2^{\text{out}}$ as varying β_2 when g_2 is fixed

(approximately M) is the point where the discontinuity occurs.

On the other hand, we now investigate the allocation behavior as β_2 varies for a fixed g_2. Figure 3.7 illustrates the variation of the cost $\bar{J}_1^{\text{out}}(\beta_2 - b_2)$ as β_2 increases. When β_2 is small, the two curves meet at a convex part of $\bar{J}_1^{\text{out}}(\beta_2 - b_2)$. As a result, the allocation behavior is quite similar to the non-outage scheduler. As β_2 increases, the allocation b_2^{out} increases up to some point as long as the two curves meet far below the flat region. When the two curve meet near the flat region as β_2 increases, the allocation becomes $b_2^{\text{out}} = 0$.

3.1.3 Optimal Scheduling Function for $t > 2$

From (3.1), a simple form of $\bar{J}_{t-1}^{\text{out}}$ is required to derive a compact scheduling function. Because of the complication associated with the outage penalty M and the boundary cases $0 \le b_t \le \beta_t$, it seems not possible to express $\bar{J}_{t-1}^{\text{out}}$ in a closed form. In particular, the outage penalty renders the future cost function intractable although the boundary cases are relaxed. Notice that we cannot relax the terms related to the outage penalty.

As an alternative, we can rely on numerical methods, i.e., making a lookup table of the cost function $\bar{J}_{t-1}^{\text{out}}$ by discretization and then solving the dynamic optimization (3.1) numerically. Figure 3.2 illustrates $\bar{J}_t^{\text{out}}(\beta)$ for a truncated exponential fading channel.

Figure 3.8 illustrates the outage probability with respect to B as the outage penalty M varies. We can see that the outage probability increases very slowly when B is small, and increases abruptly when B is larger than a certain value, depending on the outage penalty M.

As we did for the non-outage case, we can develop heuristic suboptimal algorithms similar to the expectation substitution and the boundary-relaxed approach, which are left for future work. In the next subsection, we examine a linear bit-energy relationship, the solution of which is given

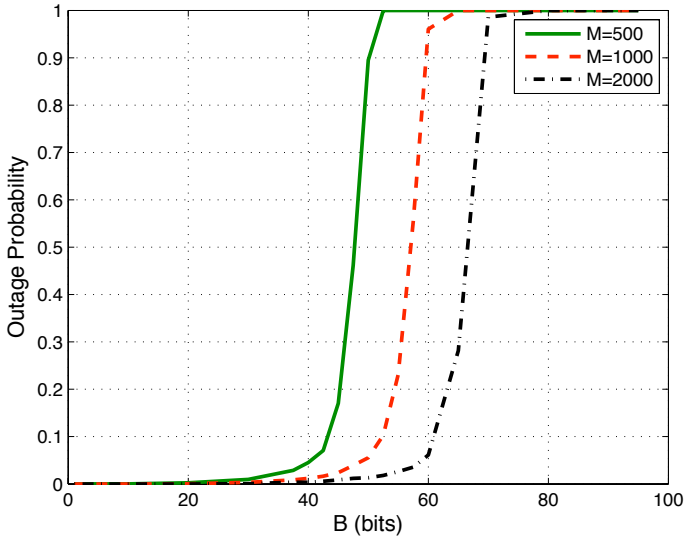

Figure 3.8: Outage probabilities of the discretized optimal scheduler for several M when $T = 10$ and the fading is i.i.d. truncated exponential with threshold 0.001

in an analytic form.

3.1.4 Linear Cost with Outage Penalty

In this subsection we investigate outage scheduling with a linear energy cost function. This linear cost function is suitable for small B environment because

$$e^x - 1 \approx x \tag{3.13}$$

for small x. With this approximated linear cost function, the optimization (3.1) can be written as

$$J_t^{\text{out,lin}}(\beta_t, g_t) = \begin{cases} \min\limits_{0 \le b_t \le \beta_t} \left\{ \frac{b_t}{g_t} + \bar{J}_{t-1}^{\text{out,lin}}(\beta_t - b_t) \right\}, & t = T, \cdots, 2 \\ \min\left\{ \frac{\beta_1}{g_1}, M \right\}, & t = 1, \end{cases} \tag{3.14}$$

where $\bar{J}_{t-1}^{\text{out,lin}}(\beta) = \mathbb{E}[J_{t-1}^{\text{out,lin}}(\beta, g_{t-1})]$.

Lemma 3.1. *If the pdf f of the channel state g is continuous, then the cost-to-go function $\bar{J}_t^{out,lin}$ is concave.*

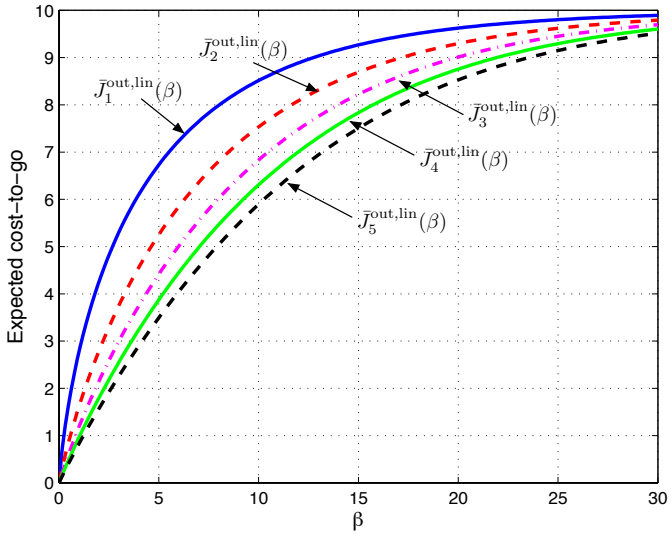

Figure 3.9: Expected cost-to-go for the linear cost M-outage scheduling $\bar{J}_t^{\text{out,lin}}$ when the fading is i.i.d. truncated exponential with threshold 0.001 and the outage penalty is $M = 10$

Proof. See Section 3.6.1. □

Figure 3.9 illustrates the concavity of the cost-to-go function for i.i.d. truncated exponential fading distribution with threshold 0.001. Because of the concavity of the cost-to-go function in a minimization problem, the optimal solution to the optimization in (3.14) lies at one of the boundary points, and thus a threshold policy is the optimal. This is precisely stated as:

Theorem 3.2. *For the linear cost M-outage penalty scheduling problem as in* (3.14)*, the optimal solution is given by*

$$b_t^{out,lin}(\beta_t, g_t) = \begin{cases} \beta_t, & \text{if } g_t \geq \frac{\beta_t}{\bar{J}_{t-1}^{out,lin}(\beta_t)}, \\ 0, & \text{else}, \end{cases} \tag{3.15}$$

and the cost-to-go function is given recursively by

$$\bar{J}_t^{out,lin}(\beta_t) = \begin{cases} \mathbb{E}\left[\frac{\beta_t}{g_t} \middle| g_t \geq \frac{\beta_t}{\bar{J}_{t-1}^{out,lin}(\beta_t)}\right] \Pr\left\{g_t \geq \frac{\beta_t}{\bar{J}_{t-1}^{out,lin}(\beta_t)}\right\} + \bar{J}_{t-1}^{out,lin}(\beta_t) \Pr\left\{g_t < \frac{\beta_t}{\bar{J}_{t-1}^{out,lin}(\beta_t)}\right\}, & t \geq 1 \\ M, & t = 0. \end{cases} \tag{3.16}$$

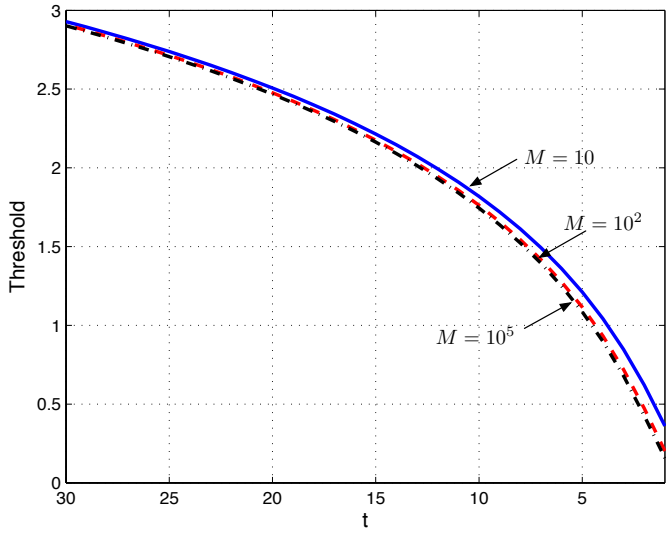

Figure 3.10: Threshold $\beta/\bar{J}_{t-1}(\beta)$ in (3.15) for the linear cost M-outage problem when $\beta = 1$ and the fading is truncated exponential with $\gamma_0 = 0.001$

Proof. See the proof of Lemma 3.1 (Section 3.6.1). □

If we compare the threshold policy in (2.33) and (2.34) for the non-outage problem with this threshold policy in (3.15) , we can see that the threshold of this policy depends on the amount of the unserved bits while the threshold of the former does not depend on the unserved bits. We can deduce that the threshold in (3.15) decreases as t increases because $\bar{J}_t^{\text{out,lin}}(\beta)$ decreases in t for a fixed β, the behavior of which can be shown in Fig. 3.9. It is interesting to note that the threshold does not depend much on the outage penalty M, especially for large t as illustrated in Fig. 3.10. It is because outage is hardly expected to occur for small bits, and also the determination of outage is only made at the final time step.

3.2 Multi-User Scheduling

In this section, we consider scheduling for multiple users, e.g., two-user scheduling is illustrated in Fig. 3.11. From a higher layer, a packet of B^1 bits arrives for user 1, B^2 bits for user 2, and so

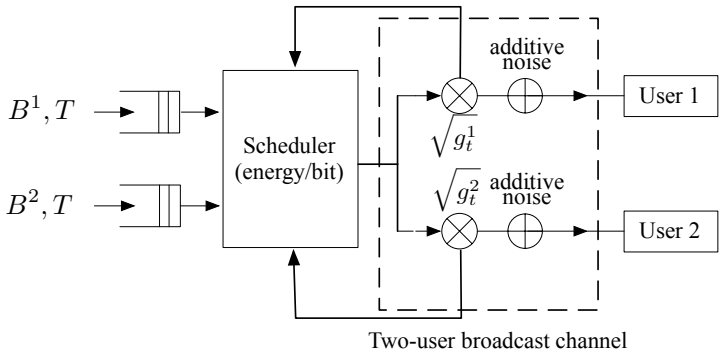

Figure 3.11: Two-user broadcast channel scheduling of delay constrained traffic

on. These packets are required to be transmitted within T time slots[2] . The channel state for user k and slot t is denoted by g_t^k in power units, which is assumed to be iid across users and time slots and to be available causally. A non-causal case is considered in the context of fairness among users for delay-limited traffic in [CMK07]. As formulated for single-user scheduling in Chapter 2, the scheduler determines the number of bits to transmit at every time slot for each user using the fading realization/statistics to minimize the total expected transmit energy while satisfying the deadline constraint.

We assume that the additive noise is Gaussian with unit variance and operate on the boundary of the capacity region of the broadcast channel (BC). This Gaussian broadcast channel forms a degraded broadcast channel such that the boundary of the capacity region is known, while the capacity region of the general broadcast channel is unknown [CT91]. If we let $\pi(\cdot)$[3] be the permutation such that

$$g_t^{\pi(1)} \geq g_t^{\pi(2)} \geq \cdots \geq g_t^{\pi(K)}, \tag{3.17}$$

then the boundary of the capacity region is characterized by [CT91, LG01b]

$$b_t^{\pi(k)} = \begin{cases} \log\left(1 + g_t^{\pi(1)} E_t^{\pi(1)}\right), & k = 1, \\ \log\left(1 + \frac{E_t^{\pi(k)}}{1/g_t^{\pi(k)} + \sum_{l=1}^{k-1} E_t^{\pi(l)}}\right), & k = 2, \cdots, K, \end{cases} \tag{3.18}$$

which represents the maximum number of bits that can be transmitted for each user at time slot t when the amount of energy allocated to the $\pi(k)$th user is $E_t^{\pi(k)}$ and the sum energy is

[2] The deadlines are identical for all users.

[3] This ordering is also a function of time. But we drop time index t in this function to simplify notation. Time index can be understood from the context in most cases.

constrained by E_t, i.e.,

$$\sum_{k=1}^{K} E_t^{\pi(k)} = E_t. \tag{3.19}$$

By inverting these, the energy cost for each user is given by [LG01b]

$$E_t^{\pi(k)} = \begin{cases} \left(e^{b_t^{\pi(1)}} - 1\right) \frac{1}{g_t^{\pi(1)}}, & k = 1, \\ \left(e^{b_t^{\pi(k)}} - 1\right) \left(\frac{1}{g_t^{\pi(k)}} + \sum_{l=1}^{k-1} E_t^{\pi(l)}\right), & k = 2, \cdots, K. \end{cases} \tag{3.20}$$

Therefore, the sum energy cost is given by

$$\begin{aligned} E_t(\{b_t^k\}_{k=1}^K, \{g_t^k\}_{k=1}^K) &= \sum_{k=1}^{K} E_t^{\pi(k)} \\ &= \sum_{k=1}^{K} \left\{ e^{\sum_{l=k+1}^{K} b_t^{\pi(l)}} \left(e^{b_t^{\pi(k)}} - 1\right) \frac{1}{g_t^{\pi(k)}} \right\} + \left(e^{b_t^{\pi(K)}} - 1\right) \frac{1}{g_t^{\pi(K)}}. \end{aligned} \tag{3.21}$$

With this sum energy cost function (3.21), we can formulate the K-user energy-efficient scheduler that minimizes

$$\min \mathbb{E}\left[\sum_{t=1}^{T} E_t\left(\{b_t^k\}_{k=1}^K, \{g_t^k\}_{k=1}^K\right)\right] \tag{3.22}$$

subject to $\sum_{t=1}^{T} b_t^k = B^k$ and $b_t^k \geq 0$ for all $k = 1, \cdots, K$. Under the causal CSI and introducing the queue size variable β_t^k representing the unserved bits at the beginning of slot t and user k, the optimization (3.22) can be formulated as a DP:

$$J_t^{\text{multi}}(\{\beta_t^k\}_{k=1}^K, \{g_t^k\}_{k=1}^K) = \begin{cases} \min\limits_{0 \leq b_t^k \leq \beta_t^k} \left\{E_t(\{b_t^k\}_{k=1}^K, \{g_t^k\}_{k=1}^K) + \bar{J}_{t-1}^{\text{multi}}(\beta_t^1 - b_t^1, \cdots, \beta_t^K - b_t^K)\right\}, & t = T, \cdots, 2, \\ E_1(\{b_1^k\}_{k=1}^K, \{g_1^k\}_{k=1}^K), & t = 1, \end{cases} \tag{3.23}$$

where $\bar{J}_{t-1}^{\text{multi}}(\{\beta_{t-1}^k\}_{k=1}^K) = \mathbb{E}\left[J_{t-1}^{\text{multi}}(\{\beta_{t-1}^k\}_{k=1}^K, \{g_{t-1}^k\}_{k=1}^K)\right]$ denotes the cost-to-go function.

3.2.1 Two-User Scheduling Problem

For the sake of simplicity, we only consider a two-user scheduling problem (i.e., $K = 2$) of (3.23) in the sequel.

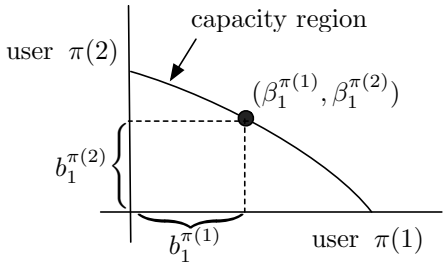

Figure 3.12: Optimal bit allocation in the capacity region at $t = 1$

At the final time step $t = 1$, all the unserved bits of each user should be served regardless of the channel states:

$$b_1^1(\beta_1^1, g_1^1) = \beta_1^1, \tag{3.24}$$

$$b_1^2(\beta_1^2, g_1^2) = \beta_1^2, \tag{3.25}$$

where β_1^1 and β_1^2 denote the unserved bits at the beginning of time slot 1 in our convention. Figure 3.12 illustrates this bit allocation with the capacity region. The total energy cost at $t = 1$ to transmit $\beta_1^{\pi(1)}$ and $\beta_1^{\pi(2)}$ for the two users can be calculated using (3.21) [JG03] as:

$$\frac{e^{\beta_1^{\pi(2)}}\left(e^{\beta_1^{\pi(1)}} - 1\right)}{g_1^{\pi(1)}} + \frac{e^{\beta_1^{\pi(2)}} - 1}{g_1^{\pi(2)}}. \tag{3.26}$$

Thus, the resulting expected energy cost-to-go is given by

$$\begin{aligned} \bar{J}_1^{\text{multi}}(\beta_1^1, \beta_1^2) = \mathbb{E}\left[\frac{e^{\beta_1^2}(e^{\beta_1^1} - 1)}{g_1^1} + \frac{e^{\beta_1^2} - 1}{g_1^2}\middle| g_1^1 > g_1^2\right] \Pr\left\{g_1^1 > g_1^2\right\} + \\ \mathbb{E}\left[\frac{e^{\beta_1^1} - 1}{g_1^1} + \frac{e^{\beta_1^1}(e^{\beta_1^2} - 1)}{g_1^2}\middle| g_1^1 \le g_1^2\right] \Pr\left\{g_1^1 \le g_1^2\right\}. \end{aligned} \tag{3.27}$$

From the assumption that g_1^1 and g_1^2 are iid,

$$\Pr\left\{g_1^1 > g_1^2\right\} = \Pr\left\{g_1^1 \le g_1^2\right\} = \frac{1}{2}. \tag{3.28}$$

By letting,

$$\frac{1}{\gamma} = \mathbb{E}\left[\frac{1}{\min(g_1^1, g_1^2)}\right], \tag{3.29}$$

$$\frac{1}{\Gamma} = \mathbb{E}\left[\frac{1}{\max(g_1^1, g_1^2)}\right], \tag{3.30}$$

we can simply write

$$\bar{J}_1^{\text{multi}}(\beta_1^1,\beta_1^2)=\frac{1}{2}\left[\frac{e^{\beta_1^2}(e^{\beta_1^1}-1)}{\Gamma}+\frac{e^{\beta_1^2}-1}{\gamma}+\frac{e^{\beta_1^1}-1}{\gamma}+\frac{e^{\beta_1^1}(e^{\beta_1^2}-1)}{\Gamma}\right]. \tag{3.31}$$

We now look for the scheduling function and the corresponding cost for $t=2$. At $t=2$, g_2^1 and g_2^2 are deterministic quantities while g_1^1 and g_1^2 are random. Without loss of generality, we assume that $g_2^1 > g_2^2$. From (3.21) and (3.23), the total energy cost at $t=2$ is given by the following optimization:

$$\begin{aligned} J_2^{\text{multi}}(\beta_2^1,\beta_2^2,g_2^1,g_2^2) = &\text{minimize } \left\{\frac{e^{b_2^2}(e^{b_2^1}-1)}{g_2^1}+\frac{e^{b_2^2}-1}{g_2^2}+\bar{J}_1^{\text{multi}}(\beta_2^1-b_2^1,\beta_2^2-b_2^2)\right\}, \\ &\text{subject to } 0\le b_2^1\le\beta_2^1, \\ &\qquad\qquad 0\le b_2^2\le\beta_2^2, \end{aligned} \tag{3.32}$$

where $\bar{J}_1^{\text{multi}}$ is specified in (3.31). Notice that the optimization in (3.32) is convex:

Proposition 3.3. *If*

$$\mathbb{E}\left[\frac{1}{\max(g_1^1,g_1^2)}\right]<\mathbb{E}\left[\frac{1}{\min(g_1^1,g_1^2)}\right]<\infty, \tag{3.33}$$

then the optimization (3.32) *is convex.*

Proof. See Section 3.6.2. □

Although the optimization in (3.32) is convex, obtaining an analytic solution is a challenging task. Instead, we can solve the optimization iteratively with the coordinate-descent method [Ber03]. With this method, the two variable optimization (3.32) can be viewed as a series of one variable optimizations. That is, solving the optimization for one user while setting the other user's bit allocation be fixed, then solving the second user's optimization with the updated first user's bit allocation, continuing this process for the first user again, and so on. Because of the convexity shown in Proposition 3.3, this iterative approach will yield the optimal solution.

For the coordinate-descent method, the two variable optimization problem (3.32) can be decomposed into the following one variable optimizations for the two users:

$$\text{User 1}: \quad \min_{0\le b_2^1\le\beta_2^1}\frac{e^{b_2^2}e^{b_2^1}}{g_2^1}+\left(\frac{e^{\beta_2^2-b_2^2}}{\Gamma}+\frac{1}{2\gamma}\right)e^{\beta_2^1-b_2^1}, \tag{3.34}$$

$$\text{User 2}: \quad \min_{0\le b_2^2\le\beta_2^2}\frac{e^{b_2^1}e^{b_2^2}}{g_2^1}+\frac{e^{b_2^2}}{g_2^2}+\left(\frac{e^{\beta_2^1-b_2^1}}{\Gamma}+\frac{1}{2\gamma}\right)e^{\beta_2^2-b_2^2}. \tag{3.35}$$

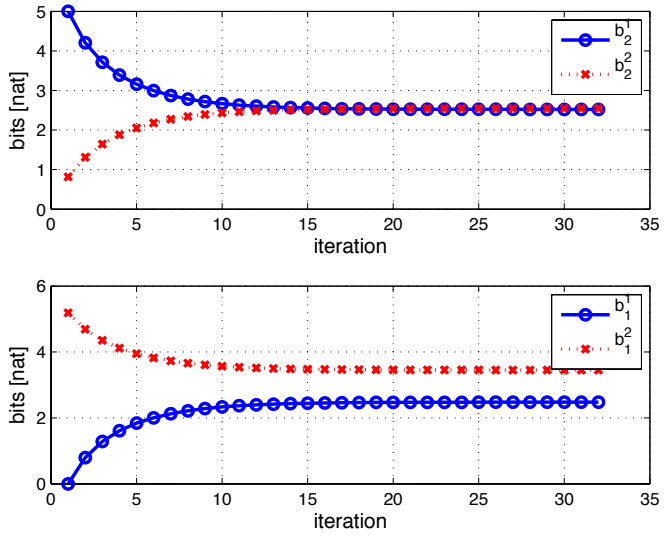

Figure 3.13: Convergence of the bit allocation algorithm for a two-user $T = 2$ scheduling problem

Since these two optimizations are convex, the optimal solutions are obtained by taking the derivative and setting it to zero:

$$b_2^1 = \left\langle \frac{1}{2}\beta_2^1 + \frac{1}{2}\log\left(\frac{\frac{e^{\beta_2^2 - b_2^2}}{\Gamma} + \frac{1}{2\gamma}}{\frac{e^{b_2^2}}{g_2^1}}\right)\right\rangle_0^{\beta_2^1}, \tag{3.36}$$

$$b_2^2 = \left\langle \frac{1}{2}\beta_2^2 + \frac{1}{2}\log\left(\frac{\frac{e^{\beta_2^1 - b_2^1}}{\Gamma} + \frac{1}{2\gamma}}{\frac{e^{b_2^1}}{g_2^1} + \frac{1}{g_2^2}}\right)\right\rangle_0^{\beta_2^2}, \tag{3.37}$$

$b_1^1 = \beta_2^1 - b_2^1$, and $b_1^2 = \beta_2^2 - b_2^2$.

Figure 3.13 illustrates a numerical example for the convergence of the iterations using the coordinate descent method. For this numerical example, we use the parameters: $\beta_2^1 = 5$, $\beta_2^2 = 6$, $g_2^1 = 0.2717$, $g_2^2 = 0.1151$, and g_1^1 and g_1^2 are i.i.d. truncated exponential variables with threshold 0.001. As can be seen, the iteration converges and moreover it converges to a boundary point of capacity regions for the two time slots as shown in Fig. 3.14. This figure shows the trace of the bit allocation with the capacity region.

There is one interesting observation regarding the tangent lines of the two capacity regions at the optimal operating points. We denote a point on the boundary of the capacity region at $t = 2$

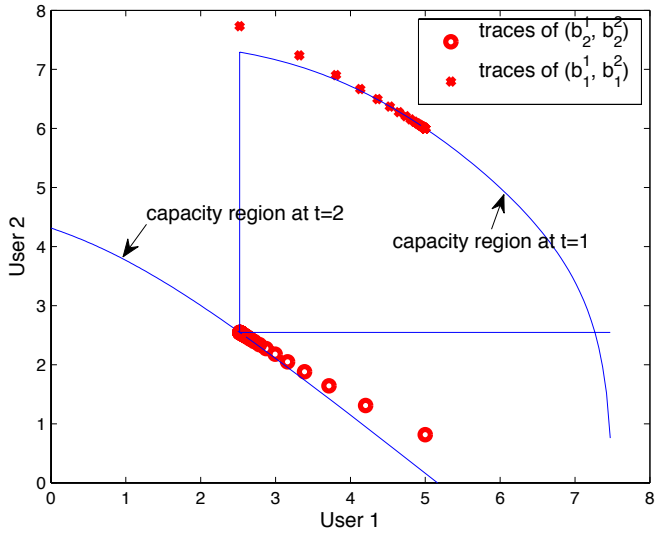

Figure 3.14: Trace of the bit allocation for a two-user $T = 2$ scheduling problem

as an ordered pair (b_2^1, b_2^2). Since one of these two values in a pair is determined, the other one is determined automatically because the pair is on the boundary of the capacity region. That is, b_2^2 is a function of b_2^1. Thus, we define the slope at a particular $(b_2^1)^*$ as (see Fig. 3.15 for illustration):

$$\Delta_2((b_2^1)^*) = \left|\frac{\partial b_2^2}{\partial b_2^1}\right|_{(b_2^1)^*}. \tag{3.38}$$

Similarly, we can define a slope for $t = 1$:

$$\Delta_1((b_1^1)^*) = \left|\frac{\partial b_1^2}{\partial b_1^1}\right|_{(b_1^1)^*}. \tag{3.39}$$

At the optimal $((b_1^1)^{\text{opt}}, (b_1^2)^{\text{opt}})$ and $((b_2^1)^{\text{opt}}, (b_2^2)^{\text{opt}})$, assuming that the optimal occurs at an interior point (i.e., $0 < (b_2^2)^{\text{opt}} < \beta_2^2$ and $0 < (b_2^1)^{\text{opt}} < \beta_2^1$), the two slopes are identical. This fact can be simply verified by

$$\Delta_2((b_2^1)^{\text{opt}}) = \left|\frac{\partial b_2^2}{\partial b_2^1}\right|_{(b_2^1)^{\text{opt}}} = \left|\frac{\partial(\beta_2^2 - b_1^2)}{\partial(\beta_2^1 - b_1^1)}\right|_{\beta_2^1 - (b_2^1)^{\text{opt}}} = \left|\frac{\partial b_1^2}{\partial b_1^1}\right|_{(b_1^1)^{\text{opt}}} = \Delta_1((b_1^1)^{\text{opt}}), \tag{3.40}$$

since $b_2^1 + b_1^1 = \beta_2^1$ and $b_2^2 + b_1^2 = \beta_2^2$.

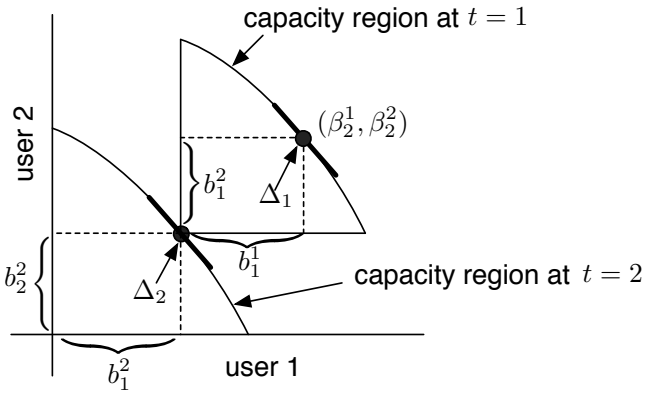

Figure 3.15: Solution to the two-user $T = 2$ scheduling problem with capacity regions

Extending the idea to an arbitrary $T(> 2)$ is pessimistic. Because we cannot analytically formulate J_2^{multi} in (3.32), we cannot obtain the cost-to-go function $\bar{J}_2^{\text{multi}} \left(= \mathbb{E}[J_2^{\text{multi}}]\right)$ analytically. Therefore, this simple method cannot be applied for $T = 3$, and thus $\bar{J}_3^{\text{multi}}$ cannot be found analytically. In this reason, the extension to $T > 2$ for a simple solution cannot be made.

In order to make the problem tractable for $T > 2$, we can instead modify the problem setup. One way is simplifying the energy-bit relations among users. According to the energy-bit relation in (3.20), the energy cost of one user affects the energy cost of some other users. If we devise a system that mitigates the interrelationship in the energy cost among users, we can employ the single-user scheduling as in Chapter 2 for a multi-user scheduling problem. For example, let us consider a base station equipped with multiple antennas that performs zero-forcing beamforming to remove the interference at all the users' terminal. Each link from the base station to a user terminal can be regarded as a single-user channel, and an equivalent channel state can be obtained with the beamforming vector. Thus, we can apply the single-user schedulers developed in Chapter 2 for this setting. Other options can be considered, such as TDM/TDMA scheduling, to avoid coupling between users.

3.3 Scheduling for Parallel/MIMO Channels

Returning to single-user scheduling, this section considers delay constrained scheduling for parallel/MIMO channels as illustrated in Fig. 3.16. Since a MIMO channel can be decomposed into a set of parallel channels [Tel95], we start with parallel channel scheduling. In another

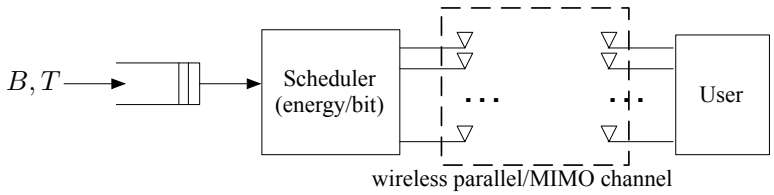

Figure 3.16: Single-user delay constrained scheduling over parallel/MIMO channels

perspective, parallel channel scheduling in itself is useful for frequency selective channels when OFDM is employed, where the set of subchannels forms a set of parallel channels.

If resource allocation (scheduling) of parallel channels is considered for one time slot, then the energy and bits are associated with the *delay-limited capacity*, which is generally not characterized in closed form. Jorswieck and Boche found upper and lower bounds of the delay-limited capacity of parallel channels [JB05]. The upper bound obtained by assuming that all the subchannels are utilized is shown to be tight for high SNR, while the lower bound obtained by assuming that only one subchannel is utilized is shown to be tight for low SNR. We will use the same technique to develop closed-form solutions for each asymptotic region. Jorswieck and Boche also studied the impact on the delay-limited capacity of fading parameters such as correlations and line-of-sight components [JB07].

3.3.1 Parallel Channel Scheduling

We consider a scheduling problem for L parallel channels at each time slot. In this case, determining the bit allocation is to be processed over two dimensions simultaneously: $t = T, \cdots, 1$ (time-domain) and $l = 1, \cdots, L$ (parallel channels). As before, we denote the discrete-time index t in subscript and denote the parallel channel index in superscript, i.e., g_t^l denotes the channel state at time slot t and the l-th parallel channel. Likewise, b_t^l denotes the bit allocation at l-th parallel channel at slot t.

Assuming i.i.d. channel states and causal CSI, the scheduler needs to determine the number of bits b_t^l allocating at slot t and l-th channel with the knowledge of the unserved bits β_t and the

current channel states $\{g_t^l\}_{l=1}^L$ but without the knowledge of $\{\{g_s^l\}_{l=1}^L\}_{s=t-1}^1$:

$$\begin{array}{cccc|ccc} g_T^1, & g_{T-1}^1, & \cdots, & g_t^1, & g_{t-1}^1 & \cdots, & g_1^1 \\ g_T^2, & g_{T-1}^2, & \cdots, & g_t^2, & g_{t-1}^2, & \cdots, & g_1^2 \\ \vdots & \vdots & \vdots & \vdots & \vdots & \vdots & \vdots \\ g_T^L, & g_{T-1}^L, & \cdots, & g_t^L, & g_{t-1}^L, & \cdots, & g_1^L \end{array}$$
unknown

The total transmitted bits at t over L parallel channels are denoted by b_t, i.e., $b_t = \sum_{l=1}^L b_t^l$. Then, the scheduling task can be formulated into two hierarchic levels:

$$J_t^{\text{parallel}}(\beta_t, \{g_t^l\}_{l=1}^L) = \begin{cases} \min\limits_{0\le b_t\le\beta_t} \left\{ E_t^{\text{parallel}}(b_t, \{g_t^l\}_{l=1}^L) + \bar{J}_{t-1}^{\text{parallel}}(\beta_t - b_t) \right\}, & t \ge 2, \\ E_1^{\text{parallel}}(\beta_1, \{g_t^l\}_{l=1}^L), & t = 1, \end{cases} \tag{3.41}$$

where

$$\begin{aligned} E_t^{\text{parallel}}(b_t, \{g_t^l\}_{l=1}^L) = \min_{b_t^1,\cdots,b_t^L} & \sum_{l=1}^L \frac{e^{b_t^l} - 1}{g_t^l} \\ \text{subject to } & \sum_{l=1}^L b_t^l = b_t \\ & b_t^l \ge 0, \quad \forall l. \end{aligned} \tag{3.42}$$

Once b_t is determined by solving (3.58), determining $b_t^1, \cdots, b_t^L$ can be done in a straightforward manner because the optimization (3.42) can be solved by an inverse waterfilling. However, determining b_t cannot be done analytically in general because of the complications of the expected future energy cost $\bar{J}_{t-1}^{\text{parallel}}$ like the single-channel case. For this reason, we will consider suboptimal policies for which $\bar{J}_{t-1}^{\text{parallel}}$ has simple forms.

Case: Large B

When B is large enough so that all the time slots are utilized (i.e., $b_t^{\text{parallel}} \gg 0$, $t = T, \cdots, 1$) and all the subchannels in the set of L parallel channels are utilized at every t (i.e., $b_t^l \gg 0$, $l = 1, \cdots, L$, $\forall t$), we can approximate

$$e^{b_t^l} - 1 \approx e^{b_t^l}, \quad \text{for } b_t^l \gg 0. \tag{3.43}$$

Then the optimization (3.42) can be approximately[4] solved by using the standard Lagrangian method [BV04] and the closed form solution is given by

$$b_t^l = \frac{b_t}{L} + \log\left(\frac{g_t^l}{\mathbb{G}(g_t^1, g_t^2, \cdots, g_t^L)}\right), \quad \forall l, \ \forall t, \tag{3.44}$$

where $\mathbb{G}(g_t^1, g_t^2, \cdots, g_t^L) = \left(\prod_{l=1}^L g_t^l\right)^{1/L}$ and the corresponding objective function value is given by

$$E_t^{\text{parallel}}(b_t, \{g_t^l\}_{l=1}^L) \approx \frac{Le^{\frac{b_t}{L}}}{\mathbb{G}(g_t^1, g_t^2, \cdots, g_t^L)}. \tag{3.45}$$

With this closed-form approximation of $E_t^{\text{parallel}}(b_t, \{g_t^l\}_{l=1}^L)$, we will prove that the expected cost-to-go function in (3.58) is given by

$$\bar{J}_t^{\text{parallel}}(\beta) = Lte^{\frac{\beta}{Lt}}\,\mathbb{G}\left(\nu_{Lt}, \nu_{L(t-1)}, \cdots, \nu_L\right). \tag{3.46}$$

When $t = 1$,

$$\begin{aligned} \bar{J}_1^{\text{parallel}}(\beta) &= \mathbb{E}\left[E_1^{\text{parallel}}(\beta, \{g_1^l\}_{l=1}^L)\right] \\ &= \mathbb{E}\left[\frac{Le^{\frac{\beta}{L}}}{\mathbb{G}(g_1^1, g_1^2, \cdots, g_1^L)}\right] = Le^{\frac{\beta}{L}}\nu_L. \end{aligned} \tag{3.47}$$

If we suppose (3.46) holds for $t-1$, the optimization (3.58) can be written as

$$J_t^{\text{parallel}}(\beta_t, \{g_t^l\}_{l=1}^L) = \min_{b_t}\left\{\frac{Le^{\frac{b_t}{L}}}{\mathbb{G}(g_t^1, \cdots, g_t^L)} + L(t-1)e^{\frac{\beta_t - b_t}{L(t-1)}}\,\mathbb{G}\left(\nu_{L(t-1)}, \cdots, \nu_L\right)\right\}, \tag{3.48}$$

which can be solved by setting the derivative of the objective to zero:

$$b_t^{\text{parallel}}(\beta_t, \{g_t^l\}_{l=1}^L) = \frac{1}{t}\beta_t + \frac{t-1}{t}L\log\left[\mathbb{G}(g_t^1, \cdots, g_t^L)\,\mathbb{G}\left(\nu_{L(t-1)}, \cdots, \nu_L\right)\right]. \tag{3.49}$$

By substituting (3.49) back into (3.48) and taking expectation, we arrive at (3.46). In doing so, a policy under the large B assumption can be obtained in two levels: first perform (3.49) and then (3.44). Notice that (3.44) is approximately obtained for a closed form solution, but $\{b_t^l\}$ can be accurately calculated by waterfilling. With this idea, a suboptimal policy is summarized in Algorithm 3.1 with appropriate truncation.

[4] We can actually solve the optimization (3.42) exactly. The motivation for this approximation is to have a closed form expression for E_t^{parallel} for the next level optimization (3.58).

Algorithm 3.1 Parallel channel scheduling when B is large

Initialization

$$\beta_T = B \tag{3.50}$$

For $t = T$ to 2 (Given: β_t, $g_t^1, \cdots, g_t^L$)

$$b_t^{\text{parallel}} = \left\langle \frac{1}{t}\beta_t + \frac{t-1}{t} L \log\left[\mathbb{G}(g_t^1, \cdots, g_t^L)\, \mathbb{G}\left(\nu_{L(t-1)}, \cdots, \nu_L\right)\right] \right\rangle_0^{\beta_t} \tag{3.51}$$

$$\beta_{t-1} = \beta_t - b_t^{\text{parallel}} \tag{3.52}$$

For $l = 1$ to L

$$b_t^l = \left\langle \frac{b_t^{\text{parallel}}}{L} + \log\left(\frac{g_t^l}{\mathbb{G}(g_t^1, g_t^2, \cdots, g_t^L)}\right) \right\rangle_0^{b_t} \tag{3.53}$$

End

End

When $t = 1$ (Given: β_1, $g_1^1, \cdots, g_1^L$)

$$b_1^{\text{parallel}} = \beta_1 \tag{3.54}$$

For $l = 1$ to L

$$b_1^l = \left\langle \frac{b_1^{\text{parallel}}}{L} + \log\left(\frac{g_1^l}{\mathbb{G}(g_1^1, g_1^2, \cdots, g_1^L)}\right) \right\rangle_0^{b_1} \tag{3.55}$$

End

End

Figure 3.17 illustrates numerical results of the suboptimal policy in Algorithm 3.1 for $L = 2$ and $L = 50$ when $T = 2$. The fading is assumed to be truncated exponential with threshold 0.001 and i.i.d. across time and parallel channels. We can observe that the performance of the suboptimal policy is close to that of the non-causal scheduling for large B. Notice that non-causal policy is a bound for any causal scheduler.

Case: Small B

When B is very small, it is highly possible that only one time slot among the T slots is utilized for the transmission of B bits, i.e., there exists t' such that $b_{t'} > 0$ and $b_t = 0$ for $t \neq t'$. Furthermore,

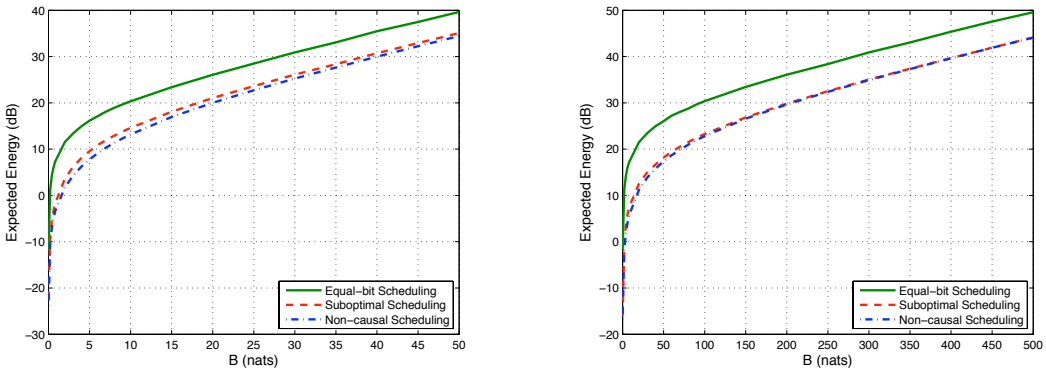

(a) $T = 2$ and $L = 5$ (b) $T = 2$ and $L = 50$

Figure 3.17: Expected energy performance comparison for parallel channel scheduling under i.i.d. block fading distribution

it is possible to utilize only one subchannel in a set of parallel channels, i.e., there exists m' such that $b_{t'}^{m'} > 0$ and $b_t^m = 0$ otherwise. This behavior can be understood by the approximation

$$e^{b_t^m} - 1 \approx b_t^m, \quad \text{for } b_t^m \approx 0 \tag{3.56}$$

in the objective function in (3.42) so that the optimization becomes a linear program (LP). The solution to this LP lies on the boundary of the constraint set such that the solution is an one-shot policy.

If we suppose that slot t is utilized, then

$$E_t^{\text{parallel}}(b_t, \{g_t^m\}_{m=1}^M) \approx \frac{b_t}{g_t^{\max}}, \tag{3.57}$$

where $g_t^{\max} = \max\{g_t^1, \cdots, g_t^M\}$. With this approximate closed form E_t^{parallel}, we can express the DP (3.58) as:

$$J_t^{\text{parallel}}(\beta_t, \{g_t^m\}_{m=1}^M) = \min_{0 \le b_t \le \beta_t} \left\{ \frac{b_t}{g_t^{\max}} + \bar{J}_{t-1}^{\text{parallel}}(\beta_t - b_t) \right\}, \tag{3.58}$$

which makes the expected cost-to-go function $\bar{J}_t^{\text{parallel}}$ also linear, and thus the overall optimization becomes an LP. Therefore, the solution lies on the boundary, i.e., an one-shot policy is the optimal for this case.

The solution to the optimization (3.58) can be obtained similar to Section 2.7.4:

$$b_t = \begin{cases} B, & \text{first } t \text{ such that } g_t^{\pi(1)} > 1/\omega_t, \\ 0, & \text{otherwise,} \end{cases} \tag{3.59}$$

where $g_t^{\pi(1)} = \max\{g_t^1, \cdots, g_t^L\}$. The threshold can be obtained by the same procedure as with (2.34) as:

$$\omega_t = \begin{cases} \mathbb{E}\left[\min\left(\frac{1}{g_t^{\pi(1)}}, \omega_{t-1}\right)\right], & t = T, \cdots, 3, \\ \mathbb{E}\left[\frac{1}{g_t^{\pi(1)}}\right], & t = 2, \\ \infty, & t = 1. \end{cases} \tag{3.60}$$

where the (conditional) expected values of $g_t^{\pi(1)}$ can be found by using order statistics [Dav81]. Because this one-shot policy is identical to the one-shot policy for a single channel, all characteristics of the single-user one-shot policy are applied here as well except using order statistics for $g_t^{\pi(1)}$.

3.3.2 MIMO Scheduling

In frequency domain, parallel channels can be provided by transmitting over multiple carriers that experience frequency selective fading. In this section, however, we consider the case that a set of parallel channel is provided in the spatial domain through multiple antennas. Let $\mathbf{H}_t (\in \mathbb{C}^{N\times M})$ be the MIMO channel state at time slot t, where M and N denote the number of transmit and receive antennas, respectively. Then, the received signal vector $\mathbf{y}_t (\in \mathbb{C}^{N\times 1})$ and the transmit signal vector $\mathbf{x}_t (\in \mathbb{C}^{M\times 1})$ are related by

$$\mathbf{y}_t = \mathbf{H}_t \mathbf{x}_t + \mathbf{z}_t, \tag{3.61}$$

where $\mathbf{z}_t (\in \mathbb{C}^{N\times 1})$ is assumed to be complex Gaussian with unit variance per vector component. From the MIMO channel capacity [Tel95], the maximum number of bits (or nats) b_t that can be transmitted with an energy constraint E_t is given by

$$b_t = \max_{\text{tr}\{\mathbf{Q}_t\} \le E_t} \log\left|\mathbf{I} + \mathbf{H}_t \mathbf{Q}_t \mathbf{H}_t^H\right|, \tag{3.62}$$

where $\mathbf{Q}_t = \mathbb{E}[\mathbf{x}_t \mathbf{x}_t^H]$. We cannot directly invert (3.62) to obtain a close-form expression for the required energy E_t, but we can still denote $E_t(\cdot,\cdot)$ as a function of b_t and $\mathbf{H}_t$ representing the

minimum energy incurred to transmit b_t (nats) under channel state $\mathbf{H}_t$. The resulting scheduling problem becomes

$$\begin{aligned} \min_{b_T,\cdots,b_1} \quad & \mathbb{E}\left[\sum_{t=1}^{T} E_t(b_t,\mathbf{H}_t)\right] \\ \text{subject to} \quad & \sum_{t=1}^{T} b_t = B \\ & b_t \geq 0, \quad \forall t. \end{aligned} \tag{3.63}$$

We assume that $\mathbf{H}_T,\mathbf{H}_{T-1},\cdots,\mathbf{H}_1$ are i.i.d. and the scheduler has only *causal* knowledge of channel states. Then, the optimization (3.63) can be formulated as a DP:

$$b_t^{\text{MIMO}}(\beta_t,\mathbf{H}_t) = \begin{cases} \arg\min\limits_{0\leq b_t\leq\beta_t} \left(E_t(b_t,\mathbf{H}_t) + \mathbb{E}\left[\sum\limits_{s=1}^{t-1} E_s(b_s,\mathbf{H}_s)\Big| b_t\right]\right), & t\geq 2, \\ \beta_1, & t=1. \end{cases} \tag{3.64}$$

At each time slot t, the scheduling task is to determine the bit allocation across antennas with the information of the current channel state $\mathbf{H}_t$ and the unserved bits β_t in order to minimize the total transmit energy satisfying the deadline constraint.

As in the procedure in [Tel95], by assuming $M<N$ and the matrix determinant identity $\left|\mathbf{I}+\mathbf{H}_t\mathbf{Q}_t\mathbf{H}_t^H\right| = \left|\mathbf{I}+\mathbf{Q}_t\mathbf{H}_t^H\mathbf{H}_t\right|$, (3.62) can be expressed as[5] $b_t = \max\limits_{\text{tr}\{\mathbf{Q}_t\}\leq E_t} \log\left|\mathbf{I}+\mathbf{Q}_t\mathbf{H}_t^H\mathbf{H}_t\right|$. With eigen-decomposition,

$$\mathbf{H}_t^H\mathbf{H}_t = \mathbf{U}_t^H\Lambda_t\mathbf{U}_t \tag{3.65}$$

such that $\mathbf{U}_t$ is unitary and $\Lambda_t = \text{diag}(\lambda_t^{\pi(1)},\lambda_t^{\pi(2)},\cdots,\lambda_t^{\pi(M)})$, where π is the permutation such that $\lambda_t^{\pi(1)}\geq\lambda_t^{\pi(2)}\geq\cdots\geq\lambda_t^{\pi(M)}$. The MIMO channel can thus be interpreted as a set of M parallel channels with its channel states (in power units) given by

$$\lambda_t^{\pi(1)},\ \lambda_t^{\pi(2)},\ \cdots,\ \lambda_t^{\pi(M)},$$

provided that the transmitter performs appropriate beamforming associated with the rotation $\mathbf{U}_t$. Thus, we can solve the MIMO scheduling problem with the parallel scheduling algorithms described in the previous subsection.

There is one interesting observation when calculating the cost-to-go function for the large B scenario. Due to symmetry, if $g^1,\cdots,g^M$ are i.i.d. random variables and $g^{(1)},\cdots,g^{(M)}$ denote the

[5] We can proceed similarly for $M\geq N$.

ordered random variables such that $g^{\pi(1)} \geq \cdots \geq g^{\pi(M)}$, then

$$\mathbb{E}\left[\frac{1}{\mathbb{G}\left(g^1,\cdots,g^M\right)}\right] = \mathbb{E}\left[\frac{1}{\mathbb{G}\left(g^{\pi(1)},\cdots,g^{\pi(M)}\right)}\right]. \tag{3.66}$$

This leads to the cost-to-go function that is identical to that of the parallel channels case:

$$\bar{J}_t^{\text{MIMO}}(\beta) \approx Mte^{\frac{\beta}{Mt}}\,\mathbb{G}\left(\nu_M, \nu_{M(t-1)},\cdots,\nu_M\right), \tag{3.67}$$

for large β.

3.4 Wideband Scheduling

Thus far, we have considered scheduling problems of minimizing energy expenditure by adjusting bit allocation to adapt to the fading behavior and delay requirements. In general, the capacity formula for a single-user/single-channel under a bandlimited additive Gaussian noise is given by [CT91]

$$b = W\log\left(1+\frac{gE}{W}\right), \tag{3.68}$$

where W denotes the bandwidth usage. For energy-efficient scheduling problems, we have assumed that the bandwidth usage at each time slot is fixed. Alternatively, this section considers efficient-bandwidth scheduling problems with fixed energy transmission at each slot.

Bandwidth scheduling will be useful for wideband systems such as OFDM, which has been adopted in many contemporary wireless systems. In an OFDM system, allocating more subcarrier channels can be simply understood by increasing the size of bandwidth. Thus, our scenario corresponds to the case that the transmitter varies the number of subchannels to adapt to fading and the deadline, with constant power in each subchannel.

Fig. 3.18a illustrates the relationship between the bandwidth usage and the size of bit allocation based on (3.68) when $g = 1$ and $E = 1$ without loss of generality, i.e.,

$$b = W\log\left(1+\frac{1}{W}\right). \tag{3.69}$$

The inverse function can be obtained with the introduction of the Lambert $\mathcal{W}$ function [CGH$^+$96]:

$$W = \frac{1}{-\frac{1}{b}\mathcal{W}_{-1}\left(-be^{-b}\right)-1}, \tag{3.70}$$

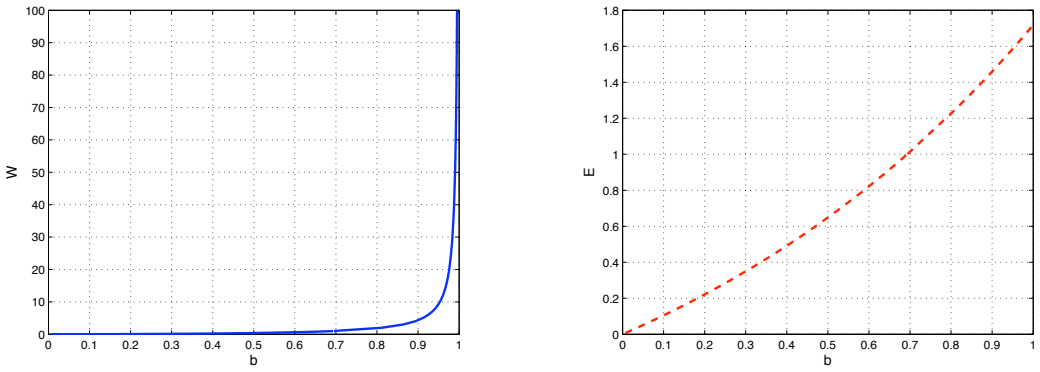

(a) Bandwidth and bit relationship, $b = W\log(1+1/W)$ (b) Energy and bit relationship, $b = \log(1+E)$

Figure 3.18: Bandwidth and energy behaviors with respect to bit allocation for the Shannon function

where $\mathcal{W}_{-1}$ denotes the -1 branch of the Lambert W function. For a comparison, we also plot the relation between the energy E and the number of bits in Fig. 3.18b. Although both W and E are increasing convex functions of b, the behavior of W is quite drastic with respect to b. One interesting fact is that b is bounded by 1 no matter how large W is, which can be shown by L'Hopital's rule. In the regime of large W, there will only be inappreciable increase in bit transmission, even though we spend a lot of bandwidth cost. This fact suggests that the bandwidth scheduling with the bandwidth cost (3.70) is not adequate for large W scheduling problem. When W is large, the maximum number of bits that can be transmitted is highly related to power/energy rather than the bandwidth. More discussion on large W can be found in [LTV03, Ver02].

3.4.1 Constant Noise Regardless of Bandwidth Expansion

In a typical OFDM system, more bits can be transmitted with more subchannels. This is because the transmission power at each subchannel is fixed and thus the total transmit power increases as the number of subchannel increases. As a result, the increase in the total transmit power compensates the the increase in noise power. To capture this, we ignore the increase in noise power due to bandwidth expansion, i.e., the second W in (3.69) is discarded. Thus, we assume that the number of bits that can be transmitted with W bandwidth under channel state g is given

by

$$b = W \log(1+g), \tag{3.71}$$

where the transmit energy is assumed to be constant $E = 1$ in (3.68). By inverting (3.71), we can relate the incurred bandwidth cost to transmit b bits under channel state g as:

$$W = \frac{b}{\log(1+g)}, \tag{3.72}$$

which is a linear cost function.

As usual, discrete-time index is denoted by t in descending order. The scheduler is to determine how many bits to transmit at each slot with constant energy $E = 1$ to minimize the expected total bandwidth usage. Thus, we form a hard-deadline scheduling problem of transmitting B bits within T time slots as:

$$\text{minimize} \quad \mathbb{E}\left[\sum_{t=1}^{T} \frac{b_t}{\log(1+g_t)}\right], \tag{3.73}$$

$$\text{subject to} \quad \sum_{t=1}^{T} b_t = B, \tag{3.74}$$

$$0 \le W_t \le W_{\max}, \ \forall t, \tag{3.75}$$

where we assume that the transmitter transmits signals with constant energy $E = 1$. Notice that (3.75) denotes a peak bandwidth constraint, which makes the problem non-trivial. Without this constraint, the optimization is a linear program and has a trivial solution of one-shot allocation. The introduction of this constraint is highly desirable in most practical systems. In an OFDM system, for example, the number of subchannels is limited. With this constraint, however, the problem may not be feasible when the channel is in deep fade continuously. To make the problem be feasible, we assume that $g_t \ge g_{\min}$ for some $g_{\min} > 0$.

The channel states are assumed to be iid and the scheduler has causal CSI. The queue state is denoted by β_t which represents the unserved bits at the beginning of slot t. Then, we can formulate the program as a DP:

$$J_t^{\text{wideband}}(\beta_t, g_t) = \begin{cases} \min\limits_{0 \le b_t \le \beta_t,\, 0 \le W_t \le W_{\max}} \left\{ W_t(b_t, g_t) + \bar{J}_{t-1}^{\text{wideband}}(\beta_t - b_t) \right\}, & t = T, \cdots, 2, \\ \min\{W_1(\beta_1, g_1), W_{\max}\}, & t = 1, \end{cases} \tag{3.76}$$

where $W_t(b_t, g_t) = b_t / \log(1+g_t)$ and $\bar{J}_{t-1}^{\text{wideband}}(\beta_{t-1}) = \mathbb{E}\left[J_{t-1}^{\text{wideband}}(\beta_{t-1}, g_{t-1})\right]$. Notice that this problem is identical to the work of Fu, Modiano, and Tsitsiklis [FMT06]. Although their

formulation is for efficient-energy scheduling rather than efficient-bandwidth scheduling, they obtained the DP (3.76) by approximating the energy cost with a linear function. Still, we cannot find a general solution to (3.76), but we can obtain a solution similar to [FMT06] by restricting fading states of g.

Because of the peak bandwidth constraint, the hard-deadline constraint (successfully transmitting B bits within T slots) may not be satisfied if $W_1(\beta_1, g_1) > W_{\max}$ in (3.76). In order to make the problem always have a feasible solution, we can add a constraint to the queue sizes according to the maximum available frequency band $W_{\max}$:

$$\beta_t \leq t W_{\max} \log(1 + g_{\min}), \tag{3.77}$$

where $g_{\min} = \inf\{\text{Support}(f)\}$ and f is the pdf of g.

3.5 Summary

We have studied extensions of the previous chapter to outage, multiple users, parallel channels, and wideband. For the M-outage scheduling problem, we observed that the outage penalty factor M plays the role of limiting peak energy transmission and making the expected cost-to-go function quasiconvex. Still, the form of stationary points at $t = 2$ is almost identical to that of the non-outage problem, and thus we have a similar balance between opportunism and delay-limitedness. For the multi-user scheduling problem, we obtained a simple coordinate-descent algorithm for the two-user $T = 2$ scheduling problem. For parallel/MIMO channels, we were able to derive analytical policies for large B and small B, which are derived with the same philosophy as the boundary-relaxed scheduler and one-shot policy in the previous chapter, respectively. Finally, we studied a bandwidth scheduling problem while fixing transmission energy at each slot. In most cases, we are not able to develop simple policies to reveal how the scheduling parameters affect the scheduling functions because of the inherent complexity in dynamic programs. To obtain analytic forms of scheduling policies one can relax or add constrains to the scheduling environments, but these are left to future work.

3.6 Proofs

3.6.1 Proof of Lemma 3.1

We want to prove this by induction.

(i) At the final time slot $t = 1$, the solution can be found by

$$b_1^{\text{out,lin}}(\beta_1, g_1) = \begin{cases} \beta_1, & \text{if } g_1 \geq \frac{\beta_1}{M}, \\ 0, & \text{else.} \end{cases} \tag{3.78}$$

Thus, the expected cost is given by

$$\bar{J}_1^{\text{out,lin}}(\beta_1) = \mathbb{E}_{g_1}[J_1^{\text{out,lin}}(\beta_1, g_1)] = M \int_0^{\frac{\beta_1}{M}} dF(x) + \int_{\frac{\beta_1}{M}}^{\infty} \frac{\beta_1}{x} dF(x), \tag{3.79}$$

where F is the fading distribution. Note that

$$\frac{d\bar{J}_1^{\text{out,lin}}(\beta_1)}{d\beta_1} = \int_{\frac{\beta_1}{M}}^{\infty} \frac{1}{x} dF(x), \tag{3.80}$$

$$\frac{d^2\bar{J}_1^{\text{out,lin}}(\beta_1)}{d(\beta_1)^2} = -\frac{1}{\beta_1} f\left(\frac{M}{\beta_1}\right) < 0, \tag{3.81}$$

where $f = F'$. Thus, $\bar{J}_1^{\text{out,lin}}$ is concave.

(ii) We suppose that $\bar{J}_{t-1}^{\text{out,lin}}$ is concave. If we define the objective function of the optimization (3.14) as $\tilde{J}_t^{\text{out,lin}}$, i.e.,

$$\tilde{J}_t^{\text{out,lin}}(b_t; \beta_t, g_t) = \frac{b_t}{g_t} + \bar{J}_{t-1}^{\text{out,lin}}(\beta_t - b_t), \tag{3.82}$$

then $\tilde{J}_t^{\text{out,lin}}$ is concave in b_t. By Lemma 3.4 (p. 100), the optimal solution is either 0 or β_t, i.e.,

$$b_t^{\text{out,lin}}(\beta_t, g_t) = \begin{cases} \beta_t, & \text{if } g_t \geq \frac{\beta_t}{\bar{J}_{t-1}^{\text{out,lin}}(\beta_t)}, \\ 0, & \text{else.} \end{cases} \tag{3.83}$$

Thus,

$$\begin{aligned}\bar{J}_t^{\text{out,lin}}(\beta_t) &= \mathbb{E}\left[\frac{\beta_t}{g_t}\middle| g_t \geq \frac{\beta_t}{\bar{J}_{t-1}^{\text{out,lin}}(\beta_t)}\right]\Pr\left\{g_t \geq \frac{\beta_t}{\bar{J}_{t-1}^{\text{out,lin}}(\beta_t)}\right\} \\ &\quad + \mathbb{E}\left[\bar{J}_{t-1}^{\text{out,lin}}(\beta_t)\middle| g_t < \frac{\beta_t}{\bar{J}_{t-1}^{\text{out,lin}}(\beta_t)}\right]\Pr\left\{g_t < \frac{\beta_t}{\bar{J}_{t-1}^{\text{out,lin}}(\beta_t)}\right\} \\ &= \mathbb{E}\left[\frac{\beta_t}{g_t}\middle| g_t \geq \frac{\beta_t}{\bar{J}_{t-1}^{\text{out,lin}}(\beta_t)}\right]\Pr\left\{g_t \geq \frac{\beta_t}{\bar{J}_{t-1}^{\text{out,lin}}(\beta_t)}\right\} + \bar{J}_{t-1}^{\text{out,lin}}(\beta_t)\Pr\left\{g_t < \frac{\beta_t}{\bar{J}_{t-1}^{\text{out,lin}}(\beta_t)}\right\}.\end{aligned} \tag{3.84}$$

By Lemma 3.5 (p. 100), $\bar{J}_t^{\text{out,lin}}$ is concave.

Therefore, by induction, $\bar{J}_t^{\text{out,lin}}$ is concave for all $t = 1, 2, \cdots$ □

Lemma 3.4. *If h is continuous on $[a,b]$ and strictly concave, then the optimal solution to*

$$\min_{a \leq x \leq b} h(x) \tag{3.85}$$

is either a or b.

Proof. Suppose the optimal minimizer x_0 is an interior point of the interval, i.e., $a < x_0 < b$. There exists $\varepsilon > 0$ such that $a < x_0 - \varepsilon < x_0 < x_0 + \varepsilon < b$. Since h is strictly concave, either $h(x_0) \neq h(x_0 - \varepsilon)$ or $h(x_0) \neq h(x_0 + \varepsilon)$ is true. By the concavity of h again,

$$h\left(\frac{1}{2}(x_0 - \varepsilon) + \frac{1}{2}(x_0 + \varepsilon)\right) > \frac{1}{2}h(x_0 - \varepsilon) + \frac{1}{2}h(x_0 + \varepsilon) \tag{3.86}$$

or $h(x_0) > \frac{1}{2}(h(x_0 - \varepsilon) + h(x_0 + \varepsilon))$. This implies that either $h(x_0) > h(x_0 - \varepsilon)$ or $h(x_0) > h(x_0 + \varepsilon)$ is true, which is a contradiction. □

Lemma 3.5. *Let x be a non-negative continuous random variable which has a pdf f. If h is concave, then*

$$\zeta(y) = \mathbb{E}\left[\frac{y}{x}\middle| \frac{y}{x} < h(y)\right]\Pr\left\{\frac{y}{x} < h(y)\right\} + h(y)\Pr\left\{\frac{y}{x} \geq h(y)\right\} \tag{3.87}$$

is concave for $y > 0$.

Proof.

$$\zeta(y) = y\int_{\frac{y}{h(y)}}^{\infty} \frac{1}{x} f(x)dx + h(y)\int_0^{\frac{y}{h(y)}} f(x)dx.$$

$$\begin{aligned}\frac{d\zeta(y)}{dy} &= \int_{\frac{y}{h(y)}}^{\infty}\frac{1}{x}f(x)dx - y\left(\frac{h(y)}{y}f\left(\frac{y}{h(y)}\right)\frac{h(y)-yh'(y)}{h^2(y)}\right)\\ &\qquad +h'(y)\int_0^{\frac{y}{h(y)}}f(x)dx + h(y)f\left(\frac{y}{h(y)}\right)\frac{h(y)-yh'(y)}{h^2(y)}\\ &= \int_{\frac{y}{h(y)}}^{\infty}\frac{1}{x}f(x)dx + h'(y)\int_0^{\frac{y}{h(y)}}f(x)dx\end{aligned}$$

$$\begin{aligned}\frac{d^2\zeta(y)}{dy^2} &= -\frac{h(y)}{y}f\left(\frac{y}{h(y)}\right)\frac{h(y)-yh'(y)}{h^2(y)} + h''(y)\int_0^{\frac{y}{h(y)}}f(x)dx + h'(y)f\left(\frac{y}{h(y)}\right)\frac{h(y)-yh'(y)}{h^2(y)}\\ &= -\left(\frac{h(y)}{y}-h'(y)\right)f\left(\frac{y}{h(y)}\right)\frac{h(y)-yh'(y)}{h^2(y)} + h''(y)\int_0^{\frac{y}{h(y)}}f(x)dx\\ &= -\frac{1}{y}f\left(\frac{y}{h(y)}\right)\left(\frac{h(y)-yh'(y)}{h(y)}\right)^2 + h''(y)\int_0^{\frac{y}{h(y)}}f(x)dx < 0.\end{aligned}$$

because $h''(y) < 0$. □

3.6.2 Proof of Proposition 3.3

If the objective of the optimization (3.32) is denoted by $\tilde{J}_2^{\text{multi}}$ as a function of b_2^1 and b_2^2, i.e.,

$$\tilde{J}_2^{\text{multi}}(b_2^1,b_2^1) = \frac{e^{b_2^2}(e^{b_2^1}-1)}{g_2^1} + \frac{e^{b_2^2}-1}{g_2^2} + \tilde{J}_1^{\text{multi}}(\beta_2^1-b_2^1,\beta_2^2-b_2^2), \tag{3.88}$$

then it is sufficient to show that $\tilde{J}_2^{\text{multi}}$ is a convex function.

The Hessian matrix of $\tilde{J}_2^{\text{multi}}(b_2^1,b_2^2)$ can be found by

$$\begin{aligned}&\nabla^2\tilde{J}_2^{\text{multi}}(b_2^1,b_2^2) =\\ &\left(\frac{e^{b_2^1}e^{b_2^2}}{g_2^1} + \frac{e^{\beta_2^1-b_2^1}e^{\beta_2^2-b_2^2}}{\Gamma}\right)\begin{bmatrix}1 & 1\\ 1 & 1\end{bmatrix} + \begin{bmatrix}\frac{e^{\beta_2^1-b_2^1}}{2}\left(\frac{1}{\gamma}-\frac{1}{\Gamma}\right) & 0\\ 0 & e^{b_2^2}\left(\frac{1}{g_2^2}-\frac{1}{g_2^1}\right)+\frac{e^{\beta_2^2-b_2^2}}{2}\left(\frac{1}{\gamma}-\frac{1}{\Gamma}\right)\end{bmatrix}.\end{aligned} \tag{3.89}$$

Let the eigenvalues of $\nabla^2\tilde{J}_2^{\text{multi}}(b_2^1,b_2^2)$ be λ_1 and λ_2. Then,

$$\lambda_1+\lambda_2 > 0, \tag{3.90}$$

$$\lambda_1\lambda_2 > 0, \tag{3.91}$$

since $\Gamma > \gamma$ and $g_2^1 \geq g_2^2$ from our construction. Therefore, $\tilde{J}_2^{\text{multi}}$ is convex since $\nabla^2\tilde{J}_2^{\text{multi}}$ is positive definite [BV04].

Chapter 4

Delay Constrained Scheduling for Monomial Cost Functions

The primal problem is identical to the problem in Chapter 2 except that the incurred energy and the transmitted bits are related by a monomial function instead of the AWGN capacity formula. That is, we study the minimization of energy expenditure subject to a hard deadline constraint assuming that the scheduler has *causal* knowledge of the channel state information. Additionally, we consider the dual (scheduling over a finite time-horizon) problem of maximizing the transmitted bits subject to a finite energy constraint. We also briefly discuss scheduling problems when the CSI is available non-causally.

The subject of this chapter is the single-packet scheduling problem of specialized to the case where the required energy E to transmit b bits under channel state g is governed by a convex monomial function, i.e., $E = b^n/g$, where n denotes the monomial order. The biggest advantage of using this monomial cost function is that it yields closed-form solutions in various scenarios, unlike the Shannon-cost function setting described in Chapter 2. As a result, it provides intuition on the interplay between the monomial order, delay deadline, and the channel states so that it ultimately suggests general ideas for a more general energy-cost function. Although the monomial cost does not hold for operating at capacity in an AWGN channel, according to Zafer and Modiano [ZM07] and their reference [NMR03], there is a practical modulation scheme that exhibits an energy-bit relation that can be well approximated by a monomial. Actually, Zafer and Modinano [ZM07] considered the same problem but for a continuous-time Markov process

channel in continuous-time scheduling, i.e., the scheduler can transmit at any time instant rather than discrete slotted time. Although they provided a solution in the form of a set of differential equations, it is not possible to give a closed-form solution. On the other hand, we are able to derive a closed-form description of the optimal scheduler for the simpler block fading model (note that the continuous model is somewhat incompatible with block fading).

In this chapter, we derive optimal scheduling policies for delay-constrained scheduling when the energy-bit cost is a convex monomial function. We also investigate the dual problem of maximizing the number of bits to transmit with a finite energy budget over a finite time horizon. In all cases, we are able to find analytical expressions that are functions of the queue state variables (energy state for the dual problem), current channel state and a quantity related to the fading distribution. Many of the results of this chapter appear in [LJ09c].

The resulting optimal schedulers determine the ratio of the number of bits to be allocated in the current slot to the deferred bits. For example, the optimal scheduling ratio of the number of bits to serve b_t (from the remaining β_t bits) at slot t (t denotes the number of remaining slots to the deadline) to the number of bits to defer $(\beta_t - b_t)$ for the primal energy minimization problem is given by

$$b_t : (\beta_t - b_t) = (g_t)^{\frac{1}{n-1}} : \eta_{n,t}, \tag{4.1}$$

where n is the order of monomial cost function, g_t denotes the current channel state, and $\eta_{n,t}$ denotes a statistical quantity determined by the channel distribution and the number of remaining slots t. It will be shown later that $\eta_{n,t}$ is increasing with respect to t. If $\eta_{n,t}$ is small, $b_t \approx \beta_t$. However, as $\eta_{n,t}$ term increases, b_t gets more affected by the channel state $(g_t)^{\frac{1}{n-1}}$. This suggests that the scheduler behaves very opportunistically when the deadline is far away (t large) but less so as the deadline approaches, since $\eta_{n,t}$ is an increasing function of t.

4.1 Primal Problem: Energy Minimization

First off, we consider the primal scheduling problem of transmitting B bits within T time slots with the objective of minimizing the total transmit energy while satisfying the delay deadline constraint. As in Chapter 2, the channel states $\{g_t\}_{t=1}^{T}$ are assumed to be independently and identically distributed (i.i.d.). If the scheduler has only causal knowledge of the channel state (i.e., at slot t, the scheduler knows $g_T, g_{T-1}, \cdots, g_t$ but does not know $g_{t-1}, g_{t-2}, \cdots, g_1$), we refer to this as *causal scheduling*. If the scheduler has non-causal knowledge of the channel state

in advance (i.e., at slot T, the scheduler knows $g_T, g_{T-1}, \cdots, g_1$), we refer to it as *non-causal scheduling*. The main focus is on causal scheduling problems.

We assume that the energy expenditure E_t is inversely proportional[1] to the channel state g_t and is related to the transmitted bits b_t by a monomial function:

$$E_t(b_t, g_t; n) = \frac{b_t^n}{g_t}, \tag{4.2}$$

where n denotes the order of monomial. If $n = 1$, the resulting optimization becomes a linear program and thus a "one-shot" policy is optimal. We assume that $n > 1$ (to be convex) and $n \in \mathbb{R}$ (n is not necessarily an integer), where $\mathbb{R}$ denotes the real number set. A practical modulation scheme that exhibits a monomial energy-cost behavior was illustrated in [ZM07], where the monomial order is $n = 2.67$.

A scheduler is a sequence of functions $\{b_t(\beta_t, g_t)\}_{t=1}^T$ with $0 \le b_t \le \beta_t$. For causal scheduling, b_t depends only on the current channel state g_t and not on the past and future states because of the i.i.d. assumption and causality.The optimal scheduler is determined by minimizing the total expected energy cost:

$$\begin{aligned} \min_{b_T, \cdots, b_1} \quad & \mathbb{E}\left[\sum_{t=1}^{T} E_t(b_t, g_t; n)\right] \\ \text{subject to} \quad & \sum_{t=1}^{T} b_t = B \\ & b_t \ge 0, \qquad \forall t, \end{aligned} \tag{4.3}$$

which is identical to (2.3) except for E_t.

4.1.1 Causal Energy Minimization Scheduling

As done in Chapter 2, a sequential formulation of the optimal causal scheduling of (4.3) can be established by introducing a state variable β_t as in standard dynamic programming [Ber05]. Recall that β_t denotes the remaining bits that summarizes the bit allocation up until the previous time step. At time step t, $g_{t-1}, \cdots, g_1$ are unknown but g_t is known. Thus, the optimization (4.3) becomes:

$$\min_{0 \le b_t \le \beta_t} \left(E_t(b_t, g_t; n) + \mathbb{E}\left[\sum_{s=1}^{t-1} E_s(b_s, g_s; n) \middle| b_t\right] \right), \ t \ge 2.$$

[1] The $1/g_t$ dependence is due to the fact that the received energy is the product of the transmitted energy E_t and the channel state g_t. Note, however, that any other decreasing function of g_t could be considered by simply performing a change of variable on g_t.

With (4.2), we obtain the following DP:

$$J_t^{\text{csl}}(\beta_t, g_t; n) = \begin{cases} \min\limits_{0 \le b_t \le \beta_t} \left(\frac{b_t^n}{g_t} + \bar{J}_{t-1}^{\text{csl}}(\beta_t - b_t; n) \right), & t \ge 2 \\ \frac{\beta_1^n}{g_1}, & t = 1, \end{cases} \tag{4.4}$$

where the first term $\frac{b_t^n}{g_t}$ denotes the current energy cost and the second term $\bar{J}_{t-1}^{\text{csl}}(\beta; n) = \mathbb{E}_g[J_{t-1}^{\text{csl}}(\beta, g; n)]$ denotes the cost-to-go function, which is the expected future energy cost (because future channel states are unknown, only expectations can be considered) to serve β bits in $(t-1)$ slots if the optimal control policy is used at each future step. Thus, the optimal bit allocation is determined by balancing the current energy cost and the expected future energy cost. Because of the hard delay constraint, all the unserved bits must be served at $t = 1$ regardless of the channel condition, i.e., $b_1 = \beta_1$ and thus the resulting energy cost is given by $\frac{\beta_1^n}{g_1}$. This dynamic optimization can be solved:

Theorem 4.1. *The optimal solution to the causal energy minimization scheduling problem* (4.4) *is given by*

$$b_t^{csl}(\beta_t, g_t; n) = \begin{cases} \beta_t \left(\frac{(g_t)^{\frac{1}{n-1}}}{(g_t)^{\frac{1}{n-1}} + \left(\frac{1}{\xi_{n,t-1}} \right)^{\frac{1}{n-1}}} \right), & t \ge 2 \\ \beta_1, & t = 1, \end{cases} \tag{4.5}$$

where the constants $\xi_{n,t}$ are determined as:

$$\xi_{n,t} = \begin{cases} \mathbb{E}\left[\left(\frac{1}{(g_t)^{\frac{1}{n-1}} + (1/\xi_{n,t-1})^{\frac{1}{n-1}}} \right)^{n-1} \right], & t \ge 2, \\ \mathbb{E}\left[\frac{1}{g} \right], & t = 1, \end{cases} \tag{4.6}$$

and the expected energy cost is given by

$$\bar{J}_t^{csl}(\beta; n) = \beta^n \xi_{n,t}, \quad t = 1, 2, \cdots. \tag{4.7}$$

Proof. See Section 4.5.1. □

The scheduling function (4.5) can be intuitively explained in the following way. The ratio of the number of allocated bits b_t to the number of deferred bits $(\beta_t - b_t)$ is equal to the ratio of

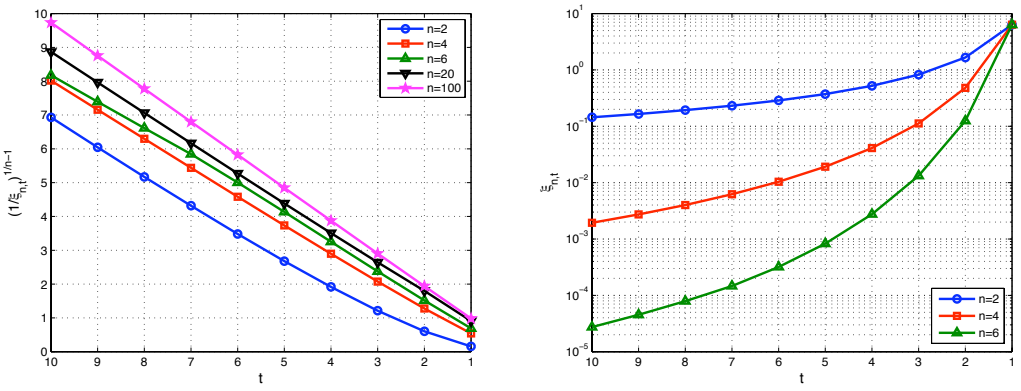

(a) $(1/\xi_{n,t})^{\frac{1}{n-1}}$ (b) $\xi_{n,t}$

Figure 4.1: $\xi_{n,t}$ for the truncated exponential random variable g with threshold 0.001

$g_t^{\frac{1}{n-1}}$ to $(1/\xi_{n,t-1})^{\frac{1}{n-1}}$, i.e.,

$$b_t : \underbrace{(\beta_t - b_t)}_{\beta_{t-1}} = (g_t)^{\frac{1}{n-1}} : \underbrace{\eta_{n,t}}_{\text{threshold}} \tag{4.8}$$

where $\eta_{n,t} = (1/\xi_{n,t-1})^{\frac{1}{n-1}}$. As expected, the optimal scheduler is *opportunistic* in that the number of transmitted bits are proportional to the channel quality. Furthermore, the thresholds $\eta_{n,t}$ are increasing in t (shown later) which implies that the scheduler is more *selective* when the delay deadline is far away (large t). When the deadline is far away, the scheduler transmits a large fraction of the unserved bits only when the channel state is very good; because many slots remain until the deadline, there is still a good chance of seeing a very good channel state. On the other hand, as the deadline approaches (small t) the scheduler is still opportunistic but must become less selective because only fewer opportunities for good channel states remain before the deadline is reached.

Figure 4.1 illustrates $\eta_{n,t}\left(=(1/\xi_{n,t})^{\frac{1}{n-1}}\right)$ and $\xi_{n,t}$ for a truncated exponential distribution. As can be seen in Fig. 4.1a, $\eta_{n,t}$ increases with respect to t and this can be shown analytically:

$$\begin{aligned}\xi_{n,t} &= \mathbb{E}\left[\left(\frac{1}{g_t^{\frac{1}{n-1}} + \left(\frac{1}{\xi_{n,t-1}}\right)^{\frac{1}{n-1}}}\right)^{n-1}\right] \\ &\leq \mathbb{E}\left[\left(\frac{1}{\left(\frac{1}{\xi_{n,t-1}}\right)^{\frac{1}{n-1}}}\right)^{n-1}\right] = \xi_{n,t-1}\end{aligned} \tag{4.9}$$

where the inequality is due to $g_t \geq 0$. This shows the delay-limited opportunistic behavior mentioned before. From (4.7), the value $\xi_{n,t}$ denotes the expected energy cost for a unit bit, i.e., $\beta_t = 1$. Thus, $\xi_{n,t}$, as illustrated in Fig. 4.1b, shows how much the expected energy unit cost (for transmitting one bit) can be reduced as the time span increases.

Another interesting fact is that the policy (4.5) utilizes[2] all the time slots. This is because both $(g_t)^{\frac{1}{n-1}}$ and $(1/\xi_{n,t-1})^{\frac{1}{n-1}}$ are always positive for typical fading distributions. For the Shannon cost function problem as in Chapter 2, however, there exist time slots that are not utilized depending on the values of B and T.

Special Cases: $n = 2$ and $n = \infty$

In this subsection, we examine the optimal policy (4.5) for two values of n: $n = 2$ and $n \to \infty$.

By substituting $n = 2$ in (4.5) and (4.6), we have

$$b_t^{\text{csl}}(\beta_t, g_t; n = 2) = \beta_t \left(\frac{g_t}{g_t + \frac{1}{\xi_{2,t-1}}}\right), \tag{4.10}$$

where

$$\xi_{2,t} = \begin{cases} \mathbb{E}\left[\frac{1}{g_t + \frac{1}{\xi_{2,t-1}}}\right], & t \geq 2, \\ \mathbb{E}\left[\frac{1}{g}\right], & t = 1. \end{cases} \tag{4.11}$$

Thus, the allocated bits b_t and the deferred bits $(\beta_t - b_t)$ have the same ratio with g_t and $1/\xi_{2,t-1}$.

Figure 4.2 illustrates the bit allocation behavior (4.10) with respect to the channel gain as t varies. If we look how strong the channel gain required to serve the half of the unserved bits, i.e., the horizontal line of $b_t^{\text{csl}}/\beta_t = 0.5$, then we can see that the half of the unserved bits are allocated for -7 dB when $t = 2$ and for 13 dB when $t = 20$.

We now examine the limiting behavior of the scheduling policy (4.5) as $n \to \infty$. First, we observe that

[2] A time slot t is called *utilized* if a positive bit is scheduled, i.e., $b_t > 0$.

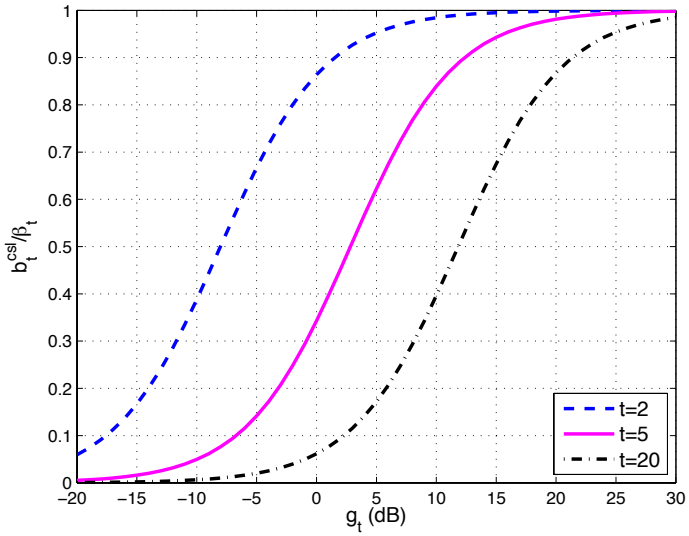

Figure 4.2: The ratio $b_t^{\text{csl}}(\beta_t, g_t; n=2)/\beta_t$ with respect to the channel state g_t when $\{g_s\}_{s=1}^{t-1}$ are i.i.d. truncated exponential variables with threshold 0.001

Lemma 4.2. *For any fading distribution for which $\mathbb{E}[1/g]$ is finite, the variable $\xi_{n,t}$ defined in* (4.6) *has the following property:*

$$\lim_{n\to\infty}\left(\frac{1}{\xi_{n,t}}\right)^{\frac{1}{n-1}} = t. \tag{4.12}$$

Proof. See Section 4.5.2. □

Figure 4.1a illustrates the values of $(1/\xi_{n,t})^{\frac{1}{n-1}}$ for the truncated exponential variable. This shows that $(1/\xi_{n,t})^{\frac{1}{n-1}}$ is increasing linearly with respect to t for large n, which agrees with Lemma 4.2.

With the limit in Lemma 4.2, we can immediately reach the simplified scheduling policy summarized below:

Theorem 4.3. *As $n\to\infty$, the scheduling policy* (4.5) *becomes the equal-bit scheduler, i.e.,*

$$b_t^{csl}(\beta_t, g_t; n=\infty) = \frac{\beta_t}{t}, \quad t = 1, 2, \cdots. \tag{4.13}$$

That is, when the order of monomial cost function tends to infinity, scheduling equal number of bits at every slot regardless of the channel state becomes the optimal policy. Note that we

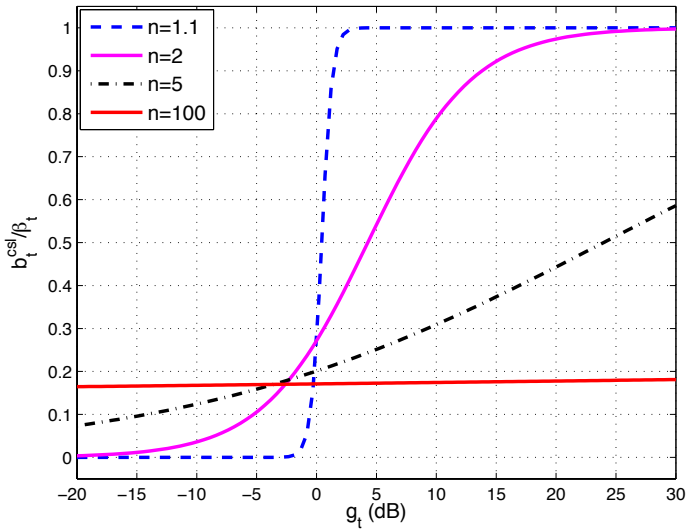

Figure 4.3: The ratio $b_t^{\mathrm{csl}}(\beta_t, g_t; n)/\beta_t$ with respect to the channel state g_t at $t = 5$ as the monomial order n varies assuming that $\{g_s\}_{s=1}^{4}$ are i.i.d. truncated exponential variables with threshold 0.001

considered only monomial orders $n > 1$ in the derivation, as when $n = 1$, the optimal policy is the one-shot policy in Chapter 2, which completely depends on the channel state. From these two extreme cases, we can deduce that the effect of channel state on the scheduling function decreases as the order of monomial cost function increases, or in other words the optimal scheduler becomes less opportunistic as the monomial order n increases.

Figure 4.3 illustrates the bit allocation behavior as the monomial order n varies. As can be seen, the scheduling function is almost a threshold policy when $n = 1.1$ and thus the function is highly dependent on the channel state value g_t. When $n = 100$, the scheduling function is almost constant with respect to g_t that means almost same amount of bits are allocated regardless of the channel condition.

4.1.2 Quadratic Polynomial Cost Function

In this subsection, we consider the case when the energy-bit cost function is given by an arbitrary quadratic function that is convex and increasing. This brings us another way of freedom when we seek an experimental cost function by fitting curves. Without loss of generality, such a quadratic

cost function be written in a form of:

$$E_t(b_t, g_t; c, d) = \frac{1}{g_t}(b_t + c)^2 + d, \tag{4.14}$$

where c and d are quadratic function parameters. To guarantee that the cost function is increasing for all $b_t \geq 0$, we assume that $c \geq 0$. Later, we will restrict more on c to have a simple cost-to-go function. Since the constant d does not contribute the optimization, this term is ignored in the sequel.

Since all other problem setups are the same with the monomial case, the DP for this quadratic cost can be obtained by replacing the energy cost (4.2) with (4.14):

$$J_t^{\text{quad}}(\beta_t, g_t; c) = \begin{cases} \min\limits_{0 \leq b_t \leq \beta_t} \left(\frac{(b_t+c)^2}{g_t} + \bar{J}_{t-1}^{\text{quad}}(\beta_t - b_t; c) \right), & t \geq 2 \\ \frac{(\beta_1+c)^2}{g_1}, & t = 1, \end{cases} \tag{4.15}$$

where $\bar{J}_{t-1}^{\text{quad}}(\beta; c) = \mathbb{E}[J_{t-1}^{\text{quad}}(\beta, g_{t-1}; c)]$. The solution to this DP can be summarized as:

Theorem 4.4. *For the hard deadline scheduling problem with a quadratic polynomial energy cost function as in* (4.15)*, if the quadratic polynomial parameter c satisfies*

$$0 \leq c \leq \min\{1, g_t \varsigma_{t-1}\} \frac{\beta_t}{|1 - (t-1) g_t \varsigma_{t-1}|}, \quad t \geq 2, \tag{4.16}$$

where

$$\varsigma_t = \begin{cases} \mathbb{E}\left[\frac{1}{g_t + \frac{1}{\varsigma_{t-1}}} \right], & t > 1, \\ \mathbb{E}\left[\frac{1}{g_1} \right], & t = 1, \end{cases} \tag{4.17}$$

then the optimal solution can be written as the following ratio relationship:

$$(b_t^{quad} + c) : (\underbrace{(\beta_t - b_t^{quad})}_{\beta_{t-1}} + (t-1)c) = g_t : \frac{1}{\varsigma_{t-1}} \tag{4.18}$$

and the cost-to-go function is given by

$$\bar{J}_t^{quad}(\beta_t; c) = (\beta_t + tc)^2 \varsigma_t. \tag{4.19}$$

Proof. See Section 4.5.3. □

4.2 Dual Problem: Rate Maximization

Thus far, we have considered problems of minimizing energy expenditure to transmit fixed B information bits in a finite time horizon T. It is of interest to consider the dual of this, i.e., maximizing the number of bits transmitted with a finite energy E over a finite time horizon T. We refer to this as the *dual scheduling problem*, while referring to the original problem as the *primal scheduling problem*. Negi and Cioffi [NC02] considered this dual problem for the Shannon energy-bit cost function and provided solutions in DP, but not in closed form. In this section, we investigate this dual scheduling problem and obtain the optimal closed-form solution for monomial cost functions.

Since the energy-bit function is assumed to be (4.2), the associated bit-energy cost function is given by inverting:

$$b_t = (g_t E_t)^{\frac{1}{n}}. \tag{4.20}$$

Then the dual problem is given by

$$\begin{aligned} \max_{E_T,\cdots,E_1} \quad & \mathbb{E}\left[\sum_{t=1}^{T} (g_t E_t)^{\frac{1}{n}}\right] \\ \text{subject to} \quad & \sum_{t=1}^{T} E_t = E \\ & E_t \geq 0, \qquad \forall t. \end{aligned} \tag{4.21}$$

To derive a DP for causal dual scheduling, we introduce a state variable $\mathcal{E}_t$ that denotes the remaining energy at slot t. Thus, the optimization (4.21) can be formulated as

$$W_t^{\text{csl}}(\mathcal{E}_t, g_t; n) = \begin{cases} \max\limits_{0\leq E_t\leq \mathcal{E}_t} \left((g_t E_t)^{\frac{1}{n}} + \bar{W}_{t-1}^{\text{csl}}(\mathcal{E}_t - E_t; n)\right), & t \geq 2 \\ (g_1 \mathcal{E}_1)^{\frac{1}{n}}, & t = 1, \end{cases} \tag{4.22}$$

where $\bar{W}_{t-1}^{\text{csl}}(\mathcal{E}; n) = \mathbb{E}_g[W_{t-1}^{\text{csl}}(\mathcal{E}, g; n)]$ denotes the cost-to-go function for the dual scheduling problem. Similar to the primal problem, the dynamic optimization in (4.22) can be solved and its optimal solution is summarized as follows:

Theorem 4.5. *The optimal causal rate maximization scheduling* (4.22) *is given by*

$$E_t^{csl}(\mathcal{E}_t, g_t; n) = \begin{cases} \mathcal{E}_t \left(\frac{(g_t)^{\frac{1}{n-1}}}{(g_t)^{\frac{1}{n-1}} + (\zeta_{n,t-1})^{\frac{1}{n-1}}}\right), & t \geq 2, \\ \mathcal{E}_1, & t = 1, \end{cases} \tag{4.23}$$

where

$$\zeta_{n,t} = \begin{cases} \left(\mathbb{E}\left[\left((g_t)^{\frac{1}{n-1}} + (\zeta_{n,t-1})^{\frac{1}{n-1}} \right)^{\frac{n-1}{n}} \right] \right)^n, & t \geq 2, \\ \left(\mathbb{E}[g^{\frac{1}{n}}] \right)^n, & t = 1. \end{cases} \tag{4.24}$$

The optimal energy scheduler (4.23) has very similar interpretation with the optimal bit scheduler (4.5) from their scheduling formulations. That is, the ratio of the amount of energy to schedule E_t to the amount of energy to defer $(\mathcal{E}_t - E_t)$ is equal to the ratio of $g_t^{\frac{1}{n-1}}$ to $\zeta_{n,t-1}^{\frac{1}{n-1}}$, and thus, the similar delay-limited opportunistic scheduling interpretation can be applied. Notice that the quantities $\zeta_{n,t}$ and $\xi_{n,t}$ are different.

4.3 Non-Causal Scheduling

This section briefly considers the case where the scheduler has knowledge of the channel states non-causally in advance, i.e., $g_T, g_{T-1}, \cdots, g_1$ are known at $t = T$.

4.3.1 Energy Minimization Scheduling

In this non-causal setting, the optimization (4.3) is simply given by

$$\min_{b_T,\cdots,b_1} \sum_{t=1}^{T} \frac{b_t^n}{g_t} \tag{4.25}$$

subject to $\sum_{t=1}^{T} b_t = B$ and $b_t \geq 0$ for all t. This is a convex optimization and can be solved as:

Theorem 4.6. *The optimal non-causal scheduling to* (4.25) *is given by*

$$b_t^{ncsl}(\beta_t, g_t; n) = \beta_t \left(\frac{g_t^{\frac{1}{n-1}}}{\sum_{s=1}^{t} g_s^{\frac{1}{n-1}}} \right). \tag{4.26}$$

Proof. The standard Lagrangian method [BV04] yields the solution:

$$b_t^{\text{ncsl}} = B \left(\frac{g_t^{\frac{1}{n-1}}}{\sum_{s=1}^{T} g_s^{\frac{1}{n-1}}} \right). \tag{4.27}$$

If we express this solution with the queue state variable β_t, we obtain the result. □

The scheduling policy (4.26) can be interpreted with the ratio argument as with the causal cases, i.e.,

$$b_T^{\text{ncsl}} : b_{T-1}^{\text{ncsl}} : \cdots : b_1^{\text{ncsl}} = g_T^{\frac{1}{n-1}} : g_{T-1}^{\frac{1}{n-1}} : \cdots : g_1^{\frac{1}{n-1}}. \tag{4.28}$$

4.3.2 Rate Maximization Scheduling

Similarly we can fomulate the non-causal rate maximition as

$$\max \sum_{t=1}^{T} (g_t E_t)^{\frac{1}{n}}, \tag{4.29}$$

subject to $\sum_{t=1}^{T} E_t = E$ and $E_t \geq 0$ for all t.

Theorem 4.7. *The optimal non-causal scheduling to* (4.29) *is given by*

$$E_t^{ncsl} = \mathcal{E}_t \left(\frac{g_t^{\frac{1}{n-1}}}{\sum_{s=1}^{t} g_s^{\frac{1}{n-1}}} \right). \tag{4.30}$$

Like (4.28), we can also observe that

$$E_T^{\text{ncsl}} : E_{T-1}^{\text{ncsl}} : \cdots : E_1^{\text{ncsl}} = g_T^{\frac{1}{n-1}} : g_{T-1}^{\frac{1}{n-1}} : \cdots : g_1^{\frac{1}{n-1}}, \tag{4.31}$$

and thus, we obtain

$$\frac{b_t^{\text{ncsl}}}{B} = \frac{E_t^{\text{ncsl}}}{E}. \tag{4.32}$$

This implies that the optimal bit distribution ratio during the T slots for the primal problem is identical to the energy distribution ratio for the dual problem.

4.4 Summary

We have investigated the problem of bit/energy scheduling over a finite time duration assuming that the energy-bit cost function is a monomial. In both the primal (minimizing energy expenditure subject to a bit constraint) scheduling and the dual (maximizing bit transmission under an energy constraint) scheduling problem, we derived closed-form scheduling functions. The optimal bit/energy allocations are determined by the ratio of $g_t^{\frac{1}{n-1}}$ and a channel statistical quantity. From the monotonicity of this statistical quantity, we interpreted that the optimal scheduler behaves more opportunistically in the initial time steps and less so as the deadline approaches.

4.5 Proofs

4.5.1 Proof of Theorem 4.1

We use mathematical induction to find $b_t^{\mathrm{csl}}(\cdot,\cdot;n)$ and $\bar{J}_t^{\mathrm{csl}}(\cdot;n)$. At $t=1$, (4.5) and (4.7) are true by definition. If we suppose that (4.7) is true for $t-1$, the optimization (4.4) becomes

$$J_t^{\mathrm{csl}}(\beta_t, g_t; n) = \min_{0\le b_t\le \beta_t} \left(\frac{b_t^n}{g_t} + (\beta_t - b_t)^n \xi_{n,t-1} \right), \tag{4.33}$$

whose solution is obtained by differentiating the objective and setting to zero to result in (4.5). Substituting (4.5) into (4.33) and then taking expectation with respect to g_t, we obtain (4.7). Therefore, the result follows by induction.

4.5.2 Proof of Lemma 4.2

This can be shown by the induction. When $t=1$, (4.12) holds trivially. If we suppose (4.12) holds for $t-1$, then

$$\begin{aligned} &\lim_{n\to\infty} (\xi_{n,t})^{\frac{1}{n-1}} \\ &= \lim_{n\to\infty} \left(\mathbb{E}\left[\frac{1}{\left(g_{t-1}^{\frac{1}{n-1}} + \left(\frac{1}{\xi_{n,t-1}} \right)^{\frac{1}{n-1}} \right)^{n-1}} \right] \right)^{\frac{1}{n-1}} \\ &= \frac{1}{t}, \end{aligned} \tag{4.34}$$

where the last equality is due $\lim_{n\to\infty} (\mathbb{E}[\phi^n])^{\frac{1}{n}} = \mathrm{Max}\phi$ and $\mathrm{Max}\phi$ denotes the "effective upper bound" of ϕ (see Chap. 6 in [HLP01] for mathematical technicality). Hence, the induction follows.

4.5.3 Proof of Theorem 4.4

At $t=1$, $b_1^{\mathrm{quad}} = \beta_1$ and

$$\bar{J}_1^{\mathrm{quad}}(\beta_1; c) = (\beta_1 + c)^2 \, \mathbb{E}\left[\frac{1}{g} \right] \tag{4.35}$$

by (4.15). We now examine the scheduling problem at $t=2$. By substituting (4.35) into (4.15), we have

$$J_2^{\mathrm{quad}}(\beta_2, g_2; c) = \min_{0\le b_2\le \beta_2} \left\{ \frac{1}{g_2}(b_2 + c)^2 + \mathbb{E}\left[\frac{1}{g} \right] ((\beta_2 - b_2) + c)^2 \right\}. \tag{4.36}$$

By differentiating the objective and setting it to zero, we have the following relation for the optimal b_2^{quad}:

$$\frac{b_2^{\text{quad}}+c}{(\beta_2-b_2^{\text{quad}})+c} = g_2\,\mathbb{E}\left[\frac{1}{g}\right], \tag{4.37}$$

and thus,

$$b_2^{\text{quad}} = \frac{g_2\,\mathbb{E}\left[\frac{1}{g}\right]\beta_2 - c\left(1-g_2\,\mathbb{E}\left[\frac{1}{g}\right]\right)}{1+g_2\,\mathbb{E}\left[\frac{1}{g}\right]}. \tag{4.38}$$

By the condition (4.16), $0 \le b_2^{\text{quad}} \le \beta_2$. Therefore, b_2^{quad} is the solution to (4.36). From (4.37), we can see that (4.18) holds for $t=2$. By taking average over g_2 with the optimal b_2^{quad}, the average cost-go-to is given by

$$\bar{J}_2^{\text{quad}}(\beta_2;c) = (\beta_2+2c)^2\,\mathbb{E}\left[\frac{1}{g_2+\frac{1}{\mathbb{E}\left[\frac{1}{g}\right]}}\right], \tag{4.39}$$

which is identical to (4.19) at $t=2$.

We now assume that the optimal solution and the cost-to-go at $t-1$ is given by (4.18) and (4.19), respectively, and we examine these values at slot t.

$$J_t^{\text{quad}}(\beta_t,g_t;c) = \min_{0\le b_t\le\beta_t}\left\{\frac{(b_t+c)^2}{g_t} + ((\beta_t-b_t)+(t-1)c)^2\,\varsigma_{t-1}\right\} \tag{4.40}$$

By the same procedure as we did for $t=2$, we can see that the relations (4.18) and (4.19) hold for slot t. Therefore, the induction follows.

Chapter 5

Resource Allocation for MIMO Broadcast Channels

The multiple antenna broadcast channel has been the subject of much research recently, primarily because impressive multiple antenna capacity benefits can be realized without requiring large numbers of mobile antennas (c.f. [CS03]). In this chapter we consider two aspects of resource allocation problem for multiple antenna broadcast channels. First, we compare the achievable throughput for the optimal strategy of dirty paper coding (DPC) to that achieved with suboptimal and lower complexity linear precoding techniques. Second, we study the symmetric capacity, which represents absolute fairness and is an important metric in which users have symmetric rate demands. For example, if severely delay-constrained voice traffic is being transmitted to multiple users simultaneously, then the symmetric capacity is a very important quantity.

The remainder of this chapter is organized as follows. Section 5.1 presents the system model and some background on MIMO broadcast channels. In Section 5.2 we compare the DPC sum capacity of MIMO BC with the sum rate achievable with linear precoding at high SNR regime. Section 5.3 studies the symmetric capacity of MIMO BC and presents algorithms achieve it. The work in this chapter is published in [LJ06a, LJ06b, LJ07].

5.1 System Model & Background

We consider a K user Gaussian MIMO broadcast channel (BC) in which the transmitter has M antennas and each receiver has N antennas. The received signal vector $\mathbf{y}_k$ for user k is given by

$$\mathbf{y}_k = \mathbf{H}_k\mathbf{x} + \mathbf{n}_k \qquad k = 1, \cdots, K, \tag{5.1}$$

where $\mathbf{H}_k (\in \mathbb{C}^{N\times M})$ is the channel gain matrix for user k, $\mathbf{x}$ is the transmit signal vector having a power constraint $\mathrm{tr}(E[\mathbf{x}\mathbf{x}^H]) \leq P$, and $\mathbf{n}_k$ $(k = 1, \cdots, K)$ is complex Gaussian noise with unit variance per vector component (i.e., $E[\mathbf{n}_k^H\mathbf{n}_k] = \mathbf{I}$). We assume that the transmitter has perfect knowledge of all channel matrices and each receiver has perfect knowledge of its own channel matrix. Note that we only consider static, or fixed, channels.

It is now well known that dirty paper coding achieves the capacity region of the MIMO BC [WSS06], which we denote as $\mathcal{C}(\mathbf{H}, P)$. We include the variable $\mathbf{H}$, which refers to the aggregate channel from the transmitter to all mobiles, to emphasize the fact that $\mathcal{C}(\mathbf{H}, P)$ is the capacity for a specific channel realization. While the rate equations describing the capacity region are somewhat intractable, the dual MIMO multiple access channel (MAC), which has the same capacity region as the MIMO BC [JVG04, VJG03], allows for a simpler characterization of the capacity region:

$$\mathcal{C}(\mathbf{H}, P) = \bigcup_{\substack{\mathbf{Q}_1,\cdots,\mathbf{Q}_K \\ \sum_{k=1}^{K}\mathrm{tr}(\mathbf{Q}_k)\leq P}} \left\{ \mathbf{R} : \sum_{k\in S} R_k \leq \log_2 \left| \mathbf{I} + \sum_{k\in S} \mathbf{H}_k^H\mathbf{Q}_k\mathbf{H}_k \right| \ \forall S \subseteq \mathcal{K} \right\}, \tag{5.2}$$

where $\mathbf{Q}_k$ is the $N \times N$ MAC transmit covariance matrix for user k, and $\mathcal{K}$ denotes the set of all possible combinations of $1, \cdots, K$. Note that a simple functional relationship between the MAC covariance matrices and the corresponding BC covariance matrices (achieving the same rates) is known [VJG03].

This dual characterization allows the boundary of the capacity region $\mathcal{C}(\mathbf{H}, P)$ to be found by solving the following convex optimization problem:

$$f(\mu) \triangleq \max \mu \cdot \mathbf{R} \ \text{ subject to } \ \mathbf{R} \in \mathcal{C}(\mathbf{H}, P), \tag{5.3}$$

where $\mu = [\mu_1 \ \mu_2 \ \cdots \ \mu_K]^T$ is the rate reward vector which will be referred to as the *weight* vector and $\mathbf{R} = [R_1 \ R_2 \ \cdots \ R_K]^T$ is the rate vector. The optimization finds the point on the boundary of

the capacity region where the tangent to the capacity region is defined by the weight vector. A steepest-descent algorithm is proposed in [VVH03] to solve this maximization for any weight vector. By solving (5.3) for all possible weight vectors satisfying $\sum_{i=1}^{K} \mu_i = 1$, the entire boundary of the capacity region can be traced out.

5.2 High SNR Analysis: Dirty Paper Coding vs. Linear Precoding

Dirty paper coding (DPC) was proved to achieve the capacity region of the multiple antenna broadcast channel (BC) [WSS06]. However, implementation of DPC requires significant complexity at both transmitter and receiver, and the problem of finding practical dirty paper codes close to the capacity limit is still open [EB05]. On the other hand, linear precoding is a low complexity but sub-optimal transmission technique (with complexity roughly equivalent to point-to-point MIMO) that is able to transmit the same number of data streams as a DPC-based system. Linear precoding therefore achieves the same multiplexing gain (which characterizes the slope of the capacity vs. SNR curve) as DPC, but incurs an absolute rate/power offset relative to DPC.

The contribution of this work is the quantification of this rate/power offset using the affine approximation developed by Shamai and Verdú [SV01]. At high SNR, the channel capacity $C(P)$ is well approximated by an affine function of SNR (P):

$$C(P) = \mathcal{S}_\infty \left(\log_2 P - \mathcal{L}_\infty\right) + o(1), \tag{5.4}$$

where $\mathcal{S}_\infty$ represents the multiplexing gain and $\mathcal{L}_\infty$ represents the power offset (in 3 dB units) that are defined as:

$$\mathcal{S}_\infty = \lim_{P\to\infty} \frac{C(P)}{\log_2(P)}, \tag{5.5}$$

$$\mathcal{L}_\infty = \lim_{P\to\infty} \left(\log_2(P) - \frac{C(P)}{\mathcal{S}_\infty}\right). \tag{5.6}$$

The multiplexing gain $\mathcal{S}_\infty$ is equal to the minimum of the number of transmit and receive antennas (for either point-to-point or downlink MIMO channels), and thus is essentially independent of the fading environment and signaling strategy. However, the power offset $\mathcal{L}_\infty$ does depend on the actual fading statistics and the signaling strategy. Reference [LTV05] provides an exact characterizations of these offset terms for point-to-point MIMO channels for the most common

fading models, such as iid Rayleigh fading, spatially correlated fading, and Ricean (line-of-sight) fading. Indeed, one of the key insights of [LTV05] is the necessity to consider these rate offset terms, because considering only the multiplexing gain can lead to rather erroneous conclusions, e.g., spatial correlation does not affect MIMO systems at high SNR.

In a similar vein, in this work we utilize the high SNR approximation to quantify the difference between optimal dirty paper coding and simpler linear precoding in an iid Rayleigh fading environment. By investigating the differential offsets between these two strategies, we are able to quantify the throughput degradation that results from using linear precoding rather than the optimal DPC strategy in spatially white fading[1] . We are also able to derive simple expressions for the average rate offset as a function of only the number of transmit and receive antennas and users for systems in which the aggregate number of receive antennas is no larger than the number of transmit antennas. Note that past work has analyzed the *ratio* between the sum rate capacity and the linear precoding sum rate [JG05, SCA$^+$06]. However, such analyses essentially capture only multiplexing gain effects and thus are limited in scope. By alternatively studying the absolute difference between the different sum rates, we are able to derive more meaningful and accurate conclusions.

In addition to the sum rate, we study weighted sum rate maximization (using DPC and linear precoding) and provide simple expressions for the rate offsets. One of the most interesting results is that weighted sum rate (for either DPC or linear precoding) is maximized at asymptotically high SNR by *allocating power directly proportional to user weights.* A similar result was recently observed in [LTV06] in the context of parallel single-user channels (e.g., for OFDMA systems). Because the linear precoding strategies we study result in parallel channels, the result of [LTV06] shows that it is asymptotically optimal to allocate power in direct proportion to user weights whenever linear precoding is used. By showing that weighted sum rate maximization when DPC is employed can also be simplified to power allocation over parallel channels, we are able to show that the same strategy is also asymptotically optimal for DPC.

[1] Although we do not pursue this avenue in the present publication, it would also be interesting to investigate the DPC-linear precoding offset in other fading environments, e.g., Ricean and spatially correlated fading. However, one must be careful with respect to channel models because some point-to-point MIMO models do not necessarily extend well to the MIMO broadcast channel. For example, in point-to-point channels spatial correlation captures the effect of sparse scattering at the transmitter and/or receiver and is a function of the angle-of-arrival. In a broadcast channel, the angle-of-arrival is typically different for every receiver because they generally are not physically co-located; as a result, using the same correlation matrix for all receivers is not well motivated in this context.

5.2.1 High SNR Sum Rate Approximations

In this subsection we compute the affine approximations to the dirty paper coding sum rate and the linear precoding sum rate at high SNR. In the following section these expressions are used to quantify the sum rate degradation incurred by linear precoding relative to DPC.

Dirty Paper Coding

The sum rate by DPC, which achieves the sum capacity [VJG03, VT03, YC04], can be written by the duality of the MIMO broadcast channel (BC) and the MIMO multiple access channel (MAC) [VJG03]:

$$C_{\mathrm{DPC}}(\mathbf{H},P) = \max_{\sum_k \mathrm{tr}(\mathbf{Q}_k)\leq P} \log_2 \left| \mathbf{I} + \sum_{k=1}^{K} \mathbf{H}_k^H \mathbf{Q}_k \mathbf{H}_k \right|, \tag{5.7}$$

where $\mathbf{Q}_k$ represent the $N \times N$ transmit covariance matrices in the dual MAC. No closed-form solution to (5.7) (which is convex) is known to exist, but it has been shown that $C_{\mathrm{DPC}}(\mathbf{H},P)$ converges (absolutely) to the capacity of the point-to-point MIMO channel with transfer matrix $\mathbf{H}$ whenever $M \geq KN$:

Theorem 5.1 (Theorem 3 in [CS03])**.** *When $M \geq KN$ and $\mathbf{H}$ has full row rank,*

$$\lim_{P\to\infty} \left[C_{DPC}(\mathbf{H},P) - \log_2 \left| \mathbf{I} + \frac{P}{KN} \mathbf{H}^H \mathbf{H} \right| \right] = 0. \tag{5.8}$$

Using this result we can make a few important observations regarding the optimal covariance matrices at high SNR. Since

$$\log_2 \left| \mathbf{I} + \frac{P}{KN} \sum_{k=1}^{K} \mathbf{H}_k^H \mathbf{H}_k \right| = \log_2 \left| \mathbf{I} + \frac{P}{KN} \mathbf{H}^H \mathbf{H} \right|, \tag{5.9}$$

choosing each of the dual MAC covariance matrices as $\mathbf{Q}_k = \frac{P}{KN}\mathbf{I}$ in (5.7) achieves sum capacity at asymptotically high SNR. Thus, uniform power allocation across the KN antennas in the dual MAC is asymptotically optimal. As a result, an affine approximation for the sum rate can be found as:

$$C_{\mathrm{DPC}}(\mathbf{H},P) \cong KN \log_2 P - KN \log_2 KN + \log_2 \left| \mathbf{H}\mathbf{H}^H \right|, \tag{5.10}$$

where $\cong$ refers to equivalence in the limit (i.e., the difference between both sides converges to zero as $P \to \infty$). Since the MIMO broadcast and the $M \times KN$ point-to-point MIMO channel are equivalent at high SNR (Theorem 5.1), the high SNR results developed in [LTV05] directly apply

to the sum capacity of the MIMO broadcast channel. It is important to be careful regarding the ordering of the equivalent point-to-point MIMO channel: due to the assumption that $M \geq KN$, the MIMO broadcast is equivalent to the $M \times KN$ MIMO channel *with CSI at the transmitter*, which is equivalent to the $KN \times M$ MIMO channel *with or without CSI at the transmitter* (i.e., open-loop MIMO). When $M > KN$, the level of CSI at the transmitter affects the rate offset of the $M \times KN$ point-to-point MIMO channel. Finally, notice that the high SNR sum rate capacity only depends on the product of K and N and not on their specific values; this is not the case for linear precoding.

Linear Precoding

Linear precoding is a low-complexity, albeit sub-optimal, alternative to DPC. When linear precoding is used, the transmit signal vector $\mathbf{x}$ is a linear function of the data symbols $\mathbf{s}_1, \ldots, \mathbf{s}_K$:

$$\mathbf{x} = \sum_{k=1}^{K} \mathbf{V}_k \mathbf{s}_k, \tag{5.11}$$

where $\mathbf{V}_k (\in \mathbb{C}^{M \times N})$ is the precoding matrix for user k and $\mathbf{s}_k (\in \mathbb{C}^{N \times 1})$ is the data symbol intended for user k. This expression illustrates linear precoding's complexity advantage: if DPC is used, the transmit signal is formed by performing dirty-paper sums, which are complex non-linear operations, whereas linear precoding requires only standard linear operations. The resulting received signal for user k is given by

$$\mathbf{y}_k = \mathbf{H}_k \mathbf{V}_k \mathbf{s}_k + \sum_{j \neq k} \mathbf{H}_k \mathbf{V}_j \mathbf{s}_j + \mathbf{n}_k, \tag{5.12}$$

where the second term in (5.12) represents the multi-user interference. In order to eliminate the multi-user interference, the precoding matrices must satisfy very stringent conditions. Note that eliminating multi-user interference is desirable at high SNR in order to prevent interference-limited behavior.

In this paper, we consider two linear precoding techniques that cancel out the multi-user interference: block diagonalization (BD) and zero-forcing (ZF). To perform BD, the precoding matrices $\{\mathbf{V}_j\}_{j=1}^{K}$ are required to be chosen such that for all $j (\neq k) \in [1, K]$,

$$\mathbf{H}_k \mathbf{V}_j = \mathbf{O}, \tag{5.13}$$

when $M \geq KN$. To perform ZF, which is a special case of BD, the precoding matrices are further imposed to be

$$\mathbf{h}_{k,n}\mathbf{v}_{j,l} = 0, \qquad \forall j(\neq k) \in [1,K], \ \ \forall n,l \in [1,N], \tag{5.14}$$

$$\mathbf{h}_{k,n}\mathbf{v}_{k,l} = 0, \qquad \forall l(\neq n) \in [1,N], \tag{5.15}$$

where $\mathbf{v}_{j,l}$ denotes the lth column vector of $\mathbf{V}_j$, this will zero force all inter-antenna inferences and consequently equivalent to a channel KN single antenna receivers (known as zero-forcing *beamforming*); this ZF can be employed for $N > 1$. Note that $\mathbf{H}$ having full row rank is sufficient to ensure ZF and BD precoding matrices exist. In iid Rayleigh fading $\mathbf{H}$ has full row rank with probability one.

The sum rate by BD is given by [CM04, SSH04]

$$C_{\mathrm{BD}}(\mathbf{H},P) = \max_{\mathbf{Q}_k:\ \sum_{k=1}^{K} \mathrm{tr}\{\mathbf{Q}_k\} \leq P} \ \sum_{k=1}^{K} \log_2 \left|\mathbf{I} + \mathbf{G}_k^H \mathbf{Q}_k \mathbf{G}_k\right|, \tag{5.16}$$

where $\mathbf{G}_k (= \mathbf{H}_k \mathbf{V}_k)$ is the effective channel matrix and the optimal rate is achieved asymptotically by uniform power allocation at high SNR since the channel can be decomposed into parallel channels. Hence, the sum rate is asymptotically given by

$$C_{\mathrm{BD}}(\mathbf{H},P) \cong KN \log_2 P - KN \log_2 KN + \log_2 \prod_{k=1}^{K} |\mathbf{G}_k \mathbf{G}_k^H|. \tag{5.17}$$

As a special case, the sum rate by ZF is similarly given by [Jin05],

$$C_{\mathrm{ZF}}(\mathbf{H},P) \cong KN \log_2 P - KN \log_2 KN + \log_2 \prod_{k=1}^{K} \prod_{n=1}^{N} |g_{k,n}|^2, \tag{5.18}$$

where $g_{k,n} = \mathbf{h}_{k,n}\mathbf{v}_{k,n}$.

Equivalent MIMO Interpretation

Due to the properties of i.i.d. Rayleigh fading, systems employing linear precoding like zero-forcing or block diagonalization are equivalent to parallel point-to-point MIMO channels, as shown in [CM04]. When ZF is used, the precoding vector for each receive antenna (i.e., each row of the concatenated channel matrix $\mathbf{H}$) must be chosen orthogonal to the other $KN-1$ rows of $\mathbf{H}$. Due to the isotropic nature of iid Rayleigh fading, this orthogonality constraint consumes

Table 5.1: Sum rates at high SNR and their equivalent MIMO interpretation

	$C(\mathbf{H},P)$	MIMO Interpretation
DPC	$\log\left\|\frac{P}{KN}\mathbf{H}^H\mathbf{H}\right\|$	one $M \times KN$
BD	$\sum_{k=1}^{K}\log\left\|\frac{P}{KN}\mathbf{G}_k\mathbf{G}_k^H\right\|$	K parallel $(M-(K-1)N)\times N$
ZF	$\sum_{k=1}^{K}\sum_{n=1}^{N}\log\left(\frac{P}{KN}\|g_{k,n}\|^2\right)$	KN parallel $(M-KN+1)\times 1$

$KN-1$ degrees of freedom at the transmitter, and reduces the channel from the $1\times M$ vector $\mathbf{h}_{k,n}$ to a $1\times(M-KN+1)$ Gaussian vector. As a result, the effective channel norm $|g_{k,n}|^2$ of each parallel channel is chi-squared with $2(M-KN+1)$ degrees of freedom (denoted $\chi^2_{2(M-KN+1)}$). Therefore, a ZF-based system with uniform power loading is exactly equivalent (in terms of ergodic throughput) to KN parallel $(M-KN+1)\times 1$ MIMO channels (with CSIT).

When BD is used, the orthogonality constraint consumes $(K-1)N$ degrees of freedom. This reduces the channel matrix $\mathbf{H}_k$, which is originally $N\times M$, to a $N\times(M-(K-1)N)$ complex Gaussian matrix. As a result, the $N\times N$ matrix $\mathbf{G}_k\mathbf{G}_k^H$ is Wishart with $M-(K-1)N$ degrees of freedom, and therefore a BD-based system is equivalent to K parallel $(M-(K-1)N)\times N$ parallel MIMO channels (with CSIT).

Finally, when DPC is used, the MIMO broadcast channel is equivalent to the $M\times KN$ point-to-point MIMO channel, where $M\geq KN$ and CSIT is again assumed. Note that a MIMO channel of this dimension can be interpreted as a series of parallel channels as well: in this case, the $M\times KN$ channel is equivalent to $M\times 1, M-1\times 1,\ldots,M-KN+1\times 1$ channels in parallel [FG98].

For all three cases, the MIMO equivalence is exact when uniform power loading is used, which is summarized in Table 5.1. If optimal power allocation is performed, for either ZF, BD, or DPC, the MIMO broadcast systems can achieve a larger ergodic throughput than the MIMO equivalent at finite SNR. However, because waterfilling provides a vanishing benefit as SNR is increased, this advantage disappears at asymptotically high SNR.

Fig. 5.1 illustrates the equivalent MIMO channels for $M=7, N=2, K=3$. In this case ZF is equvalent to 6 parallel 2×1 channels, BD is equivalent to 3 parallel 3×2 channels, and DPC is equivalent to a 7×6 channel. The absolute difference in throughput at asymptotically high SNR is indeed due to the diference in the degrees of freedom in the available parallel channels, as made precise in the following section.

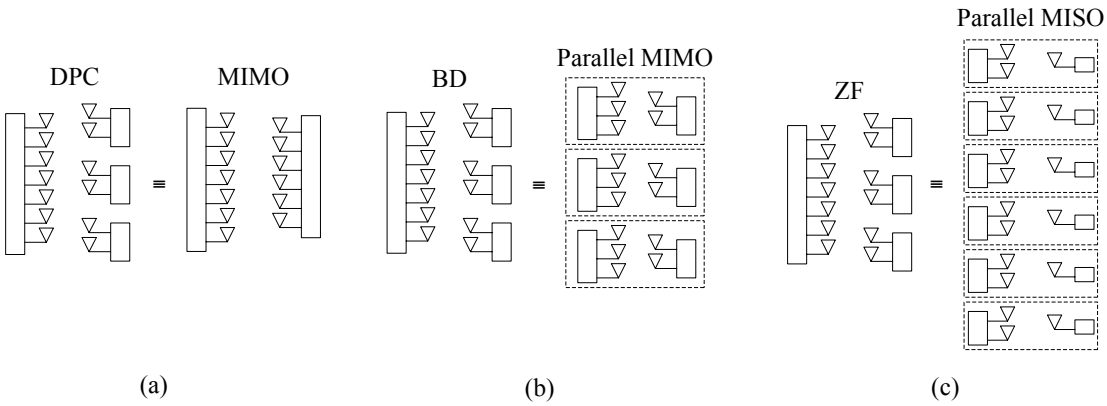

Figure 5.1: The broadcast channel with $M = 7$, $N = 2$, and $K = 3$ can be interpreted in terms of its sum rate as (a) 7×6 DPC is employed, (b) 3 parallel 3×2 MIMO channels when BD is employed, and (c) 6 parallel 2×1 MISO channels is employed

Our analysis is limited to channels in which $M \geq KN$. If $M < KN$, i.e., there are strictly less transmit antennas than aggregate receive antennas, then no MIMO equivalent channel exists for either DPC or linear precoding. The sum capacity (DPC) is smaller than the capacity of the $M \times KN$ (forward) cooperative channel (in which CSIT is not required at high SNR), but is larger than the capacity of the reverse $KN \times M$ cooperative channel without CSIT. Zero forcing and block diagonalization are clearly only feasible when the number of data streams is no greater than M. Thus, if there are more than M receive antennas, some form of selection (of users and possibly of the number of data streams per receiver) must be performed. As a result of these complications, it does not appear that the high SNR framework will yield closed-form solutions for either DPC or linear precoding when $M < KN$.

5.2.2 High SNR Offset Calculations

We define the rate loss as the asymptotic (in SNR) difference between the sum rate capacity (DPC) and the BD sum rate:

$$\beta_{\text{DPC-BD}}(\mathbf{H}) \triangleq \lim_{P\to\infty} \left[C_{\text{DPC}}(\mathbf{H}, P) - C_{\text{BD}}(\mathbf{H}, P)\right]. \tag{5.19}$$

Since each of the capacity curves has a slope of $\frac{KN}{3}$ in units of bps/Hz/dB, this rate offset (i.e., the vertical offset between capacity vs. SNR curves) can be immediately translated into a

power offset (i.e., a horizontal offset): $\Delta_{\text{DPC-BD}}(\mathbf{H}) = \frac{3}{KN}\beta_{\text{DPC-BD}}(\mathbf{H})$ dB. Because $\Delta_{\text{DPC-BD}}$ is in dB units, we clearly have $\Delta_{\text{DPC-BD}}(\mathbf{H}) = 3(\mathcal{L}_\infty^{\text{BD}}(\mathbf{H}) - \mathcal{L}_\infty^{\text{DPC}}(\mathbf{H}))$. In terms of the high SNR approximation, the rate offset is precisely the difference between the $\mathcal{L}_\infty$ terms for DPC and linear precoding multiplied by $\mathcal{S}_\infty$.

From the affine approximation to DPC and BD sum rate found in (5.10) and (5.17), the rate loss incurred by BD is:

$$\beta_{\text{DPC-BD}}(\mathbf{H}) = \log_2 \frac{|\mathbf{H}^H\mathbf{H}|}{\prod_{k=1}^{K} |\mathbf{G}_k\mathbf{G}_k^H|}. \tag{5.20}$$

By averaging across the fading distribution, we can calculate the average rate offset: $\bar{\beta}_{\text{DPC-BD}} \triangleq \mathbb{E}_{\mathbf{H}}[\beta_{\text{DPC-BD}}(\mathbf{H})]$, which allows a comparison of ergodic throughput. Likewise, the average power offset (denoted as $\bar{\Delta}_{\text{DPC-BD}}$) can be calculated in the same fashion. Since the matrices $\mathbf{H}^H\mathbf{H}$ and $\mathbf{G}_k\mathbf{G}_k^H$ are Wishart under iid Rayleigh fading, we can get a simple closed form expression for the rate offset[2] :

Theorem 5.2. *The expected loss in Rayleigh fading due to block diagonalization is given by*

$$\bar{\beta}_{DPC\text{-}BD}(M,K,N) = (\log_2 e) \sum_{k=0}^{K-1} \sum_{n=0}^{N-1} \sum_{i=kN+1}^{(K-1)N} \frac{1}{M-n-i} \quad \text{(bps/Hz)}. \tag{5.21}$$

Proof. See Section 5.4.1. □

If the number of transmit antennas M is kept fixed but N is increased and K is decreased such that KN is constant, i.e., the number of antennas per receiver is increased but the aggregate number of receive antennas is kept constant, then the rate offset decreases. Recall that the DPC sum rate depends only on the product of K and N not the individual values. In the degenerate case $M = N$ and $K = 1$ the channel becomes a point-to-point MIMO channel and the offset is indeed zero.

We can easily determine the zero forcing offset by noting that it depends only on the product KN:

$$\bar{\beta}_{\text{DPC-ZF}}(M,K,N) = \bar{\beta}_{\text{DPC-ZF}}(M,KN,1) = \bar{\beta}_{\text{DPC-BD}}(M,KN,1). \tag{5.22}$$

In the following subsections we gain some insight into these results by first further studying zero forcing and then considering block diagonalized systems.

[2] It is straightforward to use this result to determine the rate offset of BD in terms of the rate offset $\mathcal{L}_\infty^{\text{MIMO}}(KN,M)$ of a $KN \times M$ MIMO channel in iid Rayleigh fading given in Proposition 1 of [LTV05]: $\mathcal{L}_\infty^{\text{BD}}(M,K,N) = \mathcal{L}_\infty^{\text{MIMO}}(KN,M) + \frac{1}{KN}\bar{\beta}_{\text{DPC-BD}}(M,K,N)$.

Zero Forcing

To understand the rate penalty associated with zero forcing, we study the behavior of the offset as system size increases. The first case of interest is when $M = KN$, i.e., the total number of receive antennas is equal to the number of transmit antennas. In Section 5.4.2 we show that the offset in this scenario can be well approximated as:

$$\bar{\beta}_{\text{DPC-ZF}}(M,M,1) \approx M \log_2 M \quad \text{(bps/Hz)} \tag{5.23}$$

in the sense that the ratio of both sides converges to one as M grows large. In this scenario, the ZF sum rate is associated with the capacity of M parallel 1×1 (SISO) channels while the DPC sum rate is associated with an $M \times M$ MIMO channel. This corresponds to a power offset of $3\log_2 M$ (dB), which is very significant when M is large. Numerical results show that the approximation $3\log_2 M$ (dB) overstates the power penalty by 1 to 1.5 dB for reasonable values of $M(< 20)$, but it does capture the growth rate correctly. Such a large penalty is not surprising, since the use of zero-forcing requires inverting the $M \times M$ matrix $\mathbf{H}$, which is poorly conditioned with high probability when M is large.

The behavior of zero-forcing is quite different if the number of receivers is strictly smaller than M. If system size increases such that $M, K \to \infty$ with $M = \alpha KN$ for some $\alpha > 1$, the power offset converges to a constant (see proof in Section 5.4.3):

$$\bar{\Delta}_{\text{DPC-ZF}}(\alpha) = -3\left(\log_2 e + \alpha \log_2\left(1 - \frac{1}{\alpha}\right)\right) \qquad \text{(dB)}. \tag{5.24}$$

Thus for large systems, ZF is a viable low-complexity alternative to DPC if the number of transmit antennas can be made suitably large. A similar conclusion was drawn in [HV02] where the ratio of the rates achievable with ZF relative to the sum capacity is studied. Note that using ZF on the MIMO downlink channel is identical to using a decorrelating receiver on the multiple antenna uplink channel or in a randomly spread CDMA system; see Eq. (152) of [SV01] for the asymptotic performance of the decorrelating CDMA receiver.

Block Diagonalization

To gain some insight into Theorem 5.2, we first note a simple property of the rate offset. If the number of transmit antennas M is kept fixed but N is increased and K is decreased such that KN is constant, i.e., the number of antennas per receiver is increased but the aggregate number of

receive antennas is kept constant, then the rate offset decreases. Indeed, this observation can be reached by simply considering the equivalent MIMO channels discussed in Section 5.2.1.

It is also very useful to analyze the offset between BD (K receivers with N antennas each) and ZF (equivalent to KN receivers with 1 antenna each). Some simple manipulations of the earlier results yield the following theorem:

Theorem 5.3. *If $M = \alpha KN$ with $N > 1$ and $\alpha \geq 1$, the expected throughput gain of BD relative to ZF is:*

$$\begin{aligned} \bar{\beta}_{BD\text{-}ZF} &\triangleq \bar{\beta}_{DPC\text{-}ZF}(M,NK) - \bar{\beta}_{DPC\text{-}BD}(M,N,K) \\ &= (\log_2 e)K \sum_{j=1}^{N-1} \frac{(N-j)}{(\alpha-1)KN+j} \quad \text{(bps/Hz)}. \end{aligned} \tag{5.25}$$

Proof. See Section 5.4.4. □

Furthermore, when $M = KN$ the power offset between BD and ZF is a function only of N (i.e., is independent of the particular values of M and K):

$$\bar{\Delta}_{\text{BD-ZF}}(N) = \frac{3(\log_2 e)}{N} \sum_{j=1}^{N-1} \frac{N-j}{j} \quad \text{(dB)}. \tag{5.26}$$

For example, consider two system configurations: (i) $\frac{M}{2}$ receivers each have two antennas, and (ii) M receivers each have one antenna. Equation (5.26) indicates that the power advantage of using BD in the $N = 2$ system is $\bar{\Delta}_{\text{BD-ZF}}(2) = 2.1640$ (dB) relative to performing ZF that is independent of M. That is, it is the same for $M = 4$ and $K = 4, N = 1$ vs. $K = 2, N = 2$ systems as well as for $M = 6$ and $K = 6, N = 1$ vs. $K = 3, N = 2$ systems. To illustrate the utility of the asymptotic rate offsets, sum rates are plotted in Fig. 5.2 for systems with $M = 12$ and $N = 3$, $K = 4$, and $N = 2$, $K = 6$. Notice that the asymptotic offsets provide insight at even moderate SNR levels (e.g., 10 dB). When $M = 12,\ N = 3,\ K = 4$, $\bar{\beta}_{\text{BD-ZF}} = 14.4270$ (bps/Hz) and $\bar{\Delta}_{\text{BD-ZF}} = 3.6067$ (dB) while the numerical values are 14.6 (bps/Hz) and 3.65 (dB), respectively.

Unequal Average SNR's

Near-far effects in a wireless broadcast channel environment can lead to asymmetric channel gains; i.e., the channel gain of user k is now $\mathbf{H}_k = \sqrt{\gamma_k}\tilde{\mathbf{H}}_k$, where γ_k denotes the average SNR of user k. The elements of $\tilde{\mathbf{H}}_k$ have Gaussian distribution with mean zero and unit variance

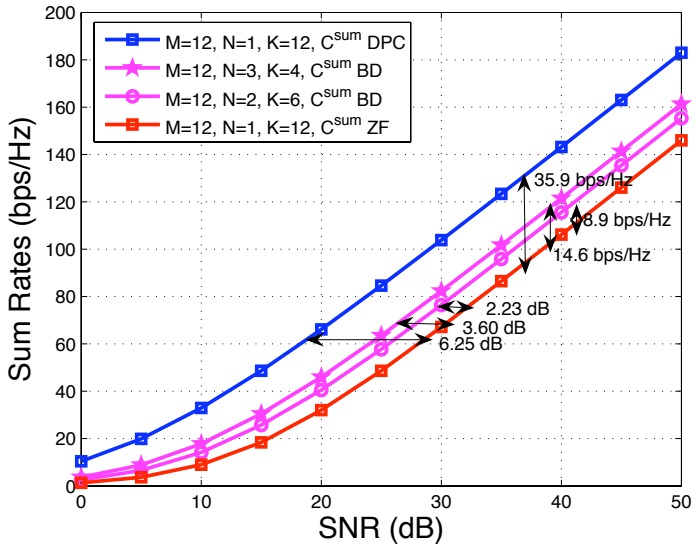

Figure 5.2: Comparison of (5.21) and (5.26) with simulated rate losses and power offsets

by assumption. It is important to note that the uniform power allocation is still asymptotically optimal even when users' SNR are asymmetric since $M \geq KN$. Thus, we can derive that all the sum rates by DPC, ZF, and BD are shifted equally by $N\sum_{k=1}^{K}\log_2\gamma_k$, i.e., (see Section 5.4.5 for derivation)

$$C_{\mathrm{DPC}}(\mathbf{H},P) \;\cong\; C_{\mathrm{DPC}}(\tilde{\mathbf{H}},P)+N\sum_{k=1}^{K}\log_2\gamma_k, \tag{5.27}$$

$$C_{\mathrm{ZF}}(\mathbf{H},P) \;\cong\; C_{\mathrm{ZF}}(\tilde{\mathbf{H}},P)+N\sum_{k=1}^{K}\log_2\gamma_k, \tag{5.28}$$

$$C_{\mathrm{BD}}(\mathbf{H},P) \;\cong\; C_{\mathrm{BD}}(\tilde{\mathbf{H}},P)+N\sum_{k=1}^{K}\log_2\gamma_k, \tag{5.29}$$

where $C_{\mathrm{DPC}}(\tilde{\mathbf{H}},P)$, $C_{\mathrm{ZF}}(\tilde{\mathbf{H}},P)$, and $C_{\mathrm{BD}}(\tilde{\mathbf{H}},P)$ are the sum rates under the symmetric channel gain scenario. As a result, the DPC-ZF and DPC-BD offsets are unaffected.

Fig. 5.3 illustrates that the sum rates by optimal power allocation and uniform power allocation tend to zero as power grows both for DPC and ZF. Unlike the symmetric channel gain case, more transmit power is required to make the difference sufficiently small.

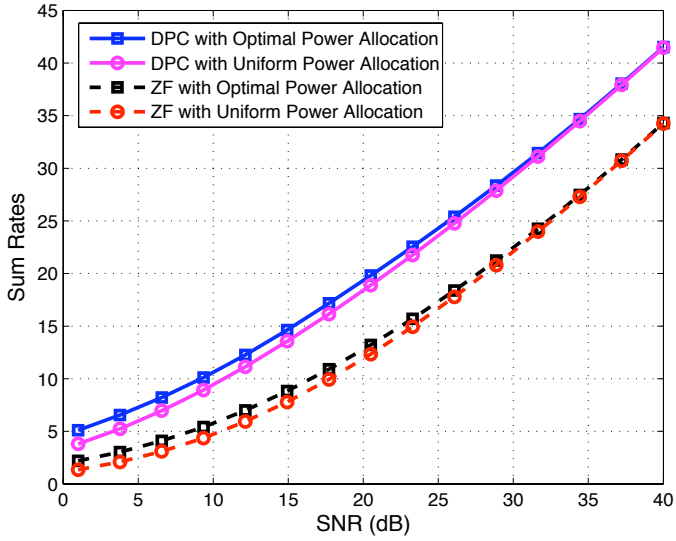

Figure 5.3: Average sum rates with the optimal power allocation and the uniform power allocation when $M = 4$, $N = 1$, $K = 4$, with unequal SNR: $\gamma_1 = 0.1$, $\gamma_2 = 0.5$, $\gamma_3 = 1$, $\gamma_4 = 2$

5.2.3 Weighted Sum Rate Analysis

In this section we generalize the rate offset analysis to weighted sum rate. The sum rate offset quantifies the difference between the sum rate points of both regions; the weighted sum rate offset is intended to describe the offset for the other portions of the rate region.

We first show that allocating power in proportion to user weights is asymptotically optimal for either DPC or BD, and then use this result to compute the associated rate offsets.

Asymptotically Optimal Power Allocation

Without loss of generality, we assume user weights are given in descending order: $\mu_1 \geq \mu_2 \geq \cdots \geq \mu_K \geq 0$ with $\sum_{k=1}^{K} \mu_k = 1$. The maximum weighted sum rate problem (DPC) can be written in terms of the dual MAC as:

$$C_{\text{DPC}}(\mu, \mathbf{H}, P) = \max_{\sum_{k=1}^{K} \text{tr}(\mathbf{Q}_k) \leq P} \sum_{k=1}^{K} \mu_k \log_2 \frac{|\mathbf{A}^{(k)}|}{|\mathbf{A}^{(k-1)}|}, \tag{5.30}$$

where $\mathbf{A}^{(k)} = \mathbf{I} + \sum_{j=1}^{k} \mathbf{H}_j^H \mathbf{Q}_j \mathbf{H}_j$ for $k \geq 1$ and $\mathbf{A}^{(0)} = \mathbf{I}$. Notice that the uplink (or the dual MAC) decoding is done in order of increasing weight, i.e., user K does not get the benefit of any

interference cancellation while user 1's signal benefits from full interference cancellation and is thus detected in the presence of only noise. From the construction of $\mathbf{A}^{(k)}$, we have

$$\frac{|\mathbf{A}^{(k)}|}{|\mathbf{A}^{(k-1)}|} = \left|\mathbf{I} + \mathbf{Q}_k \mathbf{H}_k (\mathbf{A}^{(k-1)})^{-1} \mathbf{H}_k^H\right|.$$

The following lemma shows that if we limit ourselves to linear power allocation policies of the form $\mathrm{tr}(\mathbf{Q}_k) = \alpha_k P$, then the objective function in (5.30) can be decoupled at high SNR:

Lemma 5.4. *Let $\mathbf{F}_k$ ($k = 1, \cdots, K$) be the projection of $\mathbf{H}_k$ onto the nullspace of $\{\mathbf{H}_j\}_{j=1}^{k-1}$. If $M \geq KN$, then*

$$\lim_{P\to\infty} \left[\mathbf{H}_k (\mathbf{A}^{(k-1)})^{-1} \mathbf{H}_k^H - \mathbf{F}_k \mathbf{F}_k^H\right] = 0, \qquad k = 1, \cdots, K. \tag{5.31}$$

Proof. See Section 5.4.6. □

Once the weighted sum rate maximization has been decoupled into the problem of maximizing weighted sum rate over parallel single-user channels, we can use the result of [LTV06] to show that the optimal power allocation is of the form $P_k^* = \mu_k P + O(1)$.

Theorem 5.5. *When $M \geq KN$, allocating power according to*

$$\mathbf{Q}_k = \frac{\mu_k P}{N} \mathbf{I}, \qquad k = 1, \cdots, K. \tag{5.32}$$

asymptotically achieves the optimal solution to (5.30) *at high SNR.*

Proof. See Section 5.4.7. □

Theorem 5.5 generalizes the fact that uniform power allocation achieves the maximum sum rate asymptotically at high SNR. That is, for the sum rate problem the weights are the same (i.e., $\mu_1 = \cdots = \mu_K = 1/K$), thus the uniform power policy is asymptotically optimal.

Meanwhile, the weighted sum rate of BD is given by

$$C_{\mathrm{BD}}(\mu, \mathbf{H}, P) = \max_{\mathbf{Q}_k \,:\, \sum_{k=1}^K \mathrm{tr}(\mathbf{Q}_k) \leq P} \sum_{k=1}^K \mu_k \log_2 \left|\mathbf{I} + \mathbf{Q}_k \mathbf{G}_k \mathbf{G}_k^H\right|, \tag{5.33}$$

where $\mathbf{G}_k$ is the projection of $\mathbf{H}_k$ onto the null space of $\{\mathbf{H}_1, \cdots, \mathbf{H}_{k-1}, \mathbf{H}_{k+1}, \cdots, \mathbf{H}_K\}$. (cf. $\mathbf{F}_k$ in Lemma 5.4 is the projection of $\mathbf{H}_k$ onto the null space of $\{\mathbf{H}_1, \cdots, \mathbf{H}_{k-1}\}$.) Likewise, the optimization (5.33) is the same as the optimization (5.55) and (5.56) except that $\mathbf{F}_k$ is replaced

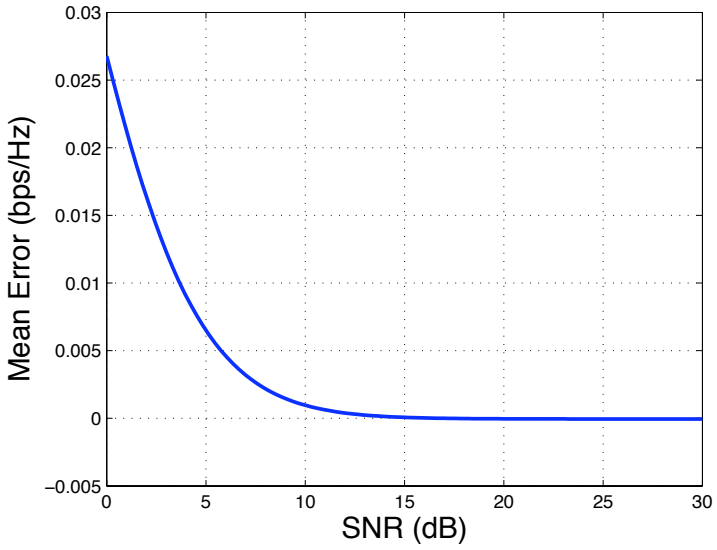

Figure 5.4: Averaged weighted sum rate difference between the exact solution and the asymptotic solution when $\mu_1 = 0.6$ and $\mu_2 = 0.4$ for Rayleigh fading channel

by $\mathbf{G}_k$ which does not contribute to the asymptotic solution. Thus, the power allocation policy in (5.32) is also the asymptotic solution to (5.33). By the same token, the weighted sum rate optimization by ZF can be easily solved at high SNR.

In Fig. 5.4 the difference between the true weighted sum rate (5.33) and the weighted sum rate achieved using $P_k = \mu_k P$ is plotted as a function of SNR. This difference is averaged over iid Rayleigh channel realizations for a $(M = 4, K = 2, N = 1)$ system with $\mu_1 = 0.6$ and $\mu_2 = 0.4$. The approximate power allocation is seen to give a weighted sum rate that is extremely close to the optimum even at very low SNR values.

Rate Loss

Using the asymptotically optimal power allocation policy of (5.32), the difference between the weighted sum rates by DPC and BD can be found as

$$\beta_{\text{DPC-BD}}(\mu, \mathbf{H}) = \sum_{k=1}^{K} \mu_k \log_2 \frac{|\mathbf{F}_k \mathbf{F}_k^H|}{|\mathbf{G}_k \mathbf{G}_k^H|} \tag{5.34}$$

per realization. In Rayleigh fading, the distribution of $\mathbf{F}_k\mathbf{F}_k^H$ is Wishart with $M-(k-1)N$ degrees of freedom while the distribution of $\mathbf{G}_k\mathbf{G}_k^H$ is Wishart with $M-(K-1)N$ degrees of freedom. Thus, we can compute the expected loss using the property of Wishart matrix:

$$\bar{\beta}_{\text{DPC-BD}}(\mu,M,K,N) = (\log_2 e)\sum_{k=1}^{K}\mu_k\left(\sum_{n=0}^{N-1}\sum_{j=M-(K-1)N-n}^{M-(k-1)N-n-1}\frac{1}{j}\right). \tag{5.35}$$

As done for the sum rate analysis, we can also calculate the rate/power offsets between BD and ZF with simple algebraic manipulations.

Besides that the sum rate problem is a special case of weighted sum rate problems, the sum rate has another property in terms of the rate offset. The expected rate offset is minimized at the sum rate; i.e., when $\mu_1 = \cdots = \mu_k = \frac{1}{K}$. If we let $\zeta_k = \sum_{n=0}^{N-1}\sum_{j=M-(K-1)N-n}^{M-(k-1)N-n-1}\frac{1}{j}$, then then $\zeta_1 > \zeta_2 > \cdots > \zeta_K$ and $\bar{\beta}_{\text{DPC-BD}} = (\log_2 e)\sum_{k=1}^{K}\mu_k\zeta_k$. Since $\{\mu_k\}$ has constraints of $\mu_1 \geq \cdots \geq \mu_K$, $\sum_{k=1}^{K}\mu_1 = 1$, and $\mu_k \geq 0$ $(1 \leq k \leq K)$, $\bar{\beta}_{\text{DPC-BD}}$ achieves minimum at $\mu_1 = \cdots = \mu_k = \frac{1}{K}$ for a given $\{\zeta_k\}$.

5.2.4 More Users Than Antennas

Although it is asymptotically optimal to allocate power in proportion to user weights when $M \geq KN$, this is not the case when $M < KN$. Indeed, such a strategy can easily be checked to be sub-optimal even for a single antenna broadcast channel with more than one user, as considered in [LG01a, Tse]. Allocating power directly proportional to user weights or allocating all power to only the user with the largest weight yields, for many single antenna broadcast channels, a weighted sum rate that is a bounded distance away from the true optimal weighted sum rate.

Although neither of these strategies is asymptotically optimal, numerical results do show that these approximations achieve rates that are extremely close to optimum. In general, there are two different reasonable power approximations. The first is to simply choose $P_k = \mu_k P$. However, when $K > M$, this results in sending many more data streams than there are spatial dimensions, which is not particularly intuitive. An alternative strategy is to allocate power to the users with the M largest weights, but again in proportion to their weights.

Fig. 5.5 illustrates the ergodic weighted sum rates vs SNR for a $K = 3, M = 2, N = 1$ system in which $\mu_1 = 0.5$, $\mu_2 = 0.3$, and $\mu_3 = 0.2$, averaged over Rayleigh fading. The true weighted sum rate is compared to the first strategy, where $P_k = \mu_k P$, and to the second strategy, where only users 1 and 2 are allocated power according to: $P_1 = \frac{\mu_1}{\mu_1+\mu_2}P$, $P_2 = \frac{\mu_2}{\mu_1+\mu_2}P$, and $P_3 = 0$. Both

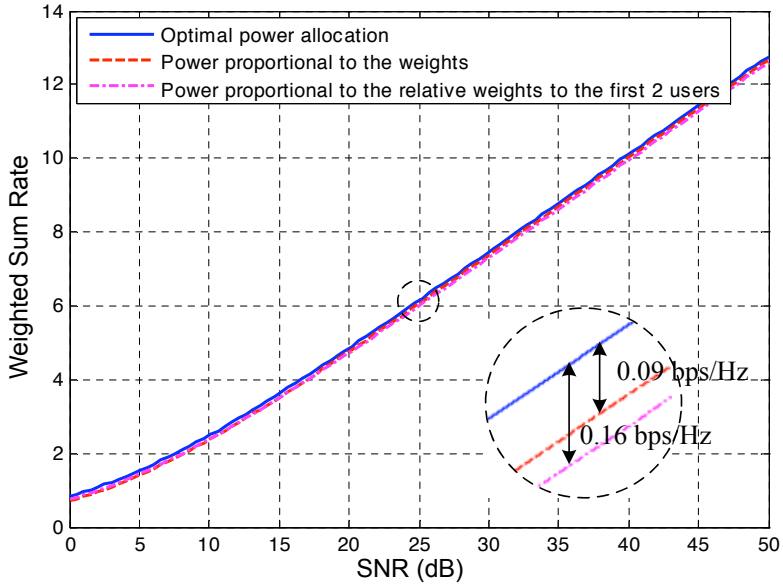

Figure 5.5: Ergodic weighted sum rates by DPC and by approximations when $M = 2$, $N = 1$, $K = 3$, with $\mu_1 = 0.5$, $\mu_2 = 0.3$, and $\mu_3 = 0.2$

approximations are a non-zero distance away from the optimum, but the rate loss is seen to be extremely small.

In a more general weighted sum rate setting, the decoding order or the precoding order is determined according to the order of weights. Empirical results show that the ratio of powers allocated to the first M users with largest weights are very close in value to the ratio of their weights. That is, if we assume that $\mu_1 \geq \cdots \geq \mu_M \geq \mu_{M+1} \geq \cdots \geq \mu_K$ without loss of generality, then at optimum, we have

$$P_1 : \cdots : P_M \approx \mu_1 : \cdots : \mu_M. \tag{5.36}$$

The remaining $K - M$ users, however, have powers either when their channel gains are high or when their weights are relatively comparable.

5.2.5 Summary

We have investigated the difference between the throughputs achieved by dirty paper coding (DPC) relative to those achieved with linear precoding strategies by utilizing the affine approximation to high SNR and computing the exact throughput/power offsets at asymptotically high

SNR for MIMO broadcast channels in which the number of transmit antennas is no smaller than the total number of receive antennas. Simple expressions in terms of the number of transmit and receive antennas are provided for the average rate/power offset in a spatially white Rayleigh fading environment. When the aggregate number of receive antennas is equal or slightly less than than the number of transmit antennas, linear precoding incurs a rather significant penalty relative to DPC, but this penalty is much smaller when the number of transmit antennas is large relative to the number of receive antennas.

Furthermore, we generalized our analysis to weighted sum rate and quantified the asymptotic rate/power offsets for this scenario as well. One of the most interesting aspects of this extension is the finding that allocating power directly proportional to user weights is asymptotically optimal for DPC at high SNR. This result is an extension at a similar result for parallel channels found in [LTV06], and this simple yet asymptotically optimal power policy may prove to be useful in other setting such as opportunistic scheduling.

5.3 Symmetric Capacity

While the sum capacity is is an extremely useful metric, the resulting rate allocation to receivers can be very non-uniform: users with strong channels are typically allocated more rate than users with weaker channels, and some users may not be allocated any rate at all. In a single antenna broadcast channel, for example, the sum capacity achieving strategy is to transmit to only the user with the largest channel gain. In a MIMO broadcast channel with M antennas at the access point (AP), sum capacity is generally achieved by simultaneously transmitting to M or more receivers. Since the rate allocation can be very unequal, and some receivers may be given no rate at all. This may be undesirable in certain systems, particularly those with unequal receiver channel qualities, and a more attractive option is to allocate rates more uniformly. Thus, the *symmetric capacity*, defined to be the maximum rate that can be allocated to every receiver [RM94], is an important capacity metric.

We focus on quasi-static channels, where the channel is fixed over the time period of interest (i.e., over the period of the delay constraints). In this scenario, the instantaneous rates achievable during a particular channel realization are of importance because no scheduling over different channel realizations can be performed. The symmetric capacity represents the fairest rate allocation in such a scenario. Note that the majority of work on scheduling and fairness for

broadcast channels (e.g., research on the proportionally-fair algorithm) concentrates on long-term average rates. We alternatively focus on instantaneous rates, which are meaningful when mobility is limited and delay constraints are very stringent.

In this section we develop an algorithm that computes the symmetric capacity of a multiple-input multiple-output (MIMO) broadcast channel. While efficient algorithms for computing the sum capacity as well as the boundary of the capacity region exist [JRV+05, VVH03, Yu03, LY04], these cannot be used to directly compute the symmetric capacity, which is the point on the boundary of the capacity region that intersects with the 45 degree line through the origin (i.e., $R_1 = \cdots = R_K$). We characterize the symmetric capacity as a convex program and then utilize the ellipsoid method to find the symmetric capacity. Note that previous work has considered a similar problem for OFDM channels [RC00], but this work only considers the rates achievable using the sub-optimal strategy of FDMA. We instead deal with the true capacity region (achievable using superposition coding for single antenna channels and dirty paper coding for multiple antenna channels).

A simple modification of the algorithm can be used to compute the intersection of the capacity region boundary and any arbitrary ray from the origin, e.g., find where the line $R_2 = 2R_1$ intersects the capacity boundary. This is of interest if differentiated service is to be provided to different sets of users: for example, a set of premium users may be guaranteed double the rate of non-premium users. This modified algorithm can also be used to compute the minimum power required to achieved a desired rate vector. This is clearly of use to operators who need to determine the power required to meet specified rate demands. Though this paper focuses on the MIMO broadcast channel, the proposed algorithms can be applied to essentially any convex capacity region, e.g., the MIMO multiple access channel as well as fading and/or wideband multiple access or broadcast channels.

We recently found a similar work in [SVL05] for a wireline channel environment, referred to as *balanced capacity* which corresponds to our differentiated service capacity. Their work considers single antenna frequency selective broadcast and multiple access channels, and the capacity is found by iteratively solving Karush-Kuhn-Tucker (KKT) conditions. However, this algorithm does not easily extend to the multiple antenna channel considered here.

In addition, we study the difference between the sum capacity and the symmetric capacity, which represents the penalty for requiring absolutely fair rate allocation, and is thus termed the *fairness penalty*. The fairness penalty is exactly quantified in the limit of high signal-to-noise

ratio (SNR) for a 2 user channel, and numerical results are provided for systems with more users. We find that this fairness penalty is quite small, which indicates that requiring fair rate allocation induces very little reduction in total system throughput. Note that a similar conclusion has been drawn for broadcast channels with an asymptotically large number of users and a fixed number of antennas [VDSH05].

5.3.1 Capacity Algorithms

In this subsection, algorithms computing the symmetric capacity and differentiated capacity as well as a method to find the minimum required power to achieve a given rate vector are described.

Symmetric Capacity

It is theoretically feasible to directly solve for the symmetric capacity using the dual multiple access channel (MAC) characterization of $\mathcal{C}(\mathbf{H}, P)$, but this would result in a convex optimization problem with more than 2^K constraints, which is impractical for even moderate values of K. As an alternative, we develop an iterative algorithm that finds the slope of the boundary of the capacity region at the symmetric capacity rate vector, and by doing so finds the symmetric capacity. We first show that the symmetric capacity can be characterized as a simple convex program:

Theorem 5.6. *The symmetric capacity is equal to the minimum weighted sum of rates, where the minimum is taken over all possible weight vectors summing to one:*

$$\begin{aligned} C^{\text{sym}}(\mathbf{H}, P) &= \min_{\mu:\mu\geq 0,\ \sum_{i=1}^{K}\mu_i=1} f(\mu) \\ &= \min_{\mu_1,\ldots,\mu_{K-1}} h(\mu_1,\ldots,\mu_{K-1}), \end{aligned} \tag{5.37}$$

where $f(\mu)$ is defined in (5.3) and $h(\mu_1,\ldots,\mu_{K-1})$ is defined as:

$$h(\mu_1,\ldots,\mu_{K-1}) \triangleq f\left(\mu_1,\ldots,\mu_{K-1},1-\sum_{i=1}^{K-1}\mu_i\right).$$

Furthermore, $f(\mu)$ and $h(\mu_1,\ldots,\mu_{K-1})$ are convex functions and thus can be efficiently minimized.

Proof. See Section 5.4.8. □

This theorem simplifies the problem of finding the symmetric capacity to a $K-1$ dimensional unconstrained convex program, for which efficient techniques exist. Note that the function $f(\mu)$, and thus $h(\cdot)$, can be computed using the algorithm in [VVH03]. Since $f(\mu)$ and $h(\cdot)$ are defined as maximums, it is not clear if they are differentiable. However, a subgradient to $h(\cdot)$ can be found: if $\tilde{\mathbf{R}} \in \mathcal{C}(\mathbf{H}, P)$ achieves $h(\tilde{\mu}_1, \ldots, \tilde{\mu}_{K-1})$, then it is straightforward to show that $\mathbf{s}$ with $s_i = \tilde{\mathbf{R}}_i - \tilde{R}_K$ for $i = 1, \ldots, K-1$ is a subgradient. This implies that for any vector μ satisfying

$$([\mu]_1^{K-1} - [\tilde{\mu}]_1^{K-1}) \cdot \mathbf{s} \geq 0,$$

we have $h([\mu]_1^{K-1}) \geq h([\tilde{\mu}]_1^{K-1})$. Furthermore, the ellipsoid algorithm, which is a standard algorithm for unconstrained convex optimization, can be used in conjunction with subgradients to provably converge to the optimum.

Algorithm Description

In order to solve the convex minimization in (5.62) we utilize the ellipsoid algorithm, which can be used if subgradients can be computed and which provably converges to the optimum. The ellipsoid algorithm is essentially a generalization of the bisection method to multi-dimensional space (see [BV01] for more details) and is directly applied to the minimization of $h(\mu_1, \ldots, \mu_{K-1})$ in (5.62), as detailed in Algorithm 5.1. Note that variables $\mathbf{s}$ and $\mathbf{x}$ are $(K-1)$-dimensional vectors, $\mathbf{E}$ is a $(K-1) \times (K-1)$ matrix, and μ and $\mathbf{R}$ are K-dimensional vectors.

The algorithm is initiated by designating an ellipse that covers all feasible optimum points ($\mu_i \geq 0$ and $\sum_{i=1}^{K-1} \mu_i \leq 1$), i.e. $\mathbf{E} = (1 - 1/K)\mathbf{I}_{K-1}$ and $x_i = \mu_i = 1/K$ for $i = 1, \ldots, K-1$ (and $\mu_K = 1/K$). In each step, the rate vector maximizing $\mu \cdot \mathbf{R}$ is found. The weights $\mu_1, \ldots, \mu_K$ are then adjusted to attempt to equalize all user rates: users with large rates have their weights decreases, while users with small rates have their weights increased. The algorithm is terminated either when all rates R_1, R_2, $\cdots$, and R_K are sufficiently identical, or when the length of the major axis (i.e. the largest eigenvalue of $\mathbf{E}$) of the ellipsoid is sufficiently small (step 2). If $K = 2$, the ellipsoid method reduces to standard one-dimensional bisection (on μ_1).

Convergence Behavior

A standard proof for the convergence of the ellipsoid algorithm is given in [BV01], and it is easily shown that $h(\cdot)$ satisfies the required Lipschitz condition. However, the rate vectors returned by

Algorithm 5.1 Symmetric capacity with ellipsoid algorithm

1. $\mathbf{R} = \arg\max \mu \cdot \mathbf{R}$ subject to $\mathbf{R} \in \mathcal{C}(\mathbf{H}, P)$ (see [VVH03])
2. if $(\max(\text{eig}(\mathbf{E})) < tol)$ or $(|R_k - R_K| < tol, \forall k)$ ($\text{eig}(\mathbf{E})$ denotes eigenvalues of $\mathbf{E}$)
   break
3. Compute subgradient

$$\mathbf{s} = [\mathbf{R}]_1^{K-1} - R_K \tag{5.38}$$

$$\tilde{\mathbf{s}} = \frac{\mathbf{s}}{\sqrt{\mathbf{s}^T \mathbf{E} \mathbf{s}}} \tag{5.39}$$

4. Update ellipse

$$\mathbf{x}^+ = \mathbf{x} - \frac{1}{K}\mathbf{E}\tilde{s} \tag{5.40}$$

$$\mathbf{E}^+ = \frac{(K-1)^2}{(K-1)^2 - 1}\left(\mathbf{E} - \frac{2}{K}\mathbf{E}\tilde{\mathbf{s}}\tilde{\mathbf{s}}^T\mathbf{E}\right) \tag{5.41}$$

$$\{\mu^+\}_1^{K-1} = \mathbf{x}^+, \;\; \mu_K^+ = 1 - \sum_{i=1}^{K-1} \mu_i^+ \tag{5.42}$$

the ellipsoid algorithm can behave unusually due to the fact that the boundary of the capacity region has many flat (i.e., linear) sections.

When there are two receivers, the capacity region boundary is flat at the sum rate plane ($\mu_1 = \mu_2$). This is illustrated in Fig. 5.6. When the symmetric rate vector lies outside of the sum rate plane, as in Fig. 5.6a, the algorithm quickly converges to the weight vector characterizing the symmetric rate vector. The ellipsoid method, which reduces to bisection for $K = 2$, will tend to overshoot the correct weight vector, then undershoot, etc., until it converges to the optimum. In Fig. 5.6b, convergence is slightly complicated because the symmetric rate vector lies along the sum rate plane. The ellipsoid method will quickly determine that the optimal weight vector is in the vicinity of $\mu_1 = \mu_2 = 0.5$, but will eventually oscillate between points A and B. This is because if μ_1 is slightly smaller than μ_2, the $\max \mu \cdot \mathbf{R}$ routine will return a rate vector very close to point A. Since $R_2 > R_1$ at this point, the weights will be slightly adjusted such that μ_1 is slightly larger than μ_2. The corresponding rate vector will then be very close to point B. The weights will continue to oscillate between $\mu_1 > \mu_2$ and $\mu_1 < \mu_2$ (and the rate vectors

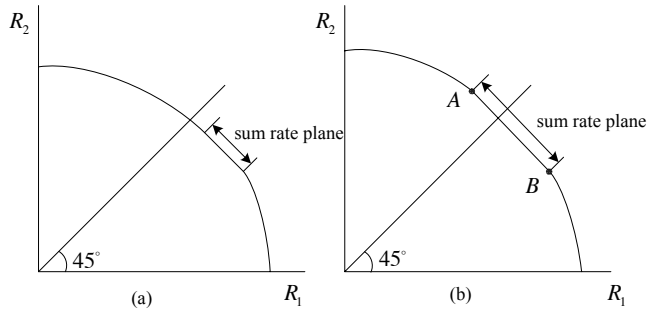

Figure 5.6: Capacity region boundary examples for two users

will oscillate between A and B), but will never exactly converge to $\mu_1 = \mu_2 = 0.5$. In order to determine the optimum point, in such scenarios the ellipsoid algorithm is terminated when the feasible ellipse is sufficiently small, and then the point within the sum rate plane is determined.

When there are more than 2 users, the capacity region boundary has a very large number of flat sections. Fig. 5.7 shows a capacity region for three users. The hexagon $ABCDEF$ is the sum rate plane, i.e. where $\mu_1 = \mu_2 = \mu_3 = 1/3$ [3] . The region $ABHG$, which corresponds to $\mu_1 = \mu_2 \geq \mu_3$, is flat in the R_1, R_2 direction, but not in R_3 (i.e. $ABHG$ is described by lines parallel to the (R_1, R_2) plane). Similarly, the regions $CDJI$ and $EFLK$ are flat in the (R_2, R_3) and (R_1, R_3) directions, respectively. Furthermore, region AFM, which corresponds to $\mu_2 = \mu_3 \leq \mu_1$, is flat in the (R_2, R_3) direction. Similarly, regions BCN and DEO are flat in the (R_1, R_3) and (R_1, R_2) directions, respectively.

When the equal rate line intersects the sum rate plane, the weight vector will be narrowed down to the vicinity of $\mu_1 = \mu_2 = \mu_3$, but will oscillate between points A, B, C, D, E, and F. If the symmetric capacity rate vector lies in region $ABHG$ ($\mu_1 = \mu_2 \leq \mu_3$), oscillation will occur between a rate vector very close to the AG line (μ_1 slightly larger than μ_2) and a rate vector close to the BH line (μ_2 slightly larger than μ_1). Regardless of these oscillations, though, the ellipse will become sufficiently small at some point and the algorithm can be properly terminated.

Figures 5.8 and 5.9 show the convergence of the weights and rates for the symmetric capacity in a three-user environment. When the weights are different at the symmetric capacity vector (i.e. the symmetric capacity vector does not lie on any of the flat sections of the capacity region boundary) as in Fig. 5.8, the rate of each user converges to the symmetric capacity point.

[3] Note that the sum rate plane is the only true plane on the boundary of the capacity region. The other sections are only flat in certain directions.

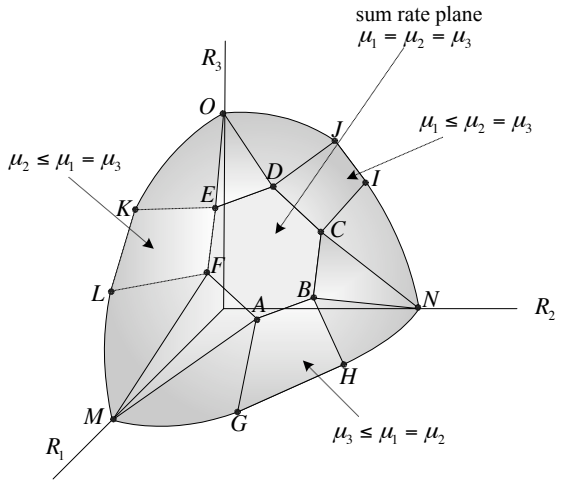

Figure 5.7: Capacity region example for a three user case

However, when the symmetric capacity vector lies on the sum rate plane, as illustrated in Fig. 5.9, the weights converge to the correct values but the rates oscillate, as described earlier. When the ellipsoid becomes sufficiently small, however, this oscillation can be recognized and the symmetric capacity can be computed.

Differentiated Service Capacity

As an alternative to providing equal rate service to all users, it may also be of interest to provide differentiated service to users, in which ratios of the rates allocated to each user are fixed. In a two user channel, as shown in Fig. 5.10, it may be of interest to compute the largest rate vector such that $R_1 = 2R_2$ (or vice versa). For arbitrary K, finding the differentiated rate vector corresponding to $R_1 = \frac{R_2}{\alpha_2} = \frac{R_3}{\alpha_3} = \cdots = \frac{R_K}{\alpha_K}$ is equivalent to finding the point where the line defined by $\alpha = (\alpha_1, \ldots, \alpha_K)$ with $\alpha_1 = 1$ intersects the boundary of the capacity region. We denote this as $C^{\text{diff}}(\alpha, \mathbf{H}, P)$, and the following is easily shown using the proof of Theorem 1:

$$C^{\text{diff}}(\alpha, \mathbf{H}, P) = \min_{\mu:\mu\geq 0,\ \sum_{i=1}^{K}\mu_i=1} \max_{\mathbf{R}\in\mathcal{C}(\mathbf{H},P)} \sum_{i=1}^{K} \frac{\mu_i}{\alpha_i} R_i. \tag{5.43}$$

As a result, the ellipsoid algorithm can also be used to find $C^{\text{diff}}(\alpha, \mathbf{H}, P)$, with the only changes being that $\sum_{i=1}^{K} \frac{\mu_i}{\alpha_i} R_i$ should be maximized in step 1, the condition in step 2 should check $|\frac{R_k}{\alpha_k} - \frac{R_K}{\alpha_K}|$, and the subgradient in step 3 is given by $\mathbf{s} = \frac{[\mathbf{R}]_1^{K-1}}{[\alpha]_1^{K-1}} - \frac{R_K}{\alpha_K}$.

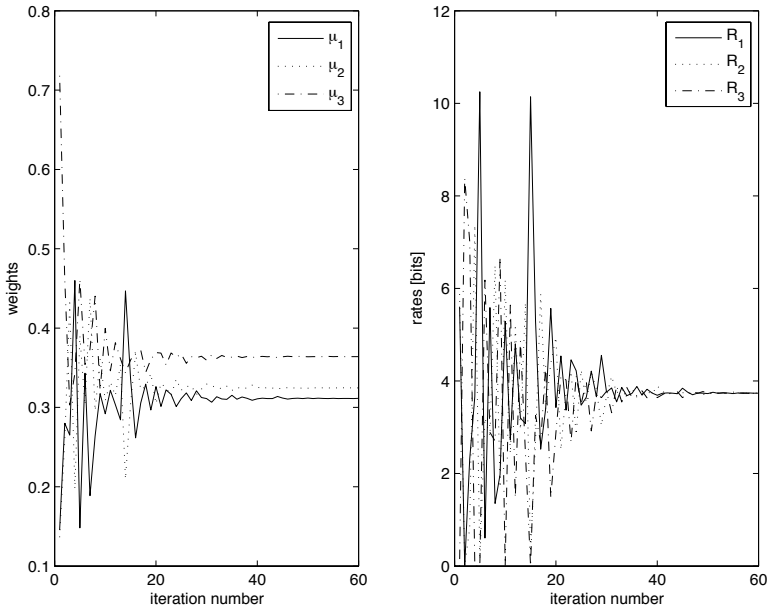

Figure 5.8: Convergence behavior when weights are distinct at C^{sym}

Minimum Power to Achieve a Rate Vector

Another important problem is determining the minimum required transmit power to achieve a given rate vector $\mathbf{R}$. For example, what is the required transmit power to serve V voice users at a specified rate and D data users at another rate for a specific channel realization? Previous research has provided sub-optimal solutions to this problem [SB04, FYL04], while we provide the optimal solution. The structure of the capacity region clearly implies that $\mathbf{R}$ lies on the boundary of $\mathcal{C}(P^{\min})$ for the minimum required power $P^{\min}$, and this minimum power can in fact easily be determined by utilizing the differentiated rate algorithm from the previous section. The key observation is that the differentiated capacity algorithm can be used to determine the intersection of the capacity region and an arbitrary line through the origin.

Note that other researchers have computed the minimum required power to achieve a desired rate vector under the assumption that there is *a priori* knowledge regarding the slope of the capacity region boundary $\mathcal{C}(P^{\min})$ at the rate vector $\mathbf{R}$ (i.e., knowledge of the ordering of the weight vectors $\mu_1, \ldots, \mu_K$) [SB04, FYL04]. However, since there is no known way to gain this knowledge other than brute force search from the $K!$ possible orderings, this is not computationally feasible.

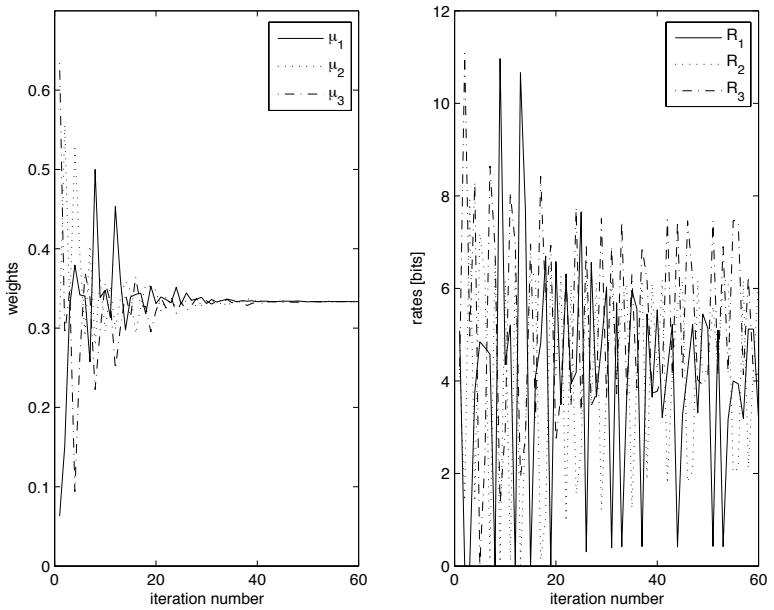

Figure 5.9: Convergence behavior when $\mu_1 = \mu_2 = \mu_3$ at C^{sym}

The algorithm can be simply described by considering a two user example, as shown in Fig. 5.11. Here the minimum required power is P_2, because the $\mathbf{R}$ lies on the boundary of $\mathcal{C}(P_2)$. In addition, the line through the origin and $\mathbf{R}$ is also drawn. The minimum power can be found by exploiting the fact that the intersection of $\mathcal{C}(\mathbf{H}, P)$ and this line can be determined using the differentiated capacity algorithm (with $\alpha_i = \frac{R_i}{R_1}$) described in Section 5.3.1. The differentiated capacity algorithm is run for some initial guess of power such as P_1. The returned rate vector (i.e. the intersection of the line and $\mathcal{C}(P_1)$) is smaller than the desired rate vector, and thus the power must be increased. This process can be continued using the one-dimensional bisection method, until the minimum power is reached.

The algorithm is explicitly described in Algorithm 2. If we denote the point-to-point capacity from the transmitter to mobile k as $C(\mathbf{H}_k, P)$, then it is easy to show the following initialization values can be chosen:

$$P_{\text{low}} = \sum_{k=1}^{K} P_k^i \tag{5.44}$$

$$P_{\text{high}} = \min\{P_1^s, P_2^s, \cdots, P_K^s\}, \tag{5.45}$$

where $P_1^i, \ldots, P_K^i$ satisfy $C(\mathbf{H}_k, P_k^i) = R_k$ and $P_1^s, \ldots, P_K^s$ satisfy $C(\mathbf{H}_k, P_k^s) = \sum_{k=1}^{K} R_k$.

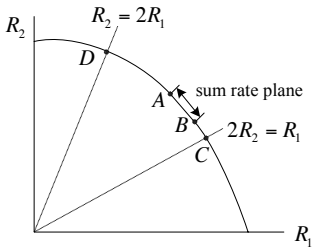

Figure 5.10: Differentiated service for 2 user channel

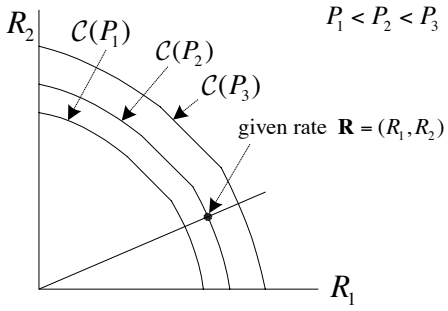

Figure 5.11: Boundaries of the capacity region with different powers

5.3.2 Symmetric Capacity vs. Sum Capacity

While symmetric capacity results in absolute fairness amongst all users, it can result in sub-optimal total system throughput. To be more specific, if the symmetric capacity vector does not lie on the sum rate plane, there is a strict reduction in system throughput. This throughput loss is referred to as the *fairness penalty*, i.e., the penalty paid for requiring absolute rate fairness. This penalty will clearly depend on the number of users and antennas, the system SNR, and the specific channel realization.

First notice that the symmetric capacity vs. SNR curve has the same slope, i.e., multiplexing gain, as the sum capacity vs. SNR curve. This is intuitively clear because all spatial degrees of freedom are used when achieving symmetric capacity. However, there can be an absolute rate difference, or equivalently a rightward shift of the capacity curve, between sum capacity and symmetric capacity which is not captured by the multiplexing gain alone. It is often useful to study the limiting behavior of this rate difference at asymptotically high SNR, using the high

Algorithm 5.2 Minimum power to achieve a desired rate vector

1. if $P_{\text{high}} - P_{\text{low}} < tol$
   break
2. $P = (P_{\text{high}} + P_{\text{low}})/2$
3. Compute differentiated service capacity: $C^{\text{diff}}(\alpha, \mathbf{H}, P)$
4: If $C^{\text{diff}}(\alpha, \mathbf{H}, P) > R_1$, then $P_{\text{high}} = P$, else $P_{\text{low}} = P$.

SNR approximation developed in [SV01]. We define the high SNR fairness penalty $\Delta(\mathbf{H})$ as:

$$\Delta(\mathbf{H}) \triangleq \lim_{P\to\infty} \left[C^{\text{sum}}(\mathbf{H}, P) - K \cdot C^{\text{sym}}(\mathbf{H}, P)\right], \tag{5.46}$$

where $C^{\text{sum}}(\mathbf{H}, P)$ is sum of the rate vector $\mathbf{R}$ in $\mathcal{C}(\mathbf{H}, P)$ that maximizes the sum of rates. Although $\Delta(\mathbf{H})$ is defined at asymptotically high SNR, it is generally quite accurate for even moderate SNR values.

Two User Case

We provide exact analytical results for the high SNR fairness penalty for two user broadcast channels with a single receive antenna ($N = 1$), and also discuss numerical results for channels with more than two users. In this scenario, the channel matrix can be reduced to vector quantities $\mathbf{h}_k (\in \mathbb{C}^{1\times M})$.

Theorem 5.7. *For 2 user broadcast channels with $N = 1$ and $M \geq 2$, the fairness penalty is given by:*

$$\Delta(\mathbf{H}) = \begin{cases} 0, & \sin^2\theta \leq \frac{\|\mathbf{h}_1\|^2}{\|\mathbf{h}_2\|^2} \leq \frac{1}{\sin^2\theta}, \\ 2\log\left(\frac{\|\mathbf{h}_i\|^2 + \left\|\mathbf{g}_j\right\|^2}{2\|\mathbf{h}_i\|\left\|\mathbf{g}_j\right\|}\right), & \text{otherwise}, \end{cases} \tag{5.47}$$

where θ is the angle between channel vectors $\mathbf{h}_1$ and $\mathbf{h}_2$, $\left\|\mathbf{g}_j\right\| = \left\|\mathbf{h}_j\right\| |\sin\theta|$, $i = \arg\min_{k\in\{1,2\}}\{\|\mathbf{h}_k\|\}$, and $j = \arg\max_{k\in\{1,2\}}\{\|\mathbf{h}_k\|\}$.

Proof. See Section 5.4.9. □

More than Two Users

No similar expression is known for channels with $K > 2$, primarily because it is very difficult to analytically characterize the symmetry capacity at high SNR in this scenario. However, numerical results indicate that the gap is also small in this scenario.

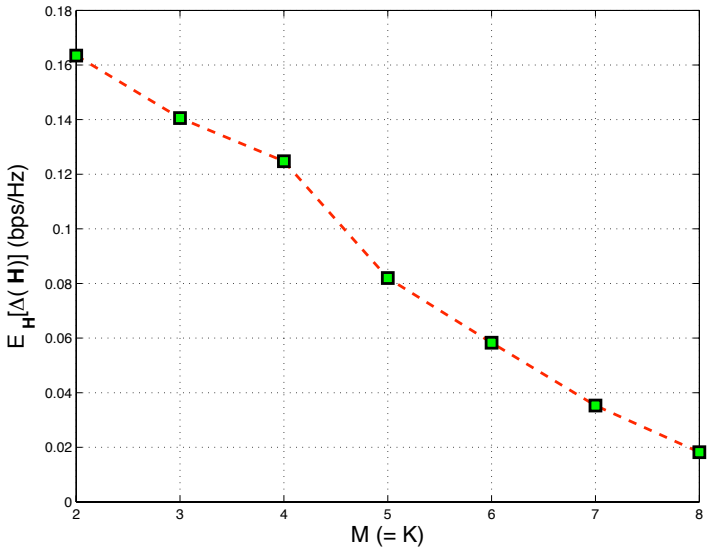

Figure 5.12: Expected fairness penalty with respect to the number of transmit antennas M (= number of users K)

In Fig. 5.12 the expectation (over iid Rayleigh fading channels for each mobile) of the fairness penalty is plotted as a function of the number of transmit antennas M for a downlink channel with $K = M$ and $N = 1$. It is clear from the figure that the fairness penalty is very small and is also decreasing to zero as M (or K) is increased.

While Fig. 5.12 indicates that the fairness penalty is very small for homogeneous users, i.e., users with the same average SNR, the heterogeneous scenario is perhaps of more practical interest. When average SNR's are asymmetric, the fairness penalty is expected to be larger, but preliminary numerical results indicate that this penalty term is again surprisingly small. For example, in a 4 user channel with $M = 4, N = 1$ and average SNR's of 30 dB, 25 dB, 20 dB, and 15 dB, the penalty is calculated to be 2.3 bps/Hz, which translates into a power penalty of less than 2 dB. Our ongoing research efforts are focused on deriving analytical expressions for the fairness penalty for downlink channels with many users and antennas, in both the homogeneous and heteregenous scenarios.

5.3.3 Summary

We proposed provably convergent algorithms for computing the symmetric capacity of the MIMO broadcast channel as well as for computing the minimum required power to achieve a desired rate vector. In fast fading scenarios where users have very loose delay constraints (e.g., file transfer), rate fairness is evaluated in terms of long-term *average* rates. When delay constraints are more stringent and fading occurs on a slow time scale, traffic demands must be met on a very fast time scale, and thus fairness must be evaluated in terms of short-term, or instantaneous, rates. In this setting, the symmetric capacity is a crucial metric for evaluating system performance. In addition, results comparing symmetric and sum capacity show that total system throughput is only slightly decreased if absolute rate fairness is required.

5.4 Proofs

5.4.1 Proof of Theorem 5.2

From (5.10) and (5.17), $\bar{\beta}_{\text{DPC-BD}}$ is given by:

$$\bar{\beta}_{\text{DPC-BD}} = \mathbb{E}[\log_2 \left|\mathbf{H}^H\mathbf{H}\right|] - K\,\mathbb{E}\left[\log_2 \left|\mathbf{G}\mathbf{G}^H\right|\right]$$

where $\mathbf{G}\mathbf{G}^H$ is $N \times N$ Wishart wth $M-(K-1)N$ degrees of freedom. Using the property of Wishart matrix [TV04], we have:

$$\begin{aligned}
\bar{\beta}_{\text{DPC-BD}} &= \log e \left[\sum_{l=0}^{KN-1} \psi(M-l) - K\sum_{n=0}^{N-1} \psi(M-(K-1)N-n)\right] \\
&= \log e \sum_{k=0}^{K-1}\sum_{n=0}^{N-1} [\psi(M-n-kN) - \psi(M-n-(K-1)N)] \\
&= \log e \sum_{k=0}^{K-1}\sum_{n=0}^{N-1} \left[\sum_{j=1}^{M-n-kN-1} \frac{1}{j} - \sum_{j=1}^{M-n-(K-1)N-1} \frac{1}{j}\right] \\
&= \log e \sum_{k=0}^{K-1}\sum_{n=0}^{N-1}\sum_{i=kN+1}^{(K-1)N} \frac{1}{M-n-i}.
\end{aligned}$$

5.4.2 Derivation of (5.23)

When $M = KN$,

$$\mathbb{E}_{\mathbf{H}}[\log_e \beta_{\text{DPC-ZF}}(\mathbf{H})] = \sum_{j=1}^{KN-1} \frac{j}{M-j} = \sum_{j=1}^{M-1}\sum_{i=1}^{M-j} \frac{1}{i}. \tag{5.48}$$

If we let S_M denote the expected rate loss with M antennas, we have:

$$S_{M+1} - S_M = \sum_{i=1}^{M} \frac{1}{i} \leq 1 + \log M, \quad \text{for } M \geq 1, \tag{5.49}$$

since $\log_e M = \int_1^M \frac{1}{x} dx \geq \sum_{i=2}^{M} \frac{1}{i}$ because $\frac{1}{x}$ is a decreasing function. If we let $f(M) \triangleq M \log_e M$, $f'(M) = 1 + \log_e M$, which is an increasing function of M, and thus $f(M+1) \geq f(M) + 1 + \log_e M$. Since $S_{M+1} - S_M \leq 1 + \log M$ and $f(1) = S_1 = 0$, $S_M \leq M \log M$ for all $M \geq 1$.

Now we show that S_M converges to $M \log M$. We do this by showing that $S_M \geq \theta M \log_e M$ for any $0 < \theta < 1$ for all M larger than some M_0. First notice that $\log_e M \leq \sum_{i=1}^{M-1} \frac{1}{i} \leq \sum_{i=1}^{M} \frac{1}{i}$ by the definition of the $\log(\cdot)$ function. Thus,

$$S_{M+1} - S_M = \sum_{i=1}^{M} \frac{1}{i} \geq \log_e M. \tag{5.50}$$

Let $g(M) \triangleq \theta M \log M$ for some $0 < \theta < 1$. Then $g'(M) = \theta + \theta \log_e M$, which is an increasing function of M. Thus $g(M+1) \leq g(M) + g'(M+1) = g(M) + \theta + \theta \log_e (M+1)$. Therefore we have

$$g(M+1) - S_{M+1} \leq (f(M) - S_M) + \theta + \theta \log(M+1) - \log M. \tag{5.51}$$

Notice that the term $\theta + \theta \log(M+1) - \log M$ is a monotonically decreasing function that goes to $-\infty$. Thus, any positive gap between $g(M)$ and S_M must close and go to $-\infty$, i.e., $S_M \geq g(M)$ for sufficiently large M. As a consequence of this, $\lim_{M\to\infty} \frac{S_M}{\theta M \log_e M} \geq 1$, or $\lim_{M\to\infty} \frac{S_M}{M \log_e M} \geq \theta$ for any $\theta < 1$. Since $\frac{S_M}{M \log_e M}$ is bounded above by 1, it must converge; i.e.,

$$\lim_{M\to\infty} \frac{S_M}{M \log_e M} = 1 \tag{5.52}$$

as desired.

5.4.3 Derivation of Equation (5.24)

From Theorem 5.2, if $M = \alpha KN$, the expected power offset, which is now a function of α and KN, can be expressed as:

$$\begin{aligned} \bar{\Delta}_{\text{DPC-ZF}}(\alpha, KN) &= \frac{3 \log_2 e}{KN} \sum_{j=1}^{KN-1} \frac{j}{M-j}, \qquad M = \alpha KN \\ &= 3 \log_2 e \sum_{j=1}^{KN-1} \frac{\frac{j}{KN}}{\alpha - \frac{j}{KN}} \frac{1}{KN} \end{aligned}$$

Let us define a function $f(x)$ as

$$f(x) = \frac{x}{\alpha - x}, \qquad x \in [0,1], \quad \alpha > 1.$$

Then $\bar{\Delta}_{\text{DPC-ZF}}$ can be expressed as

$$\bar{\Delta}_{\text{DPC-ZF}}(\alpha, KN) = 3\log_2 e \sum_{j=1}^{KN-1} f\left(\frac{j}{KN}\right)\frac{1}{KN},$$

which is a Riemann sum; i.e., as $KN \to \infty$,

$$\lim_{KN\to\infty} \bar{\Delta}_{\text{DPC-ZF}}(\alpha, KN) = 3\log_2 e \int_0^1 f(x)dx = 3\log_2 e \int_0^1 \frac{x}{\alpha - x}dx.$$

Thus,

$$\begin{aligned}\bar{\Delta}_{\text{DPC-ZF}}(\alpha) = \lim_{KN\to\infty} \bar{\Delta}_{\text{DPC-ZF}}(\alpha, KN) &= 3\log_2 e\left(-1 - \alpha\log_e \frac{\alpha-1}{\alpha}\right) \\ &= -3\left(\log_2 e + \alpha\log_2\left(1 - \frac{1}{\alpha}\right)\right).\end{aligned}$$

5.4.4 Proof of Theorem 5.3

From (5.21) and (5.22) it is known that the $\bar{\beta}_{\text{DPC-BD}}$ and $\bar{\beta}_{\text{DPC-ZF}}$ are given by

$$\begin{aligned}\bar{\beta}_{\text{DPC-BD}} &= \log e\left[\sum_{l=0}^{KN-1}\psi(M-l) - K\sum_{n=0}^{N-1}\psi(M-(K-1)N-n)\right], \\ \bar{\beta}_{\text{DPC-ZF}} &= \log e\left[\sum_{l=0}^{KN-1}\psi(M-l) - KN\psi(M-KN+1)\right].\end{aligned}$$

From the assumption, $M = \alpha KN$ ($\alpha > 1$) with $N > 1$,

$$\begin{aligned}\frac{1}{\log e}\left(\mathbb{E}[\beta_{\text{DPC-ZF}}] - \mathbb{E}[\beta_{\text{DPC-BD}}]\right) &= K\left(\sum_{n=0}^{N-1}\psi(M-(K-1)N-n)\right) - KN\psi(M-KN+1) \\ &= K\sum_{n=2}^{N}\left[\psi(M-KN+n) - \psi(M-KN+1)\right] \\ &= K\sum_{n=2}^{N}\sum_{j=M-KN+1}^{M-KN+n-1}\frac{1}{j} \\ &= K\sum_{i=1}^{N-1}\frac{N-i}{M-KN+i} \\ &= \sum_{i=1}^{N-1}\frac{K(N-i)}{(\alpha-1)KN+i}\end{aligned}$$

5.4.5 Derivation of (5.27), (5.28), and (5.29)

From (5.7) with the uniform power allocation, we have

$$C_{\mathrm{DPC}}(\mathbf{H},P) \cong \log_2 \left| \mathbf{I} + \frac{P}{KN} \tilde{\mathbf{H}}^H \Gamma \tilde{\mathbf{H}} \right|,$$

where $\Gamma = \mathrm{diag}(\gamma_1, \cdots, \gamma_K) \otimes \mathbf{I}_{N\times N}$. By $|\mathbf{I}+\mathbf{AB}| = |\mathbf{I}+\mathbf{BA}|$,

$$\begin{aligned}
C_{\mathrm{DPC}}(\mathbf{H},P) &\cong \log_2 \left| \mathbf{I} + \frac{P}{KN} \Gamma \tilde{\mathbf{H}} \tilde{\mathbf{H}}^H \right| \\
&= KN \log_2 P + \log_2 \left| \frac{1}{P}\mathbf{I} + \frac{1}{KN} \Gamma \tilde{\mathbf{H}} \tilde{\mathbf{H}}^H \right| \\
&\cong KN \log_2 P + \log_2 \left| \frac{1}{KN} \Gamma \tilde{\mathbf{H}} \tilde{\mathbf{H}}^H \right| \\
&= KN \log_2 P - KN \log_2 KN + \log_2 |\Gamma| + \log_2 \left| \tilde{\mathbf{H}} \tilde{\mathbf{H}}^H \right| \\
&\cong C_{\mathrm{DPC}}(\tilde{\mathbf{H}},P) + N \sum_{k=1}^{K} \log_2 \gamma_k
\end{aligned}$$

Since the zero-forcing vector $\mathbf{v}_{k,n}$ for $\mathbf{h}_{k,n}$ is identical to the zero-forcing vector $\tilde{\mathbf{v}}_{k,n}$ for $\tilde{\mathbf{h}}_{k,n}$, the effective channel gain is given by

$$g_{k,n} = \mathbf{h}_{k,n}\mathbf{v}_{k,n} = \sqrt{\gamma_k}\tilde{g}_{k,n}, \tag{5.53}$$

where $\tilde{g}_{k,n} = \tilde{\mathbf{h}}_{k,n}\tilde{\mathbf{v}}_{k,n}$. Thus the ZF sum rate can be modified as

$$\begin{aligned}
C_{\mathrm{ZF}}(\mathbf{H},P) &\cong \sum_{k=1}^{K}\sum_{n=1}^{N} \log_2 \left(1 + \frac{P}{KN}\gamma_k |\tilde{g}_{k,n}|^2 \right) \\
&= KN \log_2 P + \sum_{k=1}^{K}\sum_{n=1}^{N} \log_2 \left(\frac{1}{P} + \frac{1}{KN}\gamma_k |\tilde{g}_{k,n}|^2 \right) \\
&\cong KN \log_2 P + \sum_{k=1}^{K}\sum_{n=1}^{N} \log_2 \left(\frac{1}{KN}\gamma_k |\tilde{g}_{k,n}|^2 \right) \\
&\cong C_{\mathrm{ZF}}(\tilde{\mathbf{H}},P) + N \sum_{k=1}^{K} \log_2 \gamma_k
\end{aligned}$$

Likewise, for BD, $\tilde{\mathbf{V}}_k = \mathbf{V}_k$ leads to

$$\mathbf{G}_k = \mathbf{H}_k\mathbf{V}_k = \sqrt{\gamma_k}\tilde{\mathbf{G}}_k, \tag{5.54}$$

where $\tilde{\mathbf{G}}_k = \tilde{\mathbf{H}}_k \tilde{\mathbf{V}}_k$. Thus, the BD sum rate in (5.16) is modified to

$$\begin{aligned} C_{\mathrm{BD}}(\mathbf{H}, P) &\cong \sum_{k=1}^{K} \log_2 \left| \mathbf{I} + \frac{P}{KN} \gamma_k \tilde{\mathbf{G}}_k^H \tilde{\mathbf{G}}_k \right| \\ &= KN \log_2 P + \sum_{k=1}^{K} \log_2 \left| \frac{1}{P}\mathbf{I} + \frac{1}{KN} \gamma_k \tilde{\mathbf{G}}_k^H \tilde{\mathbf{G}}_k \right| \\ &\cong KN \log_2 P + \sum_{k=1}^{K} \log_2 \left| \frac{1}{KN} \gamma_k \tilde{\mathbf{G}}_k^H \tilde{\mathbf{G}}_k \right| \\ &\cong C_{\mathrm{BD}}(\tilde{\mathbf{H}}, P) + N \sum_{k=1}^{K} \log_2 \gamma_k \end{aligned}$$

5.4.6 Proof of Lemma 5.4

If we let the eigenvector matrix and eigenvalues of $\sum_{j=1}^{k-1} \mathbf{H}_j^H \mathbf{Q}_j \mathbf{H}_j$ be $\mathbf{U}$ and $\lambda_1, \cdots, \lambda_{k-1}$ with $\lambda_j > 0$, then

$$(\mathbf{A}^{(k-1)})^{-1/2} = \mathbf{U} \Lambda \mathbf{U}^H,$$

where

$$\Lambda = \mathrm{diag}\left(\frac{1}{\sqrt{1+\lambda_1}}, \cdots, \frac{1}{\sqrt{1+\lambda_{k-1}}}, 1, \cdots, 1 \right).$$

As P goes to infinity, λ's tend to infinity. Thus, the first $k-1$ eigenvalues of Λ converge to 0. The eigenvectors corresponding to the unit eigenvalues span the nullspace $\{\mathbf{H}_j\}_{j=1}^{k-1}$; i.e.,

$$\lim_{P \to \infty} \left[\mathbf{H}_k (\mathbf{A}^{(k-1)})^{-1/2} - \mathbf{F}_k \right] = 0.$$

This completes the proof.

5.4.7 Proof of Theorem 5.5

By Lemma 5.4, the optimization (5.30) can be decomposed into the two optimizations at high SNR:

$$C_{\mathrm{DPC}}(\mu, \mathbf{H}, P) \cong \max_{\sum_{k=1}^{K} P_k \le P} \sum_{k=1}^{K} \mu_k \xi_k(P_k), \tag{5.55}$$

where

$$\xi_k(P_k) = \max_{\mathrm{tr}(\mathbf{Q}_k) = P_k} \log_2 \left| \mathbf{I} + \mathbf{Q}_k \mathbf{F}_k \mathbf{F}_k^H \right|. \tag{5.56}$$

At high SNR, Eq. (5.56) can be asymptotically expressed as an affine approximation [SV01]:

$$\xi_k(P_k) = \mathcal{S}_{\infty,k}(\log_2 P_k - \mathcal{L}_{\infty,k}) + o(1), \tag{5.57}$$

where $\mathcal{S}_{\infty,k}$ and $\mathcal{L}_{\infty,k}$ are determined by the multiplexing gain and power offset. Hence, the optimization (5.55) is asymptotically equivalent to solve the following:

$$\max_{\sum_{k=1}^{K} P_k \le P} \sum_{k=1}^{K} \mu_k \log_2 P_k.$$

This leads the optimal $P_k = \mu_k P$. Furthermore, by Theorem 3 of [CS03], the optimal power allocation is asymptotically achieved by

$$\mathbf{Q}_k = \frac{\mu_k P}{N}\mathbf{I}, \qquad k = 1, \cdots, K.$$

5.4.8 Proof of Theorem 5.6

We first rewrite the symmetric capacity using the auxiliary variable s:

$$\begin{aligned} C^{\text{sym}}(\mathbf{H}, P) = \quad & \max \quad s \\ & \text{subject to} \quad R_k \ge s \quad k = 1, \cdots, K \\ & \qquad\qquad\quad \mathbf{R} \in \mathcal{C}(\mathbf{H}, P). \end{aligned} \tag{5.58}$$

We are able to efficiently solve the Lagrangian dual form of this maximization. We introduce dual variables $\lambda = (\lambda_1, \ldots, \lambda_K)$ for the K rate constraints, but keep the capacity region constraint $\mathbf{R} \in \mathcal{C}(\mathbf{H}, P)$ implicit in the problem. The resulting Lagrangian $L(s, \mathbf{R}, \lambda)$ is given by:

$$\begin{aligned} L(s, \mathbf{R}, \lambda) \quad &= s + \sum_{k=1}^{K} \lambda_k (R_k - s) \\ &= \sum_{k=1}^{K} \lambda_k R_k + s\left(1 - \sum_{k=1}^{K} \lambda_k\right), \end{aligned} \tag{5.59}$$

and the corresponding dual function $g(\lambda)$ is defined as the maximization of the Lagrangian over the primal variables s and $\mathbf{R}$:

$$g(\lambda) \triangleq \max_{s,\ \mathbf{R} \in \mathcal{C}(\mathbf{H}, P)} L(s, \mathbf{R}, \lambda).$$

Since the optimization in (5.58) is convex and satisfies Slater's condition, strong duality holds, which implies:

$$C^{\text{sym}}(\mathbf{H},P) = \min_{\lambda \succeq \mathbf{0}} g(\lambda), \tag{5.60}$$

where $\succeq$ denotes component-wise inequality.

If $\sum_{k=1}^{K} \lambda_k \neq 1$, then we get $g(\lambda) = \infty$ by choosing $s = -\infty$ if $\sum_{k=1}^{K} \lambda_k > 1$ and $s = \infty$ if $\sum_{k=1}^{K} \lambda_k < 1$. Therefore, we need only minimize $g(\lambda)$ over λ that sum to one. Thus we have:

$$\begin{aligned} C^{\text{sym}}(\mathbf{H},P) &= \min_{\lambda:\ \lambda \succeq \mathbf{0},\ \sum_{i=1}^{K} \lambda_i = 1} g(\lambda) \\ &= \min_{\lambda:\ \lambda \succeq \mathbf{0},\ \sum_{i=1}^{K} \lambda_i = 1} \max_{\mathbf{R} \in \mathcal{C}(\mathbf{H},P)} \sum_{i=1}^{K} \lambda_i R_i \\ &= \min_{\mu: \mu \geq 0,\ \sum_{i=1}^{K} \mu_i = 1} f(\mu). \end{aligned} \tag{5.61}$$

Furthermore, $g(\lambda)$ is convex because the dual function is always convex.

Addionally, notice that the weight vector μ only has $K-1$ degrees of freedom, since the entries must sum to one. We thus define a new function $h(\mu_1,\ldots,\mu_{K-1}) = g\left(\mu_1,\ldots,\mu_{K-1},1-\sum_{i=1}^{K-1}\mu_i\right)$. Thus, the non-negativity constraint on μ can be removed, giving the follow unconstrained convex program:

$$C^{\text{sym}}(\mathbf{H},P) = \min_{\mu_1,\ldots,\mu_{K-1}} h(\mu_1,\ldots,\mu_{K-1}). \tag{5.62}$$

5.4.9 Proof of Theorem 5.7

By Theorem 5.1,

$$\lim_{P\to\infty} \left[C^{\text{sum}}(\mathbf{H},P) - \log \left| \mathbf{I} + \frac{P}{2}\mathbf{h}_1\mathbf{h}_1^H + \frac{P}{2}\mathbf{h}_2\mathbf{h}_2^H \right| \right] = 0, \tag{5.63}$$

and thus,

$$C^{\text{sum}}(\mathbf{H},P) \cong \log \left| \mathbf{I} + \frac{P}{2}\mathbf{h}_1\mathbf{h}_1^H \right| + \log \frac{\left| \mathbf{I} + \frac{P}{2}\mathbf{h}_1\mathbf{h}_1^H + \frac{P}{2}\mathbf{h}_2\mathbf{h}_2^H \right|}{\left| \mathbf{I} + \frac{P}{2}\mathbf{h}_1\mathbf{h}_1^H \right|}. \tag{5.64}$$

With the matrix determinant identity $|\mathbf{I}+\mathbf{AB}| = |\mathbf{I}+\mathbf{BA}|$,

$$C^{\text{sum}}(\mathbf{H},P) \cong \log \left(1 + \frac{P}{2}\|\mathbf{h}_1\|^2 \right) + \log \left(1 + \frac{P}{2}\mathbf{h}_2^H \left(\mathbf{I} + \frac{P}{2}\mathbf{h}_1\mathbf{h}_1^H \right)^{-1} \mathbf{h}_2 \right). \tag{5.65}$$

By understanding the operation $\left(\mathbf{I}+\frac{P}{2}\mathbf{h}_1\mathbf{h}_1^H\right)^{-1}$ as a MMSE filter that achieves the best performance,

$$\begin{aligned} C^{\text{sum}}(\mathbf{H},P) &\cong \log\left(1+\frac{P}{2}\|\mathbf{h}_1\|^2\right)+\log\left(1+\frac{P}{2}\|\mathbf{h}_2\|^2\sin^2\theta\right) \\ &= 2\log\left(\frac{P}{2}\|\mathbf{h}_1\|\|\mathbf{h}_2\|\sin\theta\right), \end{aligned} \tag{5.66}$$

where θ is the angle between $\mathbf{h}_1$ and $\mathbf{h}_2$.

By Lemma 5.8, which can be found later in Section 5.4.9,

$$C^{\text{sym}}(\mathbf{H},P) \cong \begin{cases} C^{\text{sum}}(\mathbf{H},P), & \sin^2\theta \le \frac{\|\mathbf{h}_1\|^2}{\|\mathbf{h}_2\|^2} \le \frac{1}{\sin^2\theta}, \\ \log(\alpha P), & \text{else}, \end{cases} \tag{5.67}$$

where α is defined in (5.69).

Therefore, we obtain the result with algebraic manipulations by (5.46). □

Lemma 5.8. *If* $\|\mathbf{h}_1\|^2 < \|\mathbf{h}_2\|^2\sin^2\theta$, *or* $\|\mathbf{h}_1\|^2\sin^2\theta > \|\mathbf{h}_2\|^2$ *where* θ *is the angle between* $\mathbf{h}_1$ *and* $\mathbf{h}_2$, *then*

$$\lim_{P\to\infty}\left[C^{\text{sym}}(\mathbf{H},P)-\log\left(1+\alpha P\right)\right]=0, \tag{5.68}$$

where α *is defined as*

$$\alpha \triangleq \frac{\|\mathbf{h}_1\|^2\|\mathbf{h}_2\|^2\sin^2\theta}{\min(\|\mathbf{h}_1\|^2,\|\mathbf{h}_2\|^2)+\max(\|\mathbf{h}_1\|^2,\|\mathbf{h}_2\|^2)\sin^2\theta}. \tag{5.69}$$

Proof. We consider the case $\|\mathbf{h}_1\|^2 < \|\mathbf{h}_2\|^2\sin^2\theta$. The right corner point $(R_1^{\text{sum}},R_2^{\text{sum}})$ on the sum rate plane can be expressed as

$$R_1^{\text{sum}} = \log\left(1+P_1^{\text{sum}}\|\mathbf{h}_1\|^2\right), \tag{5.70}$$

$$R_2^{\text{sum}} = \log\left(1+P_2^{\text{sum}}\mathbf{h}_2^H\left(\mathbf{I}+P_1^{\text{sum}}\mathbf{h}_1\mathbf{h}_1^H\right)^{-1}\mathbf{h}_2\right), \tag{5.71}$$

where P_1^{sum} and P_2^{sum} are powers for user 1 and 2 achieving the sum rate capacity satisfying $P_1^{\text{sum}}+P_2^{\text{sum}}=P$. Since the quantity $\mathbf{h}_2^H\left(\mathbf{I}+P_1^{\text{sum}}\mathbf{h}_1\mathbf{h}_1^H\right)^{-1}\mathbf{h}_2$ in (5.71) is greater than $\|\mathbf{h}_2\|^2\sin^2\theta$ where θ is the angle between $\mathbf{h}_1$ and $\mathbf{h}_2$ by regarding $\left(\mathbf{I}+P_1^{\text{sum}}\mathbf{h}_1\mathbf{h}_1^H\right)^{-1}$ as a filter, R_2^{sum} is lower bounded by

$$R_2^{\text{sum}} \ge \log\left(1+P_2^{\text{sum}}\|\mathbf{h}_2\|^2\sin^2\theta\right). \tag{5.72}$$

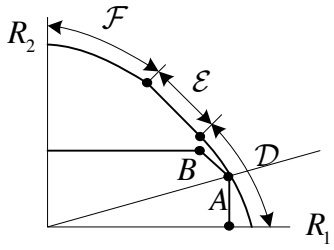

Figure 5.13: Symmetric capacity is determined in region $\mathcal{D}$

Since $\|\mathbf{h}_1\|^2 < \|\mathbf{h}_2\|^2 \sin^2\theta$, $\|\mathbf{h}_1\|^2 < \|\mathbf{h}_2\|^2$ holds so that $P_1^{\text{sum}} \leq P_2^{\text{sum}}$ [Jin05]. Thus we have $P_1^{\text{sum}} \|\mathbf{h}_1\|^2 < P_2^{\text{sum}} \|\mathbf{h}_2\|^2 \sin^2\theta$. Consequently,

$$R_1^{\text{sum}} < R_2^{\text{sum}}. \tag{5.73}$$

That is, the optimal symmetric capacity point is in the region $\mathcal{D}$ in Fig. 5.13. Since $\mu_1 > \mu_2$ and the region is convex, the optimal point is determined where point A is touching the boundary as illustrated in Fig. 5.13. The rate R_1^{sym} at an equal rate point A can be obtained by

$$R_1^{\text{sym}} = \log\left(1 + P_1 \|\mathbf{h}_1\|^2\right), \tag{5.74}$$

where P_1 is the power for user 1. Thus, the symmetric capacity is determined by doubling the rate R_1^{sym} as

$$R^{\text{sym}}(\mathbf{H}, P) = 2\log\left(1 + P_1 \|\mathbf{h}_1\|^2\right). \tag{5.75}$$

The rate R_2^{sym} at point A is obtained by

$$\begin{aligned} R_2^{\text{sym}} &= \log \frac{\left|\mathbf{I} + P_1\mathbf{h}_1\mathbf{h}_1^H + P_2\mathbf{h}_2\mathbf{h}_2^H\right|}{\left|\mathbf{I} + P_1\mathbf{h}_1\mathbf{h}_1^H\right|} \\ &= \log\left(1 + P_2\mathbf{h}_2^H\left(\mathbf{I} + P_1\mathbf{h}_1\mathbf{h}_1^H\right)^{-1}\mathbf{h}_2\right) \\ &= \log\left(1 + P_2\|\mathbf{h}_2\|^2\left(\sin^2\theta + \frac{1}{P_1\|\mathbf{h}_1\|^2}\cos^2\theta\right)\right), \end{aligned} \tag{5.76}$$

where P_2 is the power for user 2 and P_1 and P_2 satisfy $P_1 + P_2 = P$, and θ is also the angle between $\mathbf{h}_1$ and $\mathbf{h}_2$. Since $P_1 + P_2 = P$ and $R_1^{\text{sym}} = R_2^{\text{sym}}$, we have

$$P_1 = \frac{\|\mathbf{h}_2\|^2\left(\sin^2\theta + \frac{1}{P_1\|\mathbf{h}_1\|^2}\cos^2\theta\right)}{\|\mathbf{h}_1\|^2 + \|\mathbf{h}_2\|^2\left(\sin^2\theta + \frac{1}{P_1\|\mathbf{h}_1\|^2}\cos^2\theta\right)}P. \tag{5.77}$$

Note that $P_1^{\text{sum}} \leq P_1 \leq P$ since $R_1^{\text{sum}} < R_2^{\text{sum}}$ under the condition $\|\mathbf{h}_1\|^2 < \|\mathbf{h}_2\|^2 \sin^2\theta$. In addition, P_1^{sum} and P_2^{sum} satisfy that $P_1^{\text{sum}} = \frac{P}{2} - c$ and $P_2^{\text{sum}} = \frac{P}{2} + c$ where c is a positive constant not depending on P satisfying $P \geq 2c$. For sufficiently large enough P like $P \geq 6c$, $P_1^{\text{sum}} \geq \frac{P}{3}$ so that $\frac{P}{3} \leq P_1 < P$. Thus the ratio P_1/P can be upper and lower bounded by

$$\frac{\|\mathbf{h}_2\|^2 \left(\sin^2\theta + \frac{1}{P\|\mathbf{h}_1\|^2}\cos^2\theta\right)}{\|\mathbf{h}_1\|^2 + \|\mathbf{h}_2\|^2 \left(\sin^2\theta + \frac{2}{P\|\mathbf{h}_1\|^2}\cos^2\theta\right)} \leq \frac{P_1}{P} \leq \frac{\|\mathbf{h}_2\|^2 \left(\sin^2\theta + \frac{2}{P\|\mathbf{h}_1\|^2}\cos^2\theta\right)}{\|\mathbf{h}_1\|^2 + \|\mathbf{h}_2\|^2 \left(\sin^2\theta + \frac{1}{P\|\mathbf{h}_1\|^2}\cos^2\theta\right)}. \tag{5.78}$$

Since $\log\left(1 + P_1\|\mathbf{h}_1\|^2\right) = \log\left(1 + \frac{P_1}{P}\|\mathbf{h}_1\|^2 P\right)$ and $\log(\cdot)$ is monotonic,

$$\log\left(1 + \frac{\|\mathbf{h}_2\|^2 \left(\sin^2\theta + \frac{1}{P\|\mathbf{h}_1\|^2}\cos^2\theta\right)}{\|\mathbf{h}_1\|^2 + \|\mathbf{h}_2\|^2 \left(\sin^2\theta + \frac{2}{P\|\mathbf{h}_1\|^2}\cos^2\theta\right)} P\right) \leq \log\left(1 + P_1\|\mathbf{h}_1\|^2\right) \leq$$
$$\log\left(1 + \frac{\|\mathbf{h}_2\|^2 \left(\sin^2\theta + \frac{2}{P\|\mathbf{h}_1\|^2}\cos^2\theta\right)}{\|\mathbf{h}_1\|^2 + \|\mathbf{h}_2\|^2 \left(\sin^2\theta + \frac{1}{P\|\mathbf{h}_1\|^2}\cos^2\theta\right)} P\right) \tag{5.79}$$

As $P \to \infty$, we have

$$\lim_{P\to\infty}\left[\log\left(1 + P_1\|\mathbf{h}_1\|^2\right) - \log\left(1 + \frac{\|\mathbf{h}_1\|^2\|\mathbf{h}_2\|^2\sin^2\theta}{\|\mathbf{h}_1\|^2 + \|\mathbf{h}_2\|^2\sin^2\theta} P\right)\right] = 0. \tag{5.80}$$

Consequently, we have

$$\lim_{P\to\infty}\left[R^{\text{sym}}(\mathbf{H}, P) - 2\log\left(1 + \frac{\|\mathbf{h}_1\|^2\|\mathbf{h}_2\|^2\sin^2\theta}{\|\mathbf{h}_1\|^2 + \|\mathbf{h}_2\|^2\sin^2\theta} P\right)\right] = 0. \tag{5.81}$$

We can also find the similar result for $\|\mathbf{h}_1\|^2\sin^2\theta > \|\mathbf{h}_2\|^2$, that is, the optimal symmetric capacity point is in the region $\mathcal{F}$ as

$$\lim_{P\to\infty}\left[R^{\text{sym}}(\mathbf{H}, P) - 2\log\left(1 + \frac{\|\mathbf{h}_1\|^2\|\mathbf{h}_2\|^2\sin^2\theta}{\|\mathbf{h}_1\|^2\sin^2\theta + \|\mathbf{h}_2\|^2} P\right)\right] = 0. \tag{5.82}$$

Combining (5.81) and (5.82), we can get (5.68) and (5.69). □

Chapter 6

Conclusions and Future Work

In this dissertation we studied dynamic resource allocation of delay-constrained communication traffic. Our main focus was to understand the interplay between the scheduling parameters such as channel state, delay constraints, queue size. This interplay is important to develop intuition for system engineering. We spent a large portion on the "basic" scheduling problem of transmitting B bits over T discrete time slots and then considered various extensions assuming that the energy and the number of transmit bits are related by the Shannon function. We also considered a monomial energy-bit function, where we obtained the optimal solution in closed-form. We also studied the sum capacity and the symmetric capacity of MIMO broadcast channels.

We extensively investigated the basic hard delay deadline scheduling problem of transmitting B bits within finite T time slots with causal CSIT. We were able to find simple closed-form suboptimal scheduling functions. Although the policy functions are suboptimal, they perform very close to optimal, and moreover, they were shown to be asymptotically optimal. From the simple closed-form scheduling functions, we obtained some intuition regarding the interplay between scheduling parameters balancing opportunistic communication and delay-constrained communication. To make the basic problem tractable, we made assumptions on the information available to the transmitter, which may not be practical depending on the application. First, we assumed that the transmitter has perfect knowledge of the channel state information for the current time slot and knows the probability distribution of the fading channel state for future time slots. In practice, the transmitter obtains this information by estimation from measurements, and thus robustness and sensitivity to inaccuracy should be accounted for in practical employment of such schedulers.

We did not allow outage in the basic problem setup. This assumption may not be practical because too much power may be required when the receiver is in deep fade. To deal with this, typical practical systems allow outage for better system utilization. With this concern, we incorporated outage in the basic scheduling problem by slightly modifying the problem such that an outage can occur at the final time slot if the energy to transmit all the unserved bits at the final slot is greater than a certain value M. But this slight modification makes the problem non-convex and does not permit a closed-form solution even for the $T = 2$ case. Instead, we change the way to incorporate outage. For example, one can impose a delay deadline constraint with some probability, which is a probabilistic (or chance) constraint scheduling problem [DE05]. It is as of yet unclear which formulation can yield a closed-form solution.

In the basic problem setup, we considered scheduling only to a single user. To accomodate multiple users, we attempted to extend the basic scheduling problem to a broadcast channel environment. But we were only able to find a solution when $T = 2$. The difficulty for generalization was basically due to the complicated relationship between the incurred energy and the number of serving bits to multiple users, where the relationship we used is obtained from the boundary of the capacity region of the broadcast channel. The resulting cost-to-go function was not found in closed form because of coupling between users. To avoid coupling, we can adopt scheduling with time-division multiplexing (TDM) among users. We can also consider the deadline scheduling problem for multiple-access channels, interference channels, and relaying channels.

Besides these, we have studied other extensions of the basic scheduling problem to parallel/MIMO channels and wideband. These considerations are useful for OFDM systems where multiple frequency bands can be allocated to a single user. On the one hand, when the channel state of each frequency band experiences independent fading and the objective is to minimize the transmit energy, we can employ parallel channel scheduling, while on the other hand, when the transmission power is fixed and the objective is to minimize the frequency band usage, we can employ wideband scheduling. Because of complication in dynamic programs, however, we did not obtain the optimal solution in closed-form. We may add/relax constraints to make the problems tractable so that we can obtain simple analytical solutions and draw intuition between scheduling parameters.

In the basic scheduling problem, we assumed that the relationship between the energy consumption and the number of transmit bits is the Shannon function, which is the inverse function of the AWGN capacity formula. Instead of the Shannon function, we considered

monomial functions as well. With a monomial cost function, we were able to obtain the optimal solution in closed form for various setups such as primal energy minimization, dual rate maximization, and non-causal scheduling. Although the optimal policy function is different from the policy functions with the Shannon cost function, the optimal solution exhibits the interplay of balancing between opportunistic communication and delay-limited communication. Furthermore, we attempted to consider a general polynomial cost function but we were only able to succeed in finding the optimal solution for a second-order (quadratic) polynomial. It will bring significant contribution if we obtain a scheduling policy for a general convex polynomial since we can apply the solution for almost all cases.

In the final chapter, we studied MIMO broadcast channels. First, we investigated the rate/power offset between the optimal DPC sum capacity and the achievable rate with linear precoding. With random matrix techniques, we were able to characterize the rate gap and power offset at high SNR and obtain some intuition through the equivalent MIMO interpretation. Furthermore, we generalized the sum rate analysis to a weighted sum rate analysis. One of the most interesting aspects was the finding that allocating power directly proportional to user weights is asymptotically optimal at high SNR. This result can be applied to queue-based scheduling [TE92], in which it is necessary to repeatedly maximize the weighted sum rate for different user weights. All of these findings are valid when the total number of transmit antennas is no smaller than the total aggregate receive antennas. When there are more antennas on the receiver side, a sophisticated scheme is needed, such as user selection. Second, we investigated the symmetric capacity of MIMO broadcast channels. The symmetric capacity represents absolute fairness and is important for delay-constrained traffic.

Bibliography

[Bel03] R. Bellman. *Dynamic Programming*. Dover Publications, Inc., 2003.

[Ber75] D. P. Bertsekas. Convergence of discretization procedures in dynamic programming. *IEEE Trans. Automat. Contr.*, AC-20(3):415–419, Jun. 1975.

[Ber00] R. A. Berry. *Power and Delay Trade-offs in Fading Channels*. PhD thesis, MIT, 2000.

[Ber03] D. P. Bertsekas. *Nonlinear Programming*. Athena Scientific, Mass., 2 edition, 2003.

[Ber05] D. P. Bertsekas. *Dynamic Programming and Optimal Control*, volume 1. Athena Scientific, Mass., 3 edition, 2005.

[BG02] R. A. Berry and R. G. Gallager. Communication over fading channels with delay constraints. *IEEE Trans. Inform. Theory*, 48(5):1135–1149, May. 2002.

[BST74] Y. Bar-Shalom and E. Tse. Dual effect, certainty equivalence, and separation in stochastic control. *IEEE Trans. Automat. Contr.*, 19(5):494–500, Oct 1974.

[BV01] S. Boyd and L. Vandenberghe. *Introduction to Convex Optimization with Engineering Applications*. Course Reader, Stanford Univ., 2001.

[BV04] S. Boyd and L. Vandenberghe. *Convex Optimization*. Cambridge Univ. Press, Cambridge, UK, 2004.

[CC99] B. E. Collins and R. L. Cruz. Transmission policies for time varying channels with average delay constraints. In *Proc. 1999 Allerton Conf. on Commun., Control, & Comp.*, Monticello, IL, 1999.

[CGH+96] R. M. Corless, G. H. Gonnet, D. E. G. Hare, D. J. Jeffrey, and D. E. Knuth. On the Lambert w function. *Advances in Computational Mathematics*, 5:329–359, 1996.

[CM04] L.-U. Choi and R. D. Murch. A transmit preprocessing technique for multiuser MIMO systems using a decomposition approach. *IEEE Trans. Wireless Commun.*, 3(1):20–24, Jan. 2004.

[CMK07] G. Caire, R. R. Müller, and R. Knopp. Hard fairness versus proportional fairness in wireless communications: The single-cell case. *IEEE Trans. Inform. Theory*, 53(4):1366–1385, Apr. 2007.

[CNM07a] W. Chen, M. J. Neely, and U. Mitra. Energy efficient scheduling with individual delay constraints over a fading channel. In *Proc. WiOpt*, 2007.

[CNM07b] W. Chen, M. J. Neely, and U. Mitra. Energy efficient scheduling with individual packet delay constraints: Offline and online results. In *Proc. IEEE INFOCOM*, pages 1136–1144, Anchorage, AK, May 2007.

[CS03] G. Caire and S. Shamai. On the achievable throughput of a multiantenna Gaussian broadcast channel. *IEEE Trans. Inform. Theory*, 49(7):1691–1706, Jul. 2003.

[CT91] T. M. Cover and J. A. Thomas. *Elements of Information Theory*. John Wiley & Sons Inc., New York, 1991.

[CTB99] G. Caire, G. Taricco, and E. Biglieri. Optimum power control over fading channels. *IEEE Trans. Inform. Theory*, 45(5):1468–1489, Jul. 1999.

[CTV04] G. Caire, D. Tuninetti, and S. Verdú. Variable-rate coding for slowly fading gaussian multiple-access channels. *IEEE Trans. Inform. Theory*, 50(10):2271–2292, Oct. 2004.

[Dav81] H. A. David. *Order Statistics*. Wiley, 2nd edition, 1981.

[DE05] S. Dey and J. Evans. Optimal power control over multiple time-scale fading channels with service outage constraints. *IEEE Trans. Commun.*, 53(4):708–717, Apr. 2005.

[EB05] U. Erez and S. Ten Brink. A close-to-capacity dirty paper coding scheme. *IEEE Trans. Inform. Theory*, 51(10):3417–3432, Oct. 2005.

[FG98] G. J. Foschini and M. J. Gans. On limits of wireless communications in a fading environment when using multiple antennas. *Wireless Personal Commun.*, 6:311–335, 1998.

[FMT06] A. Fu, E. Modiano, and J. N. Tsitsiklis. Optimal transmission scheduling over a fading channel with energy and deadline constraints. *IEEE Trans. Wireless Commun.*, 5(3):630–641, Mar. 2006.

[FYL04] F. Fung, W. Yu, and T. J. Lim. Multi-antenna downlink precoding with individual rate constraints: power minimization and user ordering. In *Proc. IEEE Singaporepore Int. Conf. Comm. Systems (ICCS)*, Singapore, Sept 2004.

[Gol05] A. Goldsmith. *Wireless Communications*. Cambridge Univ. Press, New York, NY, 2005.

[HLP01] G. Hardy, J. E. Littlewood, and G. Pólya. *Inequalities*. Cambridge, 2 edition, 2001.

[HT98] V. Hanly and D. Tse. Multiaccess fading channels. Part II: Delay-limited capacities. *IEEE Trans. Inform. Theory*, 44:2816–2831, Nov. 1998.

[HT07] H. Holma and A. Toskala. *WCDMA for UMTS-HSPA Evolution and LTE*. John Wiley & Sons Inc., 2007.

[HV02] B. Hochwald and S. Vishwanath. Space-time multiple access: Linear growth in sum rate. In *Proc. 40th Annual Allerton Conf. on Commun., Contr., and Computing*, Oct. 2002.

[ITU03] ITU-T Recommendation G.114. *One-way Transmission Time*. ITU, May 2003.

[JB05] E. A. Jorswieck and H. Boche. Delay-limited capacity of parallel fading channels. In *Proc. IEEE 6th Workshop Signal Proc. Adv. Wireless Commun.*, pages 495–499, 2005.

[JB07] E. A. Jorswieck and H. Boche. Delay-limited capacity: Multiple antennas, moment constraints, and fading statistics. *IEEE Trans. Wireless Commun.*, 6(12):4204–4208, Dec. 2007.

[JG03] N. Jindal and A. Goldsmith. Capacity and optimal power allocation for fading broadcast channels with minimum rates. *IEEE Trans. Inform. Theory*, 49(11):2895–2909, Nov. 2003.

[JG05] N. Jindal and A. Goldsmith. Dirty-paper coding versus TDMA for MIMO broadcast channels. *IEEE Trans. Inform. Theory*, 51(5):1783–1794, May 2005.

[Jin05] N. Jindal. High SNR analysis of MIMO broadcast channels. In *Proc. IEEE Int. Symp. on Inform. Theory (ISIT)*, Adelaide, Australia, Sep. 2005.

[JRV+05] N. Jindal, W. Rhee, S. Vishwanath, S. A. Jafar, and A. Goldsmith. Sum power iterative water-filling for multiple-antenna gaussian broadcast channels. *IEEE Trans. Inform. Theory*, 51(4):1570–1580, April 2005.

[JVG04] N. Jindal, S. Vishwanath, and A. Goldsmith. On the duality of Gaussian multiple-access and broadcast channels. *IEEE Trans. Inform. Theory*, 50(5):768–783, May 2004.

[LG01a] L. Li and A. Goldsmith. Capacity and optimal resource allocation for fading broadcast channels–Part I: Ergodic capacity. *IEEE Trans. Inform. Theory*, 47(3):1083–1102, Mar. 2001.

[LG01b] L. Li and A. Goldsmith. Capacity and optimal resource allocation for fading broadcast channels–Part II: Outage capacity. *IEEE Trans. Inform. Theory*, 47(3):1103–1127, Mar. 2001.

[LJ06a] J. Lee and N. Jinal. Symmetric capacity of downlink MIMO channels. In *Proc. IEEE Int. Symp. on Inform. Theory (ISIT)*, Seattle, WA, 2006.

[LJ06b] J. Lee and N. Jindal. Dirty paper coding vs. linear precoding for MIMO broadcast channels. In *Proc. Asilomar Conf. Signals, Syst., and Comput.*, Pacific Grove, CA, Oct. 2006.

[LJ07] J. Lee and N. Jindal. High SNR analysis of MIMO broadcast channels: Dirty paper coding versus linear precoding. *IEEE Trans. Inform. Theory*, 53(12):4787–4792, Dec. 2007.

[LJ08] J. Lee and N. Jindal. Energy-efficient scheduling of delay constrained traffic over fading channels. In *Proc. IEEE Int. Symp. on Inform. Theory (ISIT)*, pages 604–608, Toronto, Canada, Jul. 2008.

[LJ09a] J. Lee and N. Jindal. Asymptotically optimal policies for hard-deadline scheduling over fading channels. In *Proc. Allerton Conf. Commun., Cont., and Comput.*, Allerton IL, Oct. 2009.

[LJ09b] J. Lee and N. Jindal. Asymptotically optimal policies for hard-deadline scheduling over fading channels. submitted to *IEEE Trans. Inform. Theory*, 2009.

[LJ09c] J. Lee and N. Jindal. Delay constrained scheduling over fading channels: Optimal policies for monomial energy-cost functions. In *Proc. IEEE Int. Conf. Commun.*, Dresden, Germany, Jun. 2009.

[LJ09d] J. Lee and N. Jindal. Energy-efficient scheduling of delay constrained traffic over fading channels. *IEEE Trans. Wireless Commun.*, 8(4):1866–1875, Apr. 2009.

[LTV03] A. Lozano, A. M. Tulino, and S. Verdú. Multiple-antenna capacity in the low-power regime. *IEEE Trans. Inform. Theory*, 49(10):2527–2544, Oct. 2003.

[LTV05] A. Lozano, A. M. Tulino, and S. Verdú. High SNR power offset in multiantenna communication. *IEEE Trans. Inform. Theory*, 51(12):4134–4151, Dec. 2005.

[LTV06] A. Lozano, A. M. Tulino, and S. Verdú. Multiuser mercury/waterfilling for downlink OFDM with arbitrary signal constellations. In *Proc. Int. Symp. on Spread Spectrum Tech. and Applic.*, Aug. 2006.

[LY04] T. Lan and W. Yu. Input optimization for multi-antenna broadcast channels with per-antenna power constraints. In *Proc. IEEE Globecom Conf.*, volume 1, pages 420–424, Dallas, 2004.

[NC02] R. Negi and J. M. Cioffi. Delay-constrained capacity with causal feedback. *IEEE Trans. Inform. Theory*, 48(9):2478–2494, Sep. 2002.

[NMR03] M. J. Neely, E. Modiano, and C. E. Rohrs. Dynamic power allocation and routing for time varying wireless networks. In *Proc. IEEE INFOCOM*, pages 745–755, 2003.

[Nua07] L. Nuaymi. *WiMAX-Technology for Broadband Wireless Access*. John Wiley & Sons Inc., 2007.

[PUBG01] B. Prabhakar, E. Uysal-Biyikoglu, and A. El Gamal. Energy-efficient transmission over a wireless link via lazy packet scheduling. In *Proc. IEEE INFOCOM*, pages 386–394, Anchorage, AK, Apr. 2001.

[RC00] W. Rhee and J. M. Cioffi. Increase in capacity of multiuser OFDM system using dynamic subchannel allocation. In *Proc. IEEE Veh. Tech. Conf.*, 2000.

[RM94] M. Rupf and J. L. Massy. Optimum sequence multisets for synchronous code-division multiple-access channels. *IEEE Trans. Inform. Theory*, 40(4):1261–1266, Jul. 1994.

[Roc70] R. T. Rockafellar. *Convex Analysis*. Princeton Univ. Press, 1970.

[RSA04] D. Rajan, A. Sabharwal, and B. Aazhang. Delay-bounded packet scheduling of bursty traffic over wireless channels. *IEEE Trans. Inform. Theory*, 50(1):125–144, Jan. 2004.

[Rud87] W. Rudin. *Real and Complex Analysis*. McGraw-Hill, 3 edition, 1987.

[SB04] M. Schubert and H. Boche. User ordering and power allocation for optimal multi-antenna precoding/decoding. In *ITG Workshop on Smart Antennas*, 2004.

[SCA+06] Z. Shen, R. Chen, J. G. Andrews, R. W. Heath, and B. L. Evans. Sum capacity of multiuser MIMO broadcast channels with block diagonalization. In *Proc. IEEE Int. Symp. on Inform. Theory (ISIT)*, pages 886–890, Seattle, WA, Jul. 2006.

[Sha48] C. E. Shannon. A mathematical theory of communication. *The Bell System Technical Journal*, 27, 1948.

[SL] D. Shuman and M. Liu. Energy-efficient transmission scheduling with strict underflow constraints. submitted to *IEEE Trans. Inform. Theory*.

[SL08] D. Shuman and M. Liu. Energy-efficient transmission scheduling for wireless media streaming with strict underflow constraints. In *Proc. Int. Symp. on Modeling and*

Optimization in Mobile, Ad Hoc, and Wireless Networks, Berlin, Germany, Apr. 2008.

[SSH04] Q. H. Spencer, A. L. Swindlehurst, and M. Haardt. Zero-forcing methods for downlink spatial multiplexing in multiuser MIMO channels. *IEEE Trans. Signal Processing*, 52(2):461–471, Feb. 2004.

[SV01] S. Shamai and S. Verdú. The impact of frequency-flat fading on the spectral efficiency of CDMA. *IEEE Trans. Inform. Theory*, 47(5), May 2001.

[SVL05] T. Sartenaer, L. Vandendorpe, and J. Louveaux. Balanced capacity of wireline multiuser channels. *IEEE Trans. Commun.*, 53(12):2029–2042, Dec. 2005.

[TE92] L. Tassiulas and A. Ephremides. Stability properties of constrained queueing systems and scheduling policies for maximum throughput in multihop radio networks. *IEEE Trans. Automat. Contr.*, 37(12):1936–1948, Dec. 1992.

[Tel95] I. E. Telatar. Capacity of multi-antenna gaussian channels. Bell laboratories tech. memo., Lucent Technologies, 1995.

[Tse] D. N. C. Tse. Optimal power allocation over parallel Gaussian broadcast channels. unpublished. Available at http://www.eecs.berkeley.edu/ d̃tse.

[TV04] A. M. Tulino and S. Verdú. *Random Matrix Theory and Wireless Communications*. now Publishers Inc., Hanover, MA, 2004.

[TV05] D. Tse and P. Viswanath. *Fundamentals of Wireless Communication*. Cambridge Univ. Press, 2005.

[UBG04] E. Uysal-Biyikoglu and A. El Gamal. On adaptive transmission for energy efficient in wireless data networks. *IEEE Trans. Inform. Theory*, 50, 2004.

[UBPG02] E. Uysal-Biyikoglu, B. Prabhakar, and A. El Gamal. Energy-efficient packet transmission over a wireless link. *IEEE/ACM Trans. Networking*, 10(4):487–499, Aug. 2002.

[VDSH05] A. Vakili, A. Dana, M. Sharif, and B. Hassibi. Differentiated rate scheduling for MIMO Gaussian broadcast channels. In *Proc. of 43rd Annual Allerton Conf. on Comm., Control and Comp.*, Monticello, IL, 2005.

[Ver02] S. Verdú. Spectral efficiency in the wideband regime. *IEEE Trans. Inform. Theory*, 48(6):1319–1343, Jun. 2002.

[VJG03] S. Vishwanath, N. Jindal, and A. Goldsmith. Duality, achievable rates, and sum-rate capacity of Gaussian MIMO broadcast channels. *IEEE Trans. Inform. Theory*, 49(10):2658–2668, Oct. 2003.

[VT03] P. Viswanath and D. N. C. Tse. Sum capacity of the vector Gaussian broadcast channel and uplink-downlink duality. *IEEE Trans. Inform. Theory*, 49(8):1912–1921, Aug. 2003.

[VTL02] P. Viswanath, D.N.C. Tse, and R. Laroia. Opportunistic beamforming using dumb antennas. *Information Theory, IEEE Transactions on*, 48(6):1277–1294, Jun 2002.

[VVH03] H. Viswanathan, S. Venkatesan, and H. Huang. Downlink capacity evaluation of cellular networks with known-interference cancellation. *IEEE J. Sel. Areas Commun.*, 21(5):802–811, Jun 2003.

[WSS06] H. Weingarten, Y. Steinberg, and S. Shamai. The capacity region of the Gaussian multiple-input multiple-output broadcast channel. *IEEE Trans. Inform. Theory*, 52(9):3936–3964, Sep. 2006.

[YC04] W. Yu and J. M. Cioffi. Sum capacity of Gaussian vector broadcast channels. *IEEE Trans. Inform. Theory*, 50(9):1875–1892, Sep. 2004.

[Yu03] W. Yu. A dual decomposition approach to the sum power Gaussian vector multiple-access channel sum capacity problem. In *Proc. Conf. Information Sciences and Systems (CISS)*, Baltimore, MD, 2003.

[ZM07] M. Zafer and E. Modiano. Delay constrained energy efficient data transmission over a wireless fading channel. In *Workshop on Inf. Theory and Appl.*, pages 289–298, La Jolla, CA, Jan./Feb. 2007.